

**Mechanistic Understanding and Development of Catalytic Carbon
Dioxide Utilisation Reactions**

Rachel Leanne Nicholls

Submitted in accordance with the requirements for the degree of
Doctor of Philosophy

The University of Leeds
School of Chemistry

June 2017

The candidate confirms that the work submitted is her own, except where work which has formed part of jointly authored publications has been included. The contribution of the candidate and the other authors to this work has been explicitly indicated below. The candidate confirms that appropriate credit has been given within the thesis where reference has been made to the work of others.

The work in Chapter 2 of the thesis has appeared in publication as follows:

R. Nicholls, S. Kaufhold, B.N. Nguyen, "Observation of guanidine-carbon dioxide complexation in solution and its role in the reaction of carbon dioxide and propargylamines", *Catal. Sci. Technol.*, 2014, **4**, 3458-3462

S.K. performed the *in situ* IR studies on complexation of CO₂ with guanidines, amidines and amines and initial catalyst screening for catalytic activity. R.N. evaluated catalytic activity of MTBD, TMG and DBU catalysts under the conditions reported.

Part of the work in Chapters 3-5 of the thesis is included in a manuscript which has been submitted for publication and is currently under review:

R. Nicholls, C.M. Rayner, A.J.P. White, B.N. Nguyen, "Guanidine-Catalyzed Reductive Amination of Carbon Dioxide with Silanes: Switching between Pathways and Suppressing Catalyst Deactivation", *under review (2017)*

R.N. carried out all experimental work with the exception of the crystal structure of a complex between Morpholine/CO₂/TMG/Thiourea which was prepared, measured and resolved by B.N.N. and A.J.P.

Part of the work in Chapter 6 of the thesis has appeared in publication as follows:

R.L. Nicholls, C.M. Pask, B. Nguyen. "Crystal structure of poly[μ -acetato-bis[μ -2-oxo-2-(quinolin-8-yl)ethanoate]-trisodium]", *Acta Cryst.*, 2014, **E70**, m385-m386

R.N. prepared the compound discussed. C.M.P. measured and resolved the crystal structure.

This copy has been supplied on the understanding that it is copyright material and that no quotation from the thesis may be published without proper acknowledgement.

© 2017 The University of Leeds and Rachel Leanne Nicholls

The right of Rachel Leanne Nicholls to be identified as Author of this work has been asserted by her in accordance with the Copyright, Designs and Patents Act 1988.

Acknowledgements

Firstly, thank you to Dr Bao Nguyen for your supervision and guidance. I am grateful for the many opportunities I have been given and the breadth training I have received throughout my PhD studies. In particular, the opportunity to be involved in the many synchrotron based experiments is one that I have greatly enjoyed. Thank you also to Prof. Chris Rayner for your advice, support and for always pushing me to think that bit further after every meeting. For funding, I thank the University of Leeds for a University Research Scholarship.

For all the technical support and help I have received throughout, thank you to Dr Chris Park for measuring and resolving many crystal structures. Thanks to Mr Simon Barrett for helping with various NMR experiments and to Dr Stuart Warriner for assistance with MSMS studies. Thanks also to Dr Mary Bayana for general help and guidance with all things iPRD and GC related, and to Dr Balazs Kulik for training and help with the high pressure CO₂ equipment. Thank you to Dr Jon Goode, Caroline Edwards and Mettler-Toledo for a loan of the ReactIR system. For help with proof reading thanks also to Grant, Jo and Rhiann.

To all of the past and current members of the Nguyen group and iPRD. Thank you for technical assistance, chemistry discussions and of course the countless enjoyable Friday pub nights and many other random activities over the last few years. Particular thanks to Chris, Mike, James and Grant for making the last few years more enjoyable; for the joint conference trips, synchrotron runs, and general day-to-day laughs and entertainment. To Grant, thank you for always being there to talk through the low times and challenges with and to jointly celebrate the successes (no matter how small). From week one to the end you've made every stage of this PhD more enjoyable.

Outside of the Leeds chemistry bubble, thanks to fellow members of Leeds Jazz Orchestra for a most welcome escape from chemistry on Thursday nights. To friends and family thank you for constant support and encouragement over the last few years. With special thanks to Naomi and Jo for many fun times, friendship and for always providing a refreshing and realistic outlook. And finally, thank you to my family: Jon and Miriam and my parents Trish and Dave. Thank you for your unconditional and continual support, and for always encouraging me to believe in myself and simply to just go for it.

Abstract

To enable the rational development of CO₂ utilisation processes, it is vital to understand the mechanisms of involved reactions. This thesis reports studies to improve the mechanistic understanding of two catalytic CO₂ utilisation reactions and work towards the development of a novel CO₂ utilisation process.

In Chapter 2, the role of guanidines in the reaction of propargylamines and CO₂ to give cyclic carbonates is discussed. Guanidines have multiple potential mechanisms of catalytic activity. Through correlating the catalytic activity and solvent effects with observed guanidine-CO₂ complexation, the origin of catalytic activity was determined.

Chapters 3-5 report results of a mechanistic investigation into the guanidine catalysed reductive functionalisation of CO₂ with amines and hydrosilanes to yield formylamides, methylamines and aminal products. Through monitoring the reaction using GC, ¹H & ¹³C NMR, *in situ* FT-IR and mass spectrometry, a number of competitive intertwined reaction pathways and intermediates were identified. At low temperatures formylamides are produced via transformylation of a formoxysilane intermediate with an amine. However, at higher temperatures a competing pathway enables further reduction of the formoxysilane to a bis(silyl)acetal, its subsequent reaction with amines yields aminal intermediates which can be further reduced under reaction conditions to yield methylamines and formylamides. A catalyst deactivation pathway was identified whereby formylation of the catalyst itself occurs. By using alkylated guanidines, the deactivation pathway was prevented and the alkylated catalysts could be used at 0.1 mol% loadings and achieved TON of 805 and TOF of 33.5 h⁻¹.

In Chapter 6, efforts towards the development of a novel CO₂ utilisation reaction are discussed. α -Ketocarboxylic acids were targeted from the insertion of CO₂ into an aldehyde C-H bond, inspired by analogous hydroacylation chemistry. A range of reaction conditions, rhodium catalysts and substrates were investigated; however, although a number of products were identified, no incorporation of CO₂ was observed.

Table of Contents

Acknowledgements	iii
Abstract.....	iv
Abbreviations	x
Chapter 1 Introduction.....	1
1.1 Introduction to CO ₂ Utilisation.....	1
1.2 Activation of CO ₂	4
1.2.1 Activation of CO ₂ with Transition Metal Complexes	4
1.2.2 Activation of CO ₂ with Organic Molecules	5
1.3 Organocatalysis in CO ₂ Utilisation.....	6
1.4 Organocatalysed Reductive Functionalisation of CO ₂ with Amines and Hydrosilanes.....	10
1.4.1 Formylation of Amines with CO ₂	10
1.4.1 <i>N</i> -Methylation of Amines with CO ₂	18
1.5 Summary	21
Chapter 2 Role of Guanidine Catalysts in the Reaction of Propargylamines and CO₂.....	22
2.1 Introduction	22
2.2 Catalytic Activity in Cyclic Carbamate Synthesis	26
2.3 Applicability to Cyclic Carbonate Synthesis.....	29
2.4 Conclusions	30
Chapter 3 Guanidine Catalysed Reductive Functionalisation of CO₂: Mechanism of Amine Formylation.....	31
3.1 Introduction	31
3.1.1 Project Aims.....	33
3.2 Reaction Development & Kinetic Profiling	34
3.2.1 Catalyst Selection.....	34
3.2.2 Reaction Kinetics	38
3.3 Intermediate Identification by Reaction Monitoring	41
3.3.1 <i>In situ</i> IR Monitoring	41

3.4	Role of Silylcarbamate Intermediate	44
3.4.1	<i>In Situ</i> Reaction Monitoring	44
3.4.2	Characterisation & Formation Kinetics of Silylcarbamate Intermediate ..	45
3.4.3	Proposed Mechanism of Silylcarbamate Formation	48
3.4.4	Reactivity of Silylcarbamate Intermediate	53
3.4.5	Summary of the Role of the Silylcarbamate Intermediate	56
3.5	Role of Formoxysilane Intermediate	59
3.5.1	<i>In Situ</i> Reaction Monitoring	59
3.5.2	Formation of Formoxysilane Intermediate	60
3.5.3	Addition of Morpholine to Products from Hydrosilylation of CO ₂	63
3.5.4	Summary of Formoxysilane Intermediate Involvement	66
3.6	Role of Morpholinium Carbamate	67
3.7	Role of TMG Catalyst	68
3.7.1	Carbamate Formation	69
3.7.2	Activation of CO ₂	70
3.7.3	Activation of Silane	70
3.7.4	Precursor to Carbamate as Catalyst	71
3.8	Summary of Pathways to Formylmorpholine	72
3.9	Conclusions	75

Chapter 4 Guanidine Catalysed Reductive Functionalisation of CO₂: Catalyst Optimisation and Scope of Amine Formylation..... 77

4.1	Introduction	77
4.2	Reducing Catalyst Loadings	78
4.2.1	Catalyst Deactivation	78
4.2.2	Catalyst Optimisation	82
4.3	Reaction Scope	85
4.3.1	Alternative Reductant	85
4.3.2	Substrate Scope	88
4.4	Conclusion	90

Chapter 5 Guanidine Catalysed Reductive Functionalisation of CO₂: Mechanism of Amine Methylation 91

5.1	Introduction	91
5.2	Factors Affecting <i>N</i> -Methylmorpholine Formation	93
5.3	Role of Aminal Intermediate	95

5.3.1	Routes to Amino Intermediate	98
5.3.2	Reactivity of Amino to Methylmorpholine and Formylmorpholine	102
5.3.3	Mechanistic Considerations	105
5.4	Reduction of Formylmorpholine to Methylmorpholine	110
5.5	Involvement of Methoxysilane Species.....	114
5.6	Rate Enhancement with Alkylated TMG Catalysts.....	115
5.7	Summary of Pathways to Methylmorpholine	118
5.8	Summary of Product Selectivity.....	119
5.9	Conclusions and Future Work	122

Chapter 6 Developing a Process for Reaction of CO₂ with Biomass Derived Compounds
..... **123**

6.1	Introduction to Hydroacylation Reactions.....	123
6.1.1	Mechanistic Overview	123
6.1.2	Substrate Control.....	124
6.1.3	Additive Control.....	127
6.1.4	Catalyst Control	127
6.1.5	Carbonyl Hydroacylation Reactions	128
6.1.6	Reaction of CO ₂ with Aldehydes	129
6.2	Aims of Study and Previous Work.....	131
6.3	Selection of Reaction Screening Conditions	132
6.4	Reactions of Quinoline-8-carbaldehyde 110 and CO ₂	133
6.4.1	Preliminary Identification of Products	133
6.4.2	Reaction Outcome	137
6.4.3	Synthesis of Target Product 166	143
6.5	Reactions of Furfural and CO ₂	146
6.5.1	Preliminary Results and Comparison with Authentic Product 186.....	146
6.5.2	Reaction Screening.....	149
6.5.3	Identification of Reaction Products.....	151
6.6	Conclusions and Further Work.....	155

Chapter 7 Experimental **157**

7.1	General Considerations	157
7.2	Chapter 2: Role of Guanidine Catalysts in the Reaction of Propargylamines and CO ₂	158
7.2.1	General Procedures	158

7.2.2	Substrate Synthesis.....	158
7.2.3	Product Characterisation	159
7.3	Chapters 3-5: Guanidine Catalysed Reductive Functionalisation of CO ₂	160
7.3.1	General Considerations	160
7.3.2	Standard Reaction Procedure	160
7.3.3	Synthesis of Organic Compounds	161
7.3.4	Procedure for Reaction Monitoring by GC	164
7.3.5	Procedure for Reaction Monitoring by <i>In Situ</i> IR	175
7.3.6	Procedure for Reaction Monitoring by NMR	176
7.3.7	Procedure for Reaction Monitoring by HRMS	179
7.3.8	Relative Solubility of CO ₂ in MeCN at 23 and 60 °C.....	181
7.3.9	Procedures for Role of Silylcarbamate Intermediate Studies.....	181
7.3.10	Procedures for Role of Formoxysilane Intermediate Studies.....	186
7.3.11	Role of Morpholinium Carbamate 19 & 20	189
7.3.12	Role of TMG Studies	191
7.3.13	Stoichiometric Catalyst Deactivation Studies	192
7.3.14	Evaluating Catalytic Activity of Alkylated Catalysts	193
7.3.15	Procedure for Use of Alternative Reductants.....	197
7.3.16	Substrate Scope	198
7.3.17	Reduction of Urea 81	202
7.3.18	GC Kinetics of Reaction of Aminal 57 to Methyl and Formylmorpholine.....	203
7.3.19	Mechanistic Study of Aminal 57 Reactivity	206
7.3.20	Reduction of Formylmorpholine 24 to Methylmorpholine 48.....	211
7.3.21	Involvement of Methoxysilane Species	214
7.3.22	Rate Enhancement with Alkylated Catalysts	214
7.4	Chapter 6: Process Development for Reaction of CO ₂ with Biomass Derived Compounds.....	216
7.4.1	General Procedures for Quinoline-8-carbaldehyde 110 Substrate.....	216
7.4.2	Substrate Synthesis.....	216
7.4.3	Catalyst Preparation	217
7.4.4	Authentic Product Synthesis	220
7.4.5	General Procedures Furfural 159 as Substrate	225
7.4.6	Authentic Product Synthesis	225
7.4.7	Characterisation of Reaction Product Component A 193	226

References.....	227
Appendix.....	240
Appendix 1	Crystal Structure of Morpholine/Thiourea/CO ₂ Complex 47 240
Appendix 2	IR Spectra of Reaction Standards 242
Appendix 3	X-ray Crystal Structure for Authentic Product 166 243
Appendix 4	X-ray Crystal Structure for Authentic Product 186 244
Appendix 5	2D Spectra Used for Identification of Component A 193 : 246

Abbreviations

ATR	Attenuated Total Reflectance
ButylTMG	2-Butyl-1,1,3,3-tetramethylguanidine
COD	1,5-Cyclooctadiene
DBU	1,8-Diazabicyclo[5.4.0]undec-7-ene
DCE	1,2-Dichloroethane
DCM	Dichloromethane
DMA	<i>N,N</i> -Dimethylacetamide
DMF	<i>N,N</i> -Dimethylformamide
DMSO	Dimethylsulfoxide
DOSY	Diffusion Ordered Spectroscopy
DPEphos	Bis[2-(diphenylphosphino)phenyl] ether
DPPB	1,4-Bis(diphenylphosphino)butane
DPPE	1,3-Bis(diphenylphosphino)ethane
DPPF	1,1'-Bis(diphenylphosphino)ferrocene
DPPM	1,2-Bis(diphenylphosphino)methane
DPPP	1,3-Bis(diphenylphosphino)propane
Equiv	Equivalents
ESI	Electron spray ionisation
FLP	Frustrated Lewis Pair
FormylTMG	2-Formyl-1,1,3,3-tetramethylguanidine
FTIR	Fourier Transform – Infrared
GC	Gas chromatography
h	Hours
HRMS	High resolution mass spectrometry
LC	Liquid chromatography
m/z	Mass to charge ratio
MethylTMG	Pentamethylguanidine
MS	Mass spectrometry
MTBD	7-Methyl-1,5,7-triazabicyclo[4.4.0]dec-5-ene
NHC	N-heterocyclic carbene
NBD	Norbornadiene / bicyclo[2.2.1]hepta-2,5-diene
NBS	<i>N</i> -Bromosuccinimide
nmr	Nuclear magnetic resonance
noe	Nuclear Overhauser effect
PMHS	Poly(methylhydrosiloxane)

ppm	Parts per million
RLS	Rate limiting step
RT	Room temperature
TBAF	Tetrabutylammonium fluoride
TEA	Triethylamine
TBD	1,5,7-Triazabicyclo[4.4.0]dec-5-ene
THF	Tetrahydrofuran
TLC	Thin layer chromatography
TMDS	Tetramethyldisiloxane
TMG	1,1,3,3-Tetramethylguanidine
TMP	2,2,6,6-Tetramethylpiperidine
TON	Turn over number
TOF	Turn over frequency
Tr	Trace

Chapter 1 Introduction

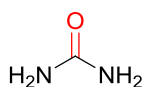
1.1 Introduction to CO₂ Utilisation

Utilising carbon dioxide (CO₂) is a key priority in current chemical research and offers an alternative carbon source over the depleting fossil fuel derived sources.¹ The use of CO₂ in chemical synthesis as a C₁ building block is an attractive process due to its ready availability, low cost and sustainability.²

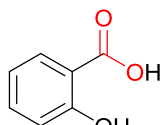
The main limitation of CO₂ as a carbon source is its thermodynamic and kinetic stability. Thermodynamic barriers are often overcome through using high energy reactants, while kinetic barriers require the use of catalysis.²⁻⁴ Currently, the use of CO₂ as a C₁ chemical feedstock is very limited and few methodologies have been developed which target products of interest to industry that are accessible under industrial scale conditions.⁵ Developments of chemical transformations which incorporate CO₂ are underway; however, they are often limited by their synthetic scope or through requirements for stoichiometric or excess amount of metal reagents, low yields and high temperatures or pressures.

Approaches to CO₂ utilisation can often be characterised into three approaches: functionalisation, polymerisation or formal reduction of CO₂, Figure 1.1.

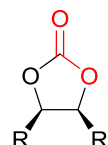
Functionalisation:



Urea

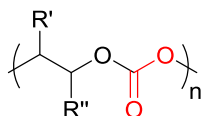


Salicylic acid

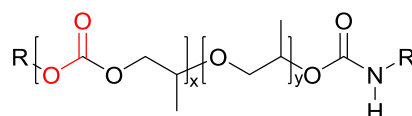


Cyclic carbonates

Polymerisation:

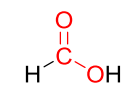


Polycarbonates

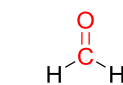


Polyurethane analogues

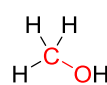
Reduction:



Formic acid



Formaldehyde



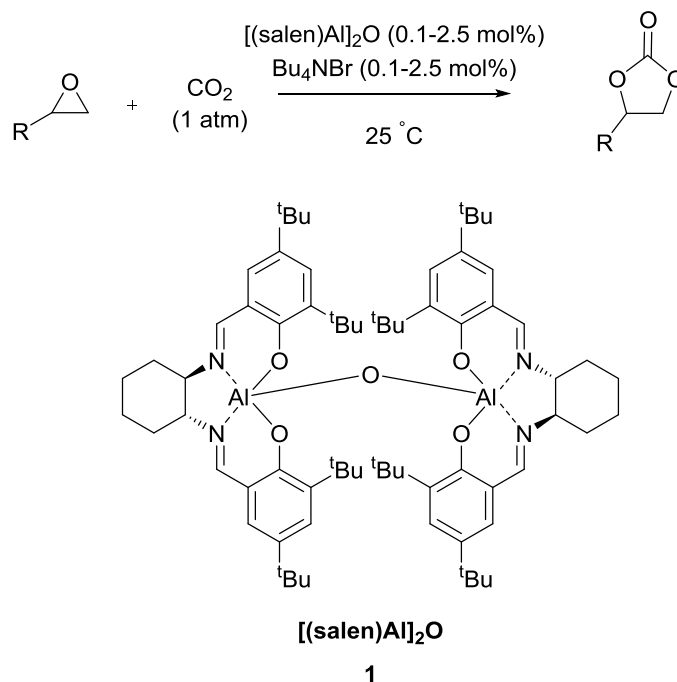
Methanol



Methane

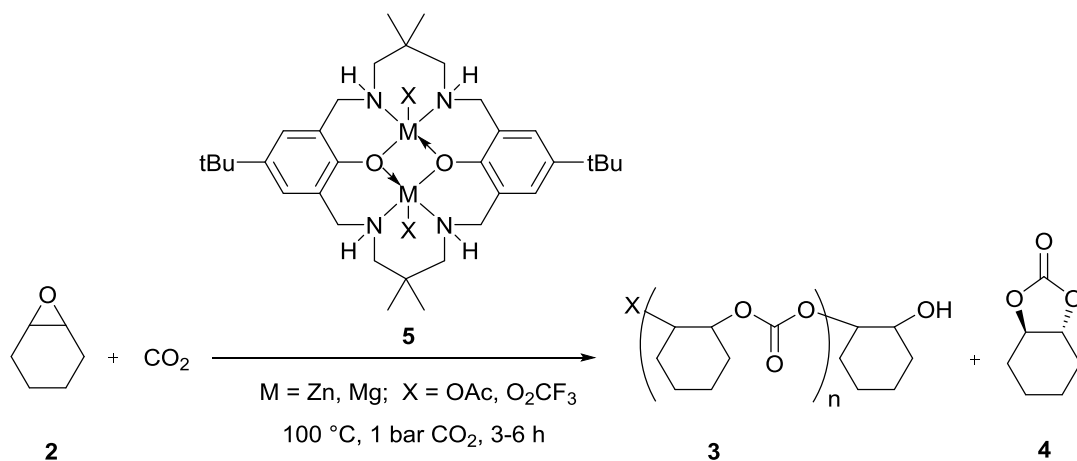
Figure 1.1: Example compounds for targets in utilisation of CO₂

For example, functionalisation transformations of CO₂ include the synthesis of urea, which is currently the largest industrial CO₂ utilisation process and the synthesis of salicylic acid at an industrial scale from the reaction of CO₂ and phenol.⁶ Cyclic carbonates are also currently synthesised on an industrial scale; however current production methods require the use of high temperatures and pressure and use ammonium or phosphonium salts as the catalyst.^{7, 8} New catalysts are under development to improve this process; for example, aluminium catalysts, e.g. salen complex **1**, developed by North enable conversion of epoxides with CO₂ to cyclic carbonates at room temperature and 1 atm CO₂ pressure using Bu₄NBr as a cocatalyst, Scheme 1.1.^{9, 10} Importantly, the process is tolerant towards common impurities in flue-gas, and this along with the mild conditions required, have enabled the development for large scale synthesis directly from industrial CO₂ emissions.^{8, 11}



Scheme 1.1: Synthesis of cyclic carbonates from epoxides and CO₂

The use of CO₂ for polymer synthesis is an attractive CO₂ utilisation process due to both the wide scope and large scale preparation of polymers and their relatively long lifespans compared to other commercial chemicals.¹ For example, Williams and co-workers have reported a series of di-zinc and di-magnesium catalysts **5** that successfully catalyse the synthesis of poly(cyclohexylene carbonate) **3**, Scheme 1.2.^{12, 13} Importantly, the reaction proceeds under mild conditions and has been proved to be tolerant to common contaminants in captured CO₂, as demonstrated by the performing the reaction with CO₂ directly captured from a carbon capture plant at Ferrybridge power station.^{12, 13}



Scheme 1.2: Synthesis of poly(cyclohexane)carbonate **3** from cyclohexane oxide **2** and CO₂ using captured and contaminated CO₂ ¹²

Already being synthesised on a pilot plant is the synthesis of polyurethane foams by the Bayer DREAM process, whereby CO₂ is incorporated into the polyol starting material through copolymerisation of propylene oxide and CO₂ using a Zn catalyst.^{14, 15} This process has a large potential for use as a CO₂ utilisation procedure, to replace the current manufacturing processes for polyurethanes, which are produced on a multi-million ton per year scale.¹⁴

While the use of CO₂ utilisation procedures for the synthesis of chemicals is unlikely to make any impact on the CO₂ levels, the direct reduction of CO₂ for use as fuels perhaps offers the greatest potential for CO₂ utilisation in terms of reducing CO₂ emissions.¹⁶ However, the main challenge associated with this is sourcing a sustainable and financially viable hydrogen source.¹ The industrial scale synthesis of methanol has been in manufacture in Iceland since 2011, however this is only possible due to the availability of geothermal energy sources which enables the sustainable production of hydrogen from the electrolysis of sea water.¹⁷

Alternative reduction processes of CO₂ include its conversion to formic acid,^{18, 19} formaldehyde,²⁰ methane^{21, 22} and carbon monoxide; however, the majority of these processes often involve transition metal catalysts or high temperatures and pressures.

1.2 Activation of CO₂

1.2.1 Activation of CO₂ with Transition Metal Complexes

Transition metal complexes are frequently employed to activate CO₂ through coordination to the metal or to activate the substrate to enable C-C bond formation.²³ There are three significant types of CO₂ coordination to transition metals commonly encountered, Figure 1.2.²³⁻²⁵

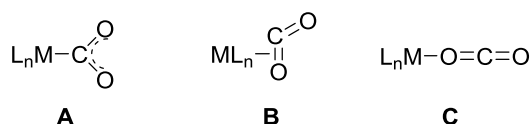


Figure 1.2: Common binding modes of CO₂ with a metal centre a) M-C σ bond, b) M-C π bond, and c) O-M σ bond

In mode A, σ bonding occurs from the transition metal centre to the carbon atom of CO₂, whilst in mode B, π bonding of the transition metal with one C=O bond occurs, whereby electron density is donated from the metal to the LUMO of the ligand, Figure 1.3. Finally in mode C, σ bonding from the oxygen in CO₂ leads to coordination, Figure 1.2. Coordination of CO₂ is most commonly observed with late transition metals of low oxidation states, e.g. iron, cobalt and nickel, due to their basicity and ability to bind to CO₂ through back bonding, Figure 1.3.^{3, 23}

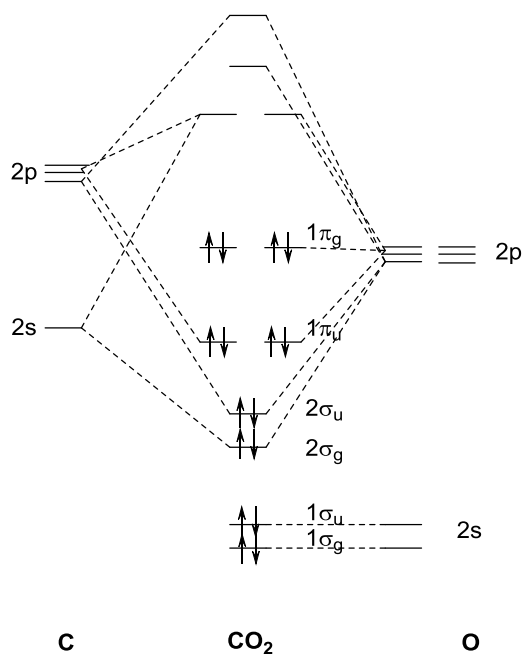
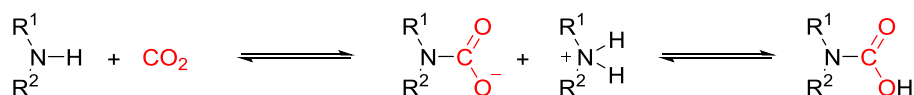


Figure 1.3: Molecular orbital diagram for CO₂

1.2.2 Activation of CO₂ with Organic Molecules

A variety of highly reactive organic molecules are also known to activate CO₂. For example, the reaction of many amines with CO₂ leads to the formation of carbamate salts or carbamic acids, the equilibrium of which is dependent on solvent and temperature (Scheme 1.3).^{26, 27} Similarly, reactions of alcohols with CO₂ leads to the formation of carbonic acids and carbonates.^{26, 27}



Scheme 1.3: Reaction equilibrium of amines and CO₂ to form corresponding carbamate and carbamic acid ^{26, 27}

Alongside amines, other organic bases such as guanidines and amidines have also been shown to activate CO₂. For example, Franco and co-workers observed DBU-CO₂ complexation by solid state NMR^{28, 29} and complexation between TBD and CO₂ has also been reported by Villiers *et al.* using NMR and X-ray crystallography, Figure 1.4.³⁰

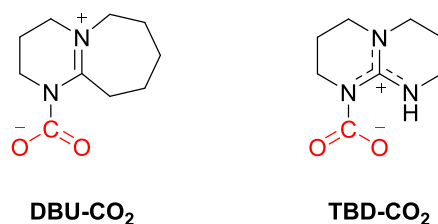
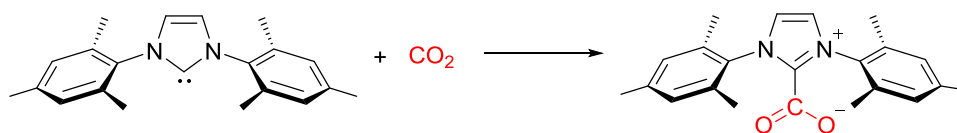


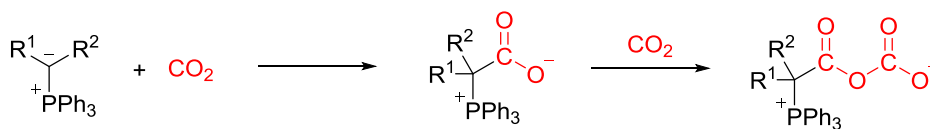
Figure 1.4: Guanidine and amidine complexes with CO₂^{28, 30}

Other examples of CO₂ activation include activation by *N*-heterocyclic carbenes (NHCs) to form imidazolium carboxylates³¹ and by phosphorous ylides,³² both of which proceed by nucleophilic attack at the carbon atom of CO₂. With diazaphosphenes however, activation of CO₂ occurs via insertion of CO₂ into the P-H bond to give a phosphorus formate, with attack from the oxygen of CO₂ to the electrophilic phosphorus atom.³³ Frustrated Lewis pairs (FLPs) have also been shown to activate CO₂ through their dual role as a Lewis acid and a Lewis base,³⁴ Scheme 1.4.

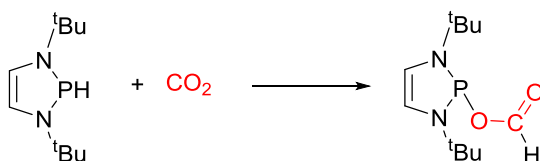
a) CO₂ Activation by NHCs



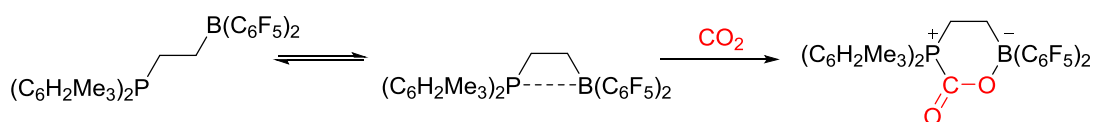
b) CO₂ Activation by P-ylide CO₂ adducts



c) CO₂ Activation by Diazaphospholenes



d) CO₂ Activation by FLPs



Scheme 1.4: Examples of CO₂ activation with: a) NHCs, b) P-ylide CO₂ adducts, c) Diazaphospholenes and d) FLPs³¹⁻³⁴

1.3 Organocatalysis in CO₂ Utilisation

Catalytic CO₂ utilisation processes predominantly use transition metal catalysts and the field of organocatalysts for use in CO₂ utilisation processes is significantly less developed. While transition metal catalysts mostly offer a greater stability and higher activities than organocatalysts, organocatalysts are generally low cost, less toxic, and importantly, more tolerant to moisture and air.³⁵

As with metal catalysis, a broad range of organocatalysts, e.g. guanidines,³⁶ NHCs,³⁷ FLPs,³⁸ diazaphospholenes,³³ ionic liquids³⁹ and polyhydroxy compounds⁴⁰ (Figure 1.5), have been shown to catalyse CO₂ utilisation reactions by either i) activation of CO₂, ii) activation of the substrate, or iii) dual activation of both CO₂ and the substrate.³⁵

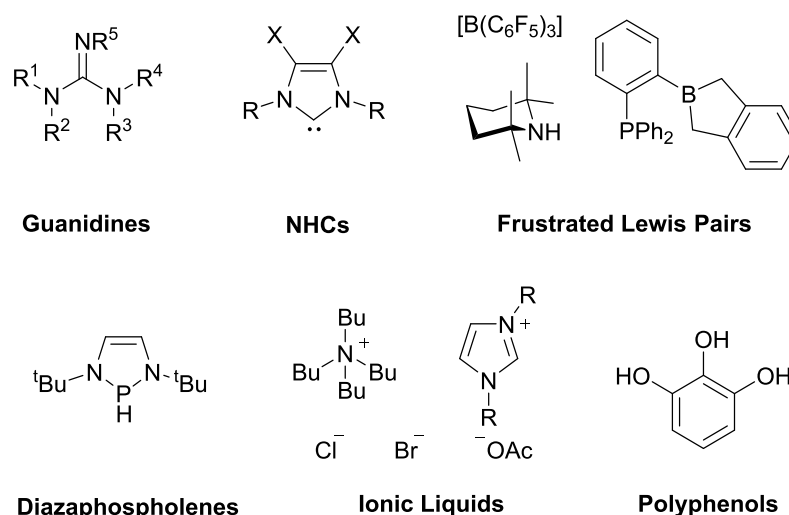
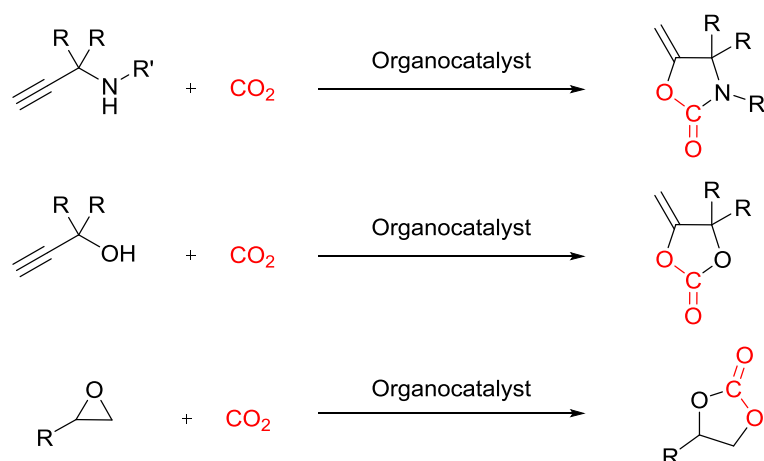


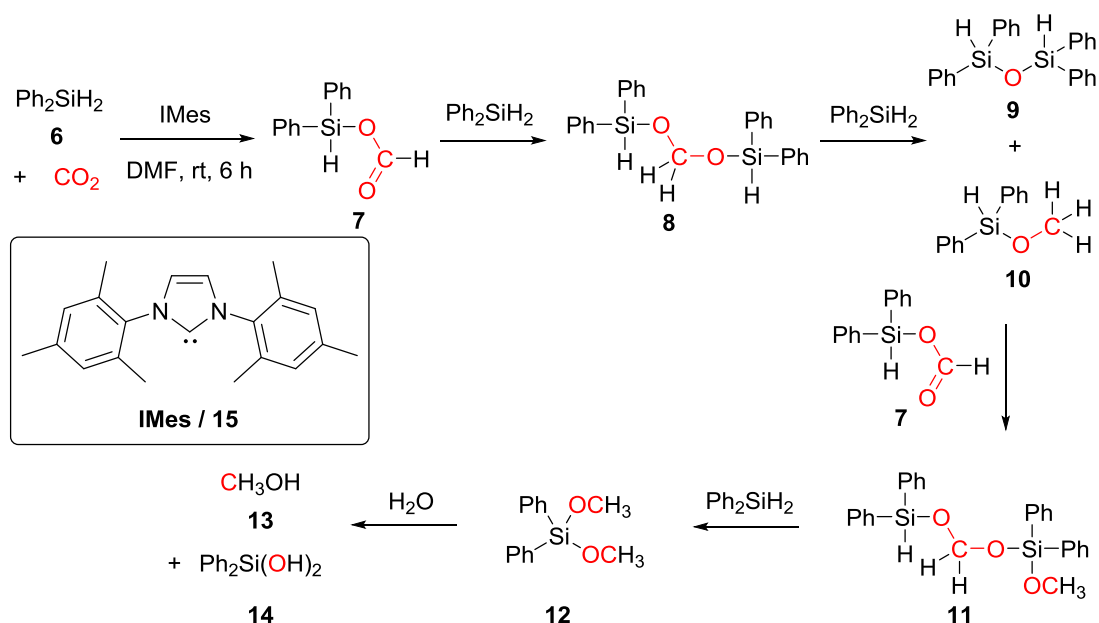
Figure 1.5: Example classes of organocatalysts used in CO₂ utilisation reactions

A variety of transformations of CO₂ using organocatalysts have been achieved. For example, many organocatalysts have been reported for the non-reductive functionalisation of CO₂ to give products such as cyclic carbamates and cyclic carbonates, Scheme 1.5.^{36, 41, 42}



Organocatalysts have also been successfully used for the reduction of CO₂ to products such as formic acid, carbon monoxide, methanol and methane.^{35, 46} Typical reductants for the reduction of CO₂ with organocatalysts include hydrosilanes and hydroboranes. The role of the organocatalyst in these transformations is typically ascribed to either activation of CO₂ or activation of the Si-H or B-H bond; however there is still discussion as to the mechanism of activation.⁴⁷ For sustainable reduction hydrosilanes derived from waste streams, such as polymethylhydrosiloxane (PMHS), are often targeted.⁴⁸

The first organocatalysed reduction of CO₂ was reported by Zhang and Ying in 2009 using a hydrosilane reductant.³⁷ A highly active NHC catalyst was reported for the reduction of CO₂ to methoxysilane which could be hydrolysed to release methanol, achieving turnover numbers (TON) and turnover frequencies (TOF) of up to 1840 and 25.5 h⁻¹ respectively, Scheme 1.6.³⁷ The proposed mechanism, based on computational and experimental studies, involves initial formation of an NHC-CO₂ adduct which can react with the hydrosilane, and following subsequent hydride transfer, produce a formoxysilane species **7**, Scheme 1.6. Reaction of the formoxysilane intermediate **7** with a second silane species yields a bis(silyl)acetal intermediate **8**, which can then further react to give the final methoxysilane species **10** and **12**. Hydrolysis of the methoxysilane then releases the desired methanol product **13** and silanol by-products **14**, Scheme 1.6.^{37, 49}



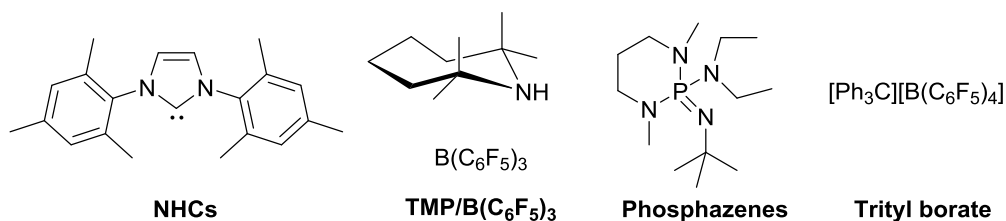
Scheme 1.6: Proposed reaction pathways for the NHC catalysed reduction of CO₂ to MeOH with hydrosilanes^{37, 49}

Following this report, the reduction of CO₂ with hydrosilanes was also demonstrated with other organocatalysts including phosphazenes⁵⁰ and solid poly-*N*-heterocyclic carbenes⁵¹ for the production of methanol, and a FLP system of 2,2,6,6-tetramethylpiperidine (TMP) and [B(C₆F₅)₃] for synthesis of methane, Figure 1.6a.⁵² Stoichiometric amounts of trityl borate have also shown to mediate the reduction of CO₂ to methanol.⁵³

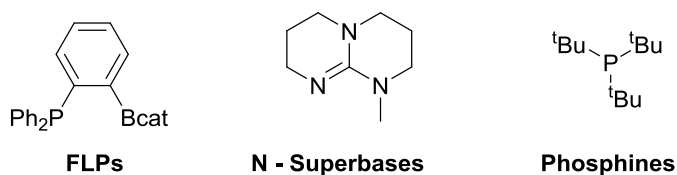
Hydroboranes have also been used as reductants for the synthesis of methanol using organocatalysts such as a phosphine-borane FLP,^{38, 54} nitrogen superbases (e.g. TBD, MTBD and DBU),⁵⁵ and phosphines, Figure 1.6b.⁵⁶ Whilst the use of hydrosilanes and boranes has enabled the reduction of CO₂ with organocatalysts, ideally a sustainable source of hydrogen

would instead be used to reduce the cost and the amount of waste generated. However, the use of hydrogen in the organocatalysed reduction of CO₂ is significantly less developed. The first reported reduction of CO₂ by hydrogen using a metal-free mediator was reported in 2009 by O'Hare.⁵⁷ The frustrated Lewis pair (TMP/B(C₆F₅)₃) was shown to stoichiometrically reduce CO₂ with hydrogen to methanol, however yields were low and reaction times long.⁵⁷ More recently, Fontaine and co-workers have also demonstrated the reduction of CO₂ with hydrogen using an intramolecular B/N FLP as the stoichiometric mediator, however harsh reaction conditions were required and low yields were achieved, Figure 1.6c.⁵⁸

a) Organocatalysts for the Reduction of CO₂ with Hydrosilanes:



b) Organocatalysts for the Reduction of CO₂ with Boranes:



c) Organocatalysts for the Reduction of CO₂ with Hydrogen:

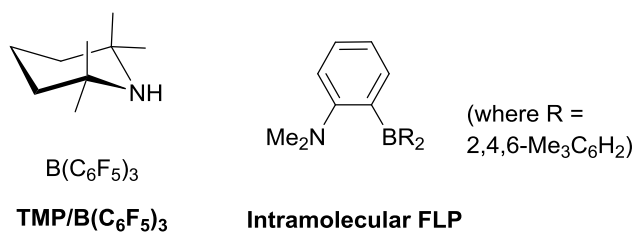


Figure 1.6: Examples of organocatalysts used for the reduction of CO₂ with hydrosilanes, hydroboranes and hydrogen reductants

1.4 Organocatalysed Reductive Functionalisation of CO₂ with Amines and Hydrosilanes

An important strategy in CO₂ utilisation to expand the synthetic scope of CO₂ is to develop processes which combine the functionalisation of CO₂ with its reduction; a process coined as the reductive functionalisation of CO₂.⁵⁹ One particular target for this type of transformation is the formation of C-N bonds, for example in the synthesis of formylamides, methylamines and amins.^{60, 61}

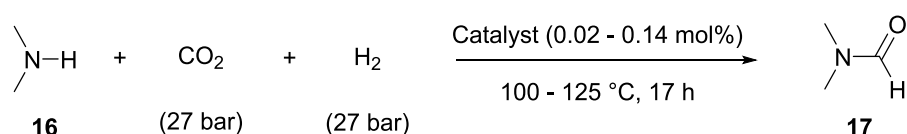
1.4.1 Formylation of Amines with CO₂

Formylamides have a wide application as solvents, protecting groups or as intermediates in many important pharmaceuticals.⁶² Typically the synthesis of formylamides is achieved through the formylation of amines using formylating agents such as carbon monoxide, formaldehyde or formic acid.⁶³ However, the use of these formylating agents is often problematic due to thermal instability, formation of by-products, toxicity and harsh or hazardous reaction conditions.

The current method for the industrial synthesis of formylamides at BASF uses an indirect two step approach: firstly carbon monoxide is reacted with methanol to yield methylformate which is subsequently reacted with the amine.⁶ However, the use of CO₂ as a formylating agent offers an excellent alternative due to its low cost, ready availability and the fact it is environmentally benign. This approach would combine the functionalisation and reduction of CO₂ and in particular would enable the alteration of the functionalising reagent independently to the reducing agent.

1.4.1.1 Early work on formylation of amines with CO₂

The first catalytic synthesis of formylamides from the formylation of primary and secondary amines with CO₂ and H₂ was reported by Kohnle in 1970, Scheme 1.7.⁶⁴ A variety of transition metal catalysts, e.g. (dppe)₂CoH (dppe = 1,3-bis(diphenylphosphino)ethane), (Ph₃P)₂(CO)IrCl and (Ph₃P)₃CuCl were shown to successfully catalyse the synthesis of dimethylformamide **17** (DMF) with high turnover numbers (TON) of up to 1200, although high pressures (27 bar CO₂, 27 bar H₂) and temperatures 100 - 125 °C were required.⁶⁴



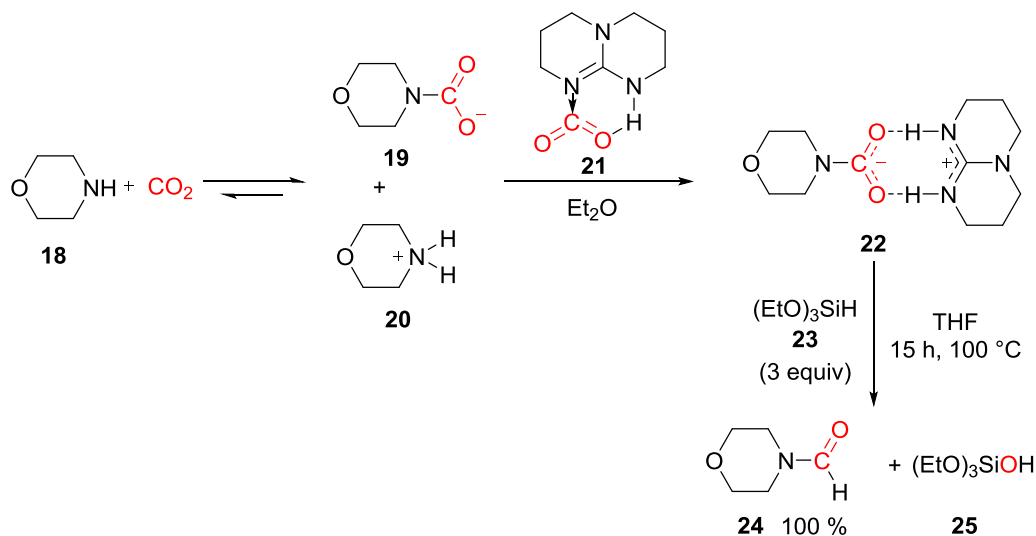
Scheme 1.7: First reported catalytic synthesis of DMF from formylation of dimethylamine with CO₂/H₂.⁶⁴

Following this initial report, many improved transition metal catalysed processes have been developed. For example, Noyori reported a highly efficient ruthenium catalyst, $\text{RuCl}_2(\text{PMe}_3)_4$, for the synthesis of DMF in scCO_2 (132 bar) with H_2 (81 bar) at 100 °C with TON of up to 370 000.⁶⁵ Subsequently, and under similar reaction conditions, Baiker further investigated the role of diphosphine ligands and reported a more efficient Ru catalyst, $\text{RuCl}_2(\text{dppe})_2$, with TON 740 000 and a rate 36 times faster than the best previously reported catalyst.⁶⁶ More recently the development of non-precious metal catalysts, such as Cu and Fe, have been targeted,^{67, 68} along with attempts to address the limited substrate scope, for example by the addition of a second base.⁶⁹ This has also led to investigations into alternative reductants to hydrogen, for example through use of electrochemistry or hydrosilanes.^{60, 70}

1.4.1.2 Organocatalysed hydrosilylation for formylamide synthesis

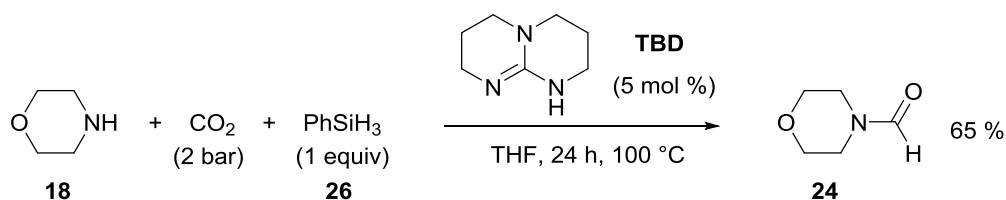
Hydrosilanes pose an excellent alternative to H_2 as a reductant in the formylation of amines with CO_2 . The Si-H bond is slightly polar and weaker (Si-H: 90 kcal mol⁻¹) than the H-H bond (H-H: 103 kcal mol⁻¹) and thus hydrosilanes should be more easily activated than H_2 .⁷¹ As shown by Zhang and Ying, and discussed early, hydrosilanes are able to reduce CO_2 in the presence of an organocatalyst at room temperature to give methoxysilanes, which can subsequently be hydrolysed to give methanol.³⁷

Using a similar approach Cantat and co-workers investigated the use of hydrosilanes and guanidine catalysts in the reduction of carbamates for the synthesis of formylamides.⁵⁹ Stoichiometric reaction of morpholine **18**, CO_2 and 1,5,7-triazabicyclo[4.4.0]dec-5-ene (TBD) gave complete conversion to the morpholine carbamate **22**, Scheme 1.8. Subsequent addition of 3 equivalents $(\text{EtO})_3\text{SiH}$ gave complete reduction of the carbamate to *N*-formylmorpholine **24**, Scheme 1.8, which is the first reported carbamate reduction by a hydrosilane.⁵⁹



Scheme 1.8: Reduction of carbamate with hydrosilane and TBD to yield *N*-formylmorpholine⁵⁹

Further development of the process demonstrated that the reaction could be performed catalytically using a more active hydrosilane, PhSiH₃ **26**, with 5 mol% TBD, Scheme 1.9. Other guanidines and amine catalysts were investigated, such as MTBD, DBU, and DMAP, however these gave significantly lower yields. It was found that polar solvents were beneficial to the reaction, however optimal conversion was achieved when the reaction was performed neat, without solvent.⁵⁹

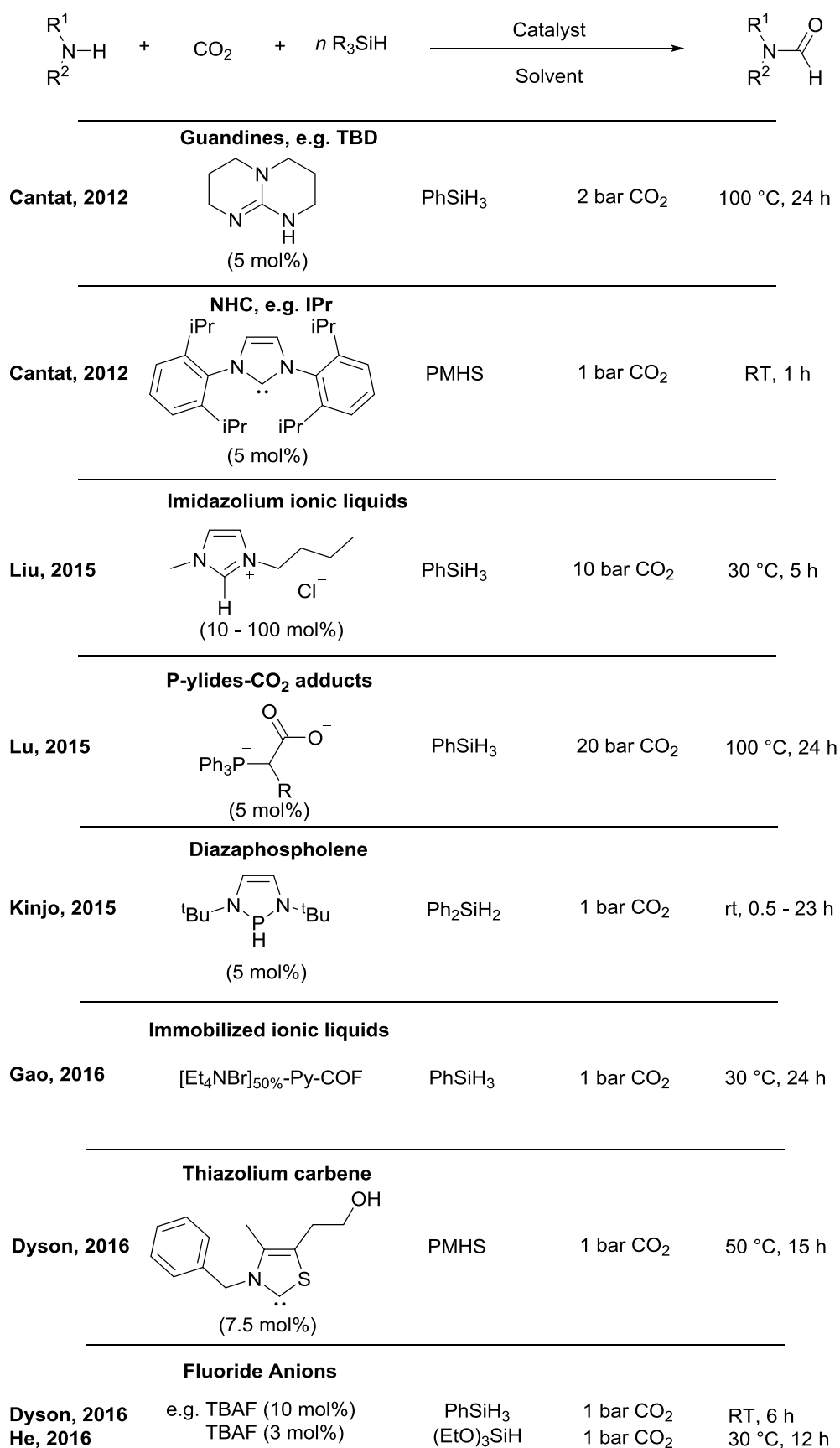


Scheme 1.9: TBD catalysed synthesis of *N*-formylmorpholine from morpholine, CO₂ and a hydrosilane reductant⁵⁹

This reaction represents a significant development as both the first organocatalysed formylation reaction with CO₂ and the first example using a hydrosilane reductant which has widened the substrate scope relative to the previous examples with H₂ as the reductant and significantly reduced the pressures required (i.e. 2 bar with hydrosilane⁵⁹ compared to 123 bar with H₂⁶⁵).

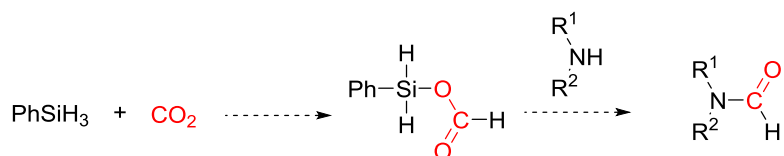
This led to the development of a number of organocatalysts able to catalyse the reaction with a hydrosilane reductant. NHC catalysts were shown to have significantly higher activity than guanidine catalysts and catalysed the complete conversion of morpholine to *N*-formylmorpholine with PhSiH₃ at room temperature within 1 hour, Scheme 1.10.⁷² NHC catalysts also enabled polymethylhydrosiloxane (PMHS) to be used as the silane source, giving 90% conversion after 24 h at room temperature.⁷² PMHS is an attractive reductant as it is a waste product from the silicone industry, moisture stable and is significantly cheaper than other hydrosilanes such as PhSiH₃.⁴⁸

Other successful organocatalysts include imidazolium-based ionic liquids, reported by Liu in 2015⁷³ and thiazolium carbene catalysts reported by Dyson in 2016 for a range of aromatic and aliphatic amines substrates, Scheme 1.10.⁷⁴ As with NHC catalysts, the use of thiazolium carbenes enabled PMHS to be used as the reductant, however the reaction did not proceed in the usual solvents for this reaction (e.g. acetonitrile or THF) and instead *N,N*-dimethylacetamide (DMA) or DMF were required.⁷⁴ Diazaphospholenes and phosphorus ylides have also been reported to catalyse the formylation reaction, however as with previously reported carbene catalysts, a glove box was required for catalyst preparation.^{32, 33}



Scheme 1.10: Examples of organocatalysts for the formylation of amines with CO₂ with hydrosilanes^{32, 33, 59, 72-77}

The development of these new organocatalytic systems, has also led to the proposal of an alternative mechanism of amine formylation. With ionic liquids and diazaphosphenes it was instead proposed that reduction of CO₂ with the hydrosilane occurs in the first step to produce a formoxysilane intermediate, which can then undergo transformylation with the amine to produce the formylamide, Scheme 1.11.^{33, 73, 75} Characterisation of the formoxysilane intermediate has predominantly been reported using ¹H NMR spectroscopy⁷³ and GC-MS analysis.³⁷

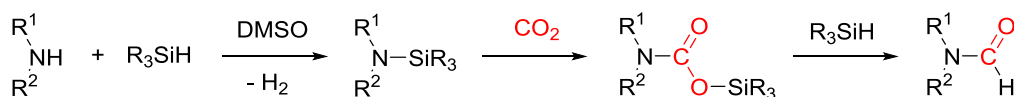


Scheme 1.11: Proposed pathway to formylamide product via a formoxysilane intermediate

The involvement of a formoxysilane intermediate was also proposed when fluoride ions e.g. tetrabutylammonium fluoride (TBAF), were used as catalysts for the formylation of amines, which were first reported simultaneously by the groups of Dyson and He in 2016.^{76, 77} In this case the fluoride and hydroxide ions are proposed to activate the Si-H bond through the formation of a hypervalent species, promoting the insertion of CO₂ into the Si-H bond to give the formoxysilane intermediate.⁷⁶

Immobilised organocatalysts have also been successfully used for the formylation reaction. For example, ionic liquids immobilised on covalent organic frameworks could be reused up to four times with catalyst recovery simply by filtering.⁷⁵ Similarly, heterogeneous poly-NHCs could be reused up to three times, however these were less active than corresponding homogeneous systems.⁵¹

Recently, a number of solvent promoted systems have been developed for the formylation of amines with CO₂. Li and co-workers have reported a DMSO promoted reaction whereby the N-H and Si-H bonds of the amine and silane respectively are activated by interactions with the solvent.⁷⁸ For this system an alternative mechanism is proposed whereby a silylamine is formed (releasing H₂), to which CO₂ is inserted to give a silylcarbamate type intermediate which is then reduced to give the formylamide, Scheme 1.12.⁷⁸



Scheme 1.12: Proposed mechanism to formylamides involving a silylamine and silylcarbamate intermediate⁷⁸

CO₂ insertion, Figure 1.7.^{80, 81} Alternatively in activation mode B an NHC-CO₂ adduct⁸² initially forms, essentially activating the CO₂, allowing for reaction with the phenylsilane.⁴⁹

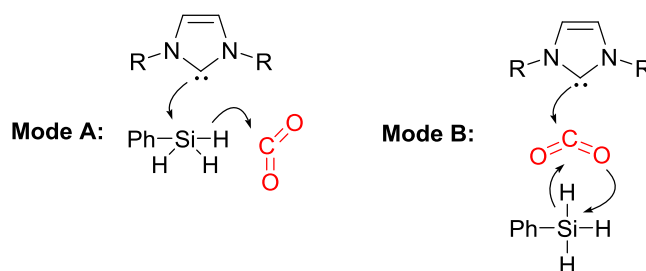


Figure 1.7: Two proposed activation modes for formoxysilane intermediate formation⁸¹

In the formylation of amines Cao calculated activation mode A to be favourable (20.7 kcal mol⁻¹ vs 31.4 kcal mol⁻¹ for mode B). The formoxysilane intermediate **28** is then proposed to couple with the amine through a general base mechanism (17.9 kcal mol⁻¹) to give intermediate **29**.⁸⁰ Thus, pathway 2 is favoured over pathway 1 whereby the carbamic acid is formed, Scheme 1.13. In the final stage, the amide **17** is formed via a base catalysis mechanism.⁸⁰

A more recent computational study reported by Li provides an alternative suggestion that the NHC is a precursor to the actual catalyst: with the actual catalytic species being the ionic liquid [NHCH]⁺[Carbamate]⁻, Figure 1.8a.⁸³ The formation of the formoxysilane intermediate is again described as a key intermediate, however an alternative activation mechanism has been calculated. It is suggested instead that the Si-H bond is activated by a concerted S_N2 attack by the amine carbamate, following which the hydride directly reacts with free CO₂ in solution, Figure 1.8a.⁸³ In the absence of the amine it is suggested that the Si-H bond is instead activated by the NHC-CO₂ adduct, similar to the proposal by Ying and Zhang⁴⁹ except that the hydride reacts with free CO₂ in solution, Figure 1.8b.⁸³ Li also proposed a mechanism for the uncatalysed reaction whereby the dimethylammonium acts to stabilise the transition state, Figure 1.8c.

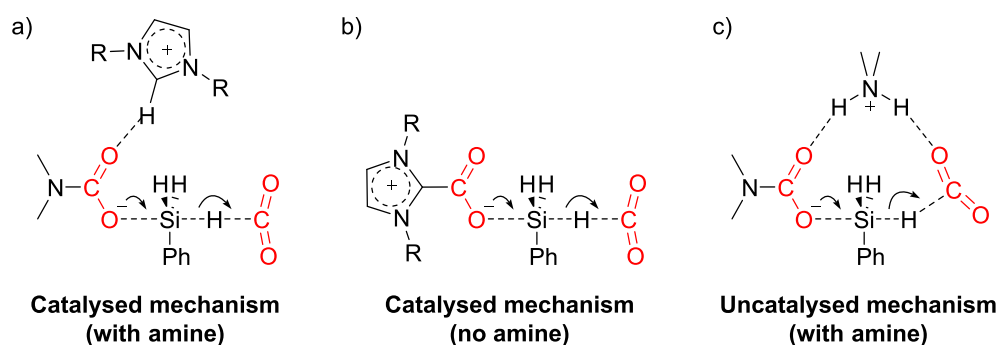
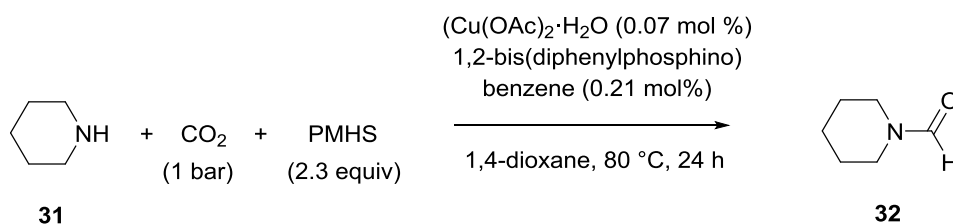


Figure 1.8: Recent activation modes proposed by Li for CO₂ reduction by Si-H bond to form a formoxysilane intermediate in a) NHC catalysed with amine, b) NHC catalysed without amine, c) uncatalysed with amine⁸³

These computational studies support evidence for the experimentally observed formoxysilane species, however, they do not account for other species observed experimentally, for example the formation of a silylcarbamate species.

1.4.1.4 Metal Catalysed Hydrosilylation

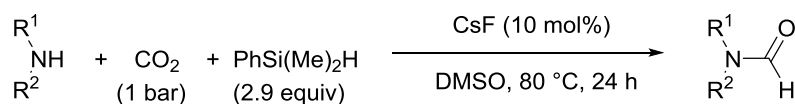
Alongside the development of organocatalysts for the formylation of amines with CO₂ and a hydrosilane, a number of metal catalysed processes utilising hydrosilane reductants were also developed. For example, Baba and co-workers reported a highly efficient copper-diphosphine complex to catalyse the formylation of amines, with PMHS as the hydrosilane.⁸⁴ The catalysts operate at low CO₂ pressures (1 bar) and moderate temperatures (80 °C) to give significantly higher TON (up to 11700) than any of the previously discussed organocatalysts, Scheme 1.14.⁸⁴ Other transition metal catalysed formylations include a nickel catalysed process with catalytic amounts of Et₃B⁸⁵ and an iron catalysed process with monodentate phosphine ligands.⁸⁶



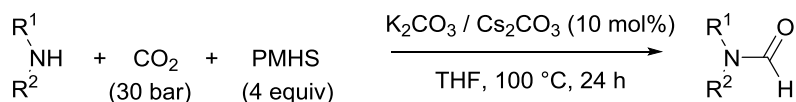
Scheme 1.14: Cu-phosphine catalysed synthesis of formylamides⁸⁴

More recently, simple metal salts and bases have been shown to catalyse the synthesis of formylamides with hydrosilane reductants. For example, Baba in 2015 reported the catalytic use of simple fluoride and carbonates salts with dimethylphenylsilane for the formylation of piperidine **32** and N-methylaniline **33**, Scheme 1.15.⁸⁷ Bhanage has also reported the use of simple base catalysts for the synthesis of formylamides, despite the need for relatively high temperatures and pressures (100 °C, 30 bar) the system demonstrates for the first time the use of K₂CO₃ as the sole catalyst.⁸⁸

Baba, 2015:



Bhanage, 2016:



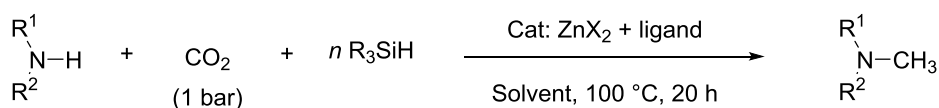
Scheme 1.15: CsF and base catalysed synthesis of formylamides with hydrosilanes^{54, 55}

1.4.1 *N*-Methylation of Amines with CO₂

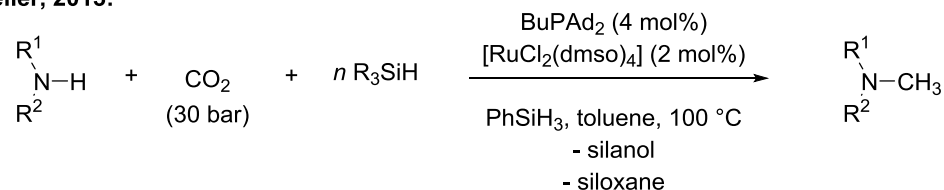
N-Methylation of amines via the reductive functionalisation of CO₂ offers an attractive process to replace the typical hazardous alkylation methods currently used, e.g. methyl iodide, dimethylsulfate or the use of formaldehyde with a reductant.⁶⁰ Initial attempts using metal catalysts and a hydrogen reductant enabled the methylation of amines with CO₂, however high temperatures or pressures were often required.

More recently the use of hydrosilanes and hydroboranes as reductants have been explored and Cantat and Beller reported the use of Zn and Ru catalysts respectively, which have enabled milder conditions to be used, Scheme 1.16.^{89, 90}

Cantat, 2013:



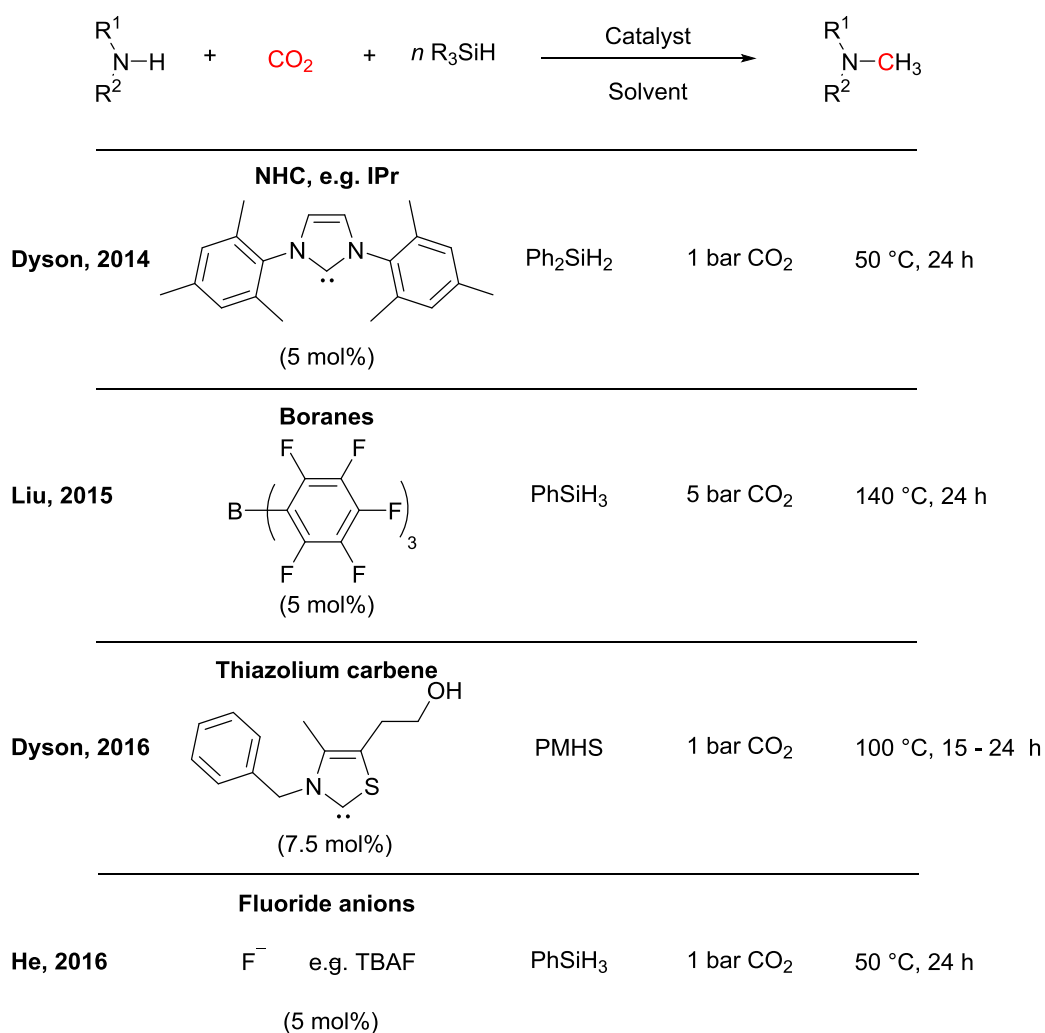
Beller, 2013:



Scheme 1.16: First reported *N*-methylation of amines using hydrosilanes and CO₂ with Zn and Ru catalysts^{89, 90}

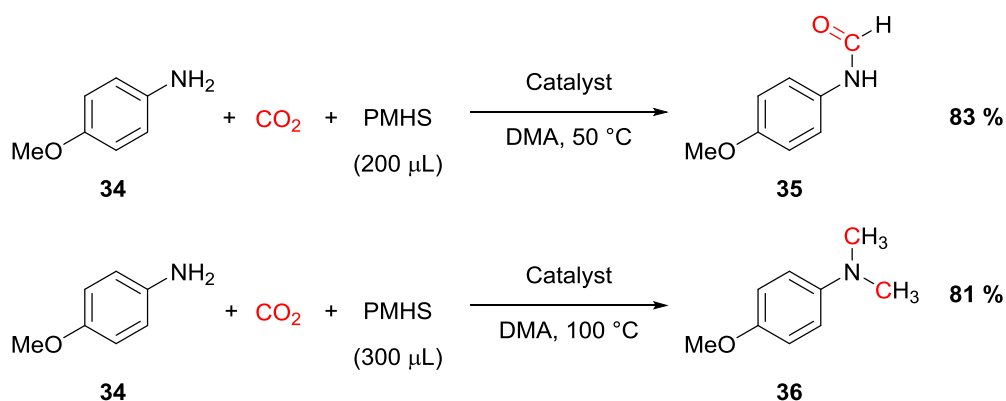
This approach has been extended and organocatalysts have since been reported to catalyse the same reaction. Dyson first reported the use of NHCs in 2014 for the *N*-methylation of amines using CO₂ and hydrosilanes under relatively mild conditions, Scheme 1.17.⁹¹ The system tolerated a broad range of amines and a wide functional group tolerance was demonstrated enabling the synthesis of a number of pharmaceutical intermediates.⁹¹

Subsequently other organocatalysts were reported to be successful for the methylation of amines with CO₂ and a hydrosilane reductant. These included boranes,⁹² thiazolium carbenes,⁷⁴ fluoride anions,⁷⁷ and a solvent promoted system with DMF,⁹³ Scheme 1.17. The use of hydroboranes as reductants has also enabled the use of proazaphosphatranes,⁹⁴ carbodicarbenes⁹⁵ and guanidines⁹⁴ as efficient organocatalysts for this transformation.



Scheme 1.17: Example organocatalysts for the methylation of amines using CO₂ with a silane reductant^{91, 92 74, 77, 96}

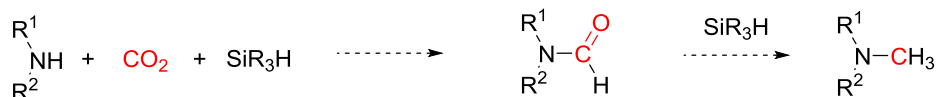
Many of the conditions and catalysts reported for the methylation of amines with CO₂ and hydrosilanes (Scheme 1.17) are very similar to those for the corresponding formylation reaction, (Scheme 1.10) and in some cases formylamides are reported as side products during the optimisation of methylation reactions. For example, Dyson showed that with thiazolium carbene catalysts, increasing the amount of reductant and increasing the reaction temperature resulted in a switch in selectivity from the formyl- **35** to the methylated product **36**, Scheme 1.18. Similarly, when fluoride catalysts were used, use of a less active silane (e.g. (EtO)₃SiH) in THF selectively gave formylation, whereas the use of a more active silane (e.g. PhSiH₃) in more polar solvent (e.g. acetonitrile) gave the methylation product.⁷⁷



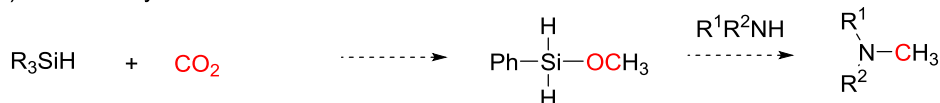
Scheme 1.18: Using thiazolium catalyst, higher reaction temperatures favour amine methylation over amine formylation⁷⁴

A number of different pathways have been proposed for the mechanism of the methylation of amines with CO_2 and hydrosilanes, Scheme 1.19. With fluoride and borane catalysts, formylamides are proposed to be intermediates to methylamines, and the corresponding formylamides have been shown to be reduced to methylamines under reaction conditions, Scheme 1.19a.^{77, 92} However, other systems have proposed that formylamides are stable products and are therefore formed in competition with methylamines, rather than as intermediates. Instead it has been proposed that reduction of CO_2 with hydrosilanes to methoxysilanes followed by nucleophilic attack of the amine is the mechanism for methylamine formation, Scheme 1.19b.⁹³

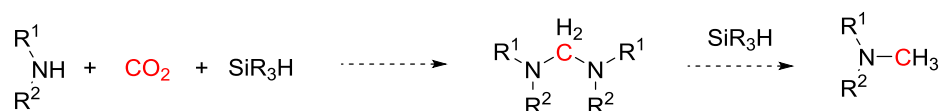
a) Via reduction of formylamide intermediates



b) Via methoxysilane intermediates



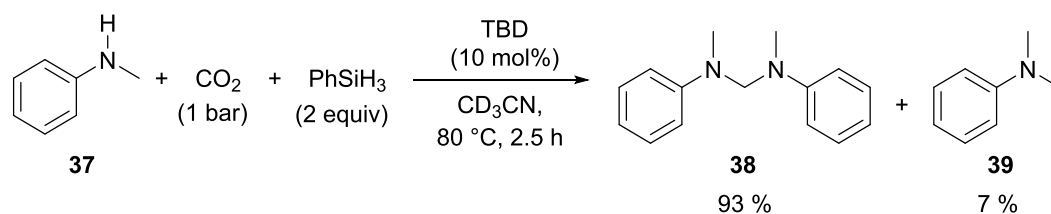
c) Via amination intermediates



Scheme 1.19: Proposed pathways to methylamine products

A third proposal is that methylamines are formed from the reduction of an amination intermediate, Scheme 1.19c. The presence of methylamines were first reported as side products when amination products **38** were targeted from the guanidine and NHC catalysed reaction of amines, CO_2 and phenylsilane, Scheme 1.20.⁹⁷ Further investigation showed that amination intermediates could be reduced to

methylamines under the same reaction conditions, therefore indicating aminals are potential intermediates to the formation of methylamines in these reductive functionalisation reactions.



Scheme 1.20: Synthesis of aminals and methylamines from reduction of CO₂ by hydrosilanes catalysed by NHCs and guanidines⁹⁷

1.5 Summary

In recent years the role of organocatalysis in CO₂ utilisation processes has been significantly developed. The report by Zhang and Ying in 2009 highlighted the first example that organocatalysts were able to promote the reduction of CO₂ using hydrosilanes as the reductant.³⁷ This led to first report of an organocatalysed process for the reductive functionalisation of CO₂ with amines to produce formylamides.⁵⁹ Following this a broad range of organocatalysts have been developed for the formylation and methylation of amines.⁶⁰ These have regularly provided mild reaction conditions and broader substrate scope in comparison to the corresponding metal catalysed reactions with hydrogen. Of particular note are the reactions which can utilise a sustainable hydrosilane source such as PMHS, therefore utilising two waste streams. A number of studies have investigated the role of organocatalysts in the activation of various hydrosilanes and hydroboranes, however a general mechanism is yet to be agreed upon and in particular the reasons behind product selectivity between formylamides, methylamines and aminals are still poorly understood.

However, despite the many advances of organocatalytic CO₂ utilisation reactions, these are still comparably less efficient than corresponding metal catalysed reaction systems suffering from low TON and TOF. No organocatalytic reaction for CO₂ utilisation is currently operable on an industrial scale. In order to develop these reactions further the mechanism of CO₂ utilisation reactions need to be well understood to enable the rational improvement of these catalytic processes.

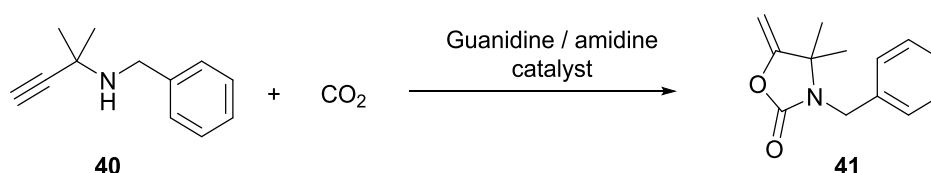
Chapter 2

Role of Guanidine Catalysts in the Reaction of Propargylamines and CO₂

2.1 Introduction

Guanidines and amidines are widely employed as organocatalysts due to their nucleophilicity and high basicity, and successfully catalyse a variety of organic reactions.⁹⁸ Of particular interest are those which involve CO₂ utilisation. Due to the high stability of CO₂, highly reactive reagents or harsh reaction conditions are often required for its conversion. However, catalysis with amidines and guanidines often offers a less energy intensive option, enabling a variety of substrates and mild conditions to be used.

The synthesis of cyclic carbamates from propargylamines and CO₂ using either an amidine, DBU, or a guanidine, TBD, as the catalyst, was first reported by Costa in 1996, Scheme 2.1.⁹⁹ Cyclic carbonates and carbamates are important classes of compounds due to their broad applications in fine chemical synthesis, pharmaceuticals and as solvents.⁸ Since the initial report by Costa⁹⁹ a broad range of amine based catalysts have been explored. Further effective catalysts include alkylated guanidines such as MTBD and TMG, Figure 2.1.^{36, 99}



Scheme 2.1: Example synthesis of cyclic carbamates from propargylamine and CO₂ using a guanidine catalyst⁹⁹

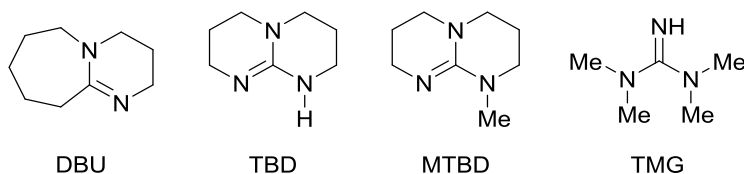
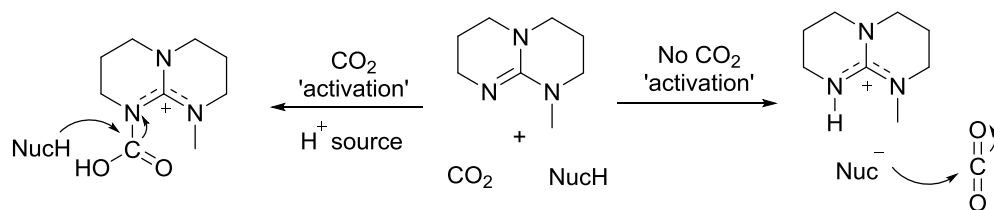


Figure 2.1: Catalysts demonstrated to be successful in reaction of propargylamines with CO₂^{36, 99}

The proposed mechanism is thought to involve the catalyst acting as a superbases to deprotonate the substrate, Scheme 2.2.³⁶ However, organic bases are also well known to form complexes with CO₂ and the formation of these complexes is proposed to account for their catalytic activity in a variety of reactions with CO₂ by enabling transcarboxylation to the substrate, Scheme 2.2.^{28,}



Scheme 2.2: Proposed mechanisms of reaction when MTBD is used as the catalyst

Complexation of organic bases with CO₂ has been widely studied due to their application in CO₂ scrubbing and capture.¹⁰³ DBU-CO₂ complexation, thought to be the cause of catalytic activity in the synthesis of cyclic carbonates from epoxides¹⁰⁴ and the synthesis of 2,4-dihydroxyquinazolines,¹⁰⁵ was observed by Franco and co-workers.²⁸ Solid state NMR data indicated that the zwitterionic form was observed (Figure 2.2); however, crystallisation saw a structural change to the bicarbonate form, suggested to be due to the presence of water.^{28, 29} Complexation between TBD and CO₂ has also been isolated and observed in the solid state by Villiers *et al.* using NMR and X-ray crystallography, Figure 2.2.³⁰ However, limited information is available for the stability of these complexes in solution under the catalytic reaction conditions of CO₂ with propargylamines.

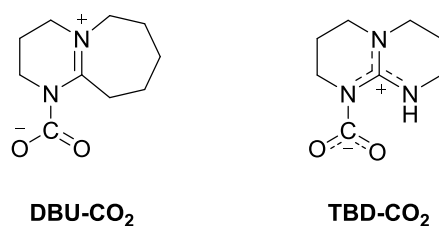
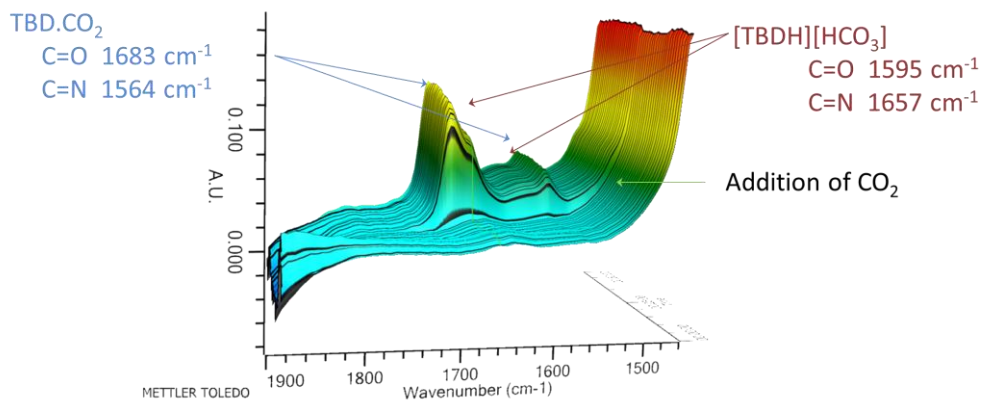


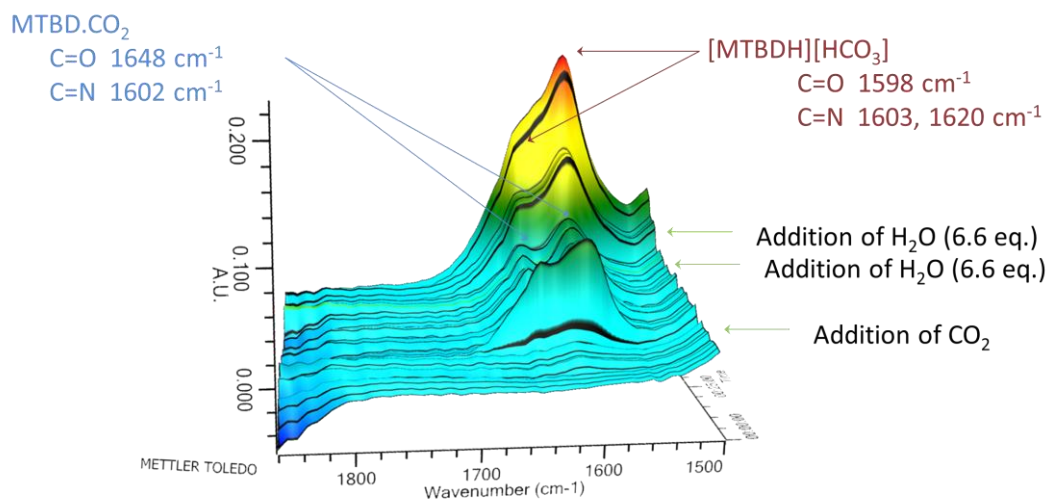
Figure 2.2: Guanidine and amidine complexes with CO₂ (isolated structures)^{28 30}

More recent work within the Nguyen group has investigated the activation of CO₂ with amines and guanidines under conditions relevant to the reaction of CO₂ with propargylamines.¹⁰⁶ The complexation between catalysts: TBD, MTBD, TMG, DABCO and TEA with CO₂ (1 atm) was monitored by ATR-FTIR spectroscopy over time, Figure 2.3.¹⁰⁶ Although the propargylamine reaction is known to be successful in acetonitrile, the reaction was studied in THF due to the poor solubility of the bases in acetonitrile.

a)



b)



c)

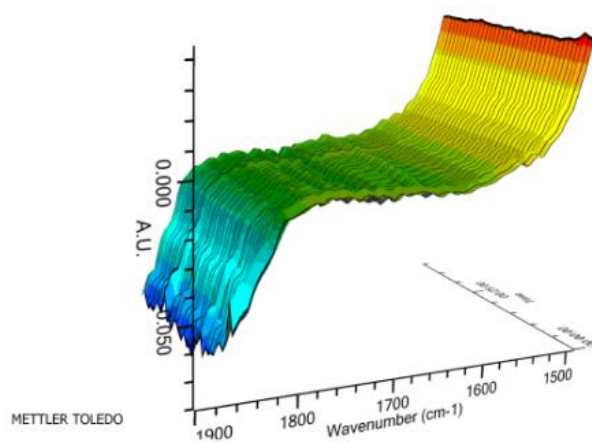


Figure 2.3: ATR-FTIR spectra of reaction in THF over time between CO₂ with amines and guanidines: a) TBD, b) MTBD, c) Representative spectra for TMG, TEA, DABCO¹⁰⁶

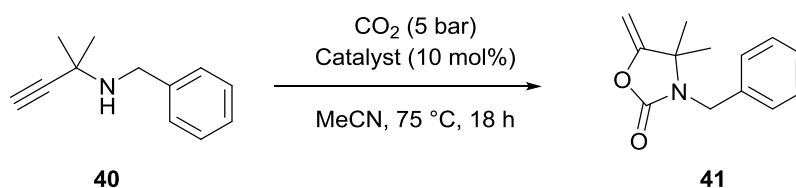
It was found that reaction of MTBD and TBD with CO₂ led to the formation of complexes MTBD·CO₂ and TBD·CO₂ respectively, identified by a change in the carbonyl region of the FT-IR spectra (Figure 2.3a&b). The bicarbonate complexes [MTBDH][HCO₃] and [TBDH][HCO₃] were also observed due to the presence of water during the reaction. This was confirmed by the addition of water during the ATR-FTIR experiment (Figure 2.3b). No change in the FT-IR spectra was observed when CO₂ was introduced to solutions of TMG, TEA and DABCO, indicating that no complex with CO₂ was formed (Figure 2.3c).¹⁰⁶

As TMG is known to be a successful catalyst in the reaction of propargylamines with CO₂^{36,99} the lack of a TMG·CO₂ complex suggested that complexation with CO₂ is not the main route of catalytic activity. Instead, the ability of the catalyst to act as a base to deprotonate the substrate appears to be more important.

With this insight there was need to re-evaluate the reaction conditions for the reaction of propargylamines with CO₂ taking into account the proposed mechanism of action. Provisional work in the group identified a range of catalysts and solvents to be investigated further;¹⁰⁶ with conditions comparable to the initial work by Costa.^{36,99} This chapter reports the evaluation of catalytic activity under the selected conditions.

2.2 Catalytic Activity in Cyclic Carbamate Synthesis

The catalytic activity of guanidine catalysts was investigated in the synthesis of cyclic carbamate **41** from propargylamine **40** and CO₂. Three catalysts were selected to investigate further: MTBD and TMG were selected as examples where CO₂ complexes were and were not observed, while DBU was investigated due to its strong basicity. Reaction conditions were selected similar to those reported by Costa:⁹⁹ catalyst (10 mol%), at 75 °C and CO₂ pressure of 5 bar, Scheme 2.3. Under these conditions use of MTBD as the catalyst in acetonitrile gave 100 % conversion, in agreement with the literature.⁹⁹



Scheme 2.3: Reaction conditions for synthesis of cyclic carbamate **41** from propargylamine **40** with CO₂

Performing the reaction in THF, the solvent of the FT-IR studies, was unsuccessful with both MTBD and TMG, Table 2.1, as previously reported by Costa.³⁶ The catalytic activity was then examined in solvents acetonitrile, ethanol and DMSO, Table 2.2.

Table 2.1: Conversion of propargylamine **40** and CO₂ with MTBD and TMG in THF

Entry	Catalyst	Loading (mol%)	Solvent	Conversion (%)
1	MTBD	10	THF	7
2	TMG	10	THF	0

Reaction Conditions: **40** (0.866 mmol), catalysts (10 mol%), THF (3 mL), 75 °C, CO₂ (5 bar), 18 h. Conversion (%) calculated by ¹H NMR

Table 2.2: Conversion of propargylamine **40** with CO₂ with MTBD, TMG or DBU

Entry	Catalyst	Loading (mol%)	Water (mL)	Solvent		
				MeCN	EtOH	DMSO
3	MTBD	10	-	100	29	54
4	MTBD	10	0.1	99		
5	MTBD	1	-	8		
6	MTBD	1	0.1	8		
7	TMG	10	-	19	40	100
8	TMG	10	0.1		39	100
9	TMG	1	-		7	6
10	TMG	1	0.1		8	61
11	DBU	10	-	100	28	64
12	DBU	10	0.1	35		

Reaction Conditions: **40** (0.866 mmol), catalysts (1-10 mol%), solvent (3 mL), 75 °C, CO₂ (5 bar), 18 h. Conversions (%) calculated by ¹H NMR as a ratio of starting material to product

At 10 mol% loading MTBD gives 100 % conversion in acetonitrile; however, it has a lower activity in EtOH and DMSO (Entry 3, Table 2.2). Contrastingly, TMG only resulted in 19 % conversion in MeCN and gives 100 % conversion in DMSO (Entry 7, Table 2.2). The lower activity of TMG in MeCN could be accounted for by its lower basicity in MeCN compared to MTBD (Table 2.3).⁹⁸ As demonstrated in the ATR-FTIR study, the addition of ethanol to the MTBD·CO₂ complex led to its decomposition. Therefore the success of TMG and MTBD in EtOH in catalysing the reaction suggests that the catalyst-CO₂ complexes are not essential for the reaction to proceed. The higher conversion achieved when TMG in DMSO was used could be accounted for by the ability of DMSO, a highly polar solvent, to stabilise the formed TMGH⁺.

Table 2.3: Basicity of studied amidine and guanidines in acetonitrile

Catalyst	pK _a (MeCN)
MTBD	25.4 ⁹⁸
DBU	23.9 ⁹⁸
TMG	23.3 ⁹⁸

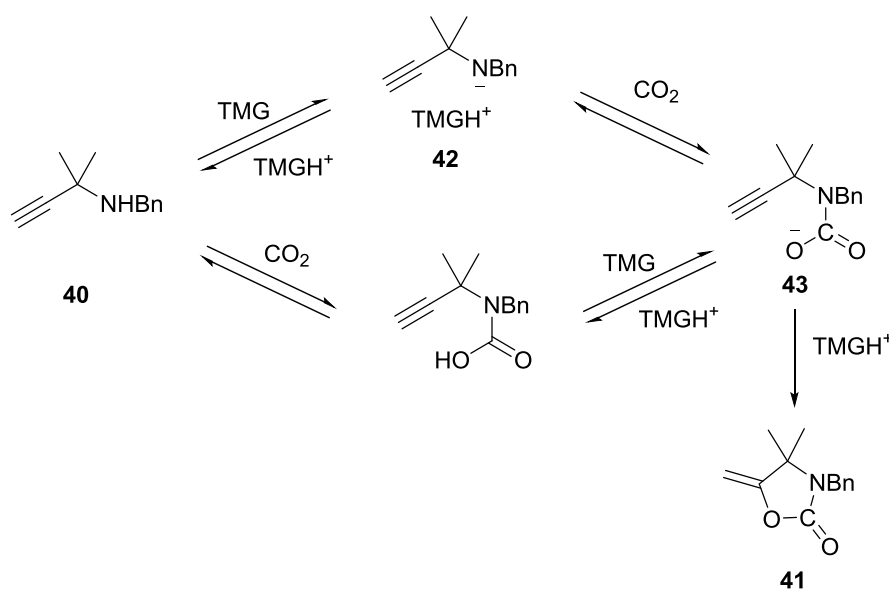
The lack of importance of the catalyst-CO₂ complexes has also been investigated by the addition of 0.1 mL water to the reaction. If the reaction proceeded by formation of the CO₂ complex, the addition of water would break down this complex, and therefore a loss in yield would be expected. The addition of water to the reaction with MTBD in acetonitrile gave no significant loss in yield (Entry 4, Table 2.2). Likewise addition of 0.1 mL water to reactions with TMG (10

mol%) in EtOH and DMSO gave no change in observed conversion (Entry 8, Table 2.2). This further supports the proposal that the reaction proceeds via a basicity controlled mechanism rather than complex formation.

At 1 mol% loading both MTBD and TMG gave low conversion in their optimal solvent (6-8 % conversion) (Entry 5&9, Table 2.2). Interestingly, addition of water to TMG (1 mol%) in DMSO led to an increased conversion to 60 % (Entry 10, Table 2.2). This could be an effect of water stabilising the TMGH^+ , produced as a result of deprotonation.

Use of DBU as the catalyst, a stronger base than TMG, also led to 100 % conversion in acetonitrile and, similarly to MTBD, gave lower conversion in EtOH and DMSO (Entry 11, Table 2.2). Addition of 0.1 mL of water to the reaction with acetonitrile gave a decrease in conversion to 35 % (Entry 12, Table 2.2). This is the only example studied whereby addition of water hinders the reaction, and perhaps indicates that DBU, an amidine, may act by an alternative mechanism to the guanidine catalysts.

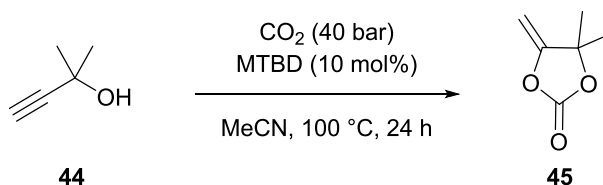
Based on the observed catalyst activity a basicity driven mechanism has been proposed, Scheme 2.4. In the first step the catalyst, e.g. TMG, deprotonates the propargylamine **40**. This can then react with CO_2 to form a carbamate intermediate **43**. Nucleophilic attack of the carbamate to the alkyne followed by proton transfer from the TMGH^+ then leads to the formation of the cyclic carbamate product **41** and regenerates the catalyst.



Scheme 2.4: Proposed mechanism for cyclic carbamate synthesis **41** from **40** and CO_2 with guanidine catalyst acting as a base

2.3 Applicability to Cyclic Carbonate Synthesis

After the success of catalyst TMG in DMSO and water for reaction of propargylamine **40**, it was investigated as to whether the TMG/DMSO system would also be effective in catalysing the synthesis of cyclic carbonate from propargyl alcohol **44**. The reaction has previously been reported by Costa, demonstrating that 99 % conversion could be achieved using MTBD in acetonitrile as the catalyst system (Scheme 2.5); however, the use of the non-alkylated guanidine, TBD, in acetonitrile was found to be unsuccessful.⁴³



Scheme 2.5: Reaction of propargyl alcohol **44** with CO₂ to give cyclic carbonate **45** in acetonitrile using MTBD catalyst as reported by Costa⁴³

Conducting the reaction with MTBD in acetonitrile gave 100 % conversion of **44**, as expected. Use of TMG in DMSO led to only a trace amount of the product formed, and the addition of water gave no effect on the reaction (Entries 2 & 3, Table 2.4). Similarly use of TMG with EtOH and/or water also gave no conversion (Entries 4 & 5, Table 2.4). These reports support work by Costa that the non-alkylated guanidines are unsuccessful in catalysing the reaction of propargyl alcohols with CO₂.⁴³ The proposed reason for this is that MTBD stabilises the carbonate intermediate by a single hydrogen bond, whereas TBD stabilises the carbonate by two hydrogen bonds, Figure 2.4. With bidentate stabilisation this would reduce the nucleophilicity of the carbonate intermediate, hence preventing cyclisation.⁴³ For TMG to be successful, it may be necessary to alkylate the N-H position preventing this bidentate stabilisation from occurring.

Table 2.4: Conversion of propargyl alcohol **44** for reaction with CO₂

Entry	Catalyst	Loading (mol %)	Solvent	Water (mL)	Conversion (%)
1	MTBD	10	MeCN		100
2	TMG	10	DMSO		trace
3	TMG	10	DMSO	0.1	trace
4	TMG	10	EtOH		-
5	TMG	10	EtOH	0.1	-

Reaction Conditions: **44** (0.866 mmol), catalyst (10 mol%), solvent (3 mL), 100 °C, CO₂ (40 bar), 23 h. Conversions calculated by ¹H NMR

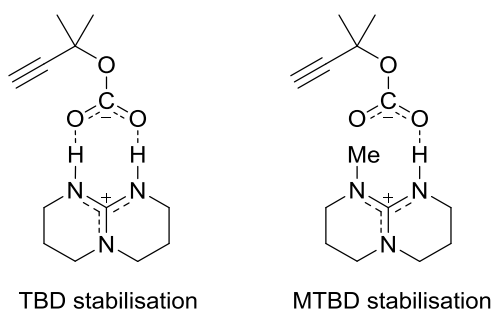


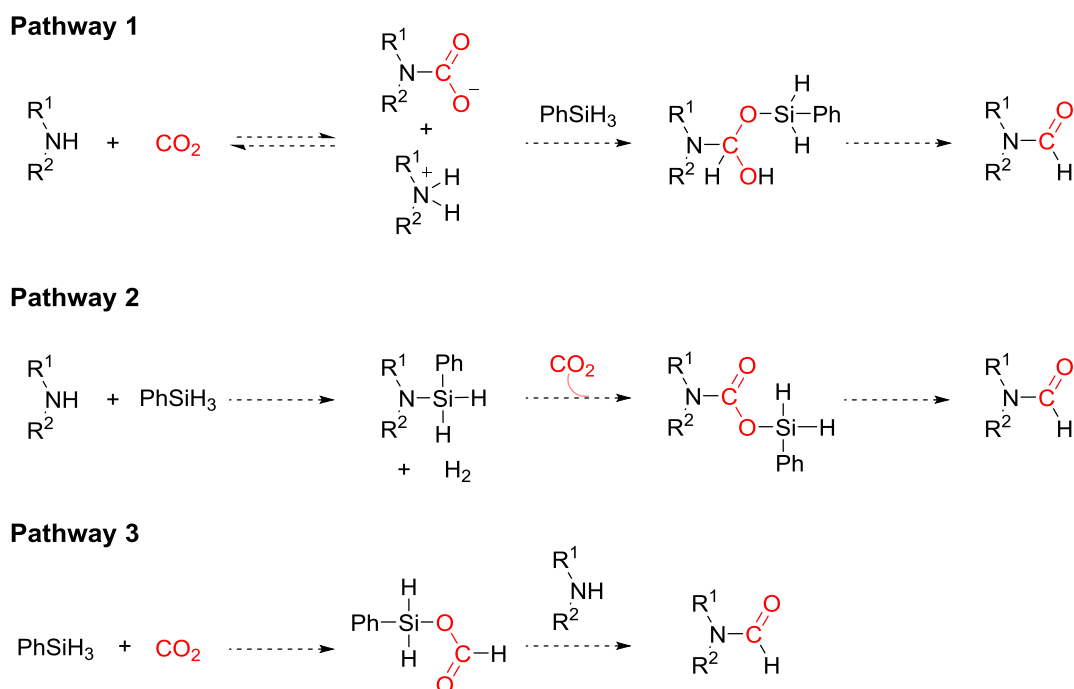
Figure 2.4: Proposed stabilisation of carbonate intermediate by TBD and MTBD ⁴³

2.4 Conclusions

The reactivity of MTBD and TMG as catalysts in the reaction of propargylamines with CO₂ to yield cyclic carbamates were re-examined after recent work demonstrated that MTBD forms a guanidine·CO₂ complex when exposed to CO₂, whereas TMG does not.¹⁰⁶ Both MTBD and TMG were shown to be successful in catalysing the reaction, indicating that the formation of guanidine·CO₂ complexes is not essential for the reaction to proceed. The basicity of the guanidine catalyst was instead suggested to be a determining factor. The importance of basicity was further supported through increased catalytic activity of TMG when ethanol and DMSO were employed as the solvents rather than acetonitrile. These highly polar solvents were proposed to stabilise the intermediate TMGH⁺ formed during the proposed deprotonation driven mechanism. Addition of water to the reaction, demonstrated to break down guanidine·CO₂ complexes, led to no reduction in catalytic activity with MTBD and TMG, further discounting the role of guanidine·CO₂ complexes in the reaction mechanism.

mechanism have been made, and the three most commonly proposed reaction pathways are summarised in Scheme 3.2, however many lack clear experimental evidence.

In proposed Pathway 1 (Scheme 3.2), a carbamate intermediate is formed which is reduced by the hydrosilane to give the formylamide product. Support for this mechanism has been provided in the initial guanidine catalysed reaction reported by Cantat, whereby the success of TBD catalyst was ascribed to its ability to stabilise the carbamate intermediate.⁵⁹ However a subsequent computational study suggested that the reduction of a carbamic acid was unfavourable.⁸⁰ Li and co-workers have instead proposed the involvement of a silylcarbamate intermediate based on ²⁹Si and ¹³C NMR monitoring studies, Pathway 2, Scheme 3.2.⁷⁸ In this mechanism, the amine and hydrosilane are proposed to react first to release H₂ to form a silylamine intermediate, into which CO₂ inserts to give the silylcarbamate. This is further reduced by a silane to yield the formylamide.⁷⁸



Scheme 3.2: General proposed mechanisms for reductive functionalisation of CO₂ with secondary amines with PhSiH₃ as the reductant to give formylamide products

The third pathway (Pathway 3, Scheme 3.2), was proposed following computational studies of the NHC catalysed reaction and involves the formation of a formoxysilane intermediate.^{33, 73, 80, 83} In this case, reduction of CO₂ occurs in the first step to produce a formoxysilane intermediate, which can then undergo transformylation with the amine to yield the formylamide. The mechanism for the organocatalysed formation of the formoxysilane has been investigated computationally both in the presence and absence of the amine substrate, leading to a number of proposed activation modes, Figure 3.1.^{49, 80, 81, 83} These can be broadly categorised as

proceeding primarily due to activation of the silane (Figure 3.1, Mode A), activation of CO₂ (Figure 3.1, Mode B) or, in a more recent study, by activation of the Si-H bond via a concerted S_N2 attack by the amine carbamate when stabilised by the NHC (Figure 3.1, Mode C).^{49, 80, 81, 83} The formoxysilane intermediate was observed experimentally as an intermediate during the NHC catalysed reduction of CO₂ to methoxysilanes³⁷ and in formylation reactions with organocatalysts such as polyNHCs,⁵¹ imidazolium ionic liquids^{73, 75} and diazaphospholenes.³³

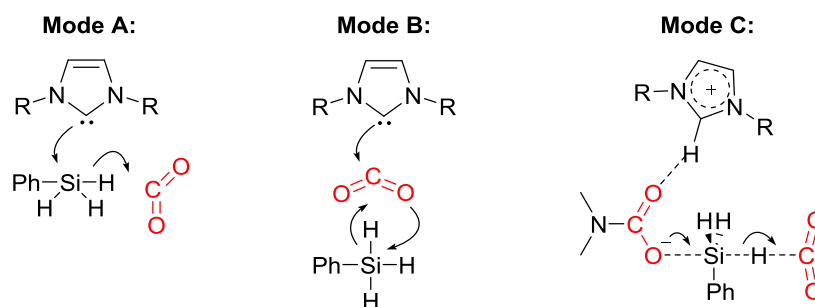


Figure 3.1: Proposed activation modes for formation of a formoxysilane intermediate with NHC as the catalyst^{49, 81, 83}

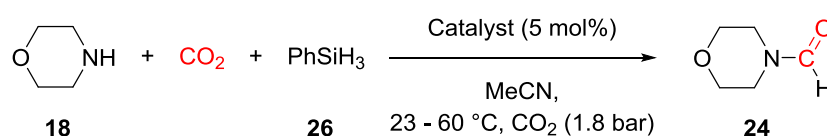
3.1.1 Project Aims

This project aimed to improve the mechanistic understanding of the reductive functionalisation of CO₂ with amines using a hydrosilane as the reductant to enable the rational improvement of organocatalysed CO₂ utilisation reactions. Guanidines were selected as the catalyst of interest due to their relative low cost, availability and ease of handling due to their tolerance to air and moisture.

This chapter reports experimental investigations specifically focussing on mechanistic pathways to formylamide products. Reaction profiling was employed to understand the reaction kinetics and to identify any involved intermediates. The role of each intermediate and individual pathways were then explored.

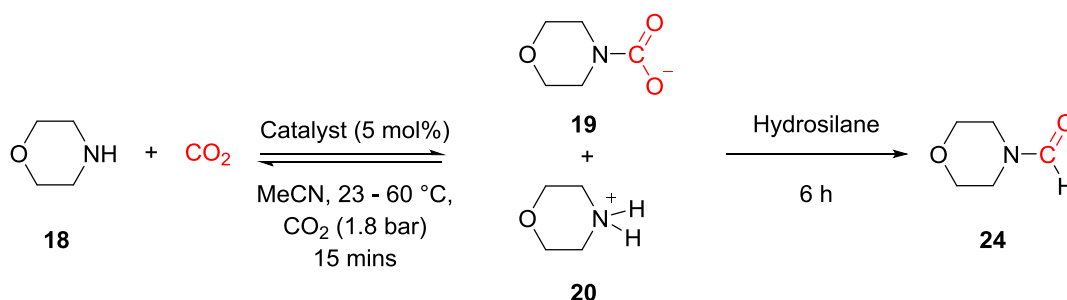
3.2 Reaction Development & Kinetic Profiling

To investigate the mechanism of the guanidine catalysed reductive functionalisation of CO₂ with amines, the transformation of morpholine **18** to *N*-formylmorpholine **24** using phenylsilane **26** as the reductant with acetonitrile as the solvent, was selected as a model system for a detailed study, Scheme 3.3.



Scheme 3.3: Reductive functionalisation of CO₂ with morpholine **18** and phenylsilane **26** to give *N*-formylmorpholine **24**

In the presence of CO₂ and under anhydrous conditions, secondary amines often lie in a temperature and pressure dependent equilibrium with the corresponding carbamates.¹⁰⁷ Furthermore, when gaseous reagents are used, reliable mixing for mass transfer of the gas into solution is required, particularly for kinetic studies. To address these requirements and to maintain a reproducible reaction set up for the reaction profiling, a 15 minute equilibrium period was employed to allow transfer of CO₂ into solution and the equilibration of carbamate formation **19** and **20** and reaction temperature before the hydrosilane was added to start the reaction, Scheme 3.4.



Scheme 3.4: Reaction set-up: 15 minutes equilibrium of amine and CO₂ at reaction temperature before reaction initiated by addition of hydrosilane

3.2.1 Catalyst Selection

Cantat and co-workers have previously screened a range of guanidine and amidine catalysts for the reductive functionalisation of CO₂ with secondary amines. This work identified the cyclic guanidine 1,5,7-triazabicyclo[4.4.0]dec-5-ene (TBD) as giving the highest levels of conversion, achieving 100 % conversion after 24 h at 100 °C.⁵⁹ Due to the success of TBD over other cyclic guanidines and amidines, the role of TBD was ascribed to its ability to stabilise a carbamate intermediate, Scheme 3.5.⁵⁹



Scheme 3.5: Proposed role of the TBD catalyst in stabilisation of a carbamate intermediate⁵⁹

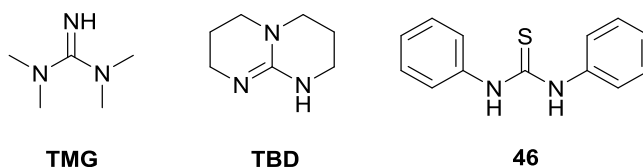


Figure 3.2: Structure of catalysts and co-catalysts

In a previous study on the guanidine catalysed synthesis of cyclic carbamates from CO_2 (discussed in Chapter 2), it was found that 1,1,3,3-tetramethylguanidine (TMG), can replace more expensive and less available cyclic guanidines (e.g. MTBD) and we again sought to use this cheaper catalyst for this transformation.¹⁰⁶ However due to the topology of TMG (Figure 3.2) it is unexpected to be able to stabilise a carbamate intermediate. Thioureas and ureas are known to stabilise carboxylate and alkylcarbamate species through hydrogen bond interactions of the N-H groups of the thiourea with the carbamate anion.^{108, 109} Thus it was proposed that the use of a *N,N'*-diphenylthiourea **46** as a co-catalyst in combination with TMG, would enable stabilisation of the carbamate by the thiourea **47**, enabling the TMG to act solely as a superbases, thus replicating the role of the TBD catalyst, Figure 3.3.

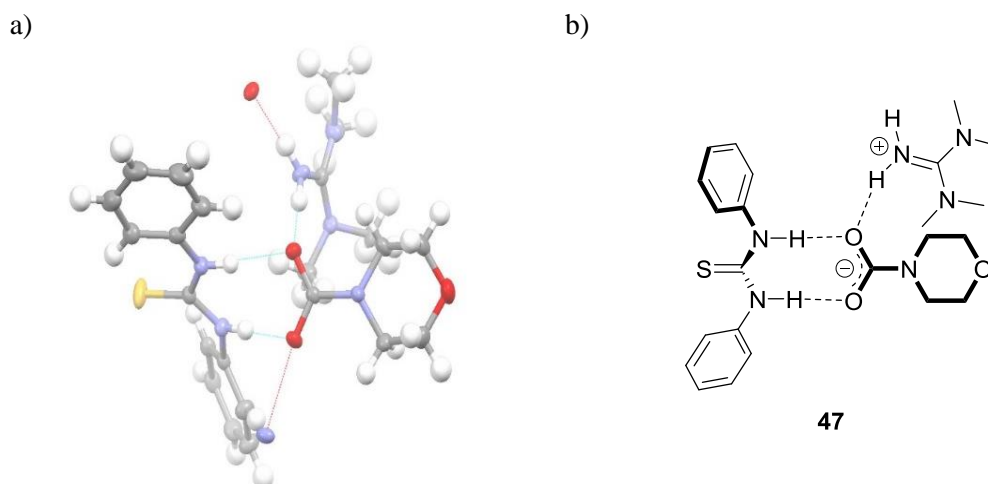


Figure 3.3: Stabilisation of morpholine carbamate by diphenylthiourea **46** a) resolved crystal structure, b) Schematic representation **47**

(Complex **47** prepared, measured and resolved by B.N. Nguyen, full details in Appendix 1)

To investigate this further, the formylation reaction was carried out using a catalyst system TMG and thiourea **46** and was compared against catalysts TBD and a control of TMG in the synthesis of formylmorpholine **24** with phenylsilane **26** as the reductant. Reactions were carried out at room temperature, 1.8 bar CO₂ at 1 M in acetonitrile. The products were identified by comparison of ¹H and ¹³C NMR spectra to those of commercial samples. The reactions were monitored by GC, Figure 3.4, and conversions were calculated relative to an internal standard of biphenyl, using calibration curves prepared using the authentic pure compounds.

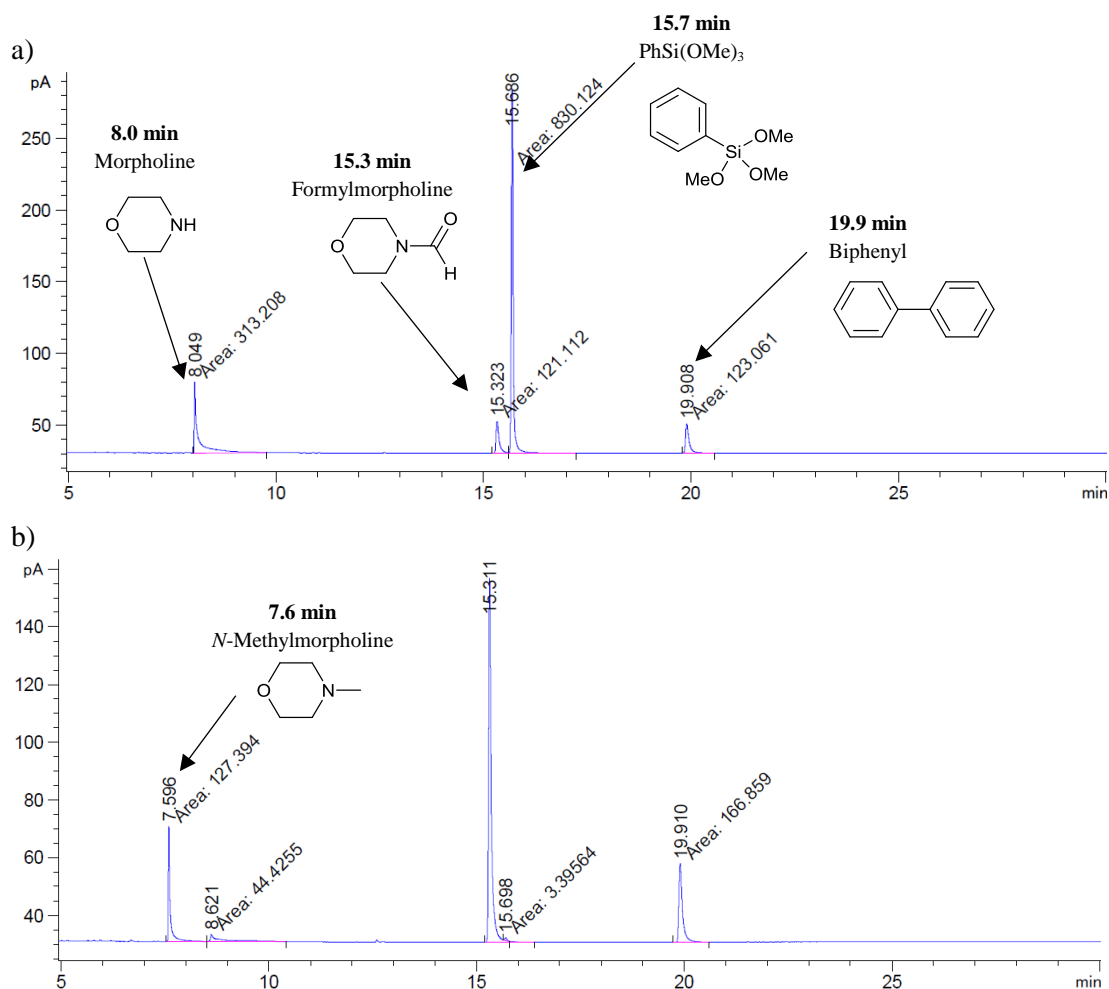


Figure 3.4: Example GC chromatograms from reductive functionalisation of CO₂ with morpholine and PhSiH₃. Samples taken at a) 30 s b) 4 hours and quenched with methanol

As shown in Figure 3.5, all catalyst systems gave 93-97 % conversion to **24** after 6 hours, however the kinetic profiles highlighted different activities. Using TMG/**46** gave a higher rate of conversion than TBD. However, TMG alone as the catalyst was more efficient than when thiourea **46** was added as a co-catalyst, reaching full conversion after only 90 mins of reaction. The higher efficiency of the TMG catalyst over the TMG/thiourea system, suggests that the stabilisation of the carbamate intermediate is not important and may even be detrimental to the reaction progress.

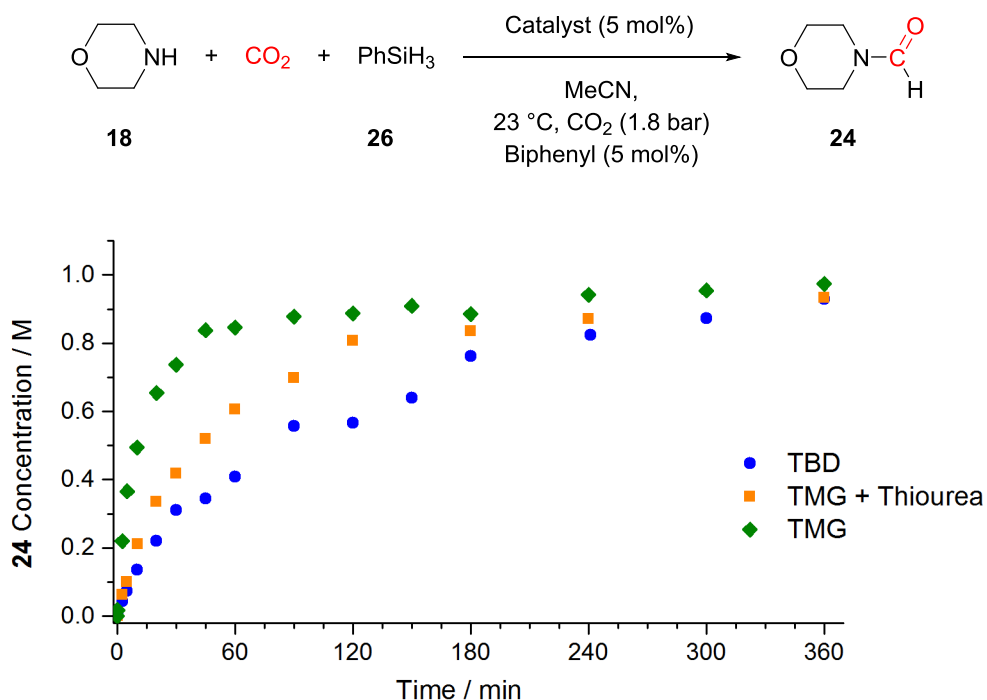


Figure 3.5: Comparison of catalyst activities in synthesis of **24** at 23 °C. Reaction conditions: **18** (2 mmol), PhSiH₃ (2 mmol), catalyst (0.1 mmol), MeCN (2 mL), biphenyl (0.1 mmol), CO₂ (1.8 bar), 23 °C, concentrations determined by GC relative to internal standard

Increasing the reaction temperature to 60 °C with TMG as the catalyst led to a lower overall conversion to formylmorpholine **24** and a slower reaction than at 23 °C, Figure 3.6. The observed decreased rate of reaction could be due to the increased solubility of CO₂ in acetonitrile at lower temperatures¹¹⁰ or the increased stability of a carbamate intermediate at lower temperatures.¹⁰⁷ However, with TBD as the catalyst, increasing the reaction temperature led to an increased rate of reaction suggesting other factors may be involved. The lower conversion to **24** at higher temperature can be accounted for by the formation of side product *N*-methylmorpholine **48** which began to form after 60 minutes of reaction and accounted for 12 % conversion after 360 minutes, Figure 3.6. This side reaction was of interest in its own right as the methylation of amines is an important transformation. The methylation of amines by CO₂ and hydrosilanes is known to occur under similar conditions,⁹⁷ and detailed investigations into the mechanism of its formation will be discussed in Chapter 5.

Next, the tolerance of the system to water was investigated. The TMG catalysed reaction at 60 °C was found to be tolerant to 10 mol% water, with no change in the rate of reaction or overall conversion observed after 6 hours. The reaction was also carried out in the absence of any catalyst. In this case, the reaction proceeded more slowly giving yields of formylmorpholine **24** of 15 and 23 % at RT and 60 °C respectively after 28 hours.

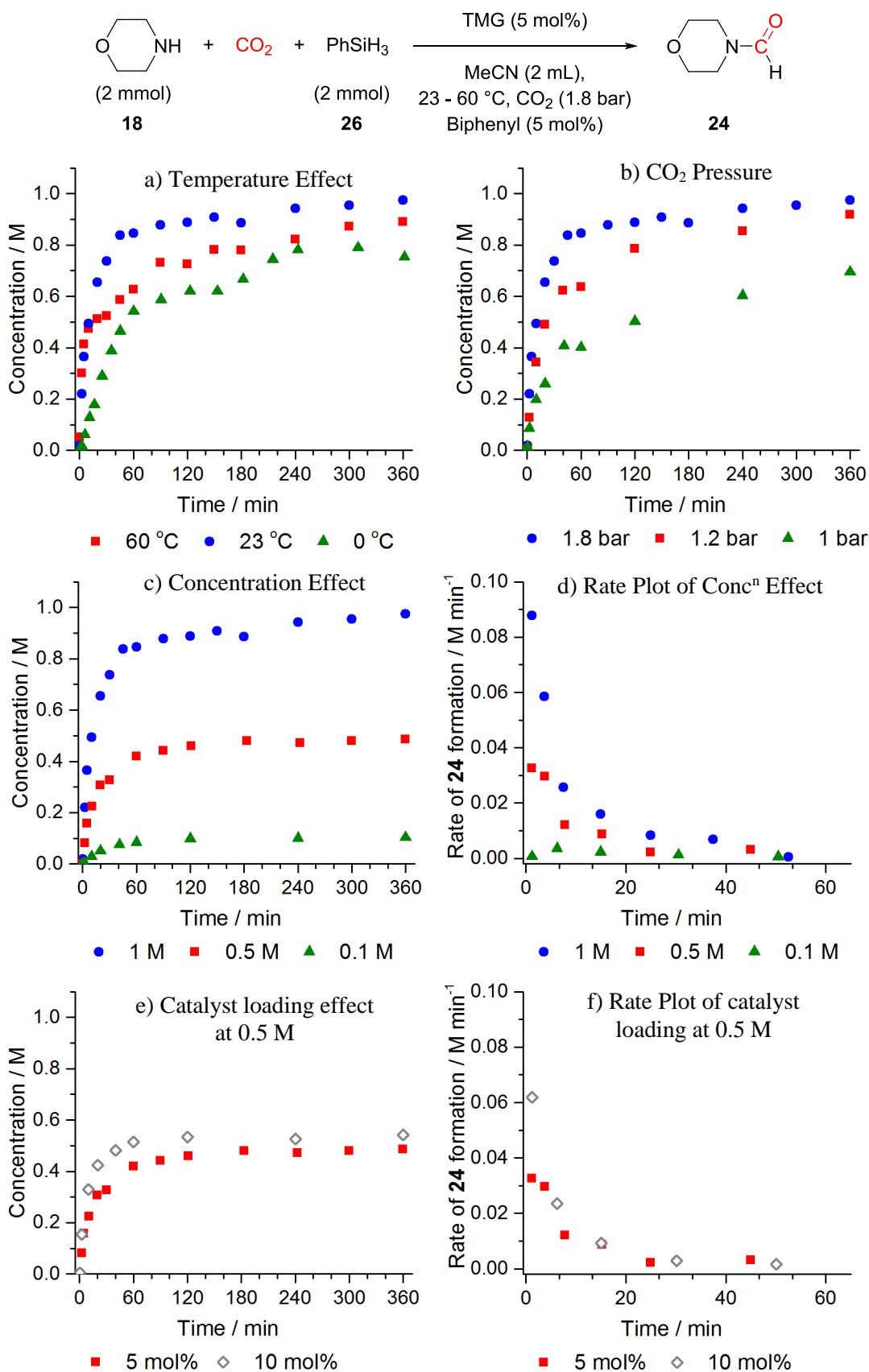


Figure 3.7: Kinetic profiles of **24** formation. Standard conditions: **18** (2 mmol), PhSiH₃ (2 mmol), TMG (0.1 mmol), MeCN (2 mL), biphenyl (0.1 mmol), CO₂ (1.8 bar), 23 °C, Concentrations determined by GC. Variations: a) 60 °C, 23 °C, 0 °C; b) CO₂ (1.8, 1.2, 1 bar); c&d) **18** (2, 1, 0.2 mmol), TMG (0.1, 0.05, 0.01 mmol); e&f) **18** (1 mmol), TMG (0.1, 0.05 mmol)

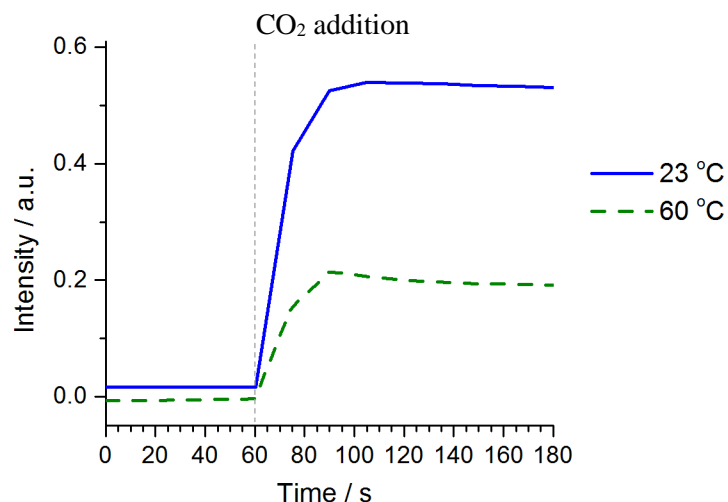


Figure 3.8: Absorption of CO₂ (1.8 bar) into acetonitrile at 23 and 60 °C monitored by *in situ* IR. Solution exposed to CO₂ after 60 s

To further explore the effect of CO₂ pressure on the reaction, the formylation of morpholine was performed at 23 °C at 1.8 bar, 1.2 bar and atmospheric CO₂ pressure, Figure 3.7b. The reaction was found to proceed faster at higher pressures, with full conversion achieved in 6 hours at 1.8 and 1.2 bar CO₂. At atmospheric pressure, only 71 % conversion was achieved after 6 h, although leaving the reaction overnight led to full conversion. Thus, all reactions were carried out at 1.8 bar to ensure mass transfer of CO₂ was not the limiting step.

The effect of concentration on reaction kinetics was investigated, however to ensure mass transfer of CO₂ into solution remained constant, the same total volume of solvent (2 mL) was used in all cases. As the reaction concentration was decreased from 1 M to 0.5 M and 0.1 M the rate of reaction decreased and was not linearly proportional, indicating that the reaction rate may be dependent on concentrations of multiple components, Figure 3.7 c & d. Increasing the catalyst loading from 5 to 10 mol% led to an increase in initial reaction rate (Figure 3.7 e & f); however, this rate increase was not linear with the increase in catalyst loading and the increased catalyst loading had no beneficial effect after the first 15 mins of reaction. In summary, these results indicate that the rate of the reaction is dependent on the concentrations of the catalyst and CO₂, as well as either morpholine and/or PhSiH₃, however the exact rate law could not be determined.

3.3 Intermediate Identification by Reaction Monitoring

Alongside initial investigations that have suggested that the stabilisation of a carbamate intermediate may not be the important role of the catalyst, the effect of temperature on catalyst activity and product selectivity suggested that multiple pathways may be in operation. Based on previously reported systems, a number of intermediates have been proposed to be involved, Scheme 3.2. To further probe the formation and identity of these intermediates, *in situ* reaction monitoring techniques were employed.

3.3.1 *In situ* IR Monitoring

Initially, monitoring by GC did not highlight any distinguishable intermediates, suggesting any intermediates may be unstable on the column or react when methanol is added to quench the reaction. Thus alternative techniques were applied to study the system. As many of the proposed intermediates possessed carbonyl moieties, *in situ* IR spectroscopy was well placed to study this system and allows consistent monitoring of the reaction.

In situ IR monitoring was performed using a ReactIR system with a diamond ATR crystal probe inserted into the reaction vessel. Spectra were recorded every 15 or 30 seconds as the reaction progressed for up to the first 120 minutes of reaction. Starting material and product peaks were identified based on reference spectra (Appendix 2), and characteristic bands were selected to monitor the reaction progress, Figure 3.9a.

On addition of PhSiH_3 to start the reaction, a rapid increase in formylmorpholine (characteristic peak at 1678 cm^{-1}) was observed in the first 10 minutes, which corresponded with a decrease in PhSiH_3 band at 921 cm^{-1} by 50 %, Figure 3.9a. As the reaction progressed, two further intermediate or side product species were identified.

Firstly, Intermediate 1 was observed with a maximum level after 120 seconds before being consumed and decreasing as the reaction progressed, Figure 3.9b. The intermediate species was identified by absorption bands at 1242 , 1253 and 1697 cm^{-1} , Figure 3.9c. A tentative assignment of a silylcarbamate species (Figure 3.10) was made based on previously reported $\text{C}=\text{O}$ stretch frequencies of *N*-alkylsilylcarbamates between 1671 - 1710 cm^{-1} .^{111, 112}

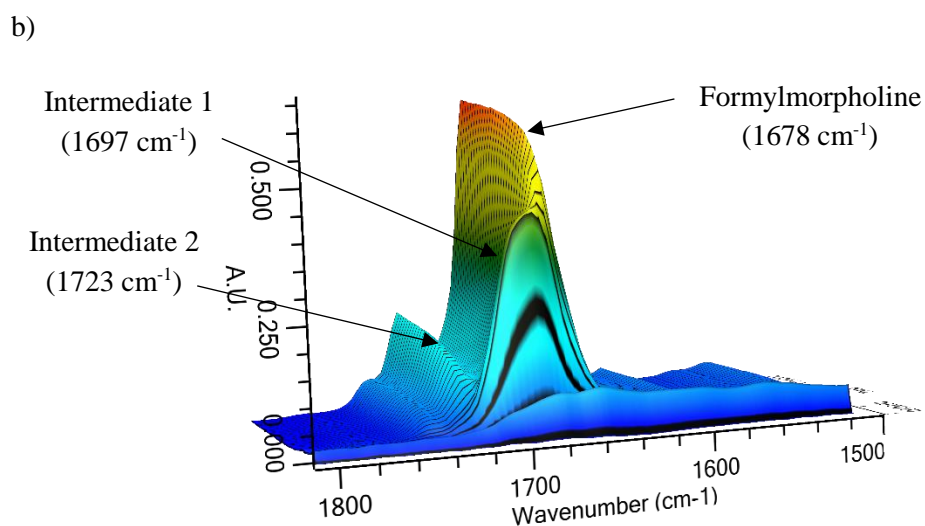
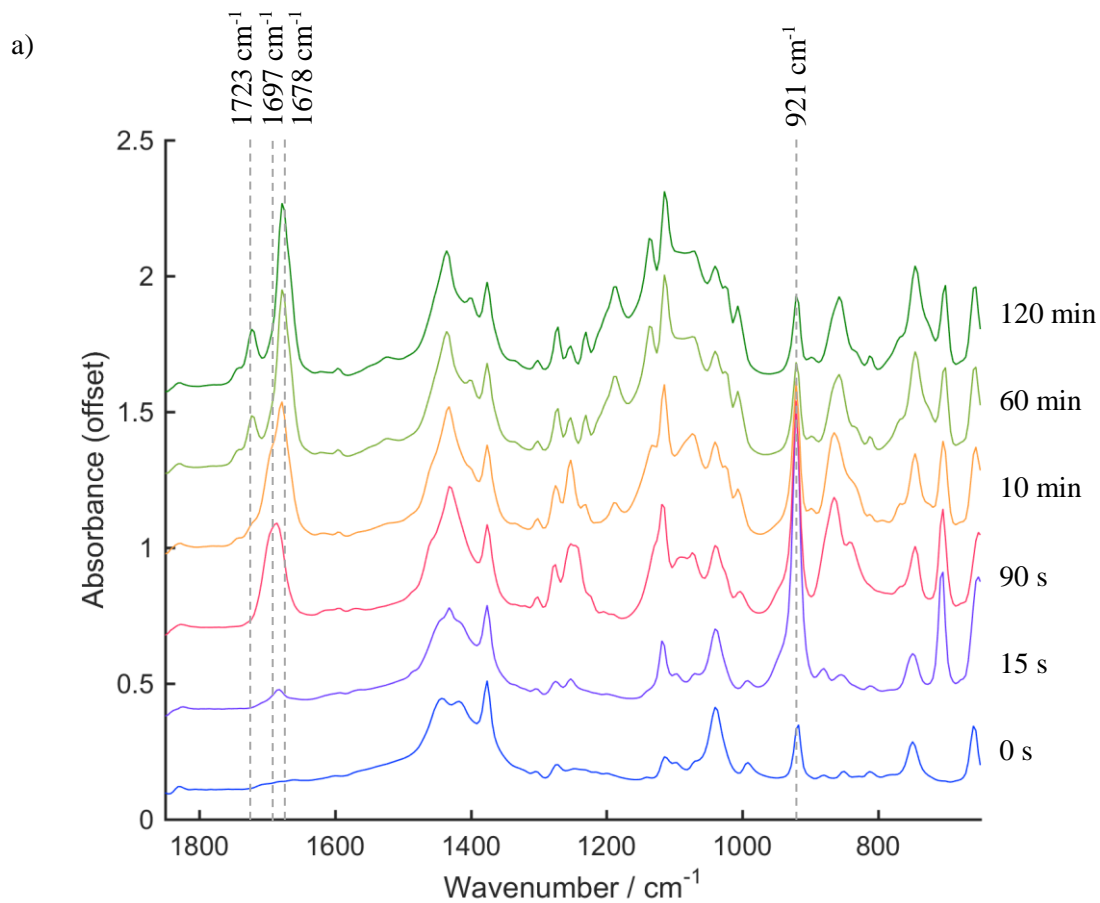
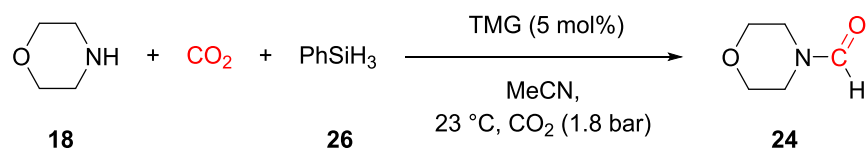


Figure 3.9: Reaction monitoring by *in situ* IR at 23°C with 5 mol% TMG a) Example reaction spectra over time, b) Example spectra of carbonyl region over time; c) Normalised trends based on peak height over first 60 mins of reaction (continued over page)

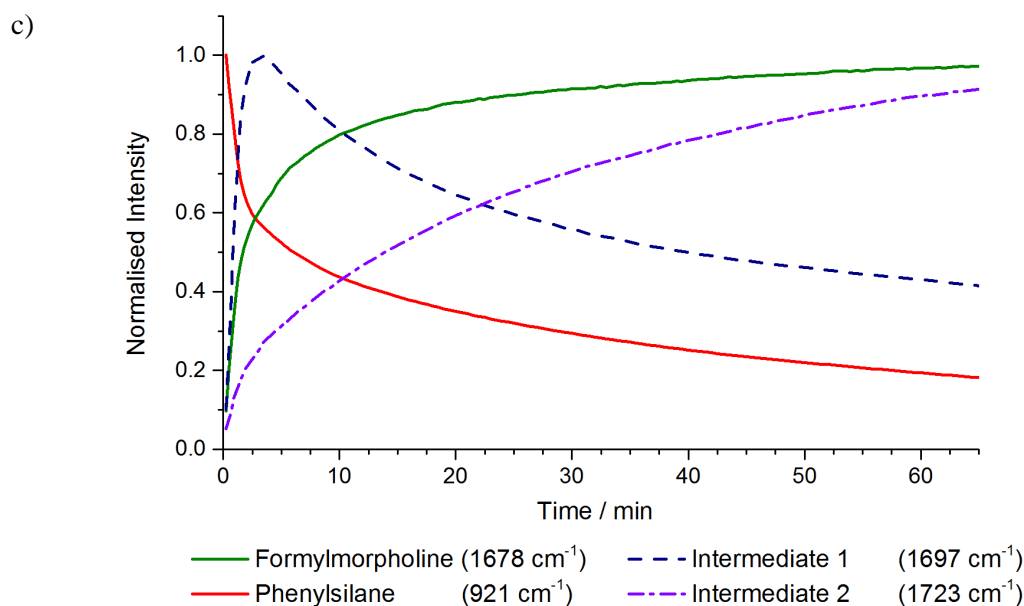


Figure 3.9 cont...: c) Normalised trends based on peak height over first 60 mins of reaction

A second species (Intermediate 2) gradually increased throughout the reaction, Figure 3.9. The species was identified by an absorption band at 1725 cm⁻¹ and tentatively assigned as a formoxysilane species, based on similar formoxysilane species with C=O stretch reported as 1708 – 1727 cm⁻¹, Figure 3.10.¹¹³⁻¹¹⁵ The involvement of formoxysilane intermediates has also previously been proposed in a number of studies.^{33, 73}

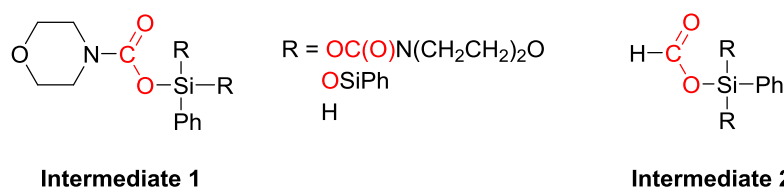


Figure 3.10: Possible assignments of intermediates 1 & 2 observed during reaction monitoring by IR

Due to the overlap of IR bands, particularly between 1650 and 1750 cm⁻¹ it was not possible to gain accurate kinetic profile of each component during the reaction. To overcome this, peak fitting was attempted based on the carbonyl region and various chemometric techniques such as concIR (Mettler-Toledo), FACPACK¹¹⁶ and multivariate curve resolution – alternating least squares (MCR-ALS)¹¹⁷ were attempted to separate out the component spectra and corresponding concentration profiles. However, due to the high number of components and low resolution (8 cm⁻¹) of measurements, these methods were unsuccessful at reliably separating out trends.

After preliminary identification and preliminary assignments of intermediates based on *in situ* monitoring by IR, full characterisation of each intermediate and the role of each intermediate in the reaction was investigated further.

3.4 Role of Silylcarbamate Intermediate

3.4.1 *In Situ* Reaction Monitoring

The formation and reactivity of the possible silylcarbamate intermediate under various reaction conditions was further explored. Monitoring the reaction by *in situ* IR at 23 °C with 1 and 5 mol% TMG, and at 60 °C with 5 mol% TMG, identified the silylcarbamate intermediate in all conditions in similar amounts, Figure 3.11. In reactions with 5 mol% TMG, the silylcarbamate intermediate was consumed faster in the reaction compared to with 1 mol%, whilst little difference in rate was observed for reactions carried out at 23 °C compared to 60 °C. However, significant overlap of peaks prevented an accurate comparison.

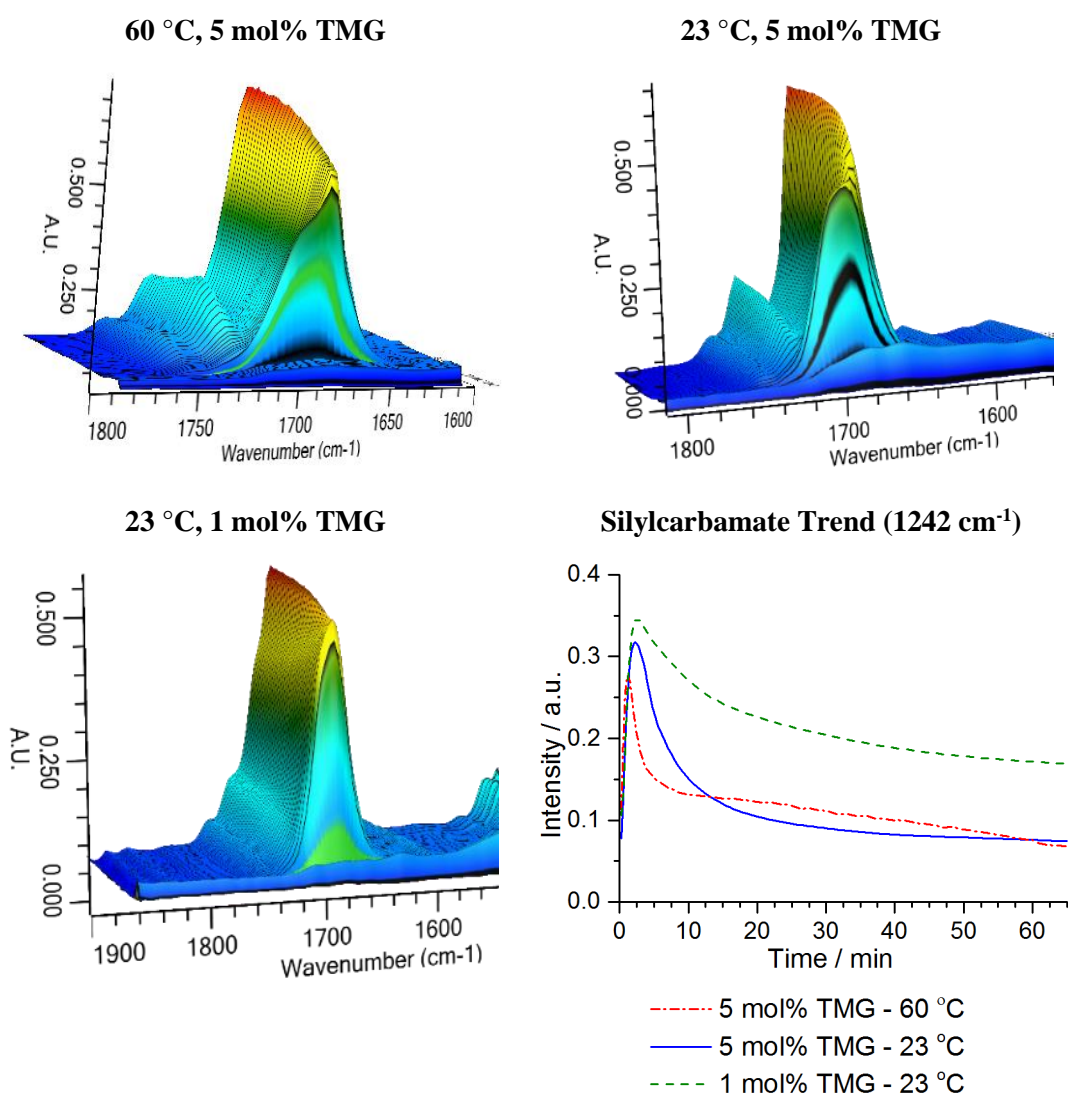
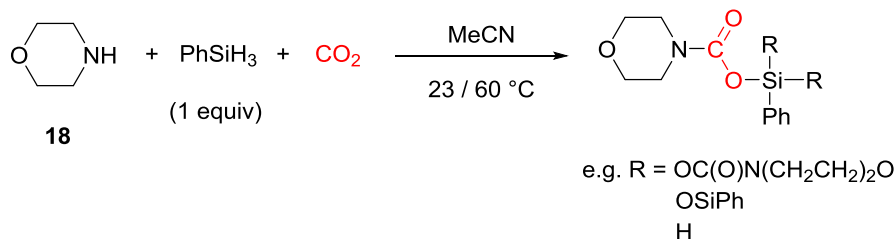


Figure 3.11: Comparison of silylcarbamate formation based on *in situ* IR monitoring a) 60 °C, 5 mol% TMG, b) 23 °C, 5 mol% TMG, c) 23 °C, 1 mol% TMG, d) comparison of trends from conditions a)-c) based on absorption at 1242 cm⁻¹

3.4.2 Characterisation & Formation Kinetics of Silylcarbamate Intermediate

Further investigation found that the silylcarbamate intermediate was formed in the absence of a catalyst at 23 and 60 °C, Scheme 3.6. ^1H , ^{13}C , ^{29}Si NMR and *in situ* IR spectroscopy were used to characterise the structure and reactivity of this intermediate.



Scheme 3.6: Reaction of morpholine, PhSiH_3 and CO_2 to give silylcarbamate species

A solution of morpholine and phenylsilane in acetonitrile at 23 and 60 °C was added to a CO_2 filled Schlenk tube at 1.8 bar, and the reaction monitored by *in situ* IR, Figure 3.12. In the absence of TMG, at 23 °C a new species was rapidly formed within 5 minutes of addition, which was concurrent with a decrease in PhSiH_3 as monitored by the SiH_3 deformation at 920 cm^{-1} , Figure 3.12. The observed species showed characteristic IR bands at 1697 ($\text{C}=\text{O}$ stretch), 1430 ($\text{Si}-\text{Ph}$ ring stretch), 1253 ($\text{C}-\text{O}$ stretch), 1242 ($\text{C}-\text{O}$ stretch) and 866 cm^{-1} ($\text{Si}-\text{H}$ and $\text{Si}-\text{H}_2$), Figure 3.13. These correspond well with literature IR spectra of silylcarbamates with typical $\text{C}=\text{O}$ stretch frequencies of $1671\text{--}1710\text{ cm}^{-1}$ for trimethylsilyl carbamates.¹¹¹

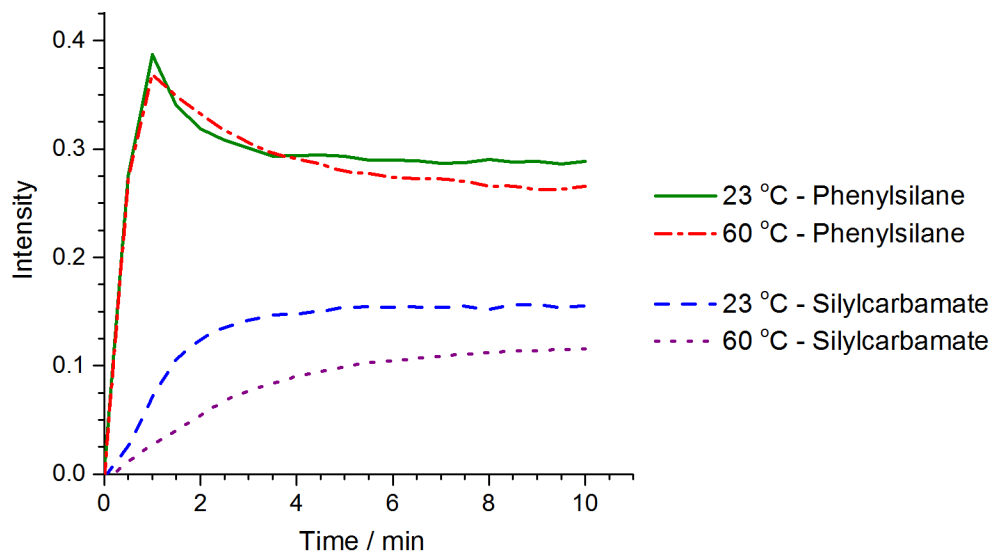


Figure 3.12: Kinetic profile for formation of silylcarbamate intermediate (IR) at 23 and 60 °C (Phenylsilane at 920 cm^{-1} and silylcarbamate at 1242 cm^{-1})

After formation, the silylcarbamate species was initially stable; however, over time it gradually degraded (7 % decrease in intensity over 30 mins) when excess PhSiH_3 was present. This was found to be due to the formation of formylmorpholine. Reaction at 60 °C also showed formation of the silylcarbamate species, however this proceeded more slowly than at 23 °C, reaching maximum conversion after 10 mins, Figure 3.12.

The observed IR species from the uncatalysed reaction resembles the IR spectra taken at 90 s of the catalysed reaction (23 °C, 5 mol% TMG) where the proposed silylcarbamate intermediate is at its maximum, Figure 3.13. This further confirms that the silylcarbamate species is present during the initial stages of the reaction.

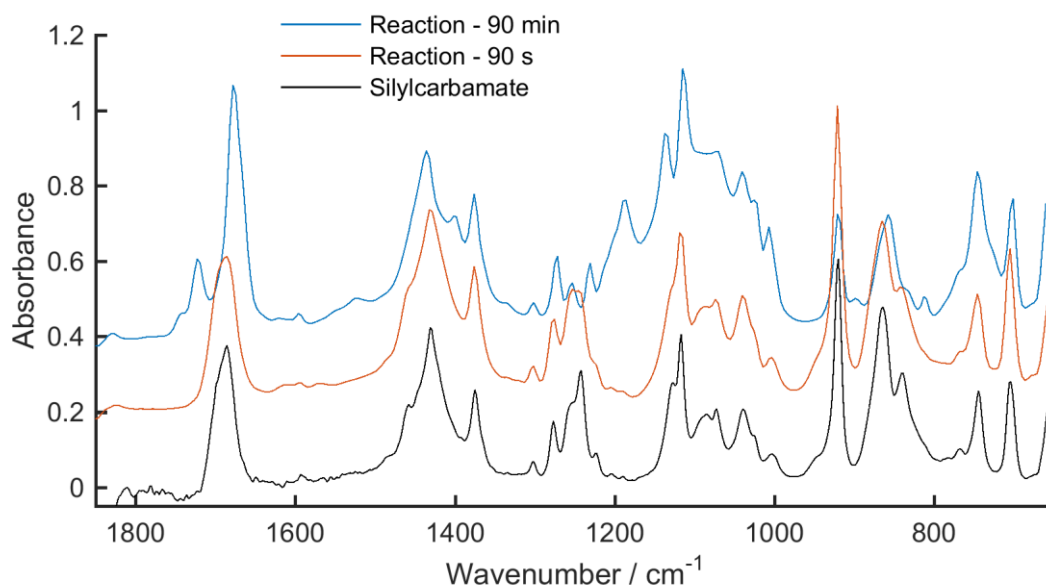


Figure 3.13: Comparison of silylcarbamate **49** spectra with entire reaction monitoring (5 mol% TMG, 23 °C) at 90 s and 90 mins

To further aid characterisation of the silylcarbamate intermediate, the uncatalysed reaction was performed in a Young's tap NMR tube at RT with regular shaking and refilling of CO₂ to ensure mixing. Initially, reaction with 1 equivalent of PhSiH₃ relative to morpholine led to full conversion of morpholine with approximately 50 % unreacted PhSiH₃ observed at the end of the reaction. Repeating the reaction with only 0.5 equiv PhSiH₃ led to almost full consumption of both morpholine and PhSiH₃ by ¹H NMR, Figure 3.14a.

Based on the NMR spectra (Figure 3.14) and IR assignments it is suggested that the dominant species is the dialkylated silylcarbamate **49**, Figure 3.15. The ¹H NMR spectra shows a singlet at 5.47 ppm correlating to the Si-H proton, and a doublet observed in the ²⁹Si NMR spectra of the carbamate at - 31.2 ppm ($J = 281$ Hz), which supports the presence of one Si-H bond. The ¹³C NMR spectra shows signals around 153.8 ppm, which are proposed to correspond to the carbonyl carbon atom present in **49**. This is comparable to ¹³C chemical shifts of 153.3 ppm for dimethylbis(diethylcarbamoyloxy)silane (Me₂Si-[O(CO)N(CH₂CH₃)₂]₂) which have previously been reported.¹¹⁸ ¹H, ¹³C and ²⁹Si NMR spectra also showed other species present in small amounts, these were preliminarily assigned to the monosilylcarbamate **50** and remaining PhSiH₃ and morpholine.

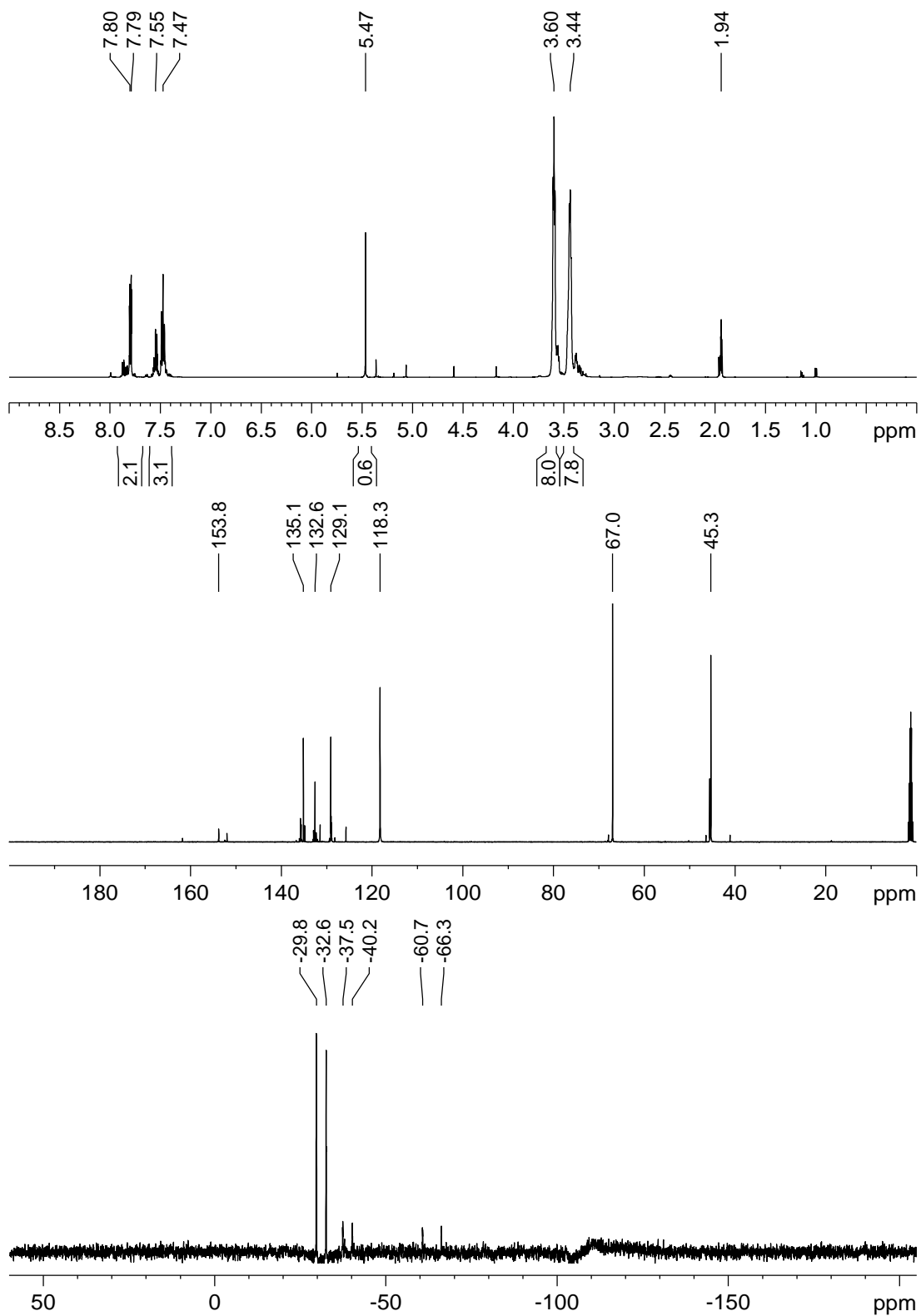


Figure 3.14: Example NMR spectra of *in situ* formation of silylcarbamate in CD₃CN prepared with 0.5 equiv PhSiH₃ to morpholine (1 equiv) a) ¹H, b) ¹³C, c) ²⁹Si

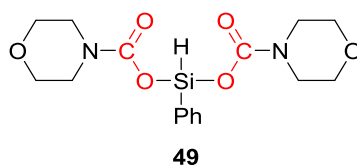
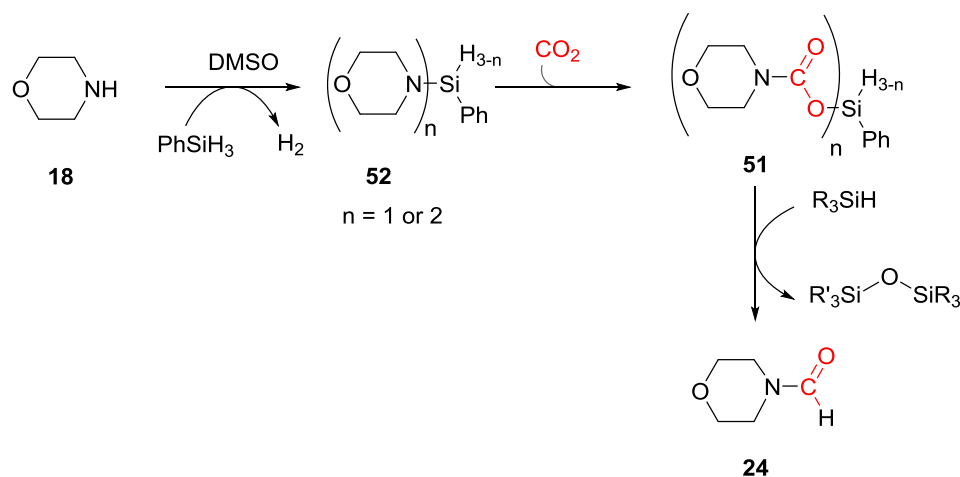


Figure 3.15: Proposed structure of dominant silylcarbamate intermediate species

3.4.3 Proposed Mechanism of Silylcarbamate Formation

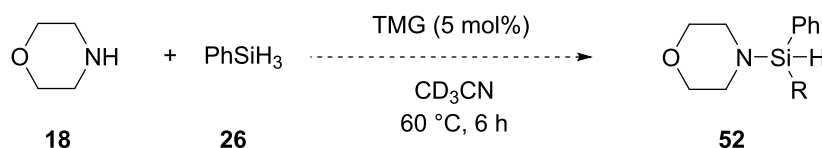
While our investigations into the identity and reactivity of the silylcarbamate intermediate were ongoing, Lei & Li and co-workers published a report on the solvent promoted synthesis of formylamides with DMSO as the promotor.⁷⁸ Based on NMR evidence it was proposed that the silylcarbamate **51** forms from insertion of CO₂ into a silylamine species **52**, and after formation is reduced with a second silane species to give the formylamide product **24**, Scheme 3.7.⁷⁸



Scheme 3.7: Proposed route by Lei & Li to formylmorpholine via silylamine and silylcarbamate intermediate for the solvent promoted reaction in DMSO⁷⁸

The dehydrocoupling of amines with hydrosilanes to form Si-N bonds has previously been reported using transition metals or heavy alkaline earth metal catalysts, or with organocatalysts such as B(C₆F₅)₃ and TBAF.¹¹⁹⁻¹²²

To investigate if this pathway to silylcarbamate formation is operative under the guanidine catalysed conditions used in this system, the reaction was performed under N₂ to probe for the silylamine species **52**, Scheme 3.8.



Scheme 3.8: Proposed formation of silylmorpholine intermediate **52**

After 6 hours at 60 °C in a Young's tap NMR tube, analysis by NMR showed the majority of morpholine (Figure 3.16 – green highlight) and phenylsilane had not reacted (Figure 3.16 – blue highlight); however a small amount (approximately 8 % conversion) of a new morpholine species was present (Figure 3.16 – red highlight).

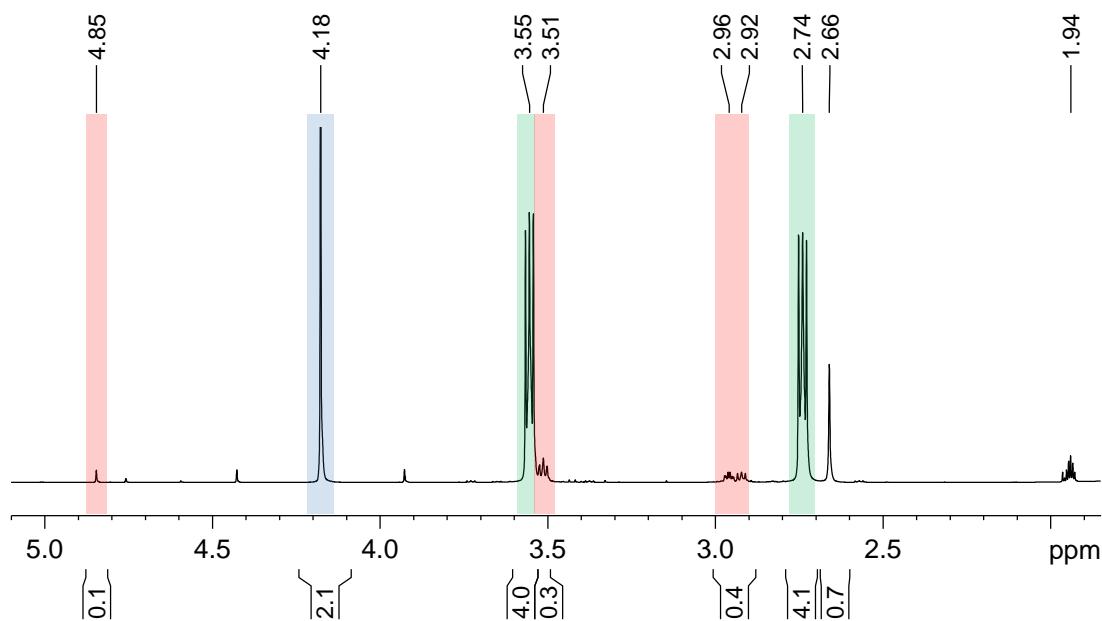
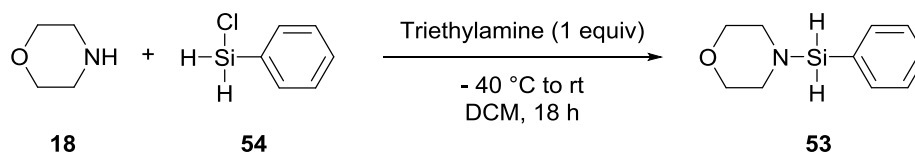


Figure 3.16: ^1H NMR spectra of reaction under N_2 in CD_3CN (given in Scheme 3.8) blue highlight – PhSiH_3 , green highlight – Morpholine, red highlight – new species

To enable identification of this new product the authentic silylmorpholine species **53** was synthesised from morpholine **18** and chlorophenylsilane **54**, based on a procedure reported by Ripoll, Scheme 3.9, to give the desired product in 64 % isolated yield.¹²³



Scheme 3.9: Synthesis of silylmorpholine **53** based on procedure reported by Ripoll¹²³

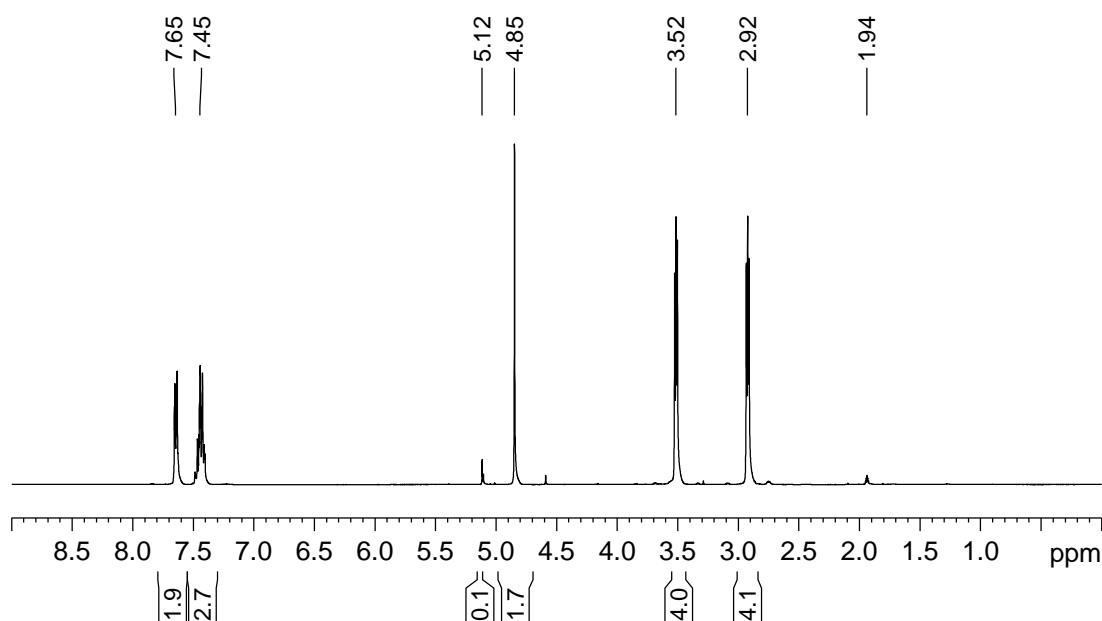
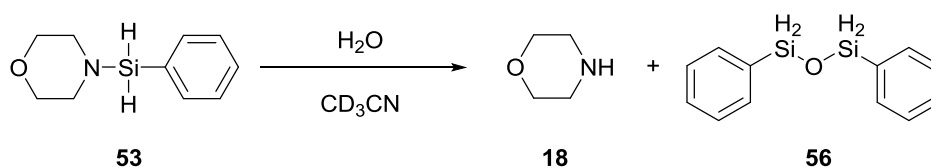


Figure 3.17: ^1H NMR spectra of *N*-phenylsilylmorpholine **53** in CD_3CN (synthesised by alternative synthetic route shown in Scheme 3.9)

The ^1H NMR spectra of **53** (Figure 3.17) corresponds well with the new morpholine species seen in the reaction under N_2 , Figure 3.16. Triplets at 3.52 and 2.92 ppm correspond to the CH_2 groups on morpholine and a singlet at 4.85 ppm from SiH_2 . The ^{29}Si NMR spectra displays a triplet at -23.3 ppm ($J_{\text{Si-H}} = 205.0$ Hz). This is comparable to literature characterisation of $\text{PhSiH}_2\text{N}(\text{Et})_2$ **55** for which a triplet at -26.16 ppm ($J_{\text{Si-H}} = 203.0$ Hz) was reported in the ^{29}Si NMR spectrum.¹²⁴

Compound **53** was found to be very moisture sensitive and despite careful handling using Schlenk line techniques and dried solvent, some contamination with trace water led to approximately 4 % decomposition to diphenylsiloxane **56** and morpholine **18**. This was identified by a peak at 5.12 ppm in ^1H NMR spectra and further correlation of ^1H and ^{13}C NMR spectra with those reported in the literature, Scheme 3.10.¹²⁵ Furthermore, on deliberate exposure to water, full decomposition of **53** to **18** and **56** was observed based on characterisation by NMR and GCMS, Scheme 3.10. Thus no characterisation of silylmorpholine **53** by GC/GCMS or HRMS was possible due to use of protic solvents and exposure to air.



Scheme 3.10: Decomposition pathway of **53** to **18** and **56** in presence of water

Lei & Li proposed, based on NMR studies, that CO_2 is then inserted into the silylmorpholine species to give the silylcarbamate species.⁷⁸ The insertion of CO_2 into Si-N bonds has been well studied and is typically reported to be catalysed by either free amine,¹²⁶⁻¹²⁸ Ru and Rh catalysts,¹²⁹ or may occur uncatalysed with aliphatic amines.^{118, 130}

Having isolated the silylmorpholine species **53**, the insertion of CO_2 into the Si-N bond was investigated in a Young's tap NMR tube, Scheme 3.11. A solution of silylmorpholine **53** in acetonitrile- d_3 was exposed to CO_2 (at 1.1 bar) with regular shaking. The silylcarbamate species **50** was assigned as the major species based on ^1H , ^{13}C and ^{29}Si NMR spectra (Scheme 3.12), with the presence of two Si-H bonds assigned by a triplet in ^{29}Si NMR at -21.4 ppm ($J_{\text{Si-H}} = 230.5, 6.0$ Hz). The dicarbamate **49** and PhSiH_3 were also observed in small amounts at the end of the reaction, Figure 3.18.



Scheme 3.11: Proposed insertion of CO_2 into silylamine **53** to give silylcarbamate **50**

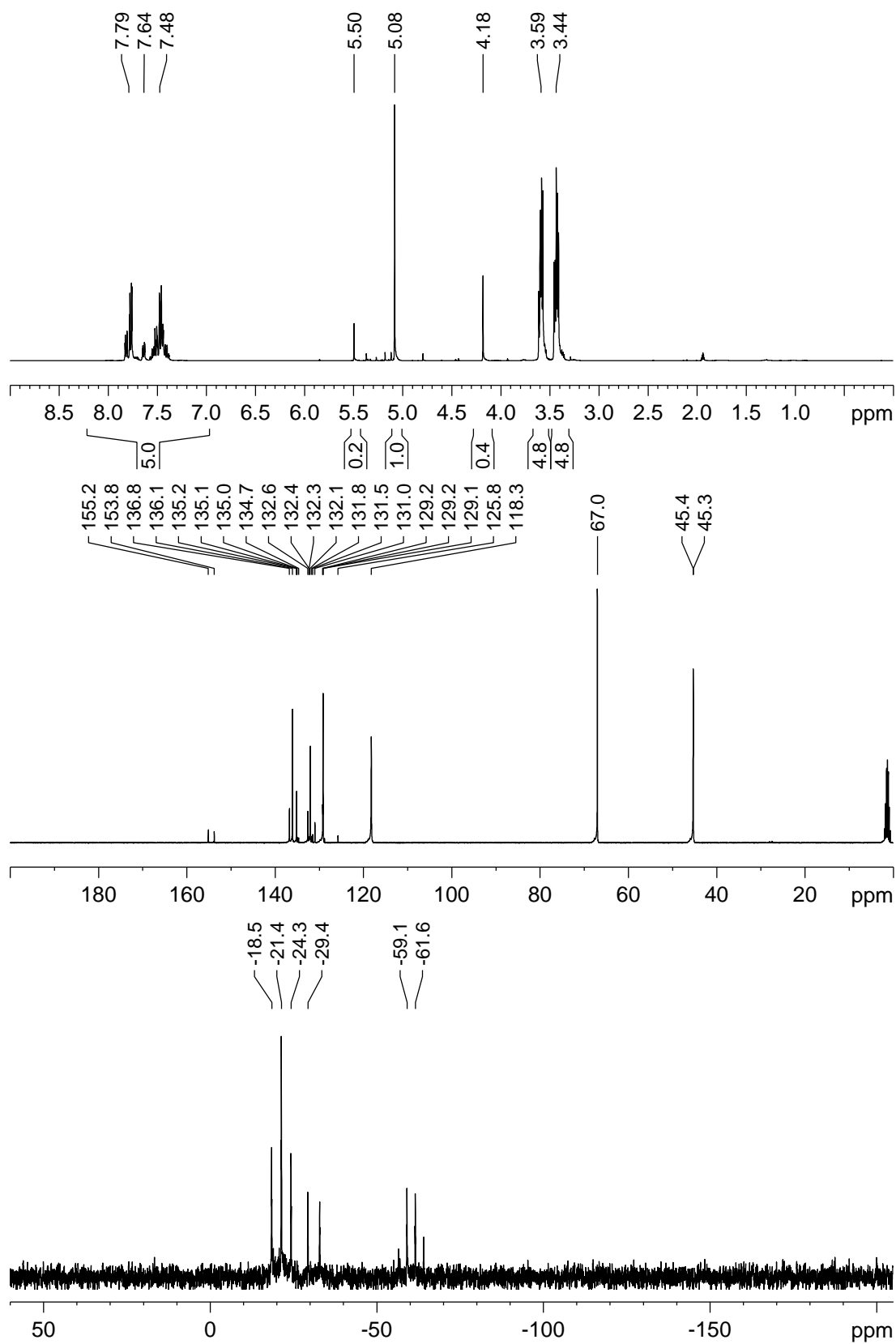
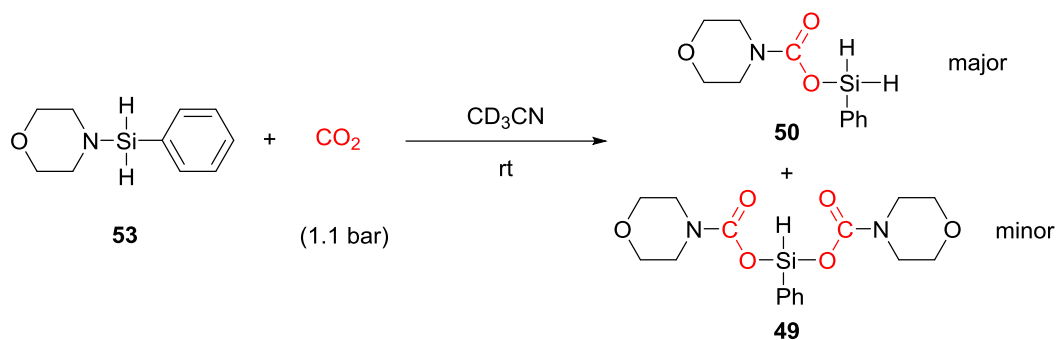


Figure 3.18: ^1H , ^{13}C and ^{29}Si NMR spectra of CO_2 insertion into **53**



Scheme 3.12: Insertion of CO₂ into silylmorpholine intermediate **53**

Monitoring the reaction by *in situ* IR spectroscopy showed that insertion of CO₂ was complete within 120 s of exposure of a silylamine **53** solution to CO₂, as monitored by the carbonyl stretch at 1686 cm⁻¹. IR spectra of **50** correspond well with characteristic peaks identified for silylcarbamate **49**, Figure 3.19. Changes in the relative intensity of absorption bands corresponding to the C-O stretch at 1242 and 1253 cm⁻¹,¹³¹ further support the difference in number of carbamate species bound to the silicon in **49** and **50**.

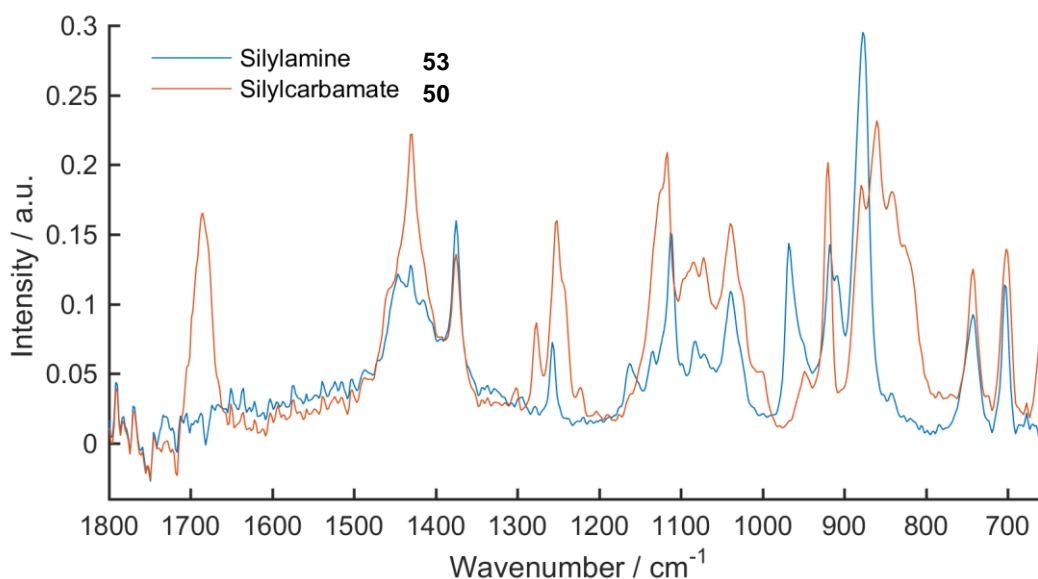
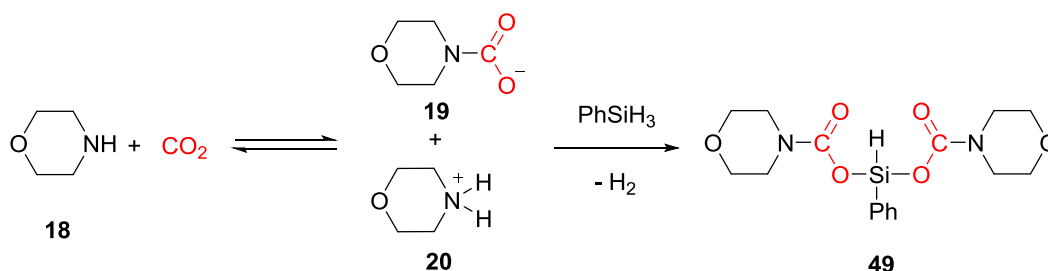


Figure 3.19: IR spectra for silylmorpholine **53** and product of CO₂ insertion to give **50**

Although CO₂ was found to rapidly insert into the Si-N bond of the silylmorpholine species **53** at room temperature, the very slow formation of silylmorpholine **53** from morpholine and PhSiH₃, even at 60 °C with 5 mol% TMG, suggests that this is not the dominant pathway to the silylcarbamate intermediate **49**. An alternative proposal for the formation of silylcarbamate at room temperature is the dehydrocoupling of the morpholine carbamate **19** with the phenylsilane,

by nucleophilic attack from the carbamate oxygen, Scheme 3.13. The rapid release of H₂ in this proposed mechanism is supported by the observation of gas evolution and generation of heat. The formation of silylcarbamates from carbamic acids and carbamates with hydrosilanes has previously been reported to occur under both uncatalysed¹³² and catalysed¹³³ conditions and thus may be a viable pathway to the formation of silylcarbamates under these reaction conditions.



Scheme 3.13: Proposed route to silylcarbamate **49** by dehydrocoupling morpholine carbamate **19** with PhSiH₃

3.4.4 Reactivity of Silylcarbamate Intermediate

The reactivity of silylcarbamate **49** in the synthesis of formylmorpholine **24** was next investigated. The silylcarbamate **49** was prepared *in situ* with 1 equiv PhSiH₃ at 1.8 bar CO₂ in the absence of TMG at 23 °C and 60 °C. After 10 mins the reaction was complete and 5 mol% TMG (in 0.2 mL MeCN) was added. The entire reaction was monitored by *in situ* IR spectroscopy to monitor the intermediates involved, Figure 3.20.

On addition of TMG, at both 23 and 60 °C, the silylcarbamate **49** (monitored by a band at 1242 cm⁻¹) and the remaining PhSiH₃ (monitored by a band at 920 cm⁻¹) rapidly decreased. Concurrently, the formylmorpholine product **24** was produced as observed by an increase in intensity of the band at 1675 cm⁻¹, Figure 3.20. The rate of formylmorpholine **24** production appeared faster at 23 °C than at 60 °C. An increase in intensity of a band at 1725 cm⁻¹, proposed to be a formoxysilane intermediate, was also observed at both 23 and 60 °C after TMG addition, Figure 3.20.

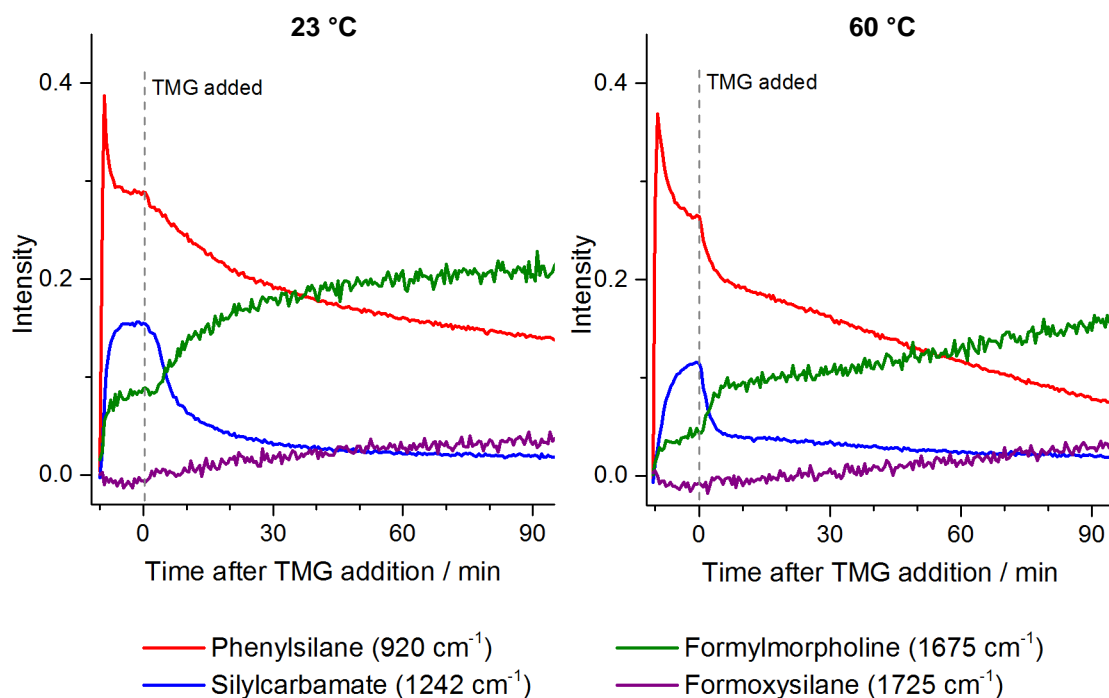
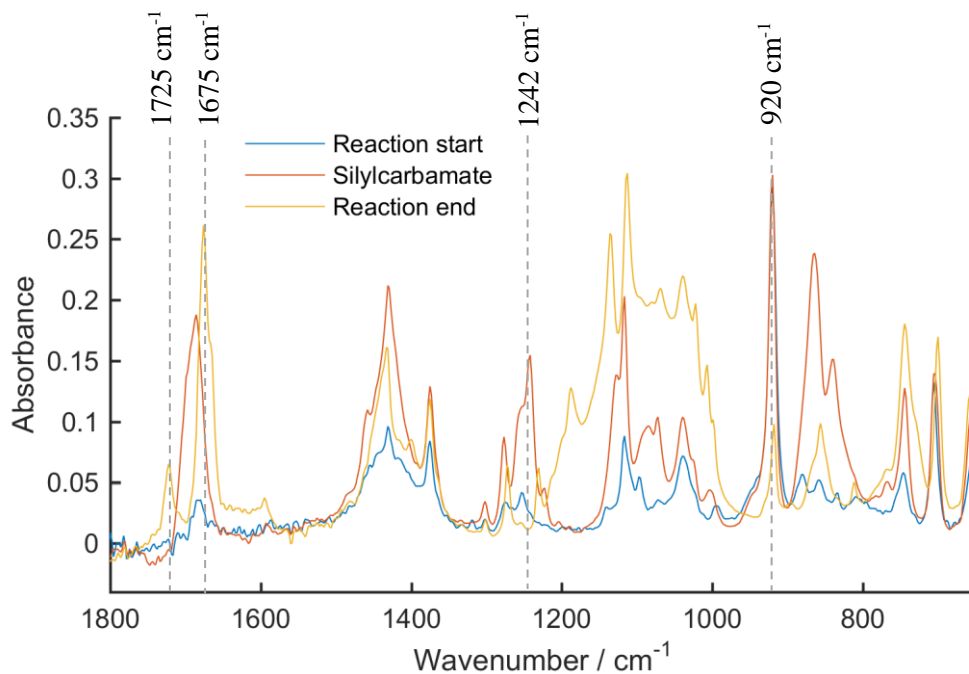
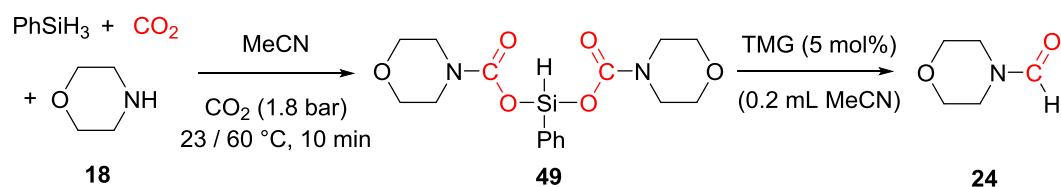


Figure 3.20: Addition of 5 mol% TMG to silylcarbamate **49** (monitored by IR) a) example IR spectra of reaction at 23 °C, b) Reaction trends at 23 °C and 60 °C determined by peak height

Due to the inability to gain accurate concentration profiles from the IR data due to significant overlapping peaks, the above reactions were repeated with regular samples for analysis by GC, Figure 3.21. On addition of 5 mol% TMG to the silylcarbamate **49**, formylmorpholine **24** was produced at a faster rate at 23 °C than at 60 °C. At 60 °C *N*-methylmorpholine **48** was also produced in 15 % yield after 6 hours. These reaction profiles at 23 and 60 °C replicate those where the silylcarbamate was not preformed and PhSiH₃ was instead added to start the reaction, Figure 3.5 & Figure 3.6. This suggests that the rate limiting step is after the formation of the silylcarbamate intermediate. However, it is not yet clear what the role of the silylcarbamate is i.e. whether it is an active intermediate or an off cycle sink of morpholine.

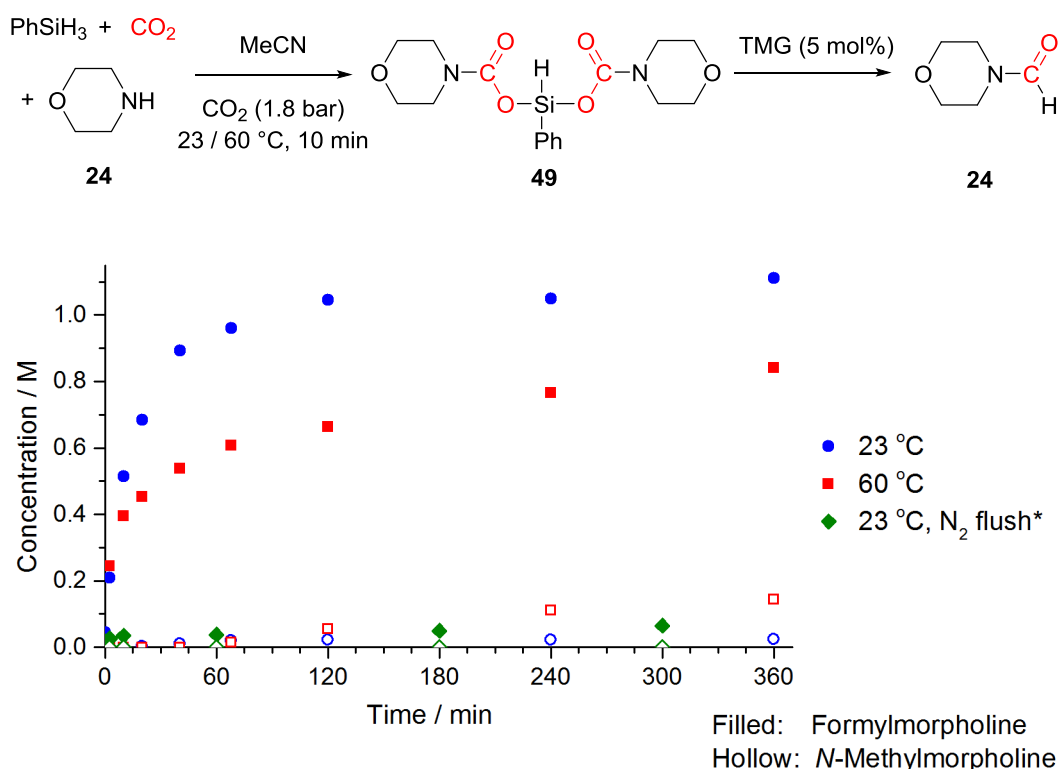


Figure 3.21: Addition of 5 mol% TMG to silylcarbamate (monitored by GC). Reaction conditions: **18** (2 mmol), PhSiH₃ (2 mmol), CO₂ (1.8 bar), MeCN (2 mL), biphenyl (0.1 mmol). After 10 min, flushed with N₂ for 60 mins and TMG (0.1 mmol) added

One possibility is that TMG may promote the reduction of silylcarbamate **49** to formylmorpholine **24**. To investigate this, the silylcarbamate was prepared in the same way as above at 23 °C with monitoring by *in situ* IR, however after its formation the reaction was flushed with N₂ to remove all CO₂ that was not incorporated into the silylcarbamate species from the solution. The loss of CO₂ was monitored by IR and flushing continued until the CO₂ absorption band at 660 cm⁻¹ reached a stable minimum, during which period the silylcarbamate remained stable, Figure 3.22. On addition of 5 mol% TMG a small decrease in the intensity of the silylcarbamate species was observed, however the majority appeared to remain stable and

no formylmorpholine product **24** was observed to form, Figure 3.22. This was again confirmed with reaction monitoring by GC, Figure 3.21. The lack of reaction on addition of TMG (in the absence of CO₂) suggests that the CO₂ incorporated into the silylcarbamate species is not the same CO₂ that was incorporated into the final product, and thus an alternative pathway to the reduction of silylcarbamate must be operating.

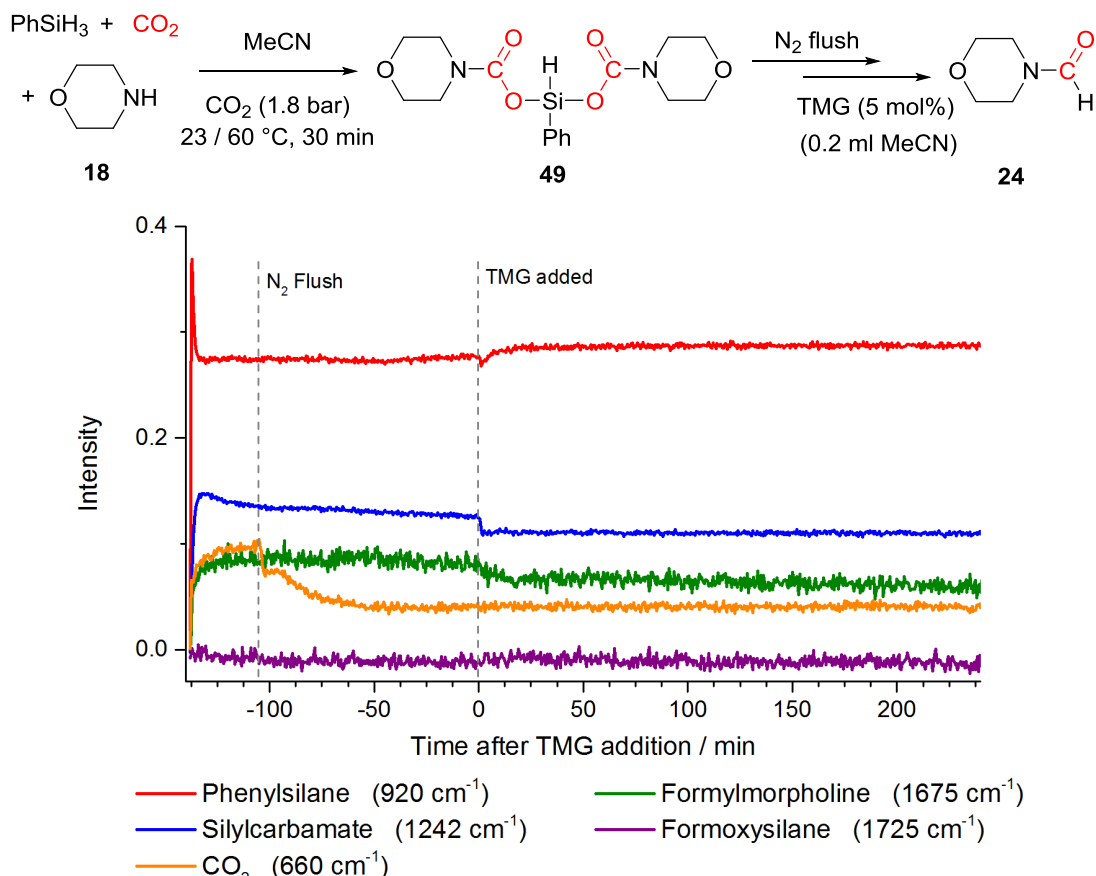


Figure 3.22: IR trends of monitoring reactivity of silylcarbamate after flushing with N₂ before adding TMG (5 mol%)

3.4.5 Summary of the Role of the Silylcarbamate Intermediate

The rapid and significant formation of the silylcarbamate species in reactions at both 23 and 60 °C shows it is an important species to consider in this reaction. After the identity of the species was confirmed by sequential ¹H NMR experiments, monitoring the entire reaction by ¹H NMR further confirmed that the silylcarbamate intermediate is rapidly formed and consumed, but also showed that both silylcarbamate species **49** and **50** are involved in the reaction, Figure 3.23. Attempts to monitor the formation of **49** and **50** during the catalytic reaction by ²⁹Si NMR were unsuccessful due to the low sensitivity of ²⁹Si NMR. As the kinetics of the reaction do not significantly change whether the silylcarbamate is pre-formed or if formed during the reaction, this suggests its formation is not the rate limiting step of the reaction.

Furthermore, as the silylcarbamate **50** requires CO₂ to form formylmorpholine **24**, it suggests that the CO₂ incorporated into the silylcarbamate cannot be reduced to give the formylmorpholine product, however a labelling experiment with ¹³CO₂ would be required to confirm this further. It could thus be that the silylcarbamate is a source of activated hydrosilane, the observation of the proposed formoxysilane species by IR monitoring (Figure 3.20) also suggests this could be involved and requires further investigation.

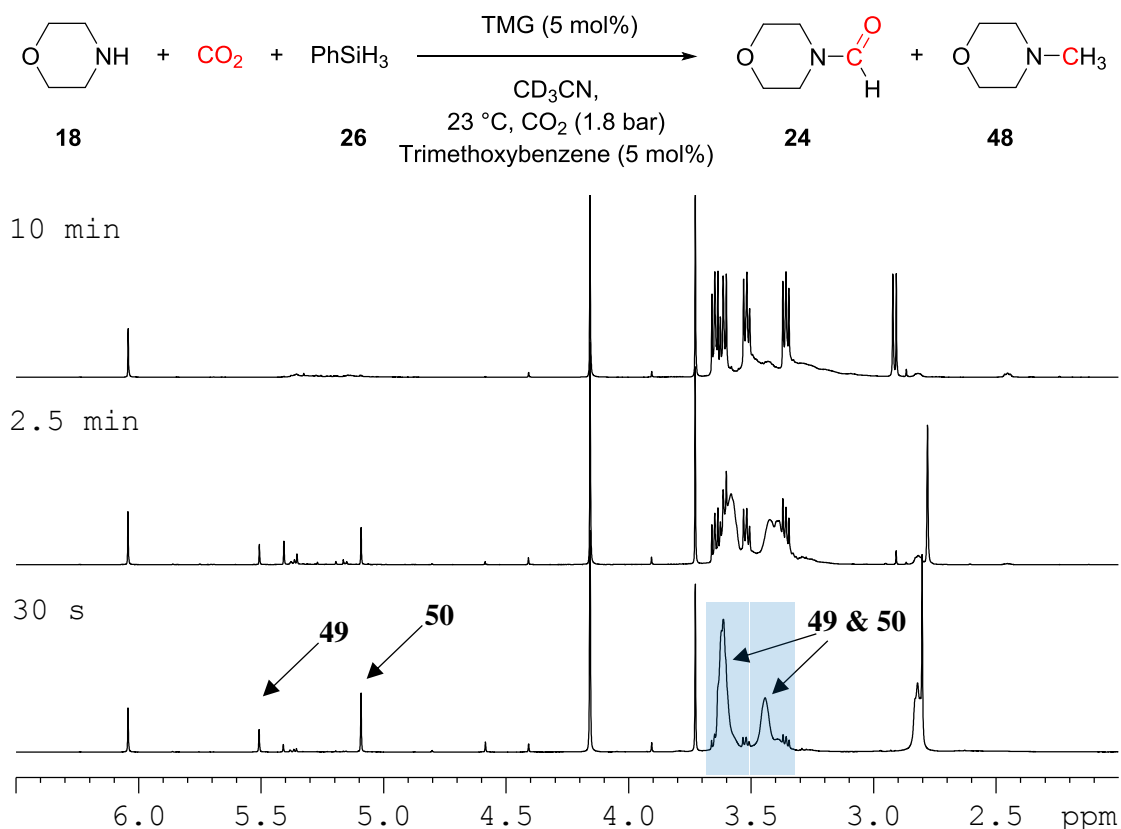
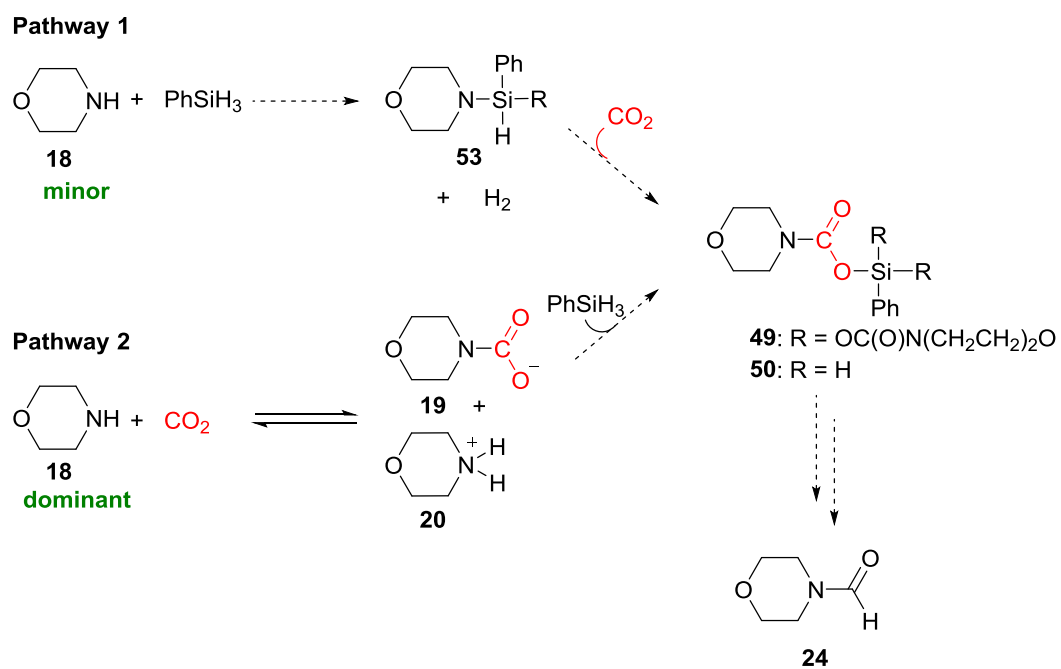


Figure 3.23: ¹H NMR spectra of silylcarbamate intermediates observed in catalysed reaction with 5 mol% TMG at 23 °C



Scheme 3.14: Possible pathways to silylcarbamate species as an intermediate to formylmorpholine **24**

3.5 Role of Formoxysilane Intermediate

3.5.1 *In Situ* Reaction Monitoring

The presence of formoxysilane (Intermediate 2) during the reaction was monitored using *in situ* IR (ReactIR system) by monitoring the carbonyl absorption band at 1725 cm^{-1} for reactions at 23 and 60 °C with catalyst loadings of 1 or 5 mol% TMG, Figure 3.24. Formoxysilane was observed to form under all conditions, however due to a significant amount of silylcarbamate present in the reaction at 1 mol% TMG at 23 °C, which significantly overlaps with the formoxysilane band, the amount present under these conditions cannot be determined.

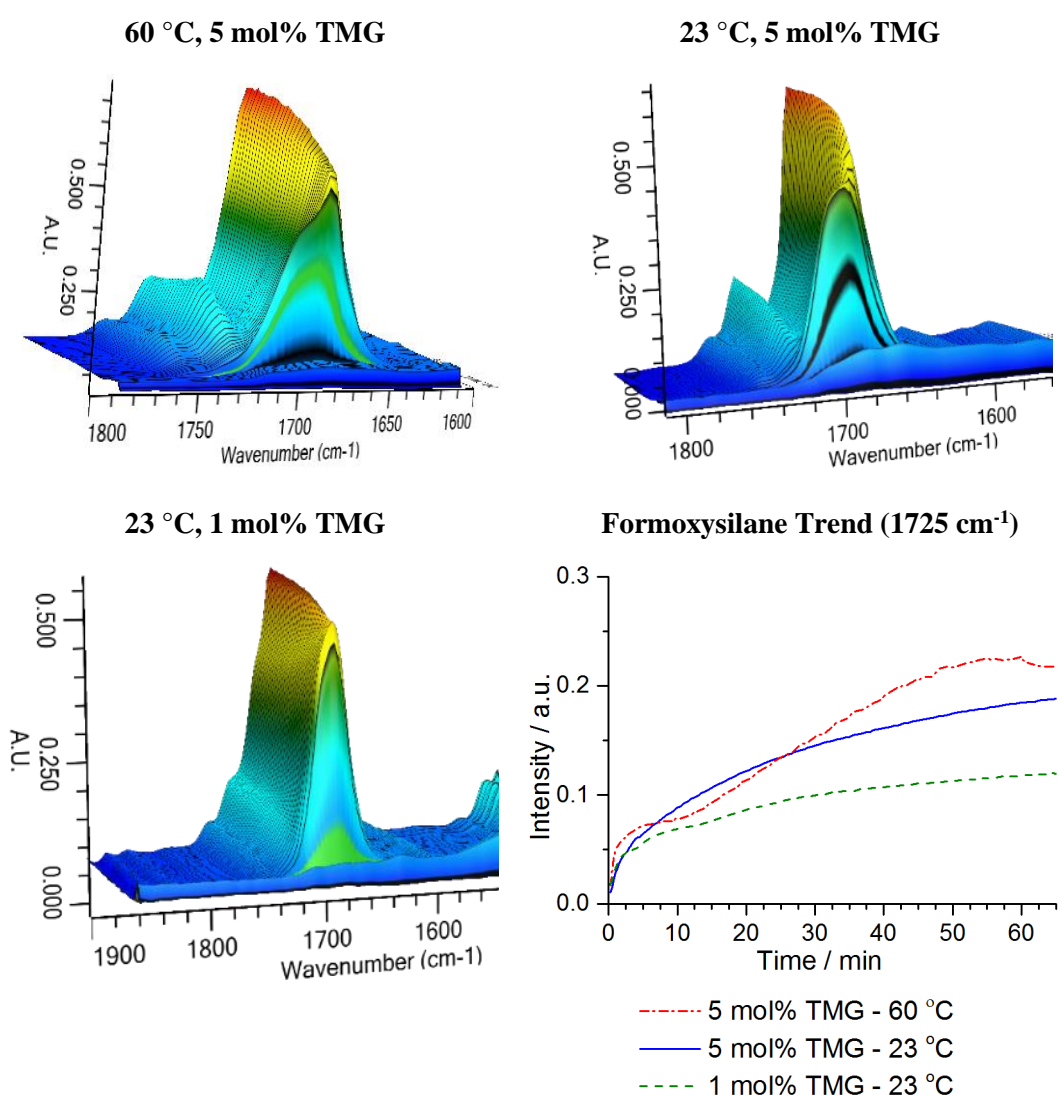


Figure 3.24: Comparison of formoxysilane formation based on *in situ* IR monitoring a) 60 °C, 5 mol% TMG, b) 23 °C, 5 mol% TMG, c) 23 °C, 1 mol% TMG, d) comparison of trends from conditions a)-c) based on absorption at 1725 cm^{-1}

3.5.2 Formation of Formoxysilane Intermediate

The reduction of CO₂ with PhSiH₃ to formoxysilane in the absence of an amine substrate was investigated using IR spectroscopy. Uncatalysed, on addition of PhSiH₃ in acetonitrile to a CO₂ flushed reaction vessel at both 23 °C and 60 °C only a very slight decrease in intensity of a band at 922 cm⁻¹ was observed over 60 minutes, corresponding to SiH₃ deformation of PhSiH₃, Figure 3.25. In the presence of 5 mol% TMG at 23 °C, a 17 % reduction in PhSiH₃ was observed over 60 mins; however, with 5 mol% TMG at 60 °C complete consumption of PhSiH₃ was observed within 40 mins, Figure 3.25.

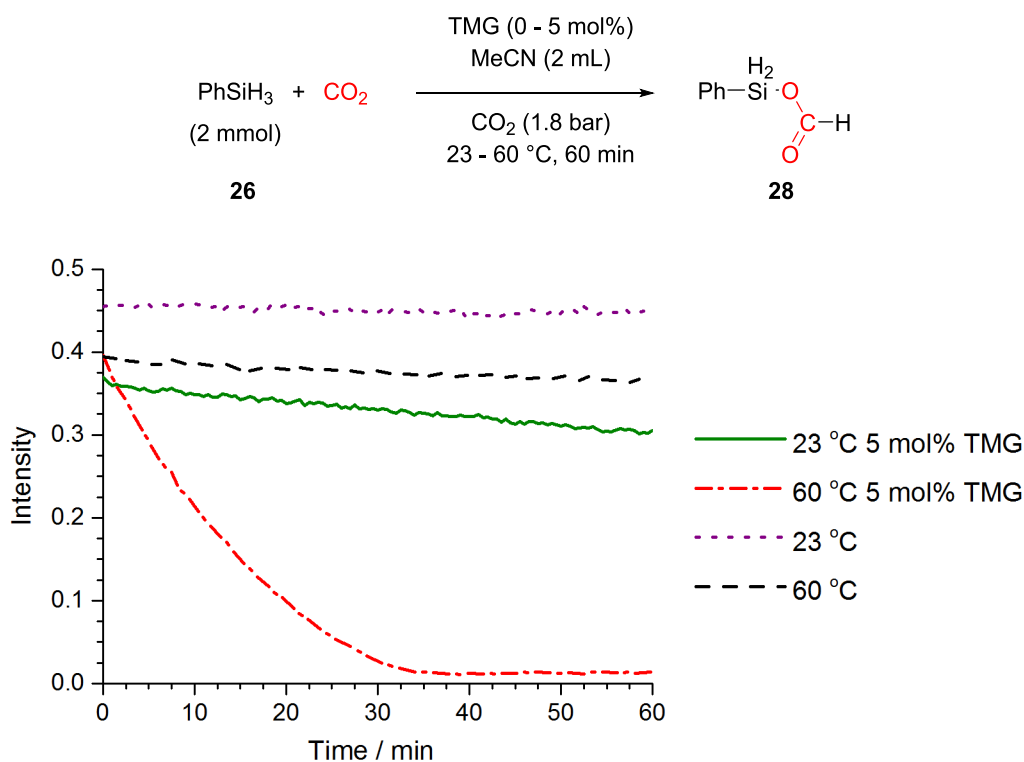


Figure 3.25: Consumption of PhSiH₃ in reduction of CO₂ (monitored by *in situ* IR, peak height at 922 cm⁻¹) from reaction at 23 & 60 °C and 0 – 5 mol% TMG

The decrease in the PhSiH₃ band at 922 cm⁻¹ corresponds with a significant increase in bands at 1725 cm⁻¹ and 1200-1000 cm⁻¹, Figure 3.26. The absorption band at 1725 cm⁻¹ is assigned to the C=O stretch of formoxysilane species based on reported frequencies of 1708-1727 cm⁻¹.^{113, 114} Absorption bands at 1000-1200 cm⁻¹ can be assigned to the formation of new Si-O and C-O bonds,¹³⁴ which correspond well with absorption bands reported in an IR study on the hydrosilylation of CO₂ with dimethylphenylsilane using a Ru based catalyst.¹³⁵

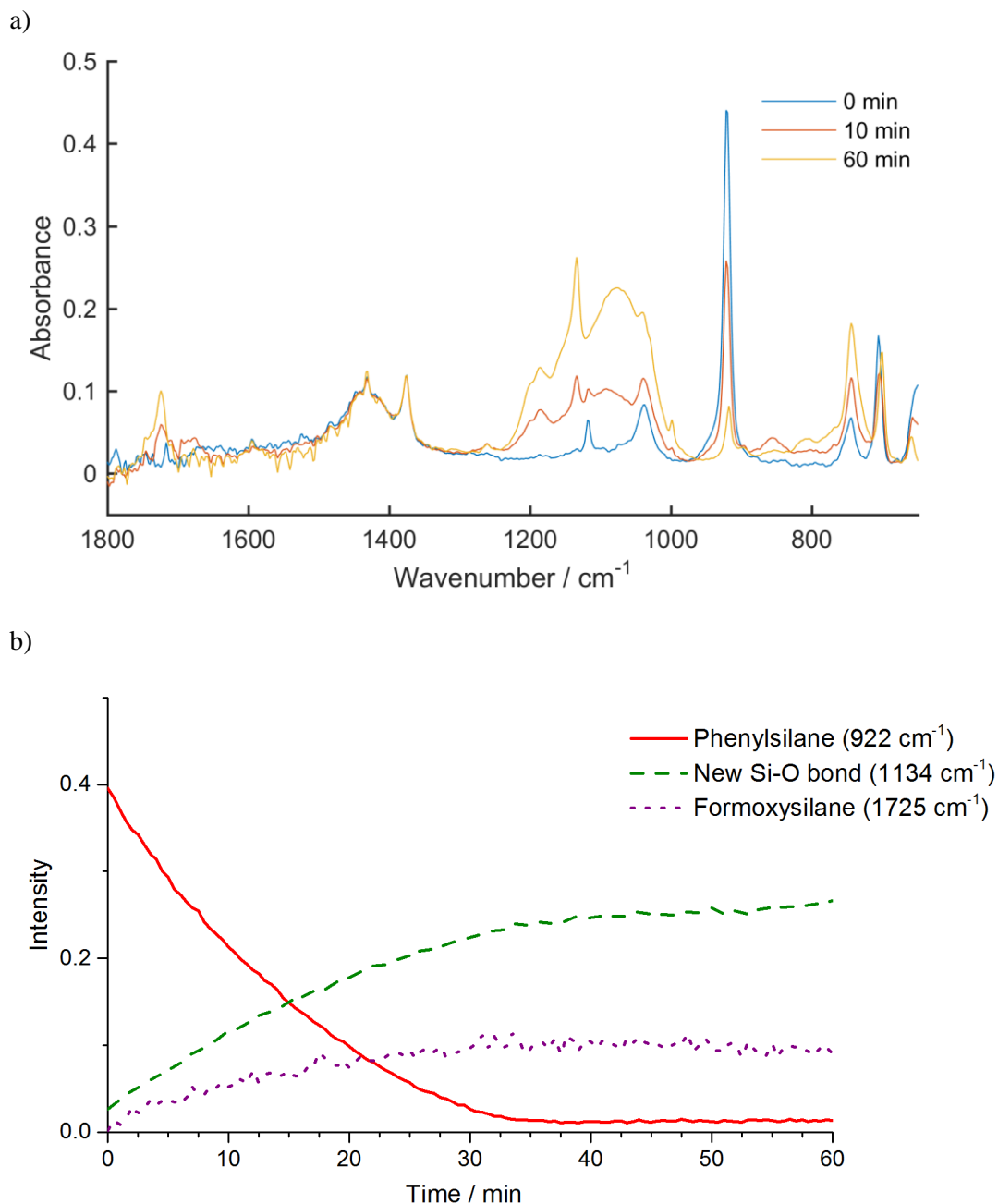
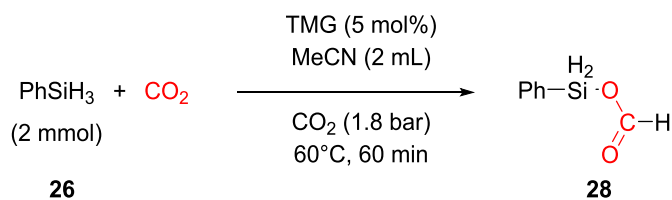


Figure 3.26: Reaction of CO_2 (1.8 bar), PhSiH_3 (2 mmol), TMG (5 mol%) at 60°C with monitoring by IR. a) Spectra at 0, 10 and 60 mins; b) IR trends of reaction

The reduction of CO_2 with PhSiH_3 at 60°C with 5 mol% TMG was further studied by ^1H NMR spectroscopy. The reaction was performed in a Schlenk tube in CD_3CN and samples diluted in CDCl_3 to ensure no change in kinetics were observed, compared to if reaction was ran in an NMR tube.

As the reaction progressed, the consumption of PhSiH_3 was observed by a decrease in the Si-H signal at 4.17 ppm, which was concurrent with the appearance of a broad band at 8.0-8.3 ppm corresponding to the formoxysilane HOCOSiR_3 proton over 40 minutes of the reaction, Figure 3.27.^{33, 37, 75} As the reaction progressed, other new species were also observed. Firstly a broad band between 5.6-4.9 ppm increased over the course of the reaction, this was followed by a second band at 3.7-3.1 ppm which began to increase after 10 minutes of reaction, Figure 3.27. These were tentatively assigned as silylactal and methoxysilane species respectively based on comparison with NMR shifts reported by Ying *et al.* in the NHC catalysed hydrosilylation of CO_2 .¹⁴

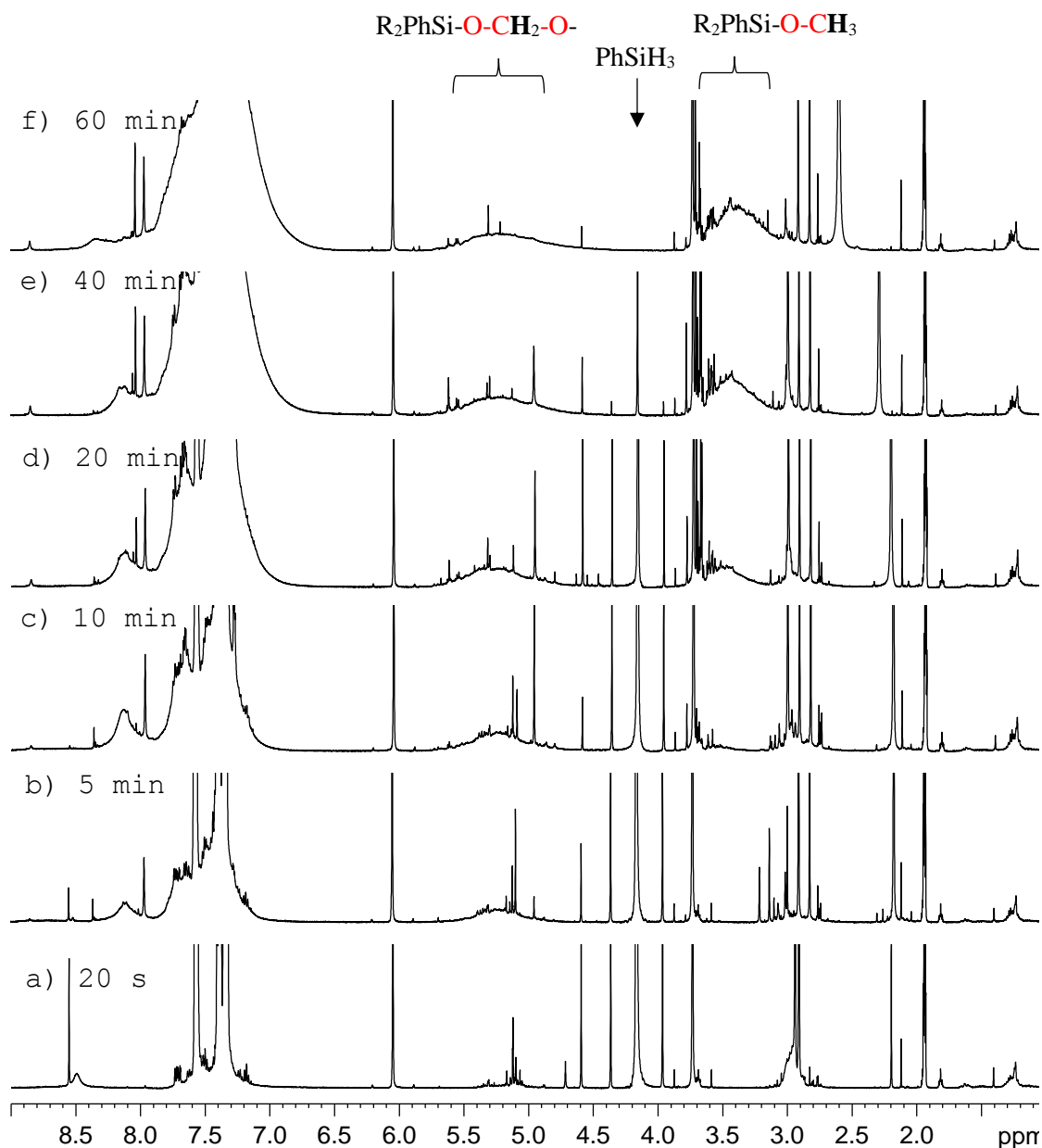


Figure 3.27: ^1H NMR spectra of reduction of CO_2 with PhSiH_3 at 60°C and 5 mol% TMG over 60 minutes

3.5.3 Addition of Morpholine to Products from Hydrosilylation of CO₂

The reactivity of the formoxysilane intermediate was next investigated. After the reduction of CO₂ with phenylsilane had reached completion (determined by monitoring by IR) 1 equivalent of morpholine was added to the reaction. On addition, the band at 1725 cm⁻¹, assigned to the C=O stretch of the formoxysilane, rapidly decreased and a band at 1675 cm⁻¹, which corresponds to the formation of the formylmorpholine product, increased, Figure 3.28. This suggests that the formyl group is transferred from the formoxysilane intermediate to morpholine **18** to yield formylmorpholine **24**. After 15 minutes a large amount of white precipitate due to siloxane and silanol by-products formed, preventing further analysis by IR due to blockage of the probe.

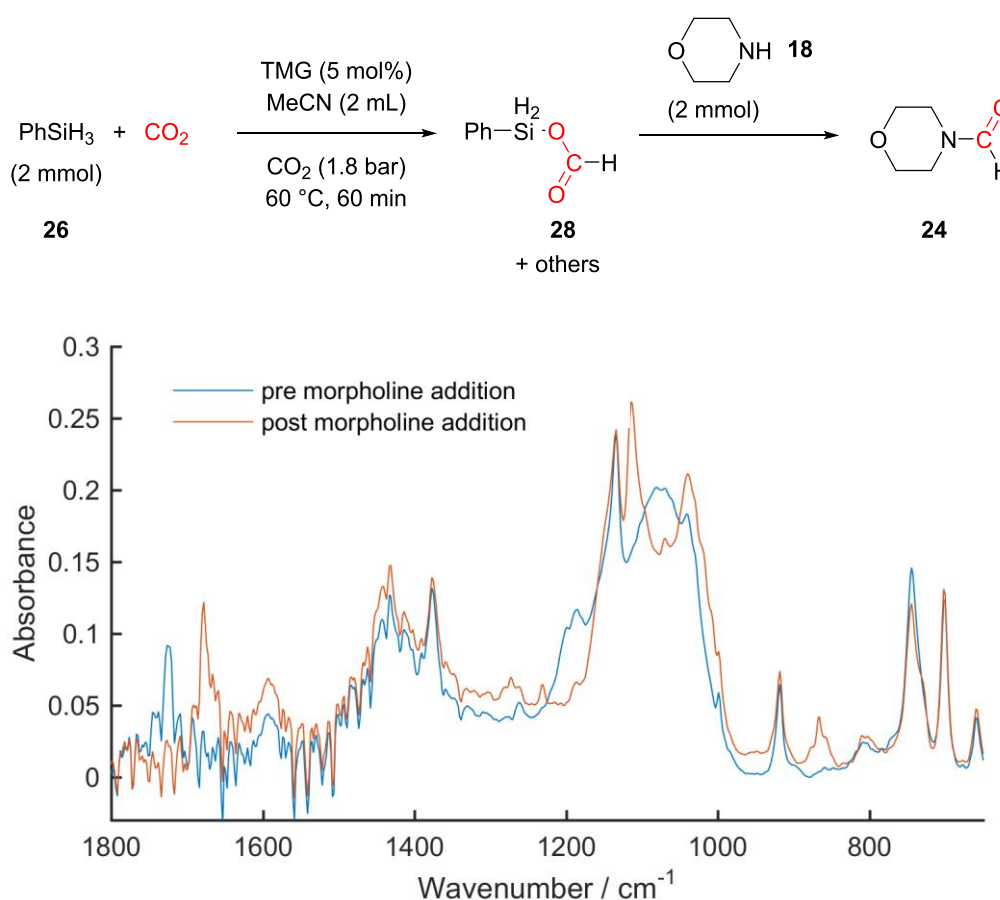
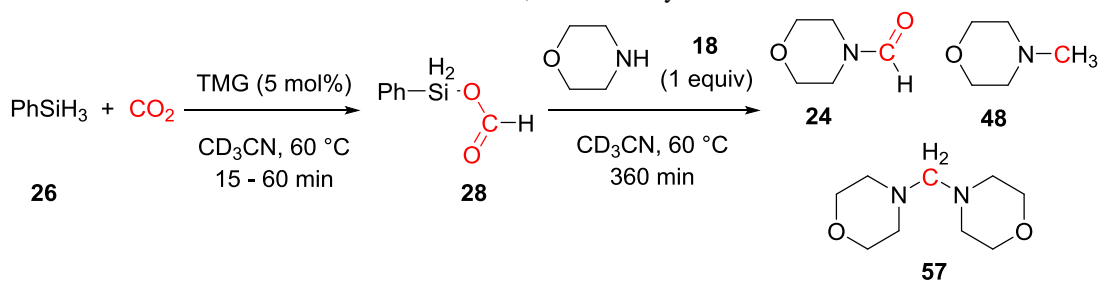


Figure 3.28: Averaged IR spectra of 5 min before and 5 min after addition of morpholine to formoxysilane species

To gain quantitative information on the conversion of morpholine and its reaction with formoxysilane, the reaction was repeated with monitoring by GC and ¹H NMR spectroscopy. After 60 mins of reaction between CO₂ and PhSiH₃ with 5 mol% TMG at 60 °C, the addition of morpholine led to 38 % conversion of formylmorpholine **24** after 6 h, Entry 2, Table 3.1. Monitoring the conversion to formylmorpholine **24** over time showed that the rate of reaction was fast achieving 30 % conversion to **24** in only 2.5 mins, Figure 3.29. The remaining

components after 6 hours were identified by ^1H NMR as unreacted morpholine **18** (28 %) and the aminor dimorpholinomethane **57** (32 %). When the pre-reaction time between PhSiH_3 and CO_2 was reduced to 15 mins, then 74 % conversion to formylmorpholine **24** was observed with the remaining 24 % as the aminor **57** and 1 % as methylmorpholine **48**, Entry 1, Table 3.1. The higher proportion of unreacted morpholine when longer pre-reaction times are used suggests the formoxysilane may be over reduced, as suggested by Ying,³⁷ to a species which is unreactive with morpholine.

Table 3.1: Ratio of products after addition of morpholine to pre reaction of PhSiH_3 and CO_2 at 60°C with 5 mol% TMG, determine by ^1H NMR



Entry	Time / min	% Conversion			
		18	24	48	57
1	15	0	75	1	24
2	60	28	38	1	32
3*	60 + N_2 flush	51	26	0	23

* After 60 mins reaction was flushed with N_2 for 60 mins before addition of morpholine

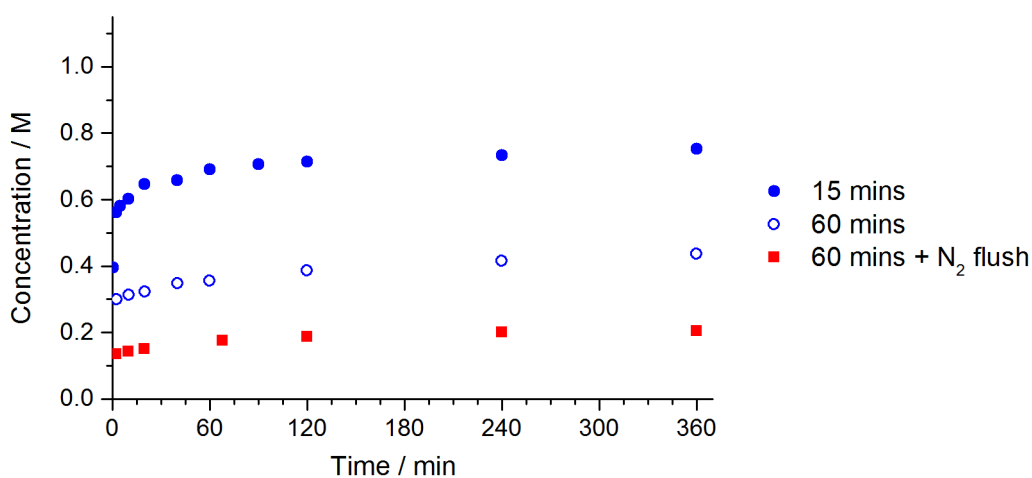
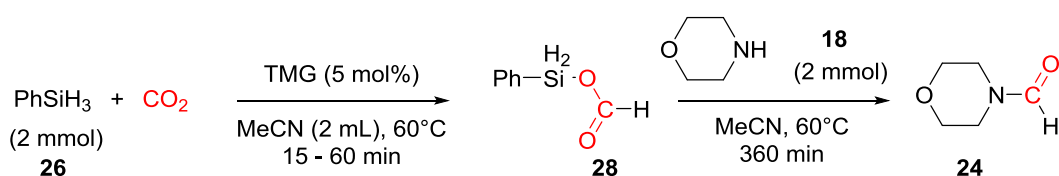


Figure 3.29: Concn of **24** following addition of **18** to formoxysilane (monitored by GC). Reaction conditions: PhSiH_3 (2 mmol), CO_2 (1.8 bar), TMG (0.1 mmol, 5 mol%), MeCN (2 mL), 60°C for 15 or 60 mins, or for 60 mins followed by N_2 flush; followed by addition of **18** (2 mmol)

To confirm that the proposed formoxysilane species is the CO₂ source incorporated into the final product, after pre-reaction of PhSiH₃ with CO₂ for 60 mins, the reaction was flushed with N₂ to remove all CO₂ (monitored by IR band at 660 cm⁻¹ until stable) before addition of morpholine, Figure 3.30. Without any CO₂ present, 26 % conversion to formylmorpholine was observed (compared to 38 % when CO₂ was present), Entry 3, Table 3.1. Thus suggesting that the CO₂ incorporated into the formoxysilane product is incorporated into the formylmorpholine **24** product. This is in contrast to reaction of the silylcarbamate intermediate **49** where additional CO₂ was required for conversion to **24**.

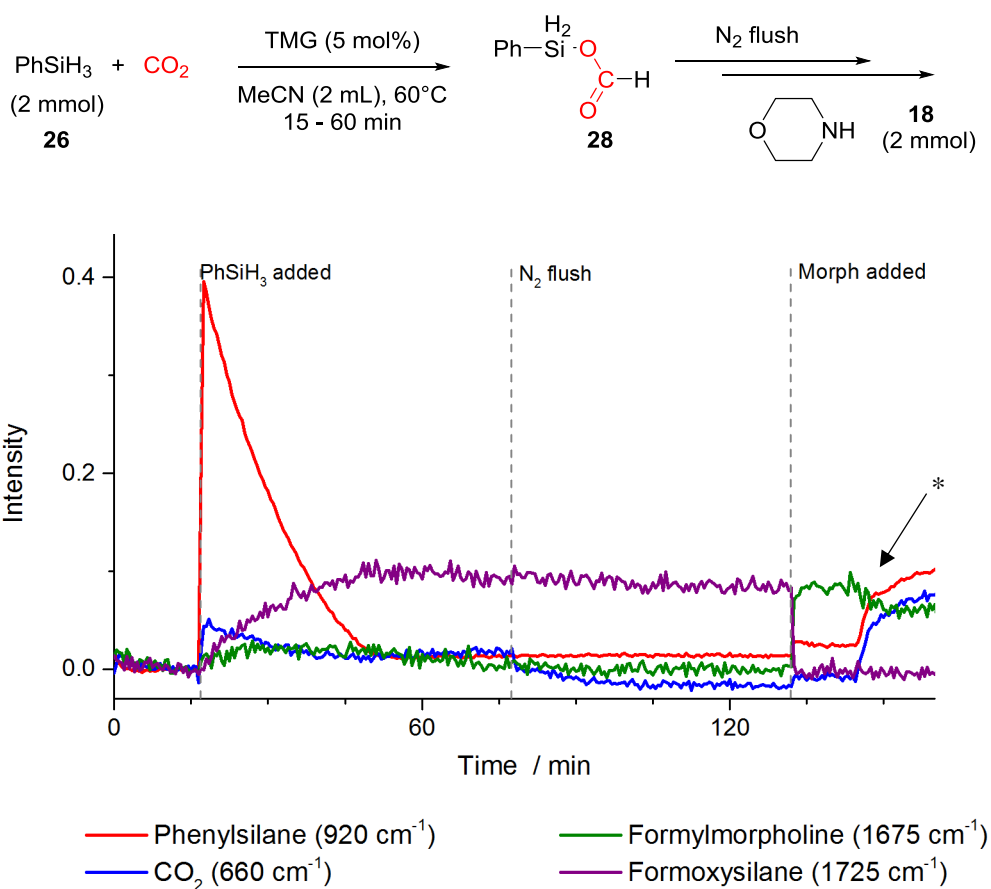
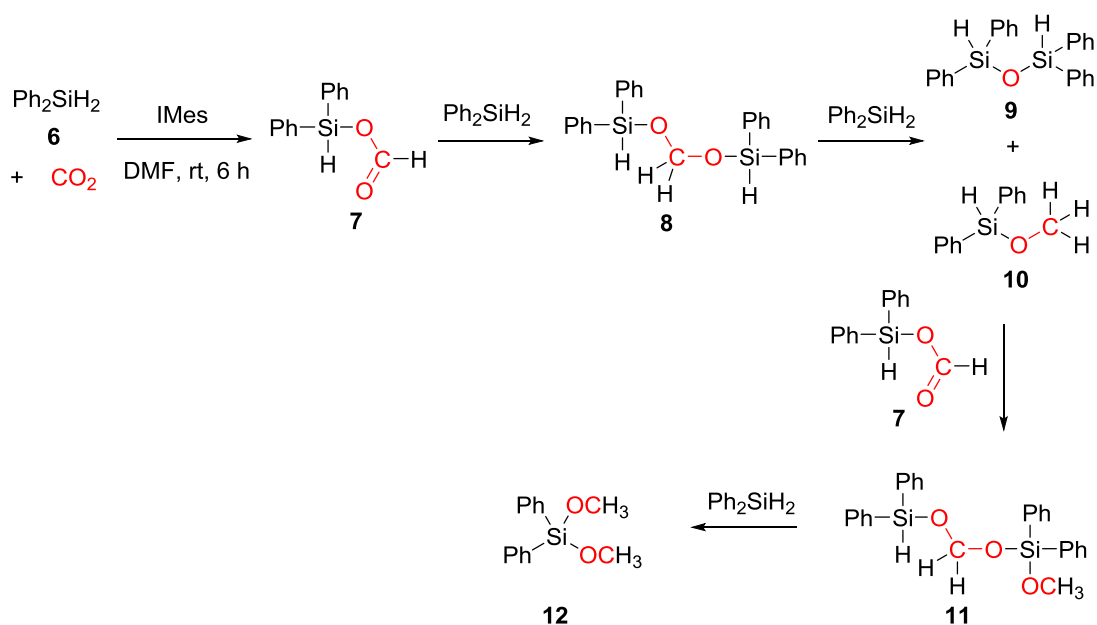


Figure 3.30: IR trends in reduction of CO₂ with PhSiH₃, flush with N₂, and subsequent addition of morpholine. *Increase in intensity at 145 min is due to formation of white solid

3.5.4 Summary of Formoxysilane Intermediate Involvement

The results discussed above have indicated that the hydrosilylation of CO₂ to give formoxysilane can occur at high temperatures when TMG is present. In accordance with previous studies,^{33, 75, 136} the formoxysilane intermediate can then undergo transformylation with morpholine to give the formylmorpholine product. Comparing the reaction kinetics, it appears that the rate limiting step of the reaction is the reduction of CO₂ to give formoxysilane, rather than the transformylation step.

These results suggest that over-reduction of the formoxysilane species can occur, which corresponds with reports of the NHC catalysed hydrosilylation of CO₂ reported by Ying et al. in which the formoxysilane species is an intermediate to silylacetal and methoxysilane species, Scheme 3.15.³⁷ The over-reduction of formoxysilane also appears to correlate with the presence of an aminor side product **57**, the role of which will be discussed in more detail in Chapter 5.

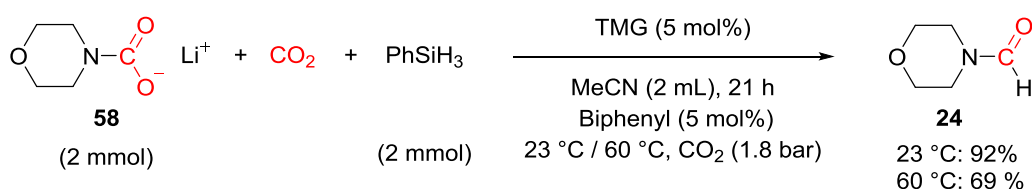


Scheme 3.15: Proposed route for reduction of CO₂ with diphenylsilane involving a formoxysilane intermediate proposed by Zhang and Ying³⁷

Whilst the reaction of PhSiH₃ with CO₂ at 60 °C led to the formation of formoxysilane within 40 mins, the corresponding reaction at 23 °C was significantly slower, Figure 3.25. However, the kinetics of the formylation reaction (i.e. including morpholine) are faster at 23 °C than at 60 °C. Furthermore, when the entire formylation reaction was monitored by IR, formoxysilane was observed under reaction conditions at both 23 °C and 60 °C. These results suggest that a different pathway to the formation of formoxysilane may be operating at lower temperatures, which would account for the fast conversion and the presence of formoxysilane at 23 °C.

3.6 Role of Morpholinium Carbamate

The role of proposed intermediate morpholinium carbamate **19** & **20** in the formylation of amines was further investigated by synthesis of the corresponding individual species. The lithium salt of morpholine carbamate **58** was prepared by lithiation of morpholine and subsequent exposure to CO₂ following a modified procedure.¹³⁷ Subjection of **58** to standard reaction conditions under CO₂ and TMG (5 mol%) led to conversion to formylmorpholine **24**, Scheme 3.16. At 23 °C, 92 % conversion to **24** was achieved after 21 h, whereas at 60 °C, 69 % conversion was observed, Figure 3.31. The reaction kinetics are slower than those observed when morpholine is used as the substrate under the same reaction conditions. This suggests that either the carbamate is not involved in the synthesis of formylmorpholine or the Li⁺ is inhibiting the reaction.



Scheme 3.16: Reaction of morpholine carbamate **58** to formylmorpholine **24** under standard reaction conditions

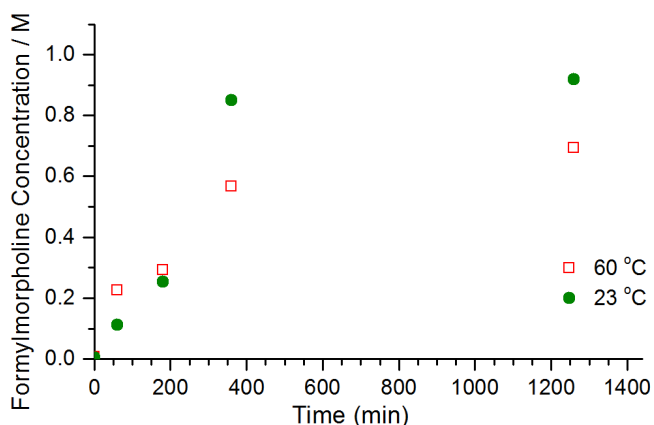
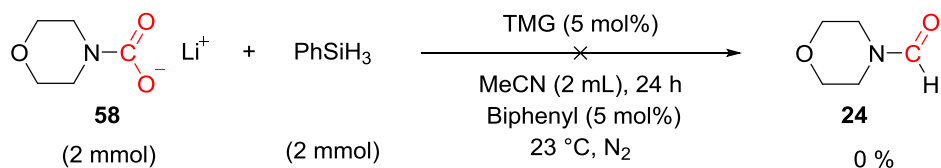


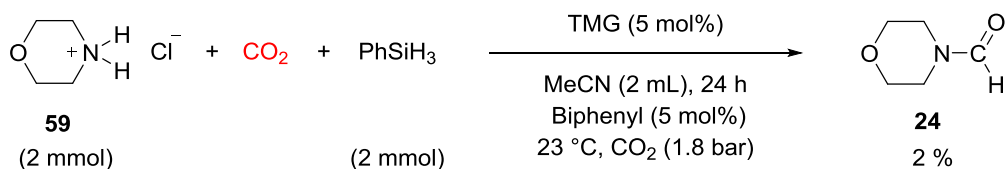
Figure 3.31: GC conversion for reaction of **58** to **24**. Reaction conditions: **58** (2 mmol), PhSiH₃ (2 mmol), CO₂ (1.8 bar), TMG (5 mol%), MeCN (2 mL), Biphenyl (5 mol%), 23 or 60 °C

To investigate if the CO₂ incorporated into the carbamate species is further reduced to the final formylmorpholine product, **58** was reacted with PhSiH₃ and TMG (5 mol%) in the absence of CO₂ under a N₂ atmosphere, Scheme 3.17. After 24 hours, no conversion to **24** was observed. This is in agreement with results of the silylcarbamate **49** which also required CO₂ to produce formylmorpholine **24**, thus **24** is not formed by the direct reduction of a morpholine carbamate species and instead another species must be involved for **24** synthesis.



Scheme 3.17: Reaction of morpholine carbamate **58** under N₂ gave no conversion to **24**

Morpholinium hydrochloride **59** was prepared by reaction of morpholine **18** with hydrogen chloride in ether, following a modified procedure reported by List.¹³⁸ Reaction of **59** with CO₂, PhSiH₃ and TMG (5 mol%) at room temperature gave only 2 % conversion to product **24**. This suggests that the morpholinium species must be deprotonated before reaction can occur.



Scheme 3.18: Reaction of morpholinium hydrochloride **59** to **24**

3.7 Role of TMG Catalyst

From the previously discussed kinetic profiling and investigations into the roles of intermediates, it is suggested that TMG is involved in the RLS of the reaction, which appears to be the reduction of CO₂. However, the exact role of TMG is unclear.

Guanidine catalysts typically operate by one of two modes of activation, either by acting as a nucleophile or as a superbases.⁹⁸ However, in the reductive functionalisation of CO₂ with amines and hydrosilanes, organocatalysts have been suggested to have a number of different potential roles. These include activation of CO₂, through either carbon or oxygen,^{32, 33, 37, 49} activation of the Si-H bond of the hydrosilane^{9, 13, 16} or stabilisation of a carbamate species,⁵⁹ Figure 3.32. Furthermore, solvent promoted systems are proposed to simultaneously activate the amine and Si-H bonds through tuning of solvation and polarisation effects and hydrogen bonding.^{73, 75, 78,}

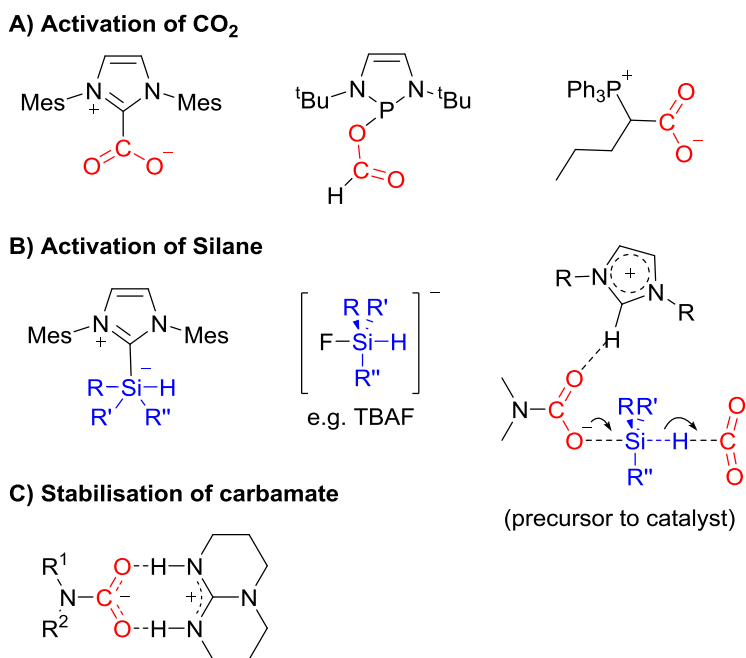
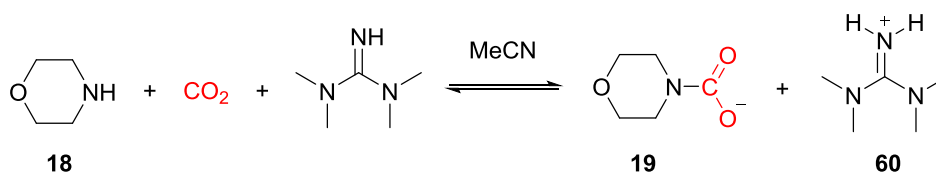


Figure 3.32: Proposed roles of organocatalysts for a) Activation of CO₂,^{32, 33, 37, 49} b) Activation of hydrosilane,^{76, 81, 83} and c) Stabilisation of carbamate⁵⁹

3.7.1 Carbamate Formation

Morpholine will react with CO₂ to form morpholinium carbamate species **19** & **20** in non-aqueous solutions.¹⁰⁷ TMG has a higher proton affinity than morpholine in acetonitrile as shown by the pK_a of conjugate acid in acetonitrile (TMG: pK_a(MeCN) = 23.3;¹³⁹ morpholine: pK_a(MeCN) = 16.6).¹⁴⁰ Thus, reaction of morpholine and TMG with CO₂ will lead instead to the formation of the morpholine carbamate **19** and guanidinium species **60** as the favoured products, Scheme 3.19. Monitoring the reaction by IR showed formation of a broad band at 1570 – 1550 cm⁻¹ corresponding to the C=O stretch and an absorption at 1269 cm⁻¹ corresponding to C-O stretch of **19**, ¹H NMR and ¹³C NMR supported formation of the species is favoured.



Scheme 3.19: Formation of morpholine carbamate **19** and TMGH⁺ **60** in CO₂

Previous work by Cantat suggested that the role of TBD as the catalyst was stabilisation of the carbamate species by hydrogen bonding, Figure 3.32c.⁵⁹ However, in this work when thiourea **46** was used to stabilise the carbamate as a co-catalyst with TMG, a slower rate of reaction was observed. These results suggest that although the morpholine carbamate **19** and corresponding

guanidinium ion **60** will form under reaction conditions, the stabilisation of the carbamate by TMG does not promote the reduction of the carbamate to the formylamide product.

3.7.2 Activation of CO₂

A number of studies have proposed that the role of the catalyst is to activate CO₂ through either the carbon or oxygen atom, Figure 3.32a.^{32, 33, 37, 49} However, in line with our previous study,¹⁰⁶ exposure of TMG to CO₂ in MeCN under reaction conditions did not lead to any observable complexation, Figure 3.33, thus suggesting that this is not the role of TMG.

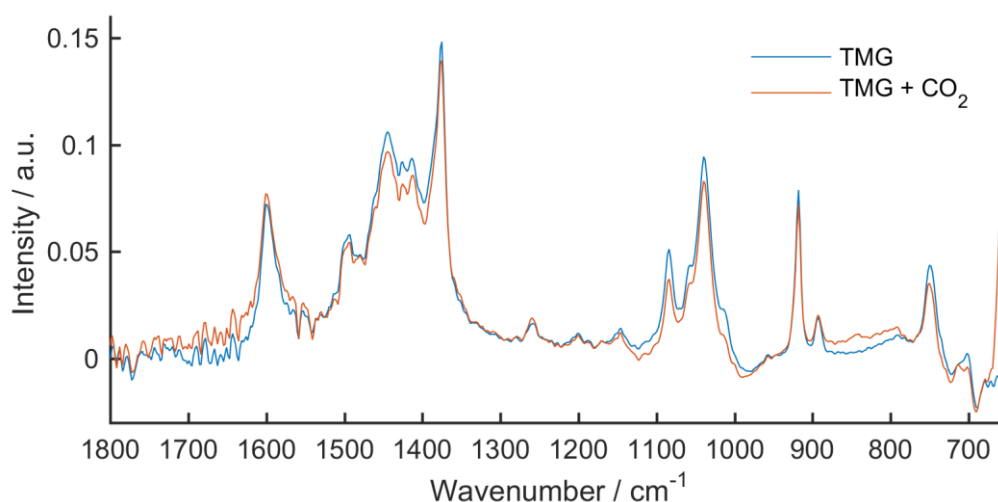


Figure 3.33: IR spectra in acetonitrile of TMG, TMG with CO₂ at 1.8 bar

3.7.3 Activation of Silane

Activation of the hydrosilane has also been proposed to occur with nucleophilic catalysts such as F⁻ ions, NHCs and ionic liquids to form pentacoordinate Si species.^{9, 16, 73} Activation of Si-H bonds has also been proposed to occur via intramolecular coordination of an amino group to give a pentacoordinate species.¹⁴¹ Thus potential interactions between TMG and PhSiH₃ were studied by ¹H NMR spectroscopy. Addition of 1 equivalent TMG to a solution of PhSiH₃ in CD₃CN gave only a small decrease in the chemical shift of the SiH signal by 0.005 ppm, Figure 3.34. A decrease in chemical shift would suggest an increase in electron density in the Si-H bond, thus potentially activating it towards CO₂. However, the change in chemical shift is small and is not conclusive as to whether the TMG alone is capable of activating the Si-H bond.

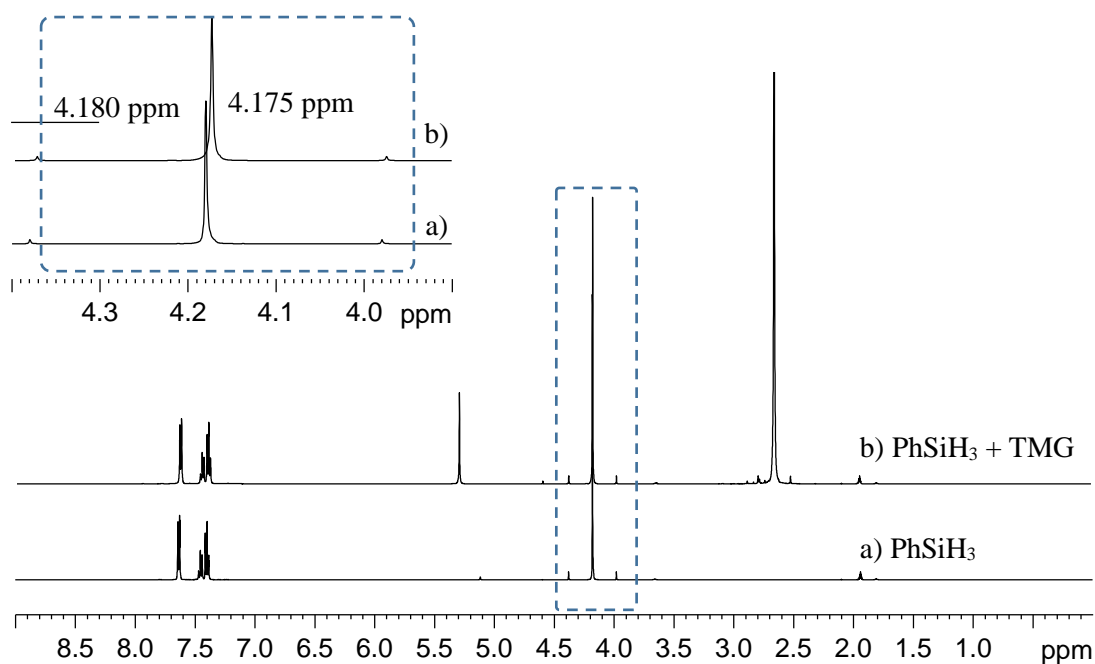
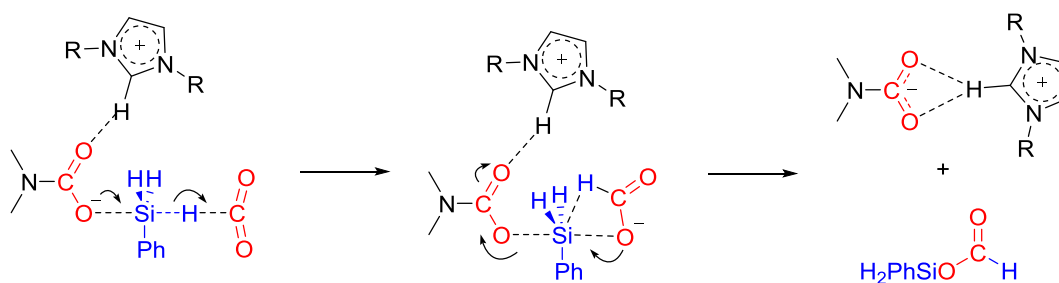


Figure 3.34: ^1H NMR spectra of a) PhSiH_3 (1 M), b) PhSiH_3 (1 M) and TMG (1 M) in CD_3CN . Inset: zoomed in spectra on SiH signal from PhSiH_3

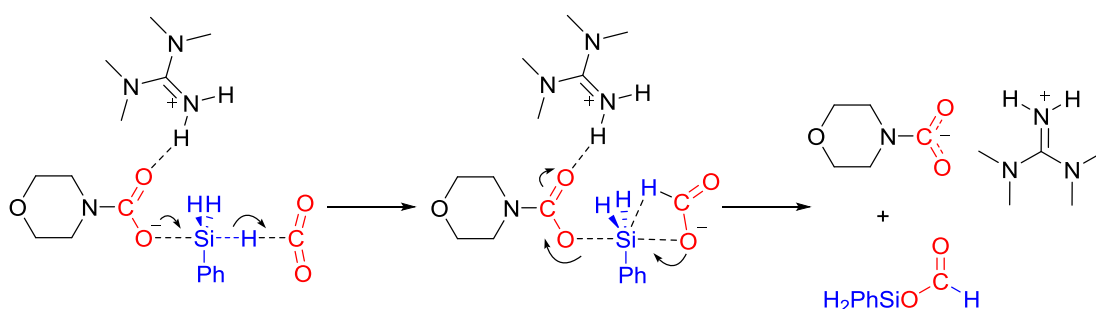
3.7.4 Precursor to Carbamate as Catalyst

Computational studies on the NHC catalysed formylation of amines have indicated that the NHC is a precursor to the actual catalyst, the ionic liquid: $[\text{NHCH}]^+[\text{Carbamate}]^-$.⁸³ In this case the NHC was found to stabilise the carbamate which in turn activates the hydrosilane via a concerted $\text{S}_{\text{N}}2$ nucleophilic attack through the O atom. The hydride can then react with free CO_2 which is more electrophilic than the CO_2 moiety in the carbamate. Reverse attack of the generated formate produces the formoxysilane intermediate, Scheme 3.20.⁸³ The NHC was also found to activate the transformylation of the amine through hydrogen bonding with NH of the free amine.⁸³



Scheme 3.20: Proposed role of NHC in route to formoxysilane intermediate reported by Li⁸³

Based on the discussed experimental evidence and suggestions from corresponding computational studies⁸³ a potential role of the TMG catalyst can be proposed. With TMG as the catalyst, it has been shown that in reaction with morpholine and CO₂, the guanidinium species TMGH⁺ **60** and morpholine carbamate **19** are produced, Scheme 3.19. Thus it is reasonable to propose that with TMG as the catalyst, the stabilised carbamate promotes the reaction by activating the silane, Scheme 3.21. This would begin to explain why the reductive functionalisation of CO₂ with amines can occur at both 23 and 60 °C (as the carbamate is formed), whereas in the hydrosilylation of CO₂ (i.e. no amine present) the reaction can only proceed at high temperatures and thus must be operating by a different pathway.



Scheme 3.21: Proposed role of TMG in route to formoxysilane intermediate

It is not clear if TMG is involved in the transformylation step of formoxysilane with morpholine as the formoxysilane intermediate has not been synthesised in the absence of catalyst. However, computational studies suggest the NHC catalyst could lower the activation barrier by interaction with the amine.⁸³ ¹H NMR studies of morpholine and TMG show interaction between the N-H of morpholine and NH of TMG and thus may also play a role in the transformylation step.

3.8 Summary of Pathways to Formylmorpholine

The results of the mechanistic study suggest that multiple pathways may be operating in the synthesis of formylmorpholine and that the catalyst may have multiple roles. These can be generalised as one pathway which proceeds predominantly at lower temperatures (i.e. RT, Scheme 3.22a) and a second that is only possible at higher temperatures, Scheme 3.22b.

In the low temperature pathway, the reaction equilibration period (Step A1) enables the formation of morpholinium carbamate **19** & **20** as a white precipitate. If TMG is present then the corresponding morpholine carbamate **19** and guanidinium species **60** will also be present in solution. Addition of PhSiH₃ (Step A2) leads to the formation of a silylcarbamate species **49** and evolution of H₂, which corresponds with the observed dissolution of the white precipitate and the evolution of a gas.

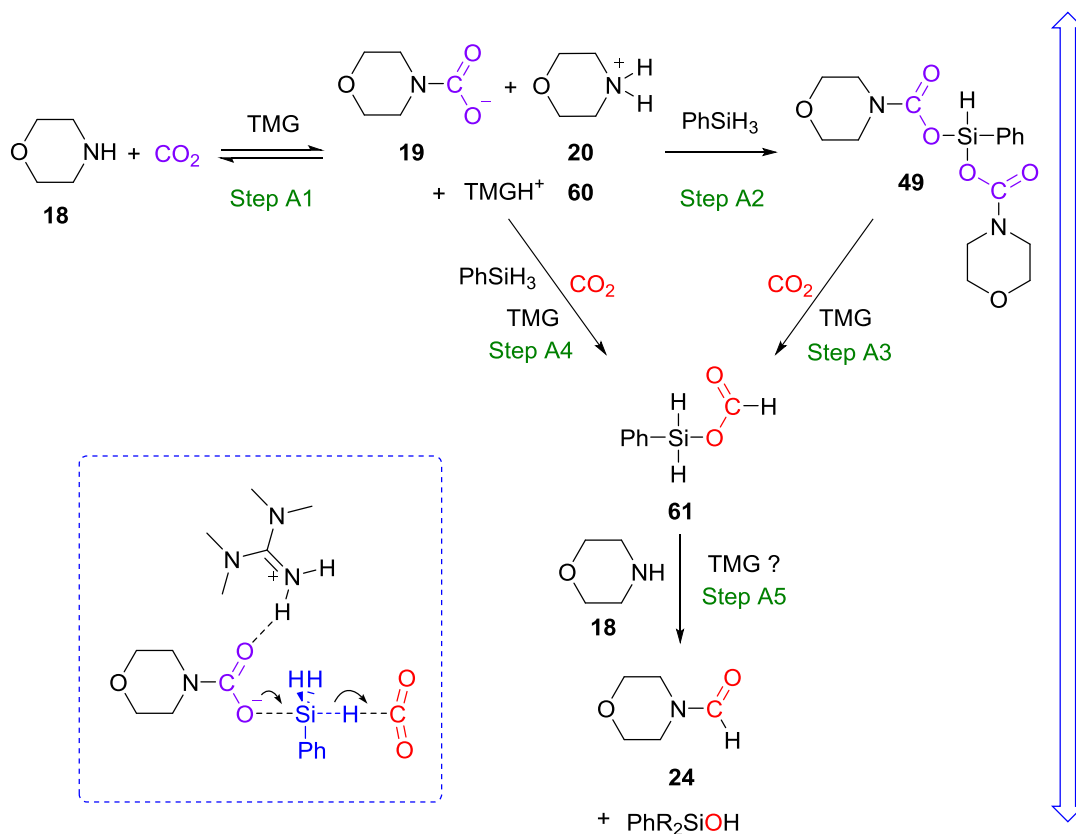
The silylcarbamate species **49** can react in the presence of TMG and CO₂ to yield the formylmorpholine product **24**. However, as this transformation requires CO₂ to proceed, it suggests that the silylcarbamate is not reduced directly to give the formylamide and instead another species must be involved. Thus, it is proposed that the carbamate activates the Si-H bond enabling hydride transfer to a free CO₂ molecule, which is more electrophilic than the CO₂ in the carbamate species, as proposed by Li.⁸³ The formate species can then react with the silane species to yield a formoxysilane intermediate (Step A3) releasing the morpholine carbamate. This is also supported by the observation of formoxysilane by *in situ* IR spectroscopy when the reactivity of the silylcarbamate species in CO₂ was monitored, and the absence of formoxysilane for the same reaction under N₂ (Figure 3.20, Section 3.4.4). It is proposed that this is the rate limiting step of the reaction and the role of TMG is proposed to be the stabilisation of the carbamate species. It is however possible that the formoxysilane species may also form directly from reaction of the morpholine carbamate **19** with PhSiH₃ and CO₂, without the formation of a discrete silylcarbamate species **49** (Step A4). However, due to the rapid formation of the silylcarbamate this could not be determined.

In the final step (Step A5) nucleophilic attack of morpholine **18** with formoxysilane intermediate **61** would then yield the formylamide product **24** and silanol byproducts. The TMG may also promote this step through activation of the morpholine.

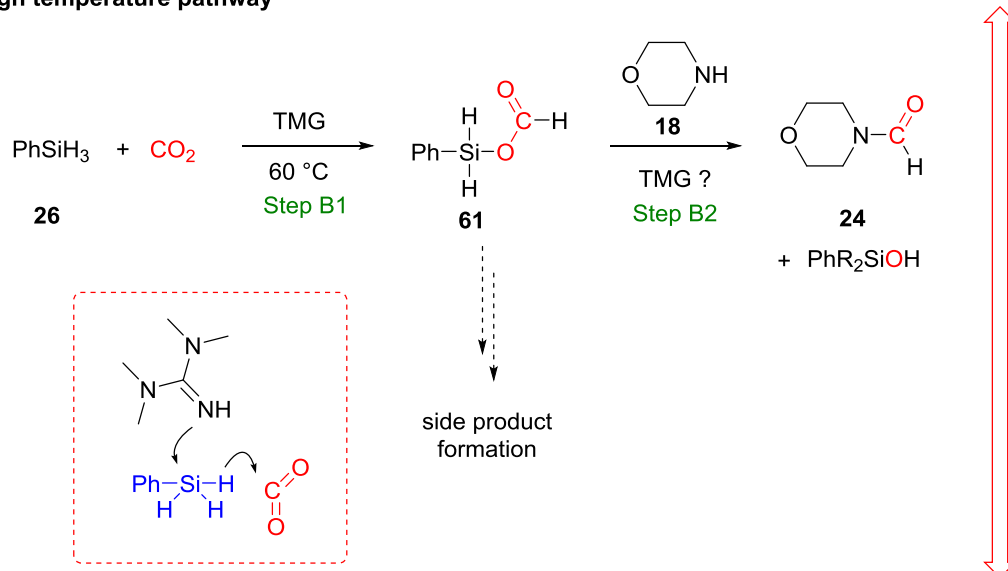
At higher temperatures (60 °C) a second pathway has also been found to be feasible, Scheme 3.22b. In this pathway the PhSiH₃ can react with CO₂ to form a formoxysilane intermediate **61**, Step B1. This reaction can only occur at high temperatures in the presence of the catalyst. As there is no amine in this reaction to form the carbamate species, a different mechanism of activation mode must be in operation. TMG cannot react with CO₂ under the reaction conditions and thus instead it is proposed that the hydrosilane is activated by co-ordination of the TMG to the Si species to form a hypervalent species. In a similar manner to above, this would enable hydride transfer to free CO₂ and the produced formate can then react again back with the Si species to produce formoxysilane. Transformylation with morpholine **18** (Step B2) would then yield the formylmorpholine **24** product.

The formation of side products methylmorpholine **48** and aminor **57** was also observed when the reactions were carried out at 60 °C. This suggests that the side products are formed from the higher temperature activation pathway, either by further reduction of the formoxysilane species or via subsequent reaction of the formylmorpholine. This pathway is discussed in more detail in Chapter 5.

a) Low temperature pathway



b) High temperature pathway



Scheme 3.22: Proposed pathways and roles of TMG at a) low and b) high temperature for the synthesis of formylmorpholine

3.9 Conclusions

Guanidine catalysts have been demonstrated to be efficient catalyst for the synthesis of formylamides via the reductive functionalisation of CO₂ with amines and a hydrosilane reductant. TMG was shown to be a favourable catalyst, as a relatively cheap and readily available guanidine, which gives high conversions within four hours at RT. This is an improvement over the previously reported guanidine, TBD, which was significantly more expensive and required longer reaction times (24 h) and high temperatures (100 °C). The reaction rate was found to be dependent upon concentration of catalyst, CO₂ and either morpholine and/or PhSiH₃, however the exact rate law could not be determined.

Mechanistic investigations highlighted that the formylamide is produced via transformylation of a formoxysilane intermediate with the amine to give the formylamide. The formoxysilane intermediate was proposed to form via two different pathways. The first pathway operates at low temperature through activation of the silane by a carbamate species stabilised by TMG, whereas the second pathway proceeds at higher temperatures by activation of the silane directly by TMG. A silylcarbamate species was also observed to form in the reaction and is proposed to be involved in activating the silane via the carbamate species at low temperatures. These results indicate that the rate limiting step is the reduction of CO₂ to form the formoxysilane, rather than the transformylation step.

The involvement of a formoxysilane intermediate supports other experimental studies into the formylation of amines with catalysts such as polyNHCS,⁵¹ imidazolium ionic liquids^{73, 75} and diazaphospholenes.³³ The proposed activation route of the silane via a carbamate species supports a computational study reported by Li with NHC catalysts and provides some of the first experimental evidence that the catalyst, CO₂ and the amine are required to give the fast reaction rate.⁸³ Based on this study it is also proposed that the silane may also be activated by TMG at high temperatures, which has previously been found to be unfavourable with carbene catalysts,⁸³ however the activation of silanes by intramolecular coordination of an amino group to give a pentacoordinate species has previously been reported.¹⁴¹ Further work is required to confirm if this pathway is feasible with guanidine catalysts.

The observation of a silylcarbamate species is consistent with a recent experimental study reported by Li, however Li proposed its formation through a silylamine species, which was not supported by our work.⁷⁸ Furthermore, Li did not report any observation of a formoxysilane species. Although we have found that the silylcarbamate cannot be directly reduced to give the formylamide species under reaction conditions, it is not known if an alternative pathway to the formylamide product (which does not involve the formoxysilane pathway) is possible. It is also

possible that the silylcarbamate is not required, and is simply a competing reaction which still provides an active sink of morpholine.

Whilst the results of this mechanistic study have provided strong experimental support for computationally proposed mechanisms, this study has only focussed on the use of morpholine as a substrate and TMG as the guanidine catalyst. The reductive functionalisation of CO₂ with aromatic amines has also been reported to be successful with a range of catalysts.^{72-74, 76} However the lower pK_a of aromatic amines compared to morpholine (e.g. pK_a(MeCN): morpholine = 16.61, aniline = 10.56),¹⁴⁰ and lower nucleophilicities (e.g. morpholine: 15.65,¹⁴² aniline: 12.64¹⁴³ in MeCN) may affect the equilibrium of amine/carbamate species as well as the formation of the silylcarbamate. Furthermore, whilst TMG cannot activate CO₂, other guanidines, such as MTBD and TBD, are known to form CO₂ adducts and as such may provide additional alternative activation pathways that need to be considered.

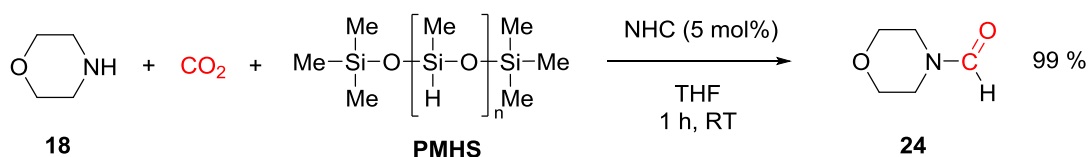
Chapter 4

Guanidine Catalysed Reductive Functionalisation of CO₂: Catalyst Optimisation and Scope of Amine Formylation

4.1 Introduction

In Chapter 3, guanidine catalysts were demonstrated to be effective catalysts for the reductive functionalisation of CO₂ with amines and hydrosilanes to yield formylamide products; however, relatively high catalyst loadings (5 mol%) were utilised. This is common for the reductive functionalisation of CO₂ with hydrosilanes, which typically requires loadings of at least 5 mol%. The most active organocatalysts reported for this system are diazaphospholenes, which gave TOF of up to 38 h⁻¹ and TON of up to 19 for secondary aliphatic amines with diphenylsilane as the reductant.³³ Compared to similar metal catalysed systems, however, these are inefficient. For example, a copper catalysed system reported by Baba operated at catalyst loadings lower than 0.1 mol% and achieved TON up to 9000 and TOFs of 2180 h⁻¹.⁸⁴ Whilst low catalyst loadings (0.05 mol%) and high TON (1840) have been reported for the NHC catalysed reduction of CO₂ with hydrosilanes,³⁷ this has not yet been extended to the organocatalysed reductive amination of CO₂ with hydrosilanes.

Another important aspect in CO₂ utilisation reactions is that the newly developed reactions are equally or more sustainable than those that they replace.⁴ Therefore a number of criteria including reaction efficiency and the reagents used must be considered. The use of hydrosilanes as reductants is attractive due to their highly tuneable reactivity and wider substrate scope, however they are typically more expensive and less atom efficient than the use of hydrogen as the reductant.⁶⁰ Consequently, there has been a drive to use alternative silane reductants derived from waste streams. Such an example is polymethylhydrosiloxane (PMHS), which is a low cost, less toxic and more stable alternative to hydrosilanes,⁴⁸ and a number of carbene catalysts have been reported to use this reductant, e.g. Scheme 4.1.^{72, 74}



Scheme 4.1: Example reaction of PMHS used as a reductant in the reductive functionalisation of CO₂ with amines using an NHC catalyst⁷²

This chapter reports attempts to understand the requirement for high catalyst loadings in the guanidine catalysed reductive functionalisation of CO₂ with amines and hydrosilanes. On the basis of the understanding gained, more efficient catalysts were developed. The use of a more sustainable reductant was also investigated and the substrate scope of the reaction studied.

4.2 Reducing Catalyst Loadings

4.2.1 Catalyst Deactivation

Lowering the catalyst loading of TMG from 5 to 1 mol% in the synthesis of formylmorpholine **24** from morpholine, PhSiH₃ and CO₂ led to a slower rate of reaction and an overall reduction in conversion, Figure 4.1. The reduction in conversion was particularly noticeable when the reaction was performed at 60 °C. One explanation for this could be deactivation of the catalyst, which occurs predominantly at higher temperatures.

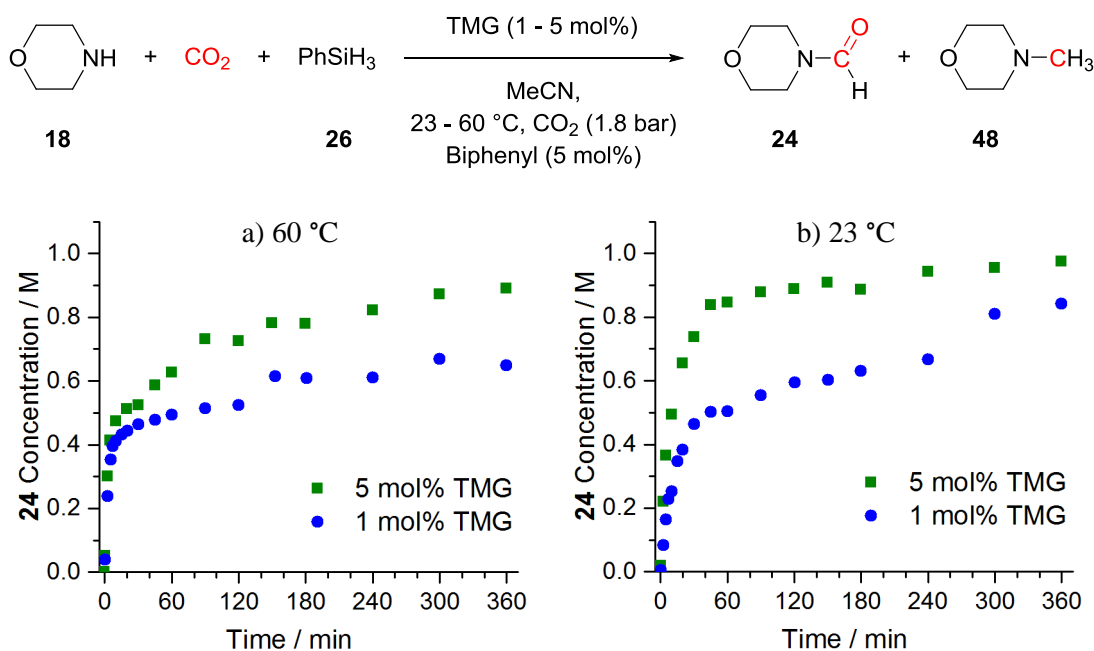


Figure 4.1: Effects of lowering catalyst loadings on formation of formylmorpholine **24** at a) 60 °C, b) 23 °C. Reaction conditions: **18** (2 mmol), PhSiH₃ (2 mmol), TMG (0.02 - 0.1 mmol), MeCN (2 mL), biphenyl (0.1 mmol), CO₂ (1.8 bar). Concentrations determined by GC

To probe possible deactivation pathways, a stoichiometric reaction of TMG with PhSiH₃ and CO₂ (i.e. no morpholine) was performed at 23 and 60 °C, Figure 4.2a. The major product of the reaction was characterised as 2-formyl-1,1,3,3-tetramethylguanidine (Formyl TMG) **62** based on HRMS-ESI ([M+H]⁺ found m/z = 144.1189, calculated: 144.1131), NMR and IR spectra which were in agreement with reported literature values, Figure 4.2b & c.¹⁴⁴ A second species was also observed at the end of the reaction (¹H NMR δ: 8.64 ppm), however the identity of this species is unknown. At 60 °C the reaction proceeded rapidly and monitoring by IR spectroscopy

showed a rapid decrease in TMG and a rapid increase in formylTMG in the first 2 minutes of reaction, Figure 4.2. The formation of a white precipitate, due to the silanol and siloxane by-products, prevented monitoring the entire reaction by IR, however analysis by HRMS showed the reaction reached completion within 20 minutes. At 23 °C, 24 hours was required to reach full conversion of TMG.

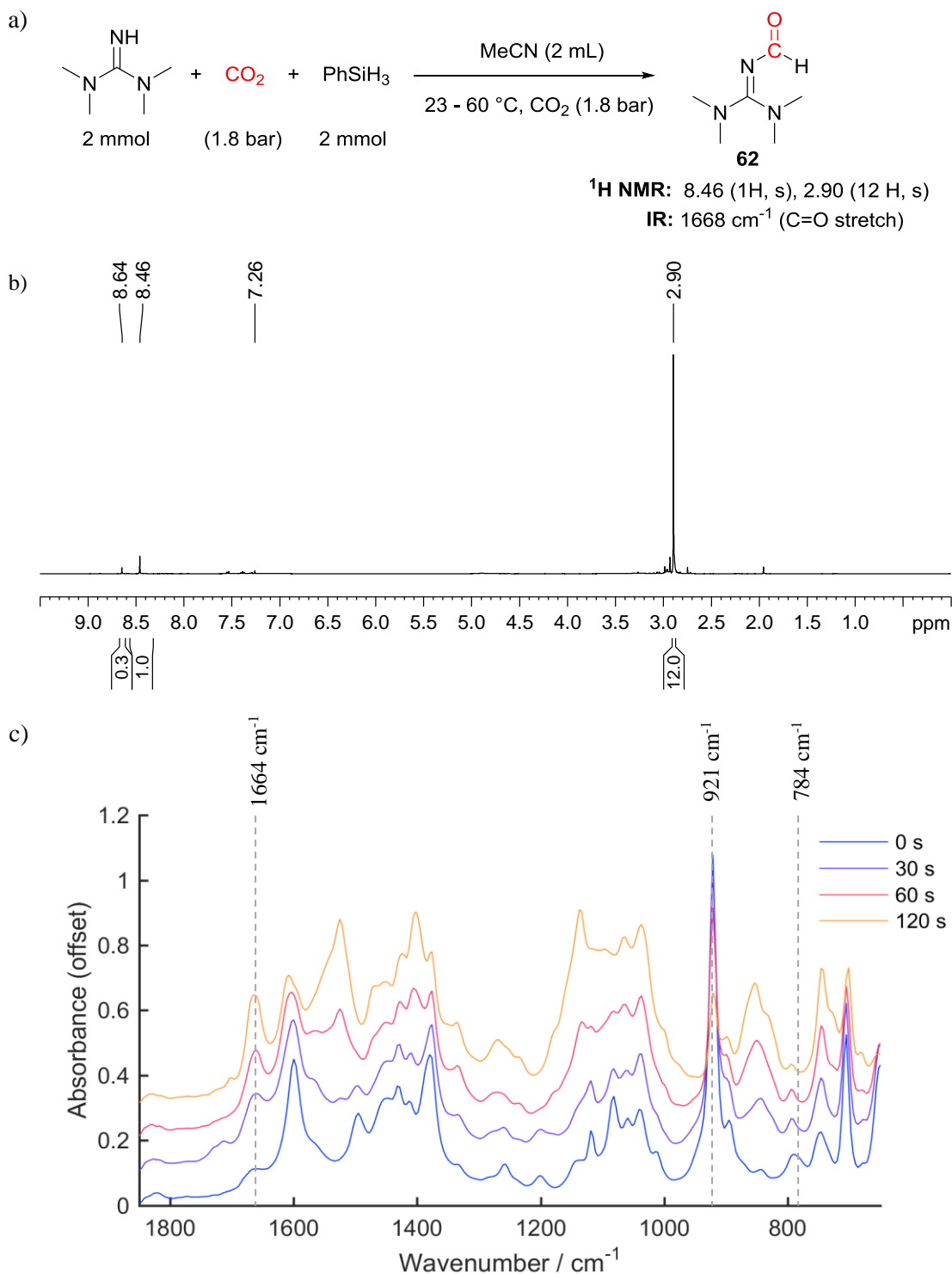


Figure 4.2: Stoichiometric reaction of TMG with PhSiH₃ and CO₂ to probe catalyst deactivation pathway. a) Reaction scheme; b) ¹H NMR spectra of formylTMG **62**; c) FTIR spectra over time of formylation of TMG at 60 °C, FormylTMG (1664 cm⁻¹), PhSiH₃ (921 cm⁻¹), TMG (784 cm⁻¹)

The deactivation of TMG to formylTMG **62** during its use as a catalyst in the reductive functionalisation of CO₂ with morpholine was investigated by monitoring the catalytic reaction at 23 °C by ¹H NMR spectroscopy. A peak corresponding to the N(Me)₂ protons in the protonated catalyst TMGH⁺ at 2.94-2.96 ppm (TMGH⁺Cl⁻ reported at 2.98 ppm)¹⁴⁵ was observed to decrease over the first 120 minutes of reaction, this was concurrent with the increase of peaks at 2.91 and 8.53 ppm assigned to the N(Me)₂ and C(O)H protons of formyl TMG, Figure 4.3a.

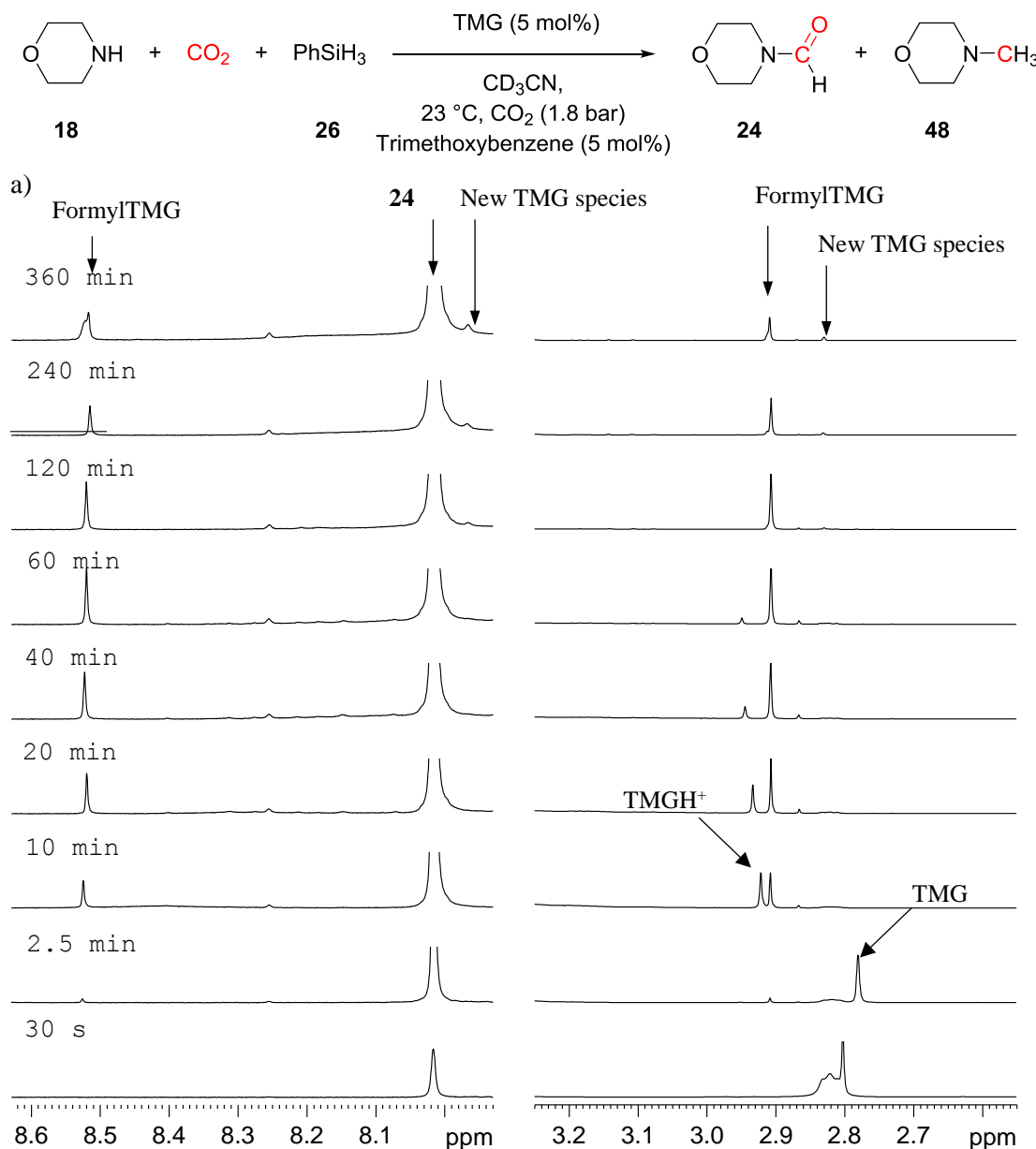


Figure 4.3: ¹H NMR monitoring decomposition of TMG in reaction to FormylTMG **62** during catalytic reaction at 23 °C. Reaction conditions: **18** (2 mmol), PhSiH₃ (2 mmol), TMG (0.1 mmol), CD₃CN (2 mL), 1,3,5-trimethoxybenzene (0.1 mmol), CO₂ (1.8 bar) a) ¹H NMR spectra, b) Trends from ¹H NMR (continued over page)

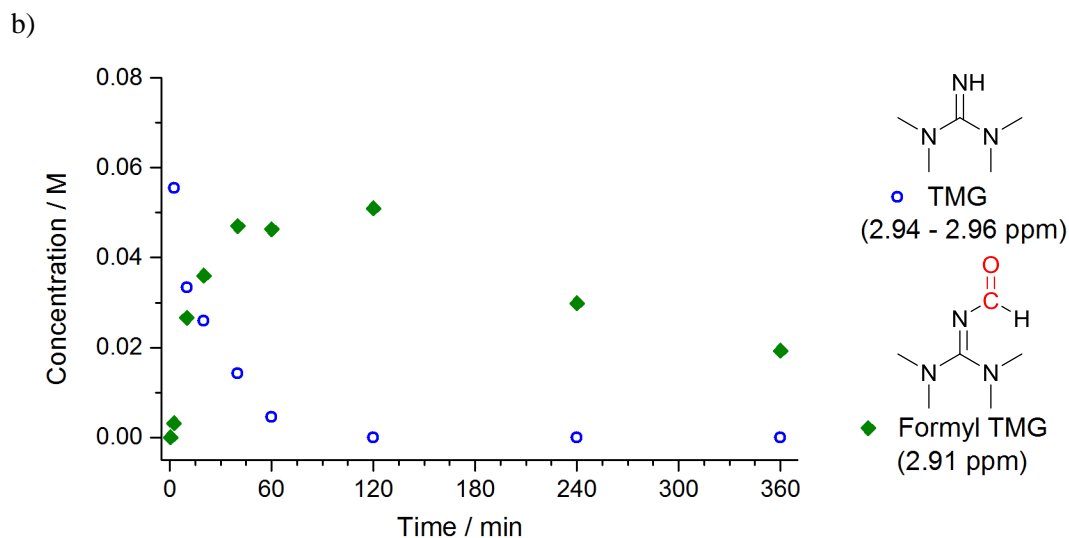


Figure 4.3 continued: b) Trends from ^1H NMR monitoring experiment

This highlights that the deactivation of TMG to formylTMG occurs faster in the catalytic reaction than the corresponding stoichiometric reaction (when no morpholine was present) which required 24 h.

After 4 hours the concentration of formyl TMG in the reaction was observed to decrease. This corresponded with an increase in signals at 7.97 and 2.82 ppm in ^1H NMR spectra, suggesting that the formylTMG may have decomposed to a different formyl species, Figure 4.3b. To probe this further, the formylTMG was prepared from the stoichiometric reaction of TMG with PhSiH_3 and CO_2 at 60°C . After completion, a second equivalent of PhSiH_3 was added and the reaction stirred overnight at 60°C . However, no further reduction of formylTMG or any new species were observed, thus suggesting that decomposition of formylTMG is dependent on the presence of morpholine species in the catalytic reaction.

Monitoring the catalytic reaction (i.e. with morpholine present) by HRMS showed the presence of species **63** (observed m/z : 213.1730) which may occur from transamidation of morpholine with formylTMG, and **62** (observed: 144.1124) which is observed more strongly in reactions with an excess of PhSiH_3 or at 60°C . However, **63** was not observed in ^1H NMR and thus may only be present in very small amounts or is undergoing exchange.

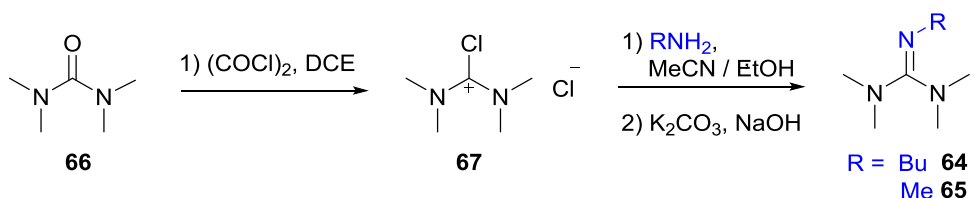
	TMG	62	63
	[M+H] ⁺	[M+H] ⁺	M
Calculated m/z:	116.1182	144.1131	213.1710
Observed m/z:	116.1212	144.1124	213.1730

Figure 4.4: Proposed catalyst deactivation species

The conversion of TMG to formylTMG within 40 minutes of initiation of the catalytic reaction may account for the reduced conversion to formylmorpholine **24** observed at lower catalytic loadings, particularly at 60 °C. It is expected that the formylation of TMG would decrease the nucleophilicity and basicity of the catalyst, thus reducing its activity.

4.2.2 Catalyst Optimisation

To prevent this deactivation, it was proposed that alkylating TMG at the NH position would prevent formylation of the catalyst, leading to a more stable catalyst of use at low catalytic loadings. Thus, alkylated catalysts, 2-butyl-1,1,3,3-tetramethylguanidine (ButylTMG) **64** and pentamethylguanidine (MethylTMG) **65**, were prepared. Guanidines **64** and **65** were prepared from tetramethylurea **66** based on modified procedures reported by Hodson and Elabd, Scheme 4.2.^{146, 147} In the first step, addition of oxalyl chloride to tetramethylurea **66** gave tetramethylchlorformamidinium chloride **67** as a yellow solid, to which addition of the corresponding amine and an aqueous work up yielded the desired guanidines **64** and **65**.



Scheme 4.2: General procedure for synthesis of alkylated TMG

The activities of the alkylated catalysts were evaluated in the reductive functionalisation of CO₂ with morpholine at 23 °C. At 5 mol% loading, alkylated catalysts **64** and **65** gave a faster rate of conversion to **24** than TMG, reaching full conversion to **24** (96 %) in 120 mins, Figure 4.5.

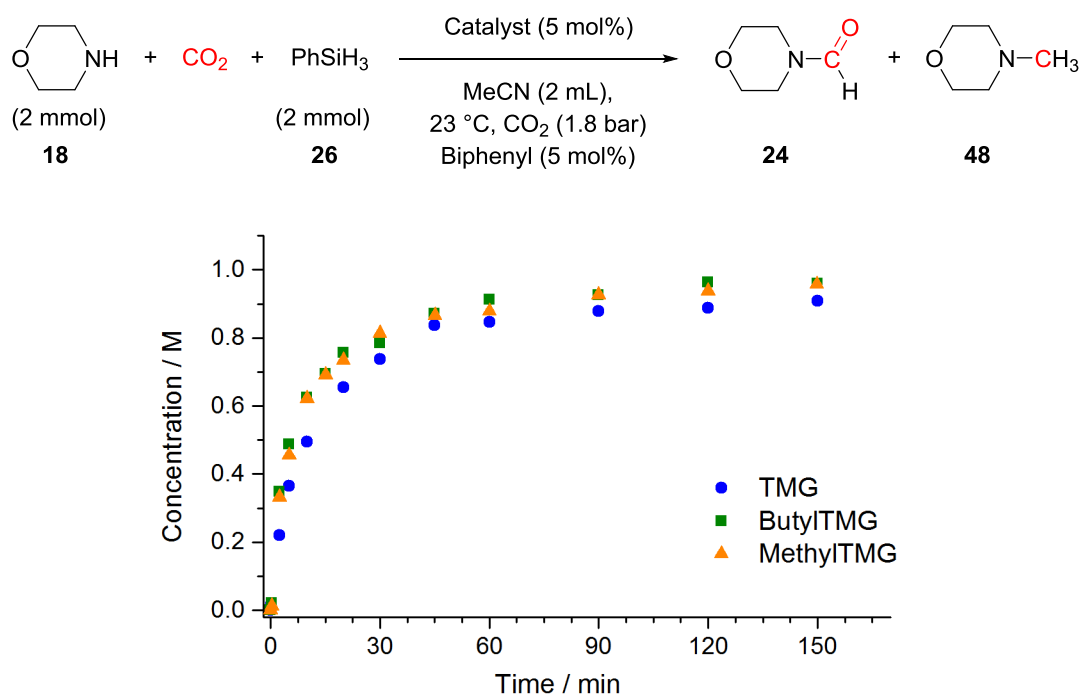


Figure 4.5: Comparison of catalyst activities at 23 °C. Reaction Conditions: **18** (2 mmol), PhSiH₃ **26** (2 mmol), catalyst (0.1 mmol), MeCN (2 mL), biphenyl (0.1 mmol), CO₂ (1.8 bar), 23 °C

Alkylated catalysts **64** and **65** also showed higher catalytic activity at 1 mol% loading than non-alkylated TMG, particularly at the later stage of the reaction after 120 mins, where the activity of TMG is significantly lower, Figure 4.6a. Comparing the effect of catalyst loading using butyl TMG **64** showed a slower rate of reaction at 1 mol% than 5 mol% loading; however full conversion was still achieved by 4 hours, suggesting that the catalyst is not being deactivated, Figure 4.6b. The faster kinetics of butylTMG over TMG may be due to prevention of deactivation, enabling more of the active catalyst to be available throughout the entire reaction. However, alkylation at the NH position would also be expected to alter the nucleophilicity and basicity of the catalyst. For example, in acetonitrile the pK_a of TMG is reported as 23¹³⁹ and methylTMG **65** was found to be 25.¹⁴⁸ Thus, alkylated catalysts may give higher conversion due to increased basicity, as well as being more stable and preventing deactivation.

Reducing the catalyst loading of butylTMG **64** further to 0.1 mol% led to a slower rate of reaction, however 80.5% conversion to formylmorpholine **24** was achieved after 24 h. This correlates to TON of 805 and TOF of 33.5 h⁻¹. A TON of 805 represents the high stability of the catalyst, only the NHC catalysed hydrosilylation of CO₂ reported by Ying *et. al* has a higher TON (1840) for an organocatalysed reduction of CO₂ with hydrosilanes.³⁷ TOF again highlights the high activity of the catalyst, however the reductive functionalisation of CO₂ with amines and hydrosilane using a diazaphospholene catalyst has been reported to achieve TOF of 38 hr⁻¹.³³

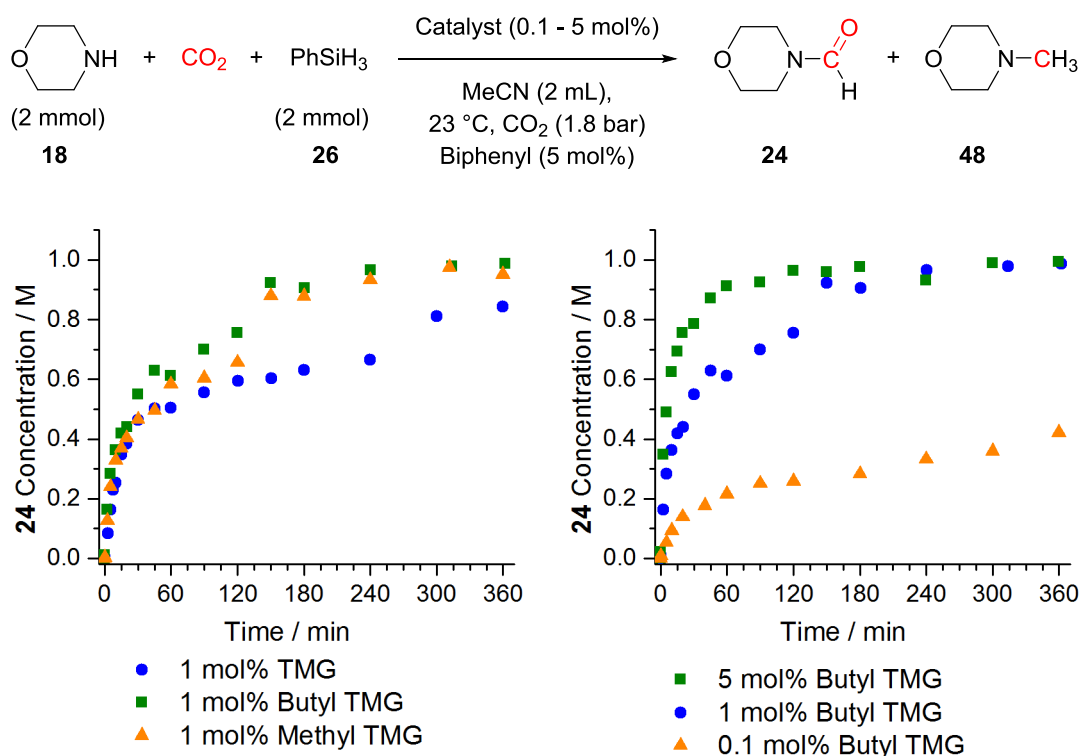


Figure 4.6: Comparison of catalytic activity at 23 °C. Reaction Conditions: **18** (2 mmol), PhSiH₃ (2 mmol), catalyst (0.002 - 0.1 mmol), MeCN (2 mL), biphenyl (0.1 mmol), CO₂ (1.8 bar), 23 °C

When the alkylated catalysts were evaluated at 60 °C, a change in selectivity of the reaction was observed. Catalysts **64** and **65** gave full conversion of **18** within 60 mins, however they gave a lower conversion to formylamide **24** compared to when TMG was used, this was accounted for by an increase in conversion to methylmorpholine **48** and the aminor, dimorpholinomethane **57**, Figure 4.7.

Use of butylTMG **64** led to a higher conversion to methylmorpholine compared to TMG, 19 % and 12 % respectively, and a small amount of aminor **57** at 12 %, Figure 4.7. Most interestingly though are the formation kinetics of methylmorpholine **48**, which is produced from the beginning of the reaction, contrasting to with TMG as the catalyst, whereby **48** only begins to form after 60 mins, Figure 4.7. With methyl TMG **65** the same rate of conversion to formylmorpholine was observed as with **64**, however the ratio of aminor **57** to methylmorpholine produced was altered giving 6 % **48** and 21 % **57** respectively, Figure 4.7. These results suggest that the alkylated catalysts may have a different effect on the reaction pathway to the methylmorpholine product than TMG, rather than solely preventing catalyst deactivation.

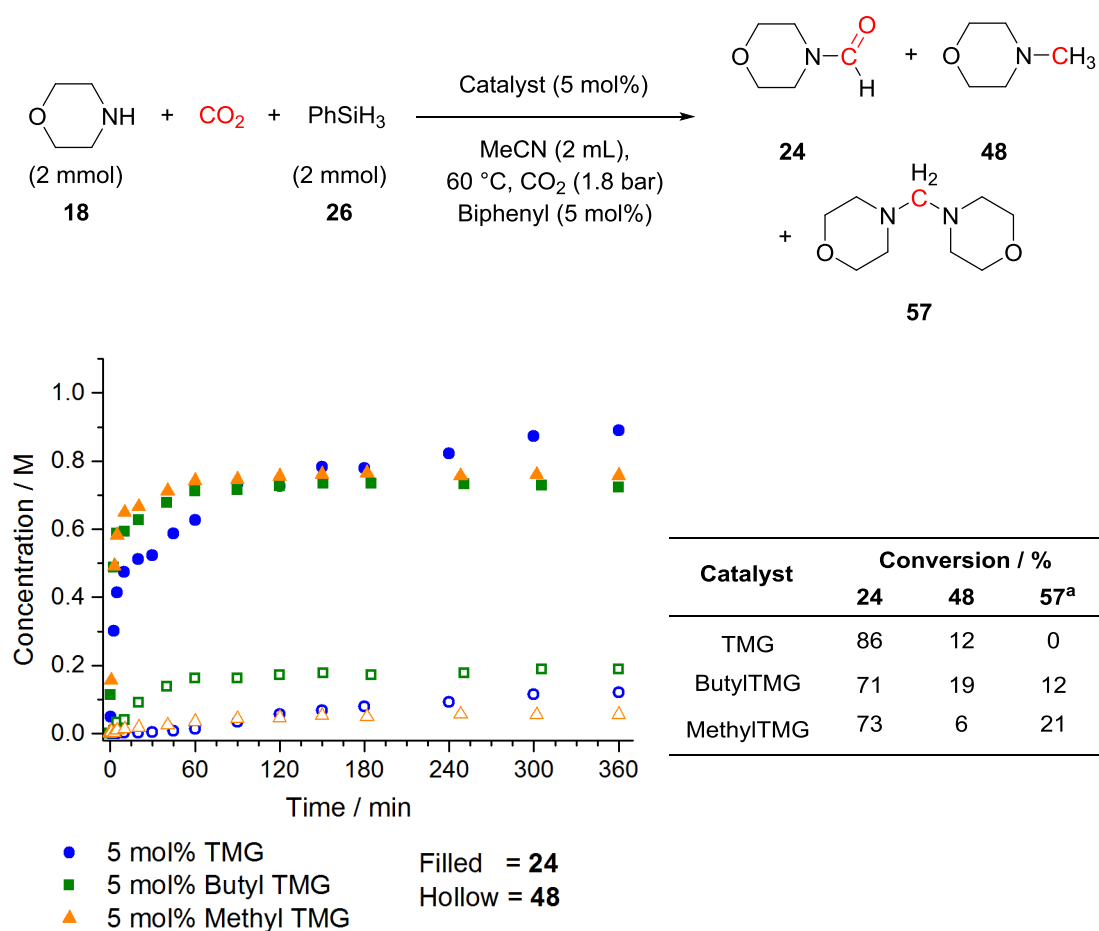


Figure 4.7: Comparison of alkylated catalysts at 60 °C at 5 mol% loading. Reaction Conditions: **18** (2 mmol), PhSiH₃ (2 mmol), catalyst (0.1 mmol), MeCN (2 mL), biphenyl (0.1 mmol), CO₂ (1.8 bar), 60 °C. Conversions determined by GC ^a Conversions to **57** determined by ¹H NMR

4.3 Reaction Scope

4.3.1 Alternative Reductant

Whilst phenylsilane has been demonstrated to be an efficient reductant in the reductive functionalisation of CO₂, it is still relatively expensive for use on a large scale and its sensitivity to moisture is unfavourable. Thus alternative polysiloxanes as reductants were sought. In particular the use of PMHS as a reductant is attractive as it is non-toxic, readily available, cheaper and more stable to moisture and air than phenylsilane.⁴⁸

The reductive functionalisation of CO₂ with morpholine was investigated using tetramethyldisiloxane (TMDS) and PMHS as the reductants. Using 5 mol% TMG as the catalyst at 60 °C, PMHS was shown to be a more active siloxane than TMDS, giving formylmorpholine **24** at a yield of 67 % as opposed to 11 % with TMDS after 6 hours, Figure 4.8a. However these are both less active than PhSiH₃ which gave 86 % conversion after 6 hours. Increasing reaction time led to higher yields of formylmorpholine with PMHS and TMDS of 78 % (22 h) and 33 %

(24 h) respectively. Whilst on the addition of PhSiH_3 evolution of gas is observed, when PMHS was added, no bubbles of gas were observed. This may indicate that an alternative reduction mechanism is occurring compared to with PhSiH_3 . The increased activity of PMHS over TMDS may suggest that intramolecular transfer of the species responsible for the activation of the Si-H between sites is promoting the reaction.⁴⁸ In all cases reduction with PMHS was selective to the formylmorpholine **24** product and none of the methylmorpholine **48** product was observed.

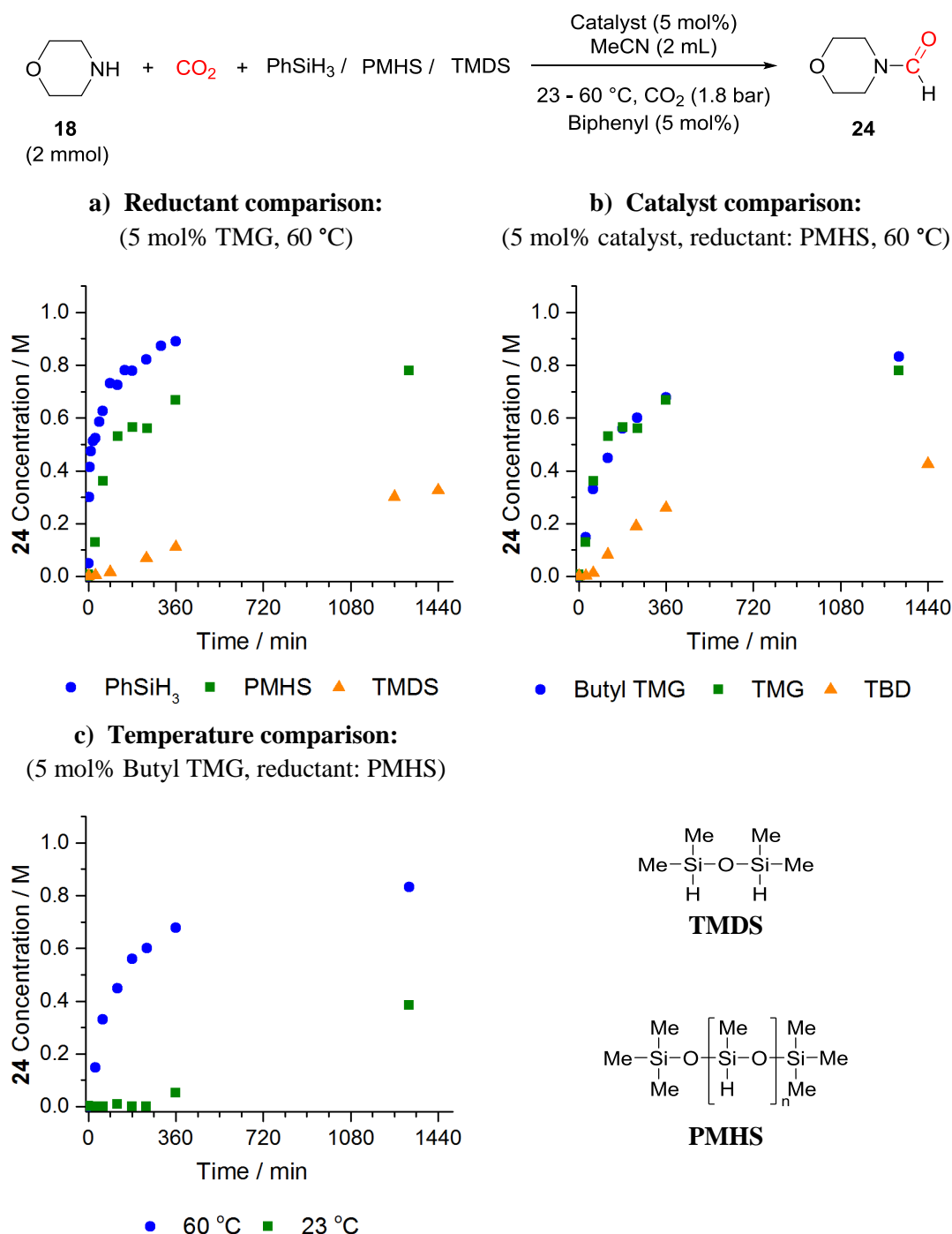


Figure 4.8: GC kinetics of reductive functionalisation of CO_2 with **18** to give **24** with alternative reductants. Standard Conditions: **18** (2 mmol), Reductant (3 Si-H equiv.), catalyst (0.1 mmol), MeCN (2 mL), biphenyl (0.1 mmol), CO_2 (1.8 bar), 60 °C. Conversions determined by GC

As the most active and cheaper siloxane reducing agent, the use of PMHS was further studied. At 60 °C use of TMG and butyl TMG made no difference to reactivity, however using TBD instead led to a lower conversion of 43 % after 24 h, Figure 4.8b. Reducing the reaction temperature to 23 °C led to a slower rate of reaction, with production of formylmorpholine only beginning after 4 hours of reaction, Figure 4.8c. However, during this initial 4 hours at room temperature, two layers were observed in solution, this may be the separation of the solution containing the morpholinium carbamate species, and the other being PMHS, Figure 4.9a. This is contrasting to the reaction at 60 °C whereby the reaction was uniformly mixed, Figure 4.9. This suggests that inefficient mixing due to the high viscosity of PMHS may be the cause of this initiation period at room temperature, and thus more effective stirring methods should be investigated.

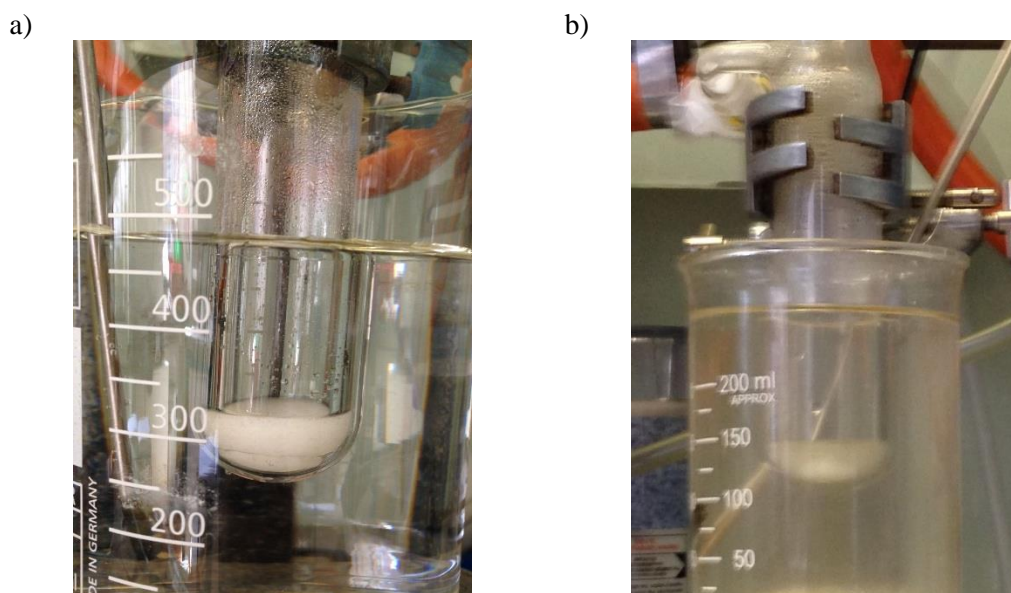
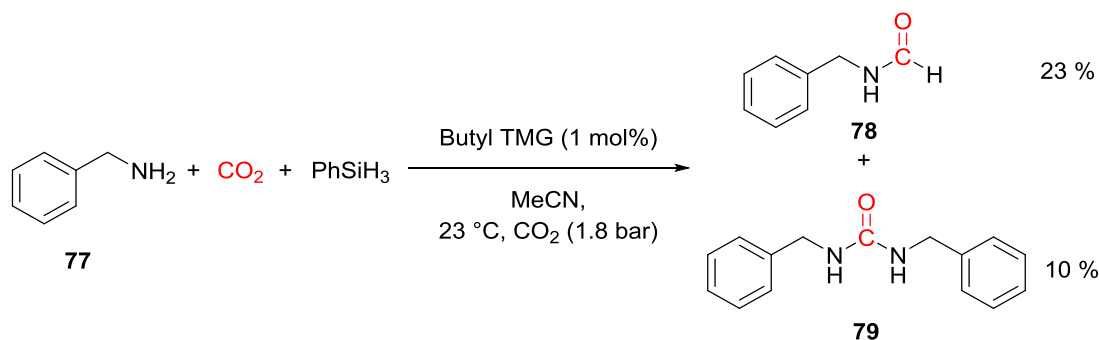


Figure 4.9: Photo of reaction mixture with PMHS reductant 60 mins into reaction a) 23 °C and b) 60 °C

4.3.2 Substrate Scope

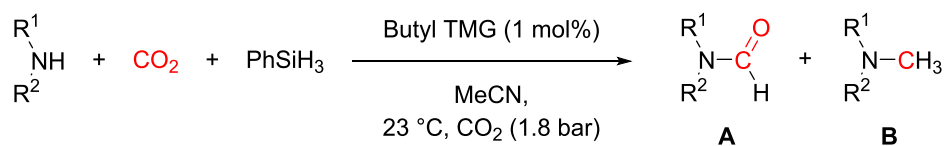
The substrate scope of the newly improved catalyst **64** at 1 mol% loading at 23 °C with phenylsilane as the reductant was explored, Table 4.1. Aliphatic and aromatic secondary amines: morpholine **18**, piperidine **31**, *N*-methylbenzylamine **68** and *N*-methylaniline **37** gave high yields (84 - 96 %) of formylated product in 8 hours (Entries 1-4, Table 4.1). Analysis by GC-MS showed the major side product of these to be the *N,N*-dimethyl product (yields 4 – 10 %). Reaction of 4-chloro-*N*-methylaniline **71** required longer reaction time to reach completion (84 % yield after 22 h), but also gave a larger amount of the methylated amine (13 %), suggesting electron poor substituents may favour *N*-methylation. Use of electron withdrawing 4-nitro-*N*-methylaniline **73** gave no conversion after 22 hours.

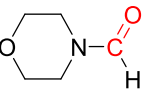
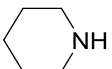
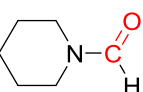
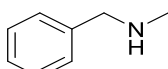
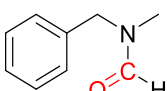
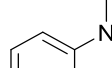
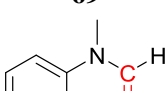
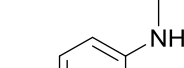
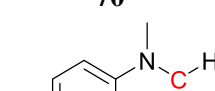
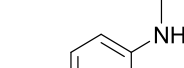
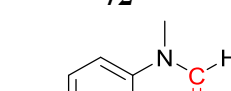
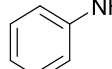
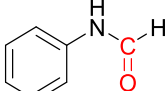
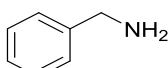
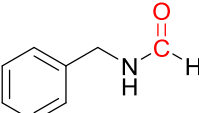
With primary amines, aniline **75** gave >99 % conversion to *N*-phenylformamide **69** with only trace amounts of the diformylated product observed in analysis by GC-MS. This highlights the high selectivity for monoformylation when only 1 equivalent PhSiH₃ was used. Reaction of benzylamine **77** with CO₂ and 1 equivalent PhSiH₃ gave a mixture of products. *N*-benzylformamide **78** was produced in 23 % yield, however *N,N'*-dibenzylurea **79** was also observed accounting for approximately 10 % conversion of benzylamine. The remaining component is unreacted benzylamine **77**. This urea product was not observed in any other of the substrate screening with secondary amines, suggesting other pathways may be possible with primary amines compared to with secondary amines.



Scheme 4.3: Products from reaction of benzylamine **77** with CO₂ and PhSiH₃ at 23 °C

These conditions represent a significant improvement on previously reported guanidine catalysed systems, which required high temperatures (100 °C), long reaction times (24 h) and 5 mol% catalyst loadings and were poorly tolerated by aromatic amines.⁵⁹

Table 4.1: Substrate scope results with alkylated catalyst at low loading (1 mol%) at 23 °C

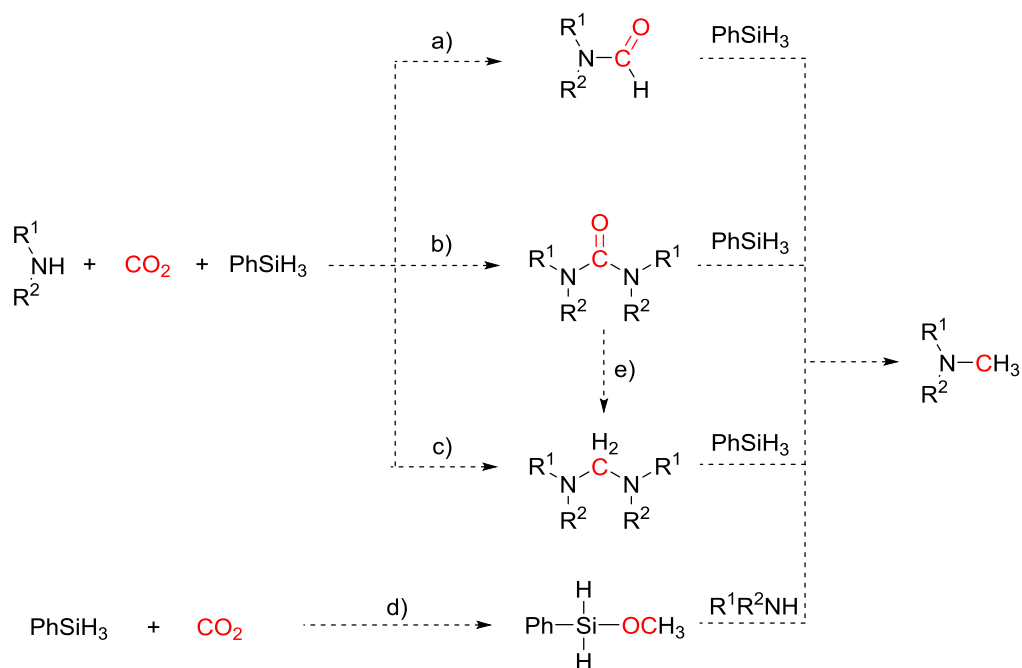
Entry	Substrate	Major Product (A)	Time	Yield of A ^a (%)	Yield of B ^a (%)
1	 18	 24	8 h	96	4
2	 31	 32	8 h	84	6 ^b
3	 68	 69	8 h	90	10
4	 37	 70	8 h	95	5
5	 71	 72	22 h	84	13
6	 73	 74	22 h	0	0
7	 75	 76	22 h	> 99	< 1
8	 77	 78	22 h	23	0

Conditions: Amine (2 mmol), PhSiH₃ (2 mmol), CO₂ (1.8 bar), **64** (1 mol%), 1,3,5-trimethoxybenzene (5 mol%), MeCN (2 mL), 23 °C. a) Conversions calculated by ¹H NMR relative to internal standard of 1,3,5-trimethoxybenzene (relative to amine substrate) b) calculated by GC

4.4 Conclusion

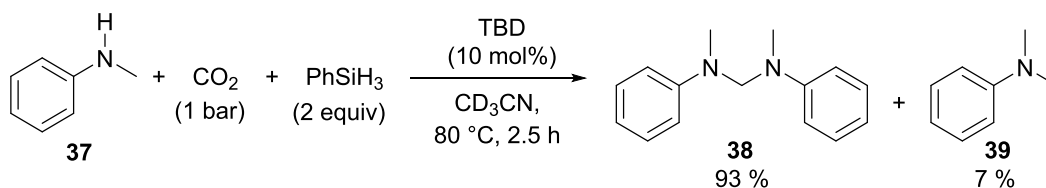
In summary, catalyst TMG was found to deactivate during the formylation of amines with CO₂ and hydrosilane by itself undergoing formylation, this prevented the reaction working at low catalyst loadings. By using alkylated guanidines, the deactivation pathway was prevented and catalyst loadings of 1 mol% gave full conversion within four hours of reaction. The new alkylated catalysts achieved TON of 805 and TOF of 33.5 h⁻¹ when used at 0.1 mol% loadings at 23 °C, yielding 81 % conversion to formylamide **24** within 24 hours at 1.8 bar. The increased activity of the alkylated catalysts, may be due to the prevention of a catalyst deactivation pathway, however alkylating the catalyst will also have changed the nucleophilicity and pK_a of the guanidine catalyst, (pK_a(MeCN) of TMG = 23,¹³⁹ methylTMG = 25)¹⁴⁸ and this is also likely to have affected its activity, suggesting the higher basicity of the catalyst maybe favourable.

Use of alkylated catalyst **64** at 1 mol% loading with PhSiH₃ at room temperature showed wide substrate tolerance with secondary amines and was successful with both aliphatic and aromatic amines; however, strongly electron withdrawing substituents hindered the reaction. The use of a more sustainable and cheaper reductant PMHS was found to work well with this system, although higher temperatures (60 °C) were required for reaction. Due to the higher temperature required and switch in product selectivity to solely formylmorpholine at 60 °C, a different mechanism or activation mode may be operating compared to that of PhSiH₃ as discussed previously.



Scheme 5.2: Possible pathways to methylamines from the reductive functionalisation of CO₂ with amines and hydrosilanes. a) reduction of formylamide, b) reduction of urea, c) reduction of aminal, d) via methoxysilane species

When guanidine catalysts were used for the synthesis of aminals from the reaction of CO₂ with amines and hydrosilanes, methylamines were also observed as a side product, Scheme 5.3.⁹⁷ Longer reaction times favoured the formation of the methylamine product, and thus it was proposed that the aminal may be an intermediate to the methylamine product. However, under some circumstances formylamides were also observed as products of the reaction.⁹⁷



Scheme 5.3: Synthesis of aminals and methylamines from the reductive functionalisation of CO₂ with amines and hydrosilanes using guanidine catalysts⁹⁷

Still, despite a number of proposed routes to the methylamines, the interplay between the products is not clear. In order to rationally develop more efficient reactions and catalysts, the route to each product and their relationship needs to be fully understood.

This chapter reports experimental investigations into the mechanism and involvement of methylamine and aminal products in the guanidine catalysed reductive functionalisation of CO₂ with amines and hydrosilane. Using the model system of morpholine and PhSiH₃ with TMG and alkylated TMG catalysts, the factors effecting the formation of each reduction product were investigated and reaction profiling used to understand the formation kinetics.

5.2 Factors Affecting *N*-Methylmorpholine Formation

Whilst investigating the reductive functionalisation of CO₂ with morpholine and phenylsilane to give formylmorpholine **24**, the formation of *N*-methylmorpholine **48** was also observed, Figure 5.1. The amount formed was found to be dependent upon temperature and stoichiometry of the reaction. At 60 °C, 12 % methylmorpholine was observed after 6 h, whereas at room temperature (23 °C) only 2 % methylmorpholine formed, Figure 5.1. Increasing the amount of PhSiH₃ in the reaction from 1 to 2 equivalents (relative to morpholine), led to an increase in methylmorpholine to 28 % after 6 hours, Figure 5.1.

Following the kinetics of formation showed that the methylmorpholine is only formed after 60 minutes of reaction, even with a higher equivalence of PhSiH₃, despite formylmorpholine being formed immediately in the reaction, Figure 5.1. Lowering the amount of PhSiH₃ to 0.5 equiv led to no conversion to methylmorpholine, whilst the addition of water to the reaction had no significant difference in conversion (14 % with water compared to 12 % without water at 60 °C). Lowering the catalyst loading to 1 mol% also led to a reduced amount of methylmorpholine. The delay in formation is intriguing and suggests either the formylmorpholine or another intermediate is required for the synthesis of methylmorpholine.

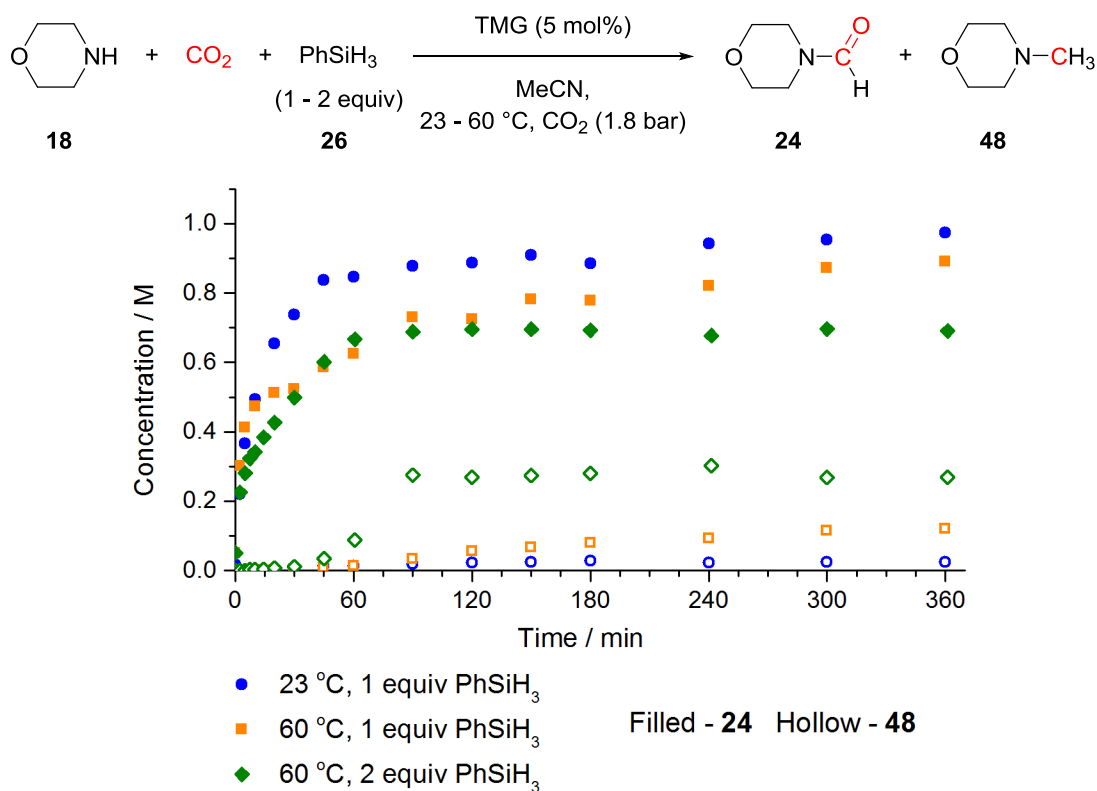


Figure 5.1: Reaction kinetics of **24** and **48** formation. Reaction Conditions: **18** (2 mmol), PhSiH₃ (2 – 4 mmol), TMG (0.1 mmol), MeCN (2 mL), biphenyl (0.1 mmol), CO₂ (1.8 bar), 23 – 60 °C. Concentrations calculated by GC relative to an internal standard.

The reaction kinetics of methylmorpholine formation were also affected by the choice of catalyst. When butyl TMG **64** was used, a faster formation of methylmorpholine within 60 minutes was observed, compared to with TMG, Figure 5.2. With Butyl TMG as the catalyst, formation of the aminal, dimorpholinomethane **57** was also observed.

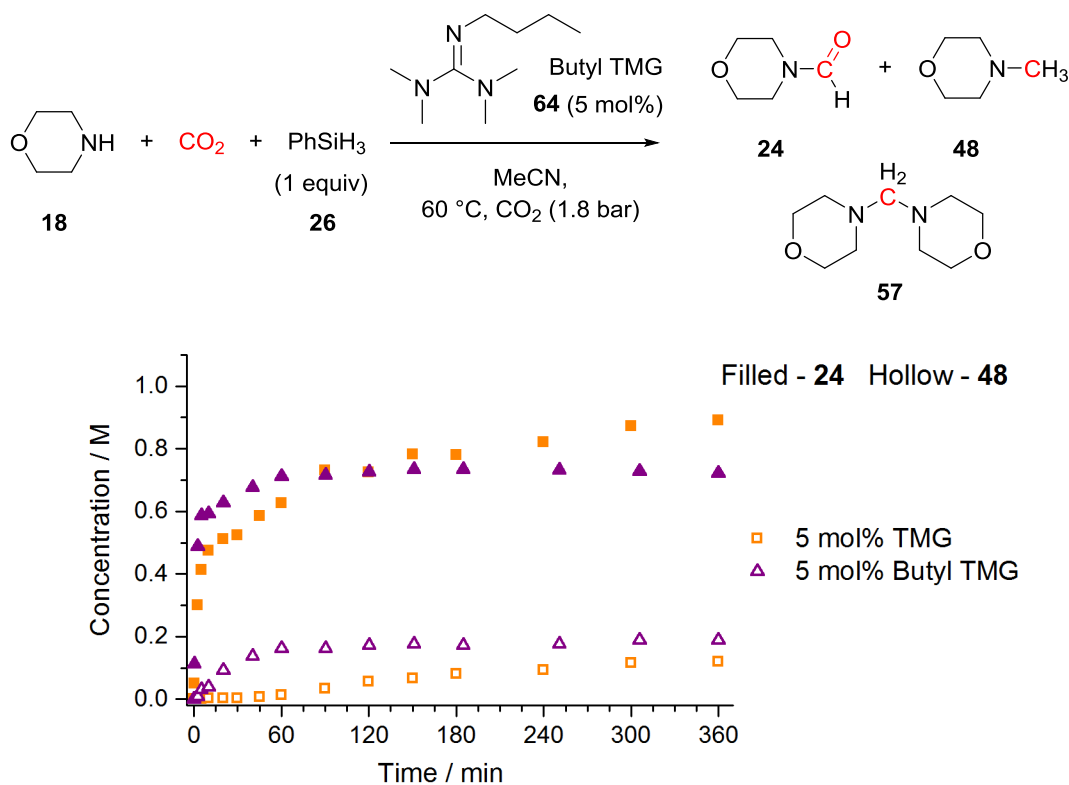
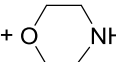


Figure 5.2: Effect of catalyst on reaction kinetics at 60 °C, reaction Conditions: **18** (2 mmol), PhSiH_3 (2 mmol), catalyst (0.1 mmol), MeCN (2 mL), biphenyl (0.1 mmol), CO_2 (1.8 bar), 60 °C

During investigations into the different roles of intermediates in formylmorpholine synthesis, it was found that changing the order of addition of reagents also led to a change in product distribution of the methylmorpholine, Table 5.1. When phenylsilane or TMG were added as the final reagent at 60 °C, 12 – 14 % conversion to methylmorpholine was observed; however, when morpholine was added last < 1% of methylmorpholine was observed and the aminal **57** was instead formed in 24 %, Table 5.1. These results highlight that catalyst loading and reaction conditions influence the different pathways and understanding this interaction may enable improved rational targeting of each product.

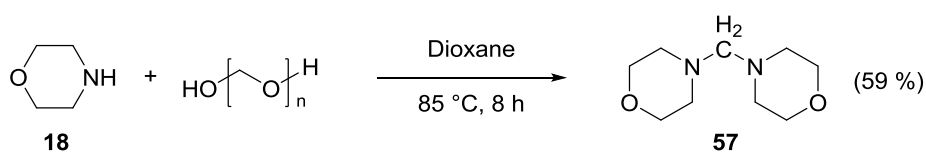
Table 5.1: Table comparing effect of order of addition on product distribution

Entry	Order of Addition	24 %	48 %	57 %
1	 + CO ₂ + TMG $\xrightarrow{15 \text{ mins}}$ + PhSiH ₃ $\xrightarrow{\hspace{1cm}}$	88	12	0
2	 + CO ₂ + PhSiH ₃ $\xrightarrow{15 \text{ mins}}$ + TMG $\xrightarrow{\hspace{1cm}}$	86	14	0
3	PhSiH ₃ + CO ₂ + TMG $\xrightarrow{15 \text{ mins}}$ +  $\xrightarrow{\hspace{1cm}}$	75	1	24

Reaction conditions: **18** (2 mmol), CO₂ (1.8 bar), TMG (0.1 mmol), PhSiH₃ (2 mmol), 60 °C, 1,3,5-trimethoxybenzene as internal standard. Conversions calculated by ¹H NMR

5.3 Role of Aminal Intermediate

It has been suggested that *N*-methylation of amines in the reductive functionalisation of CO₂ may be derived from the reduction of an aminal intermediate.⁹⁷ Early kinetic monitoring of our reaction system by GC did not identify any of the corresponding aminal species. However, once the authentic compound was prepared from morpholine and paraformaldehyde, based on a procedure reported by Huang (Scheme 5.4),¹⁴⁹ it was found that aminal **57** decomposed on the GC column and significantly overlapped with the morpholine signal. Thus alternative monitoring techniques were applied.

**Scheme 5.4:** Synthesis of dimorpholinomethane **57** from morpholine and paraformaldehyde¹⁴⁹

When the reductive functionalisation of CO₂ with morpholine at 60 °C was monitored by ¹H NMR, the presence of aminal **57** was observed, Figure 5.3 & Figure 5.4. Dimorpholinomethane **57** is produced from the start of reaction, reaching a maximum conversion of morpholine to **57** at 20 % by 120 minutes, before decreasing as the reaction progresses, Figure 5.4a & b. Methylmorpholine is only observed after 40 minutes of reaction, after **57** has begun to form, Figure 5.4b. At room temperature, a maximum of 4 % conversion to aminal **57** is observed before formation of methylmorpholine to 3 % by 6 h, Figure 5.4c & d.

These results indicate that aminal **57** is a significant species in reaction conditions when methylmorpholine is produced, and hence the mechanism for formation of **57** and its reactivity were further investigated.

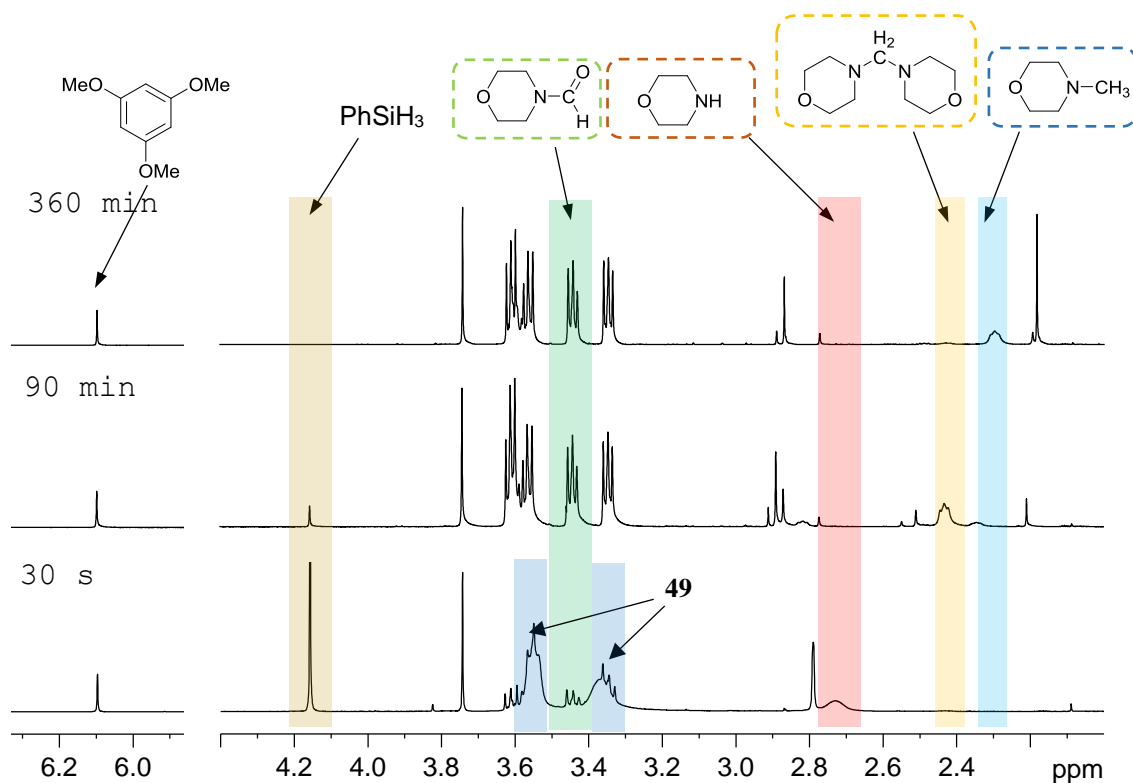


Figure 5.3: Example ^1H NMR spectra of reaction monitoring at $60\text{ }^\circ\text{C}$ with aminal **57** intermediate. Highlighted peaks were used for conversion calculations

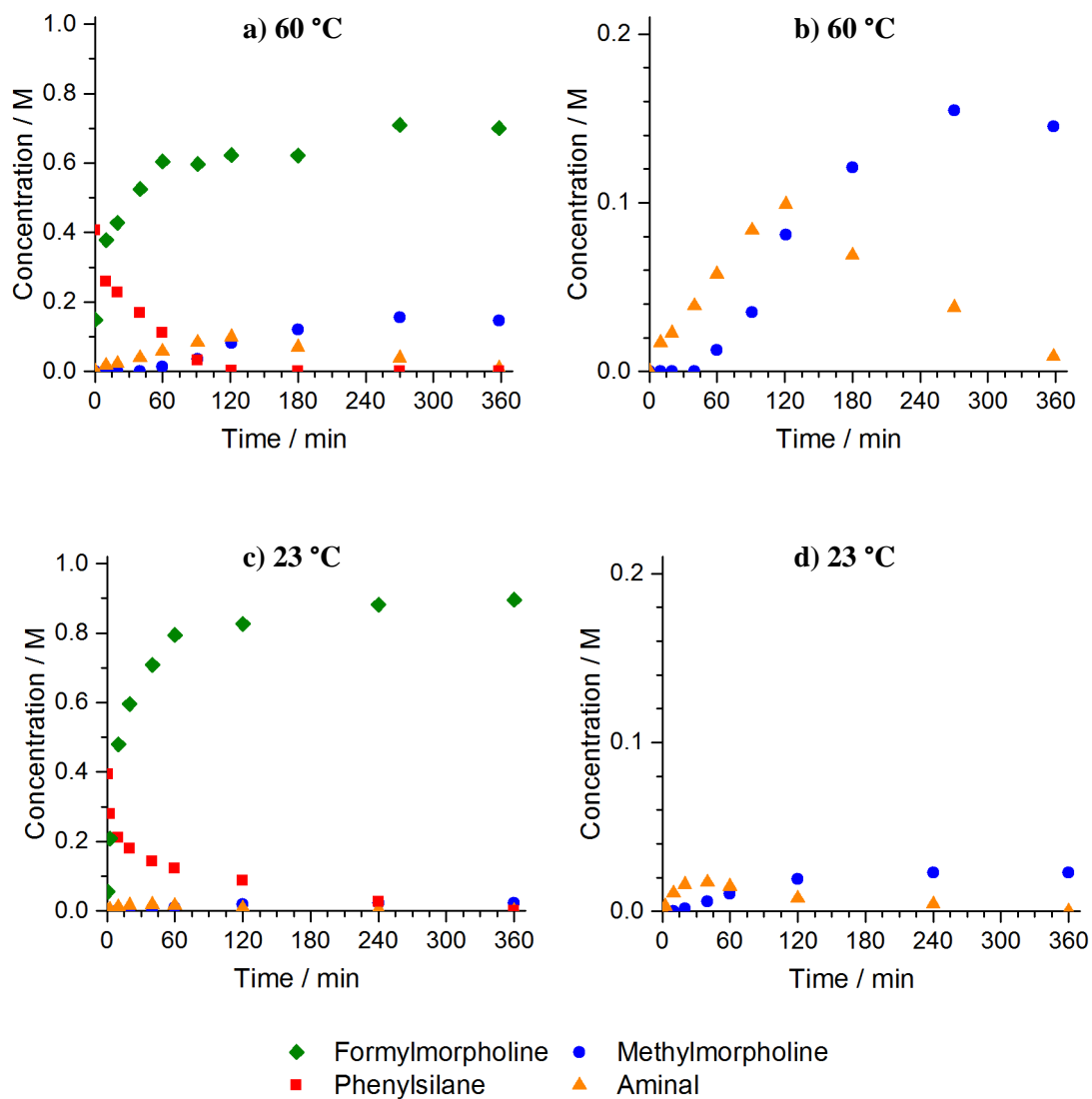
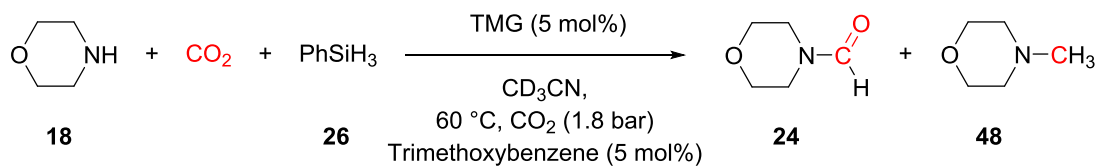
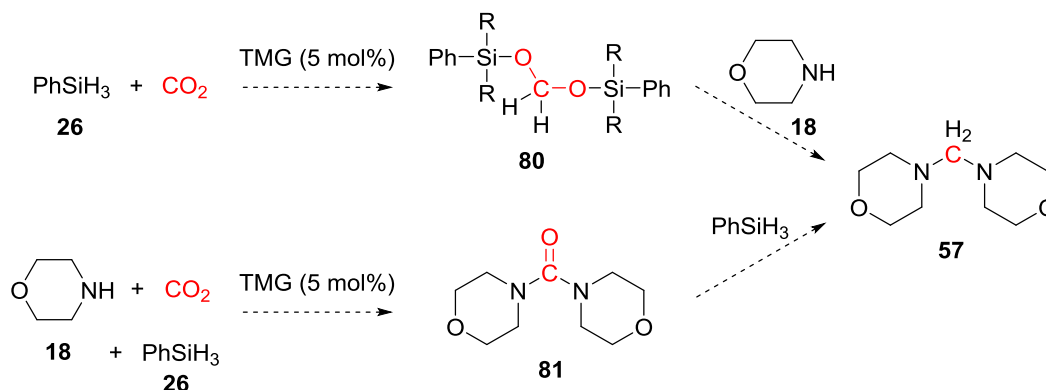


Figure 5.4: Kinetic profiles (^1H NMR) of reaction of morpholine, CO_2 and PhSiH_3 showing involvement of aminal **57** intermediate; Reaction conditions: **18** (2 mmol), PhSiH_3 (2 mmol), TMG (5 mol%), CO_2 (1.8 bar), CD_3CN (2 mL), 23-60 °C, 1,3,5-trimethoxybenzene (5 mol%), 23-60 °C. a) 60 °C, b) 60 °C zoomed in for low concentration region, c) 23 °C, d) 23 °C zoomed in

5.3.1 Routes to Aminal Intermediate

There are two main routes to the aminal product that can be thought of as likely to occur: firstly, via the reaction of morpholine with a bis(silyl)acetal species **80**,⁹⁷ and secondly via the reduction of a urea species **81**, Scheme 5.5. The feasibility of both of these routes were investigated.



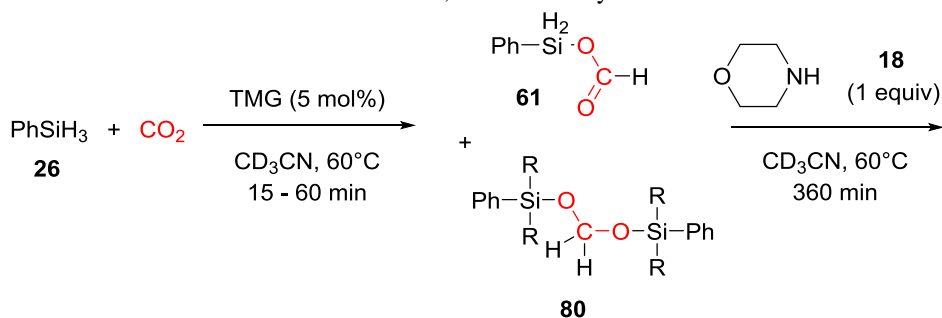
Scheme 5.5: Proposed routes to aminal intermediate via either a silylacetal species or a urea intermediate

5.3.1.1 Through a Silylacetal Intermediate

To probe the involvement of the bis(silyl)acetal species, the reduction of CO₂ with phenylsilane in the absence of morpholine was investigated. Based on earlier work reported in Chapter 3, it was found that the reduction of CO₂ with phenylsilane requires high temperatures (60 °C) and a catalyst (5 mol% TMG). Monitoring this reaction by ¹H NMR showed the formation of a number of silyl species, including formoxysilane **61**, methoxysilanes **82** and silylacetal **80** species. The bis(silyl)acetal **80** species was assigned due to a broad band that was present at (5.6 – 4.9 ppm), based on reported shifts at 4.5-5.0 ppm in d⁷-DMF by Ying.³⁷ The broad band is to be expected due to number of species which may incorporate the silylacetal group, with a number of R substituents, including: -H, -OH, -OC(O)H, -OCH₃ or other -O-[Si] species. Attempts to monitor the reaction by ²⁹Si NMR to probe the speciation of the bis(silyl)acetal species were unsuccessful due to the low concentrations of the species and low sensitivity of the technique.

The formation of the bis(silyl)acetal species **80** under these conditions may explain why the aminal **57** was observed when morpholine was added as the last component after a 15 minute pre reaction between PhSiH₃ and CO₂ at 60 °C in the presence of TMG, Table 5.1 & Table 5.2. Further investigation showed that if morpholine was added after 60 mins of pre reaction between PhSiH₃ and CO₂, then 32 % conversion to the aminal species was observed, Table 5.2. This further supports that the formoxysilane is reduced to the bis(silyl)acetal species which can then subsequently undergo nucleophilic addition of morpholine, Scheme 5.6.

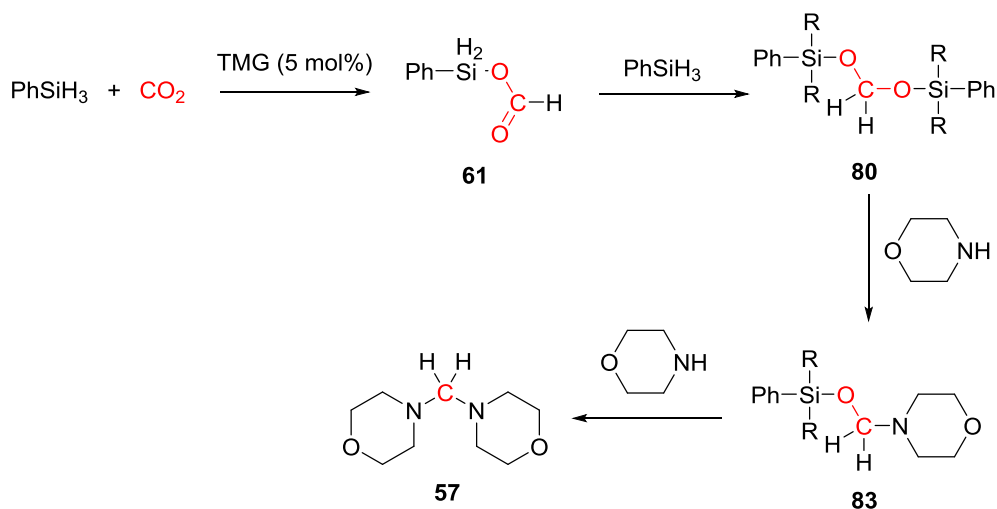
Table 5.2: Ratio of products after addition of morpholine to pre reaction of PhSiH₃ and CO₂ at 60 °C with 5 mol% TMG, determined by ¹H NMR



Entry	Time / min	% Conversion			
		Morpholine 18	Formyl- 24	Methyl- 48	Aminal 57
1	15	0	75	1	24
2	60	28	38	1	32
3*	60 + N ₂ flush	51	26	0	23

Reaction conditions: **18** (2 mmol), CO₂ (1.8 bar), TMG (0.1 mmol), PhSiH₃ (2 mmol), 60 °C, 1,3,5-trimethoxybenzene as internal standard. Conversions calculated by ¹H NMR

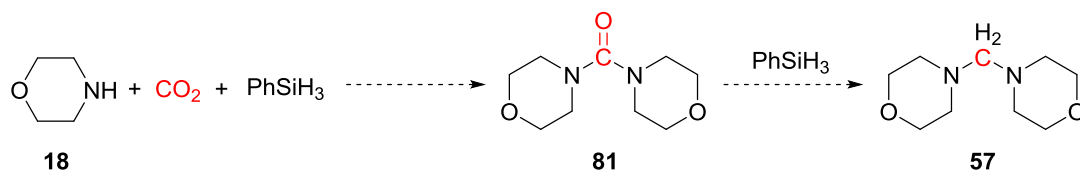
* After 60 mins reaction was flushed with N₂ for 60 mins before addition of morpholine



Scheme 5.6: Proposed route to aminal species via bis(silyl)acetal species

5.3.1.2 Through a Urea Intermediate

An alternative pathway to amina **57** is via the formation and subsequent reduction of a urea intermediate **81**, Scheme 5.7.

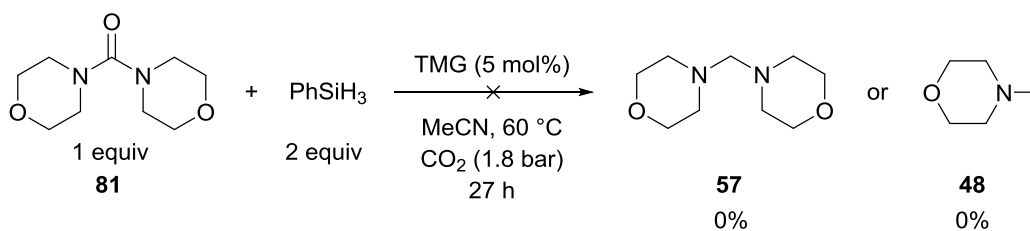


Scheme 5.7: Possible involvement of a urea intermediate **81** in the formation of the amina intermediate **57**

The formation of ureas is known to occur from the reaction of amines and CO₂ and from the decomposition of silylcarbamates; however, these transformations typically require either high temperatures and pressures or the use of a catalyst.^{111, 118, 150-152} The reduction of dialkylureas to amins with a silane reducing agent has been reported using a Ru catalyst,⁹⁰ however previous attempts to reduce 1,3-dimethyl-1,3-diphenylurea **84** with phenylsilane using an organocatalyst have been unsuccessful.⁹⁷

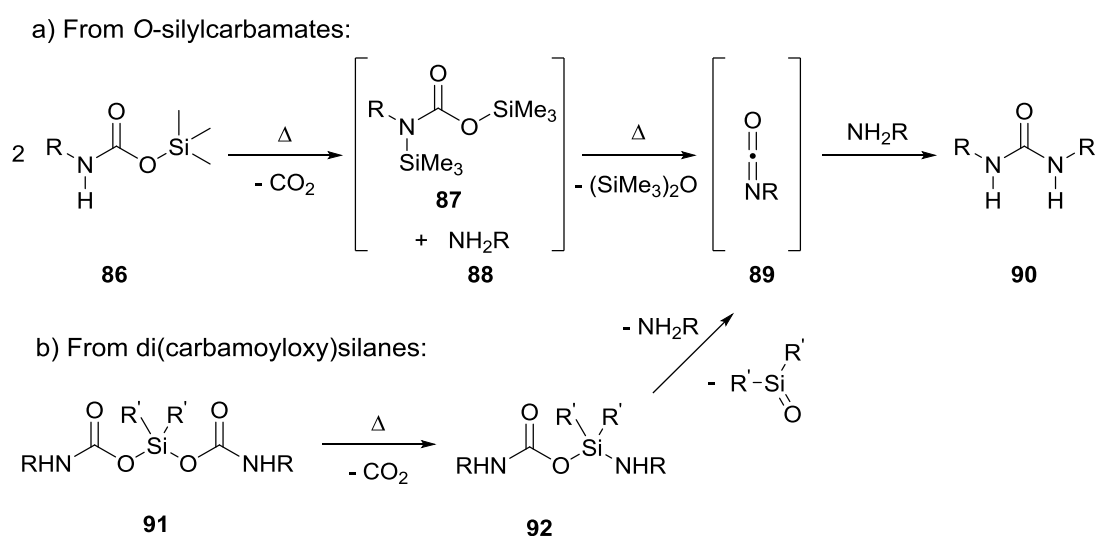
To probe the possible involvement of urea **81** in the formation of amina **57**, urea **81** was prepared by reaction of morpholine **18** with morpholine-4-carbonyl chloride **85** following a modified procedure reported by Albericio.¹⁵³ Comparing analytical data to results of NMR, IR and GC monitoring confirmed no build-up of urea **81** was observed during the reaction.

Furthermore, when urea **81** was subjected to reaction conditions at 60 °C with 5 mol% TMG; no conversion was observed after 27 h, Scheme 5.8. Thus, the reduction of a urea is not a feasible pathway to either amina **57** or methylmorpholine **48** under these reaction conditions. This corresponds with similar studies reported by Cantat⁹⁷ and Liu.⁹² Conversely, during substrate scope investigations (reported in Chapter 4) it was found that reaction of primary amine benzylamine **77**, gave *N,N'*-dibenzylurea **79** in 10 % yield after 22 h.



Scheme 5.8: Reaction of urea **81** with CO₂ and PhSiH₃ at 60 °C with 5 mol% TMG led to no conversion

This difference in reactivity could be accounted for by the necessary involvement of an isocyanate intermediate for urea formation. For example, for the formation of a urea from monoalkylated *O*-silylcarbamates the proposed route involves loss of CO₂, to yield a *N,O*-bis-silylcarbamate intermediate **87** and free amine **88**. Intermediate **87** can then be converted into an isocyanate **89** which subsequently reacts with the free amine **88** to give the dialkylurea **90**, Scheme 5.9.^{111, 118, 151} When silyldialkylcarbamates were investigated no decomposition to the corresponding tetraalkylurea was observed.¹⁵¹



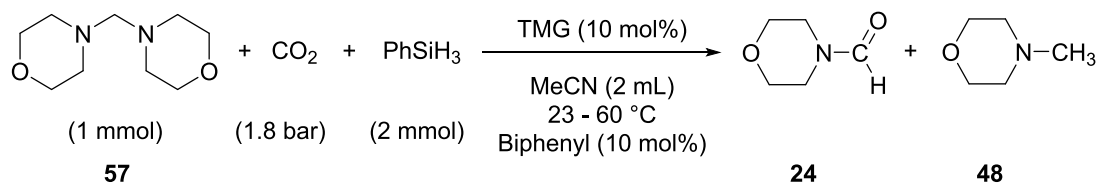
Scheme 5.9: Proposed route from a) mono alkylated *O*-silylcarbamates **86** to urea **90** via *N,O*-bis-silylcarbamate **87** and isocyanate **89** intermediates, and b) from mono alkylated dialkylsilylcarbamates **91** to urea **90** via^{111, 118, 151}

Similarly with urea formation from amines and CO₂, routes via an isocyanate intermediate were found to be favoured;¹⁵² however isocyanate intermediates are only feasible with primary amines. With secondary amines, urea formation instead requires the dehydration of a diol species, however this pathway was found to be unfavourable and thus the use of dehydrating agents, such as PPh₃, were typically required.^{152, 154, 155}

Based on the above results, the involvement of a urea in the synthesis of animal from secondary amines was deemed to be unlikely, and instead animal **57** is more likely to be formed via a bis(silyl)acetal intermediate **80**. However, the involvement of a urea intermediate in reactions with primary amines cannot be discounted without further investigation.

5.3.2 Reactivity of Ainal to Methylmorpholine and Formylmorpholine

To investigate the reactivity of ainal **57**, the authentic compound was prepared from morpholine and paraformaldehyde based on a procedure reported by Huang¹⁴⁹ and subjected to typical reaction conditions, Scheme 5.10. Catalyst loadings and equivalents of PhSiH₃ were selected relative to the number of morpholine fragments in order replicate the comparative reaction with morpholine as the substrate.



Scheme 5.10: Standard reaction conditions for reaction of ainal **57** to give formylmorpholine **24** and *N*-methylmorpholine **48**

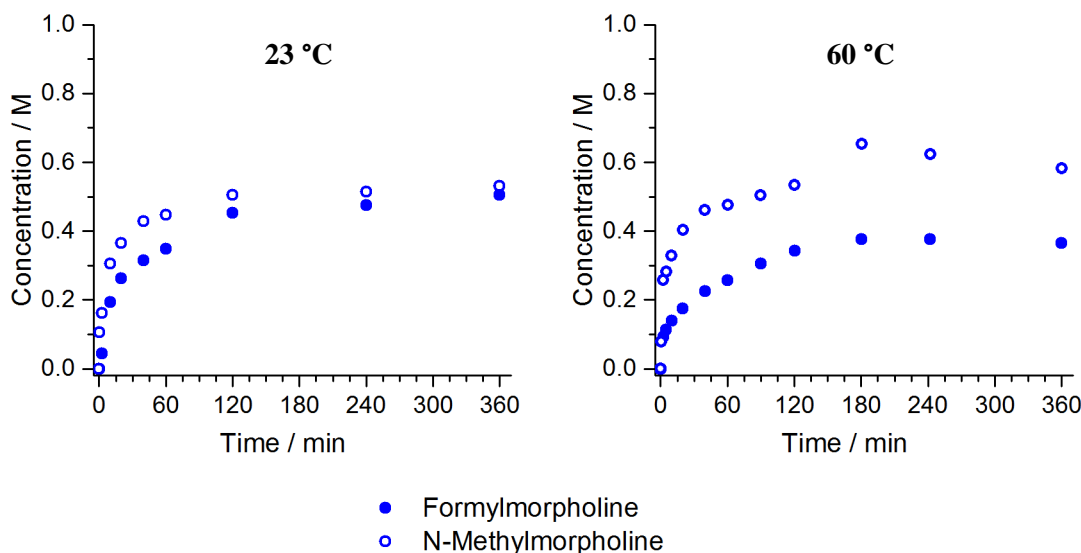


Figure 5.5: Kinetic profiles (GC) of products **24** and **48** from reaction of **57** under standard reaction conditions at a) 23 °C and b) 60 °C

Initial reactions found that both formylmorpholine and methylmorpholine were formed from the reaction of ainal **57**. The formation of formylmorpholine highlights another route to the formylamide product which was not previously found in mechanistic insights developed in Chapter 3. The ratio of products from reaction of ainal **57** with PhSiH₃ and CO₂ is dependent upon the reaction temperature. After 6 hours at 23 °C 49 % formylmorpholine and 51 % *N*-methylmorpholine is formed, whereas at 60 °C methylmorpholine is favoured over formylmorpholine giving product ratios 61 % and 39 % respectively, Figure 5.5. Interestingly methylmorpholine is produced at a faster rate than formylmorpholine in both reaction profiles suggesting that a stepwise mechanism may be involved.

Performing the reaction under N₂ led to no conversion of aminal **57** suggesting that CO₂ is required for the breakdown of this species, in agreement with preliminary work reported by Cantat.⁹⁷ Uncatalysed, the reaction proceeds at 60 °C to give products **24** and **48** in yields of 5 % and 24 % respectively after 6 hours (i.e. ratio 17:83 **24:48**) (Figure 5.6b) suggesting the catalyst is more essential for the formylmorpholine than methylmorpholine, further suggesting a second step to the formylmorpholine product. Use of TBD as the catalyst at 23 °C interestingly favours methylmorpholine over formylmorpholine with yields of 55 % and 40 % (Figure 5.6a), compared to the reaction at 23 °C with TMG where equal ratios of the product were formed, Figure 5.5a. Both the addition of water (40 mol%) and reducing the amount of PhSiH₃ to 1 mmol (1 equiv) at 23 °C made no significant change to the reaction product ratios or rate of reaction, Figure 5.6c & d. Lowering the pressure of CO₂ to 1.2 and 1 bar at 23 °C led to a slight reduction in reaction rate and overall conversion, having a larger effect on formylmorpholine conversion than methylmorpholine, Figure 5.6e & f.

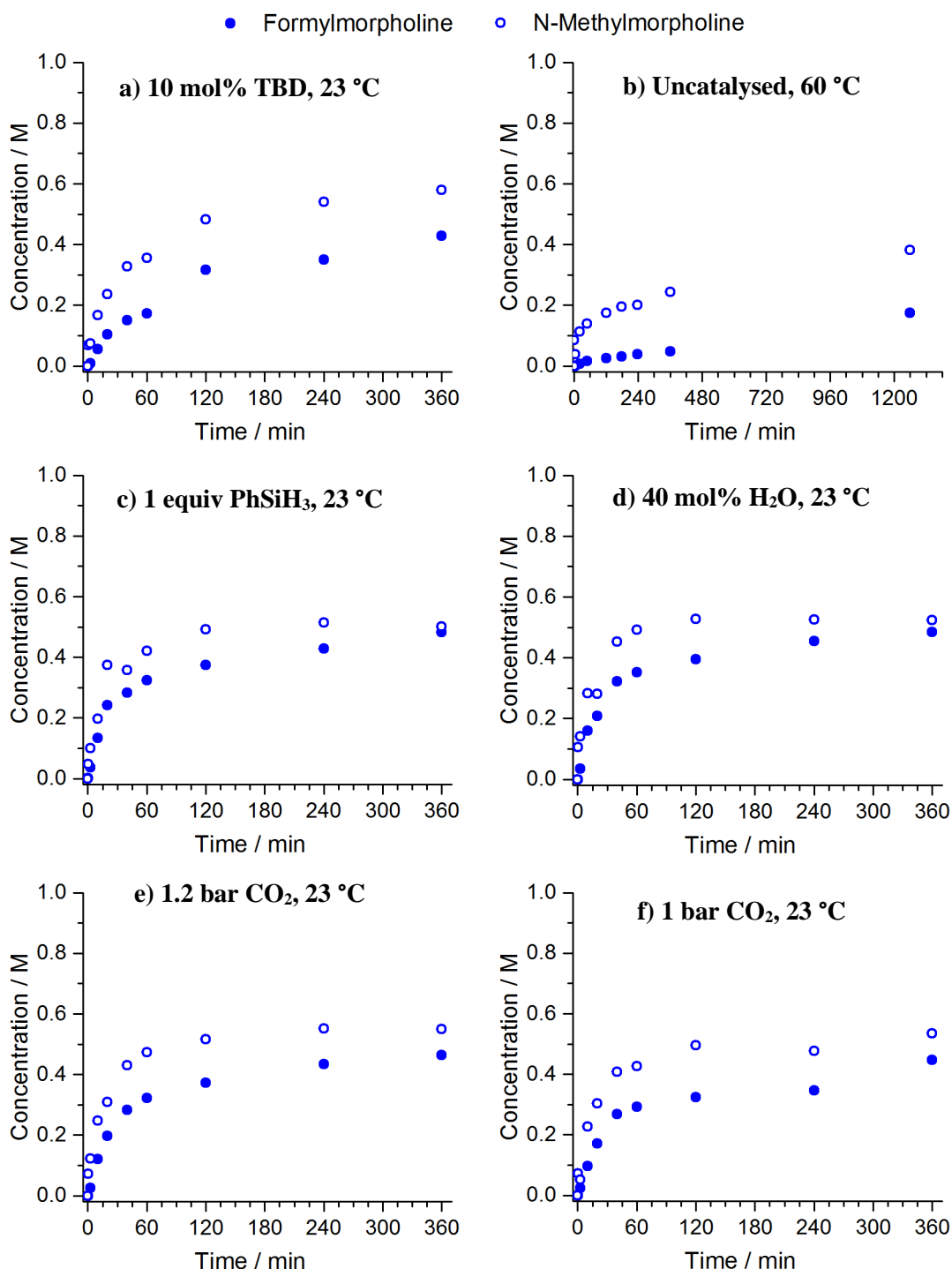
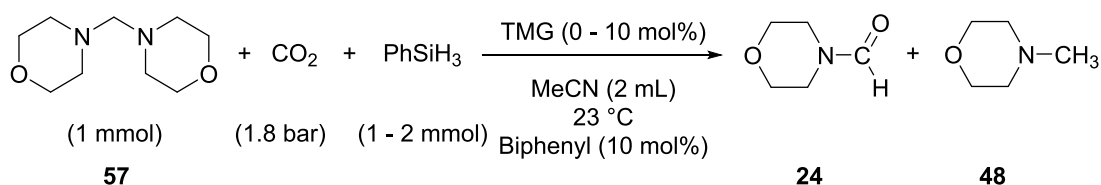


Figure 5.6: Kinetic profiles (GC) of reaction of **57** to give **24** and **48** under various conditions. Standard conditions: **57** (1 mmol), PhSiH₃ (2 mmol), TMG (0.1 mmol, 10 mol%), CH₃CN (2 mL), CO₂ (1.8 bar), biphenyl (0.1 mmol, 10 mol%), 23 °C. Product concentrations calculated by GC relative to internal standard. Variations: a) 10 mol% TBD, 23 °C; b) no catalyst, 23 °C; c) 1 equiv. PhSiH₃ (1 mmol), 23 °C; d) 0.4 mmol H₂O, 23 °C; e) 1.2 bar CO₂, 23 °C; f) 1 bar CO₂, 23 °C.

5.3.3 Mechanistic Considerations

Although the reduction of an aminor species to methylamines in the presence of CO₂ has previously been reported, the mechanism for its transformation is still unclear.⁹⁷ In particular the transformation into formylamide has not been reported. Initial screening by GC suggested that methylmorpholine is formed before formylmorpholine, suggesting an intermediate species may be formed, thus further spectroscopic monitoring of the reaction was performed.

Monitoring the reaction by ¹H NMR spectroscopy showed a kinetic profile corresponding well with that determined by GC, Figure 5.7. During the first 20 mins of the reaction, new species (approximately 2 %) were observed with signals at 2.56, 3.05, 3.64 and 4.04 ppm along with new Si-H signals between 5 and 5.2 ppm, however the identity of these species were unknown, Figure 5.8.

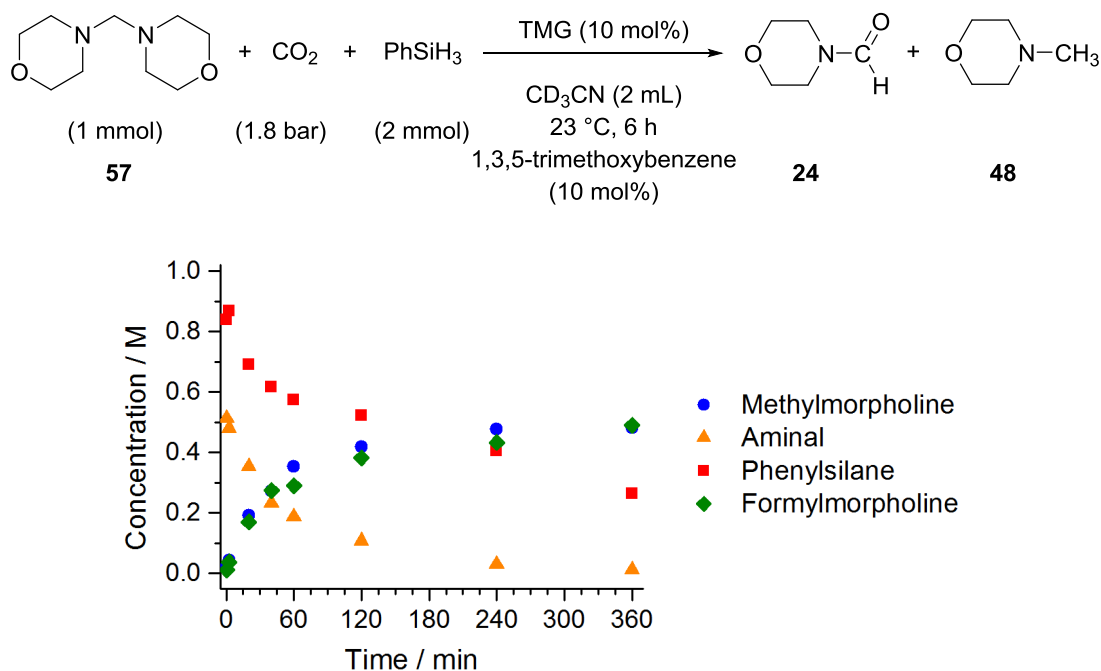


Figure 5.7: ¹H NMR monitoring of reaction of aminor **57** with CO₂ and PhSiH₃ to give **24** and **48**. Concentrations determined by ¹H NMR relative to 1,3,5-trimethoxybenzene internal standard

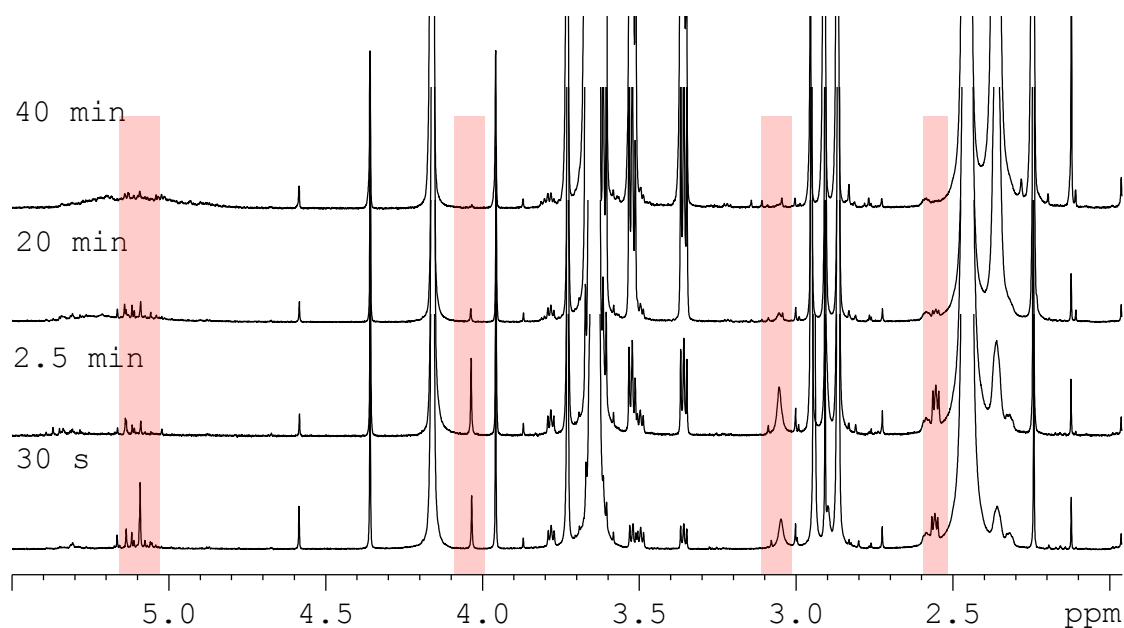


Figure 5.8: Example ^1H NMR spectra of iminal reaction with new observed species highlighted

Control NMR experiments were performed to determine the origin of the new species, Table 5.3. Reaction of iminal **57** with CO_2 and iminal **57** with TMG in CD_3CN led to no change in the ^1H NMR spectra. Reaction of iminal **57** with PhSiH_3 however, led to a small shift downfield for the $(\text{CH}_2)_2$ protons of the iminal (by 0.02 ppm) suggesting an interaction between the iminal and PhSiH_3 maybe occurring. However, this still does not account for the new species observed. Reaction of iminal **57** with TMG and CO_2 led to the formation of a white precipitate, which was found to be the guanidinium bicarbonate. This was thought to be formed due to trace amounts of water in CD_3CN , as the white precipitate was not observed when the reaction was carried out in anhydrous CH_3CN , nor were any new species observed when the reaction was monitored by *in situ* IR spectroscopy in anhydrous acetonitrile.

Table 5.3: Results of interaction study between **57**, TMG, CO_2 and PhSiH_3 at RT in $\text{CH}_3\text{CN}/\text{CD}_3\text{CN}$ by NMR and IR studies

Experiment	Outcome
57 + CO_2	No reaction
57 + TMG	No reaction
57 + CO_2 + TMG	White ppt with water: $\text{TMGH}^+ \text{CHO}_3^-$ No reaction under anhydrous conditions
57 + PhSiH_3	Interaction – upfield shift of iminal protons
57 + PhSiH_3 + TMG (10 mol%)	Interaction – upfield shift of iminal protons

Monitoring the reaction of aminal **57** by IR showed that in the first 15 mins before PhSiH₃ was added, no significant changes were observed, i.e. the aminal is stable in the presence of TMG and CO₂. On addition of PhSiH₃ the reaction commenced with formation of **24** and **48**. An intermediate species was also observed with absorption bands at 1245 and 1258 cm⁻¹, Figure 5.9. This suggests the formation of new C-O bonds and corresponds with the silylcarbamate intermediate previously observed in reactions of morpholine (Section 3.4, Chapter 3), however it could not be isolated and thus no definite characterisation can be applied. Formoxysilane was also observed by an absorption at 1725 cm⁻¹, the species slowly increased over the course of the reaction, Figure 5.9. Monitoring the reaction by HRMS confirmed formation of **24** and **48**; however, no other significant species were observed that could be assigned, except for the deactivated catalyst species formylTMG **62** and the transamination product **63** (Chapter 4).

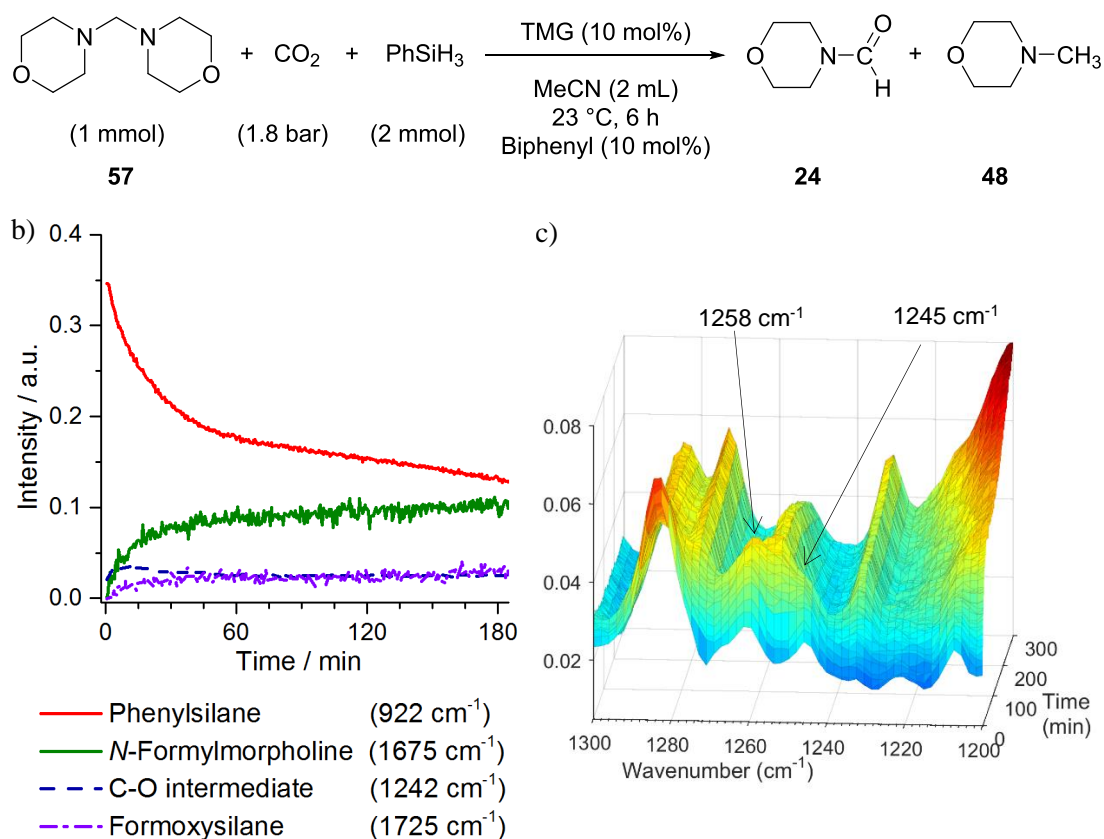
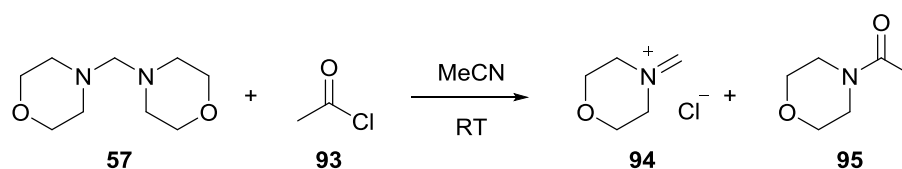


Figure 5.9: IR monitoring of aminal reaction. a) reaction scheme, b) Reaction trends by peak height of IR absorption, c) 3D plot showing possible silylcarbamate intermediate

Aminals are known to react with strong electrophiles as a means to generate iminium ions. For example, in the Mannich reaction, aminals have been reacted with acylchlorides to generate the corresponding iminium¹⁵⁶ *in situ* which can then react with a nucleophile, producing amides **95** as a side product, Scheme 5.11.^{157, 158} Chloromethylsilanes have also been used in place of acylchlorides to generate the iminium species.^{159, 160}

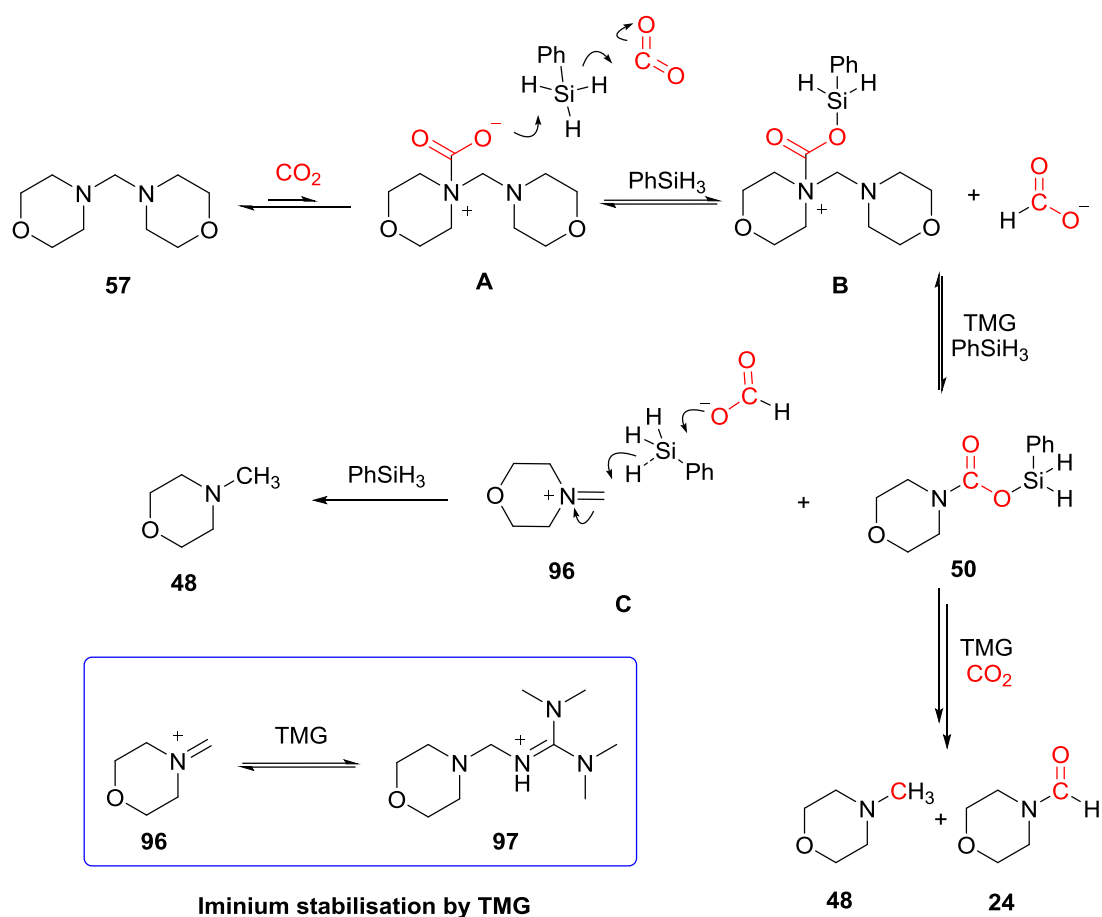


Scheme 5.11: Example reaction of aminals with acyl chlorides to generate an iminium species for use in a Mannich reaction¹⁵⁷

Based on experimental studies and previous studies on the reactivity of aminals, a tentative mechanism has been proposed, Scheme 5.12. Aminal **57** and CO₂ lie in equilibrium with the corresponding carbamate species **A**, however this was found to be unfavourable by NMR studies. Addition of PhSiH₃ adds to the carbamate yielding unstable silylcarbamate species **B**. Hydrogen may also be released during the synthesis of this silylcarbamate which would account for a small amount of gas evolution observed on the addition of PhSiH₃ at the beginning of the reaction.

Species **B** may then break down to give the silylcarbamate species **50** and *N*-methylenemorpholinium **96**, this is promoted by the catalyst (TMG) which can stabilise **96** to give the iminium **97**. In step **C** the hydrosilane is activated by formate which promotes reduction of the iminium species **96** to give methylmorpholine **48** and formation of a formoxysilane species. The silylcarbamate species **50** reacts to give formylmorpholine **24** via a formoxysilane species – as discussed in Chapter 3. At room temperature this favours formation of the formylmorpholine **24**, whereas at higher temperatures methylmorpholine **48** is also produced via regeneration of the aminal species **57** and subsequent reduction. Thus explaining why higher temperatures see a shift in ratio of products **24** and **48**.

This proposed mechanism supports experimental results that show that CO₂ is required for reduction of aminal **57** and that higher temperatures favour the methylmorpholine **48** product. The observed preference for methylmorpholine **48** in the uncatalysed reaction supports that the silylcarbamate may be an intermediate in the reaction, as this was previously found to require TMG to proceed to formylmorpholine **24**. A silylcarbamate type species is also supported by the formation of new Si-H peaks in the ¹H NMR spectra of the catalysed and uncatalysed reaction between 5.2-5.1 ppm. In the uncatalysed reaction the iminium **96** could not be stabilised by the TMG, in this case it may be that cation **B** is directly reduced to **48**, or that the produced formate stabilises **96** instead of TMG. To confirm this ¹H NMR monitoring of the uncatalysed reaction would enable identification of the silylcarbamate **50** which would be expected to accumulate. ²H and ¹³C labelling experiments of aminal **57** would also help to confirm the reactivity of the iminium species.

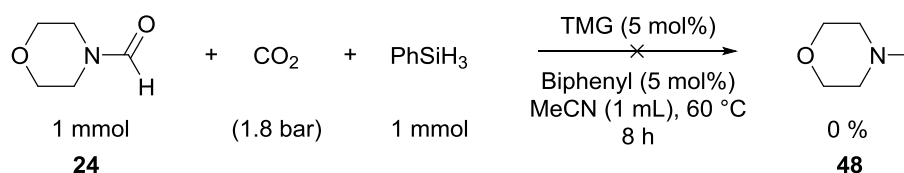


Scheme 5.12: Tentative proposed mechanism for reduction of aiminal **57** to methylmorpholine **48** and formylmorpholine **24**. Inset: proposed stabilisation of iminium species by TMG

5.4 Reduction of Formylmorpholine to Methylmorpholine

The results presented so far have indicated that the amination species formed in the reaction is a viable pathway for formation of methylmorpholine. However, other possible routes to the methylmorpholine product must still be considered. The reduction of formylamides with hydrosilanes to give methylamines has been reported using organocatalysts TBAF⁷⁷ and B(C₆F₅)₃.⁹²

Subjecting formylmorpholine to reaction conditions with 5 mol% TMG, 1 equiv. PhSiH₃ at 60 °C and 1.8 bar CO₂, led to no conversion after 8 hours, Scheme 5.13. Even when the reaction was performed at 100 °C under N₂ in a sealed tube, no conversion was observed after 18 hours.



Scheme 5.13: Reaction of **24** under reaction conditions at 60 °C gave 0 % conversion

During the investigation of the formylation reaction (as discussed in Chapter 3), it was suggested that the formation of a carbamate species is important in activating the PhSiH₃ for reaction. Thus the reduction of formylmorpholine was investigated in the presence of morpholine at 60 °C, Figure 5.10.

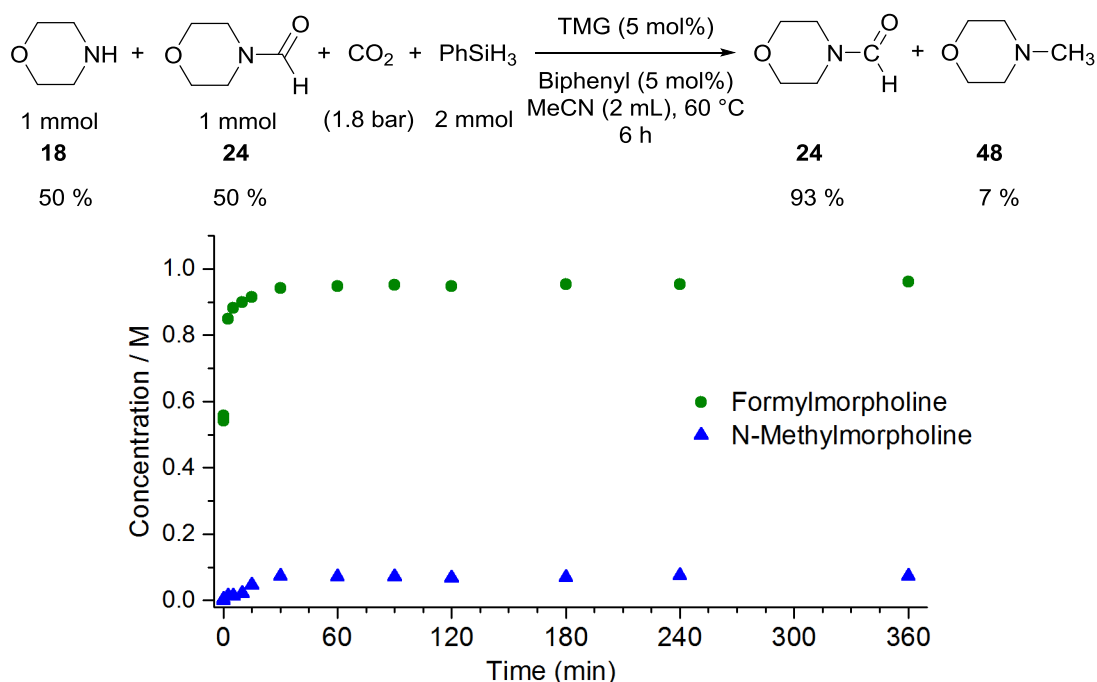


Figure 5.10: Kinetic profile (GC) of reaction of **18** and **24** in 1:1 ratio with PhSiH₃ and CO₂ at 60 °C with 5 mol% TMG. Reaction conditions: **18** (1 mmol), **24** (1 mmol), PhSiH₃ (2 mmol), TMG (0.1 mmol), Biphenyl (0.1 mmol), MeCN (2 mL), CO₂ (1.8 bar), 60 °C

Reaction of **18** and **24** in a 50:50 ratio (1 mmol each) under standard reaction conditions at 60 °C gave a final product ratio of 7 % methylmorpholine to 93 % formylmorpholine after 6 hours, Figure 5.10. These results suggest no significant increase in the amount of morpholine converted to *N*-methylmorpholine occurs in the presence of formylmorpholine. However, monitoring the reaction kinetics by GC showed interesting behaviour. When 100 % of the starting material is morpholine, methylmorpholine is normally only observed after 60 minutes; however, in the presence of formylmorpholine, methylmorpholine is observed from the beginning of reaction and reaches maximum conversion by 30 minutes. This rate enhancement may suggest that product catalysis is occurring. A weak product catalysis effect has previously been proposed by Dyson and co-workers in the formylation reaction with formylanilide, however no kinetic data was presented.⁷⁶

To ensure that the change in kinetics is due to product catalysis, rather than promoted reduction of the formylmorpholine, crossover experiments with piperidine **31** and formylpiperidine **32** as the substrates were performed. In these experiments, if the formylmorpholine was reduced in the presence of a different amine substrate (i.e. piperidine **31**), the reduced formylmorpholine to methylmorpholine would be distinguishable from the product of piperidine methyl- or formylation. The reaction of piperidine **31** was first studied to ensure that similar reactivity occurs to when morpholine is used as the substrate, Figure 5.11.

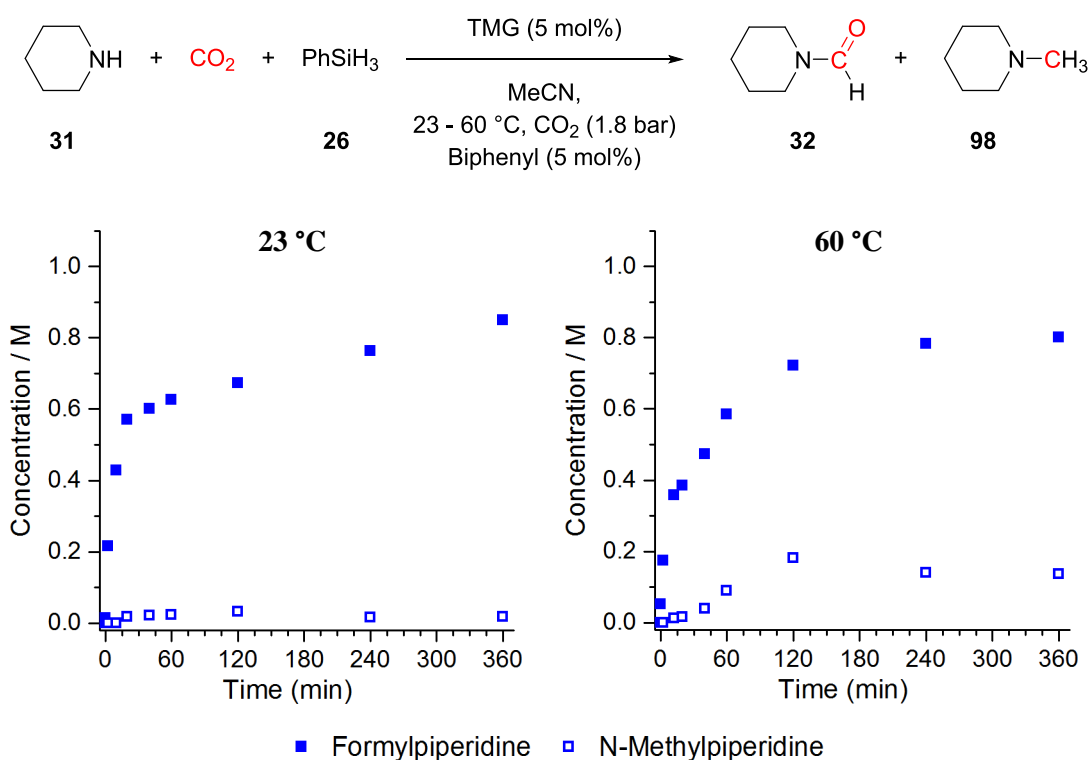


Figure 5.11: Reaction kinetics (GC) of piperidine with CO_2 and PhSiH_3 . Conditions: **31** (2 mmol), PhSiH_3 (2 mmol), TMG (0.1 mmol), Biphenyl (0.1 mmol), MeCN (2 mL), CO_2 (1.8 bar), a) 23 °C, b) 60 °C

Under comparable reaction conditions it was found that, similarly to morpholine, the reaction to formylpiperidine **32** proceeded faster at 23 °C than 60 °C, and that formation of methylpiperidine **98** formed in the later stages of the reaction in 14 % after 6 h, Figure 5.11.

As piperidine reactivity was found to be comparable to morpholine, cross over experiments were performed. Piperidine **31** and formylmorpholine **24** were reacted in a 50:50 ratio with CO₂ and PhSiH₃ at 60 °C, Figure 5.12a. After 6 hours no reduction of formylmorpholine **24** to methylmorpholine **48** was observed, and piperidine **31** was converted to formylpiperidine **32** and methylpiperidine **98** in 86 and 12 % yields respectively, relative to the piperidine starting material.

To ensure that the increased pKa and nucleophilicity of piperidine over morpholine (Table 5.4) was not effecting the reactivity, morpholine **18** and formylpiperidine **32** were also reacted in a 50:50 ratio with CO₂ and PhSiH₃ at 60 °C, Figure 5.12b. No reduction to methylpiperidine **98** was observed after 6 hours, and morpholine **18** was converted to formylmorpholine **24** and methylmorpholine **48** in 68 and 30 % yields respectively, relative to the morpholine starting material.

Table 5.4: pKa and nucleophilicity values of substrates in acetonitrile

	pKa (in MeCN)	Nucleophilicity (in MeCN)
Morpholine	16.61 ¹⁴⁰	15.65 ¹⁴²
Piperidine	18.92 ¹⁴⁰	17.35 ¹⁴²

Considering the kinetics of these reactions, formylpiperidine **32** has no rate enhancement effect on methylmorpholine **48** formation (Figure 5.12d), however formylmorpholine **24** appears to have a slight rate enhancement effect on methylpiperidine **98** formation (Figure 5.12c). The reason for this is not clear, however it has been reported that the formylamide DMF, and valerolactone can promote the reductive functionalisation of CO₂ with hydrosilanes when used as a solvent due to changes in solvation and polarisation.^{79, 93} Thus, it could be expected that significant amounts of formylmorpholine may affect hydrogen bonding interactions and promote the reaction.

In summary, both reactions show that the formylamide cannot be reduced to the corresponding methylamine under these reaction conditions, and is thus not a viable pathway.

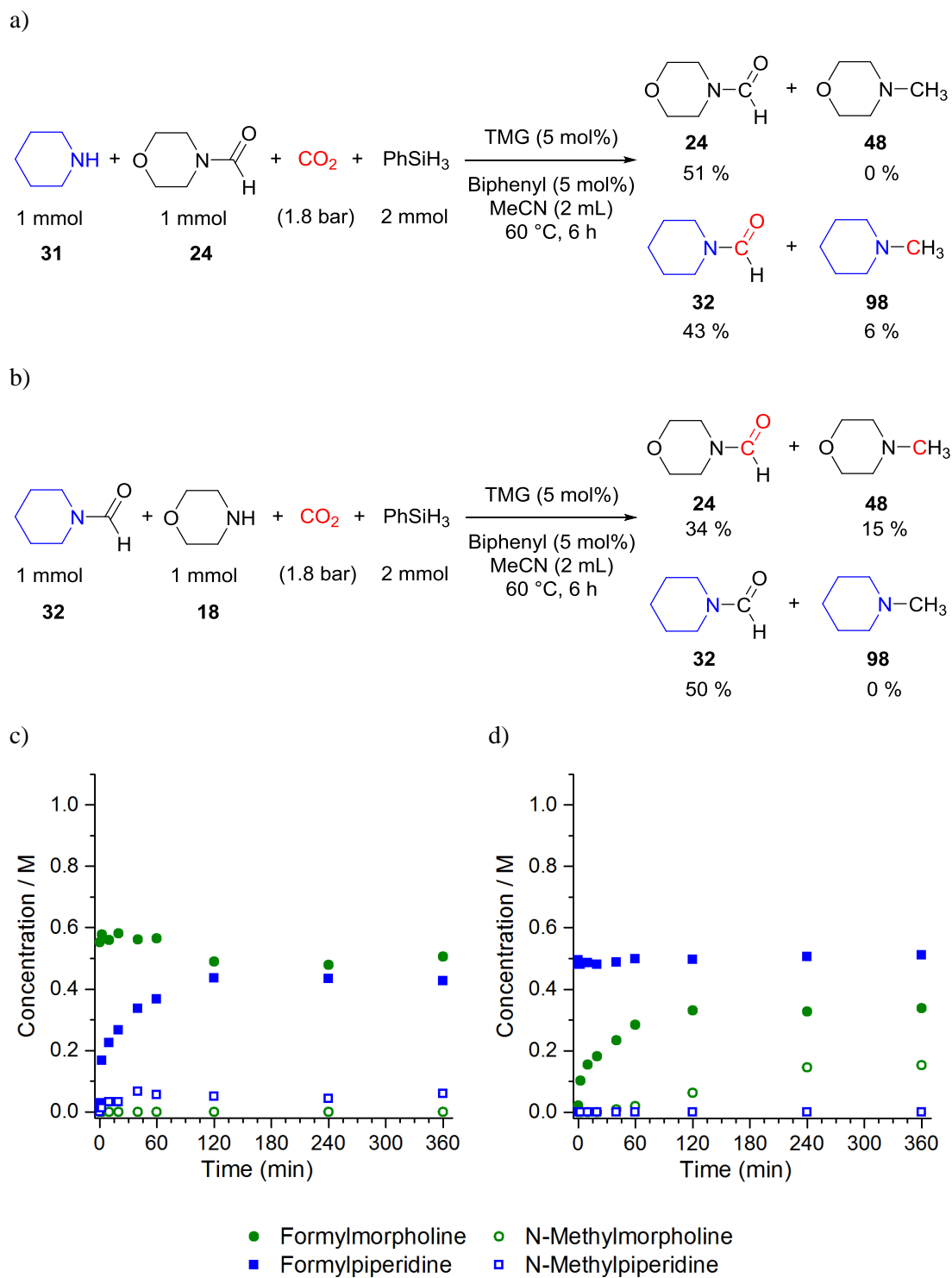
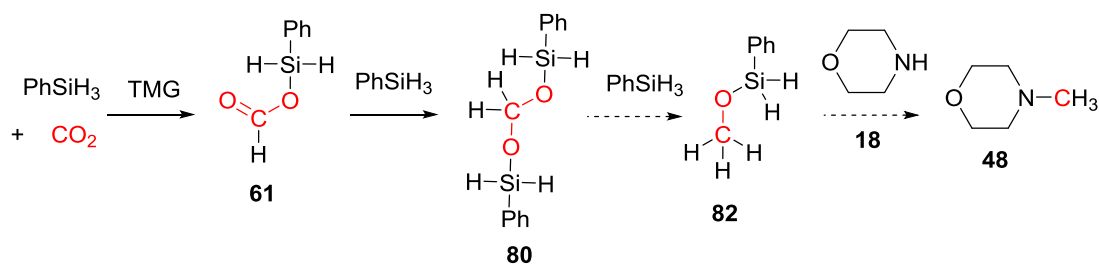


Figure 5.12: Crossover experiments of formylamide and amines. a & c) Reaction of piperidine **31** and formylmorpholine **24**, b & d) Reaction of morpholine **18** and formylpiperidine **32** Reaction conditions: Amines **31** or **18** (1 mmol), Formylamides **24** or **32** (1 mmol), PhSiH₃ (2 mmol), CO₂ (1.8 bar), TMG (0.1 mmol), Biphenyl (1 mmol), MeCN (2 mL), 60 °C, 6 h. Concentrations determined by GC

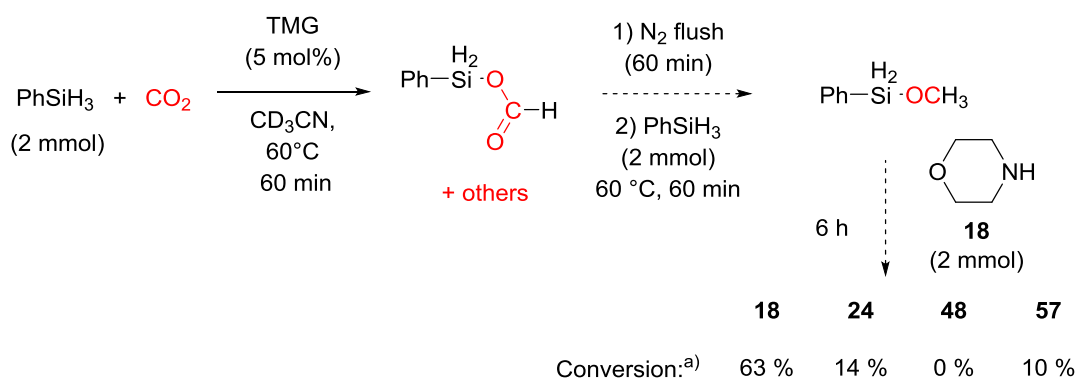
5.5 Involvement of Methoxysilane Species

An alternative route to methylmorpholine **48** is via the reduction of CO₂ to a methoxysilane species **82** which could react with morpholine to give **48**, Scheme 5.14. The reduction of CO₂ to methoxysilane species has been reported with organocatalysts such as NHCs³⁷ and subsequent nucleophilic attack of an amine on the methoxysilane was proposed to be the mechanism to methylamines in the DMF promoted reaction reported by Lei.⁹³



Scheme 5.14: Alternative route to methylmorpholine **48** via reduction of CO₂ to methoxysilane species

The formation of methoxysilane species **82** was observed during ¹H NMR monitoring of reduction of CO₂ with PhSiH₃ and TMG (5 mol%) at 60 °C by a broad band at 3.7 – 3.1 ppm, (Chapter 3, Figure 3.27). However, when morpholine was added to the reaction no conversion to methylmorpholine was observed and instead aminal **57** and formylmorpholine products were observed. To further investigate the reactivity of the methoxysilane species, CO₂ was reacted with PhSiH₃ with 5 mol% TMG at 60 °C for 60 minutes, following this the reaction was flushed with N₂ for 60 minutes to remove any unreacted CO₂ and a second equivalent of PhSiH₃ was added to further reduce any CO₂-silane species, Scheme 5.15. On addition of morpholine, no methylmorpholine was formed. This result suggests that either methoxysilane species were not formed under the reaction conditions or it is unreactive to morpholine. However, to further confirm this, a reaction between independently prepared Si(OMe)₃Ph or SiH₂(OMe)Ph and morpholine is required.



Scheme 5.15: Reduction of silylacetal and formoxysilane intermediates to investigate possible formation of Si-OMe species and its subsequent reaction with morpholine **18**. ^{a)} Conversions determined by ¹H NMR relative to **18** substrate. 13 % unidentified morpholine species

5.6 Rate Enhancement with Alkylated TMG Catalysts

The faster formation of methylmorpholine when alkylated catalysts butylTMG **64** and methylTMG **65** were used as the catalyst compared to with TMG was further investigated, Figure 5.13.

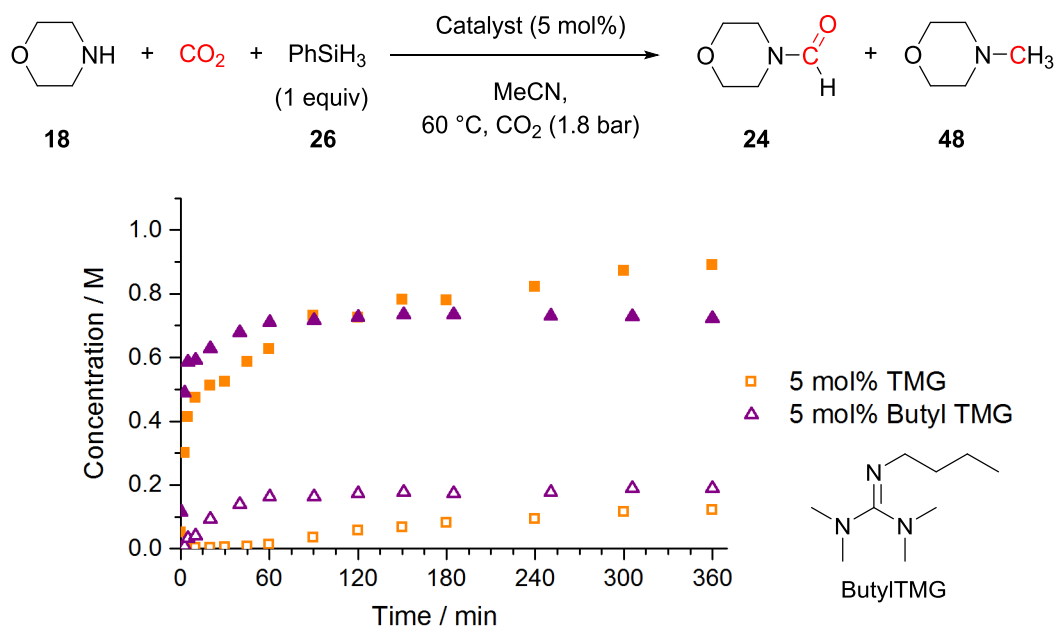
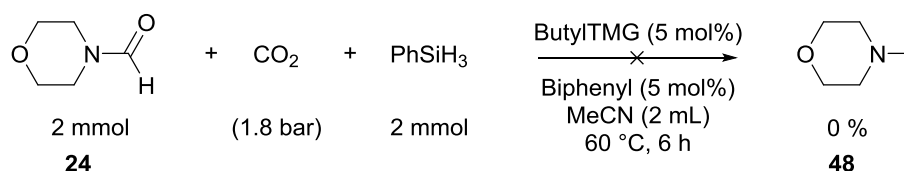


Figure 5.13: Comparison of rate of methylmorpholine formation (by GC) with TMG and butylTMG as the catalyst at 60 °C. Reaction Conditions: **18** (2 mmol), PhSiH₃ (2 mmol), catalyst (0.1 mmol), MeCN (2 mL), biphenyl (0.1 mmol), CO₂ (1.8 bar), 60 °C. Filled: **24**, Hollow: **48**

Firstly, the possibility that butylTMG can promote the reduction of formylmorpholine to methylmorpholine was studied. However, reaction of formylmorpholine under standard reaction conditions at 60 °C with 5 mol% butylTMG, led to no conversion to methylmorpholine, indicating this is not a feasible pathway, Scheme 5.15.



Scheme 5.16: Attempted reduction of formylmorpholine **24** with CO₂ and PhSiH₃ using ButylTMG as the catalyst led to no conversion

Mechanistic investigation with TMG have so far suggested that the dominant pathway to methylmorpholine formation is via an aminor **57** intermediate. Therefore the effect of butylTMG on aminor **57** reactivity was studied. Reaction of aminor **57** with CO₂ and PhSiH₃ with butyl TMG showed a slight decrease in rate of formation of **24** and **48** compared to TMG,

Figure 5.14. Thus suggesting that the rate enhancement of butylTMG is due to an increased rate of formation of the aminal, rather than the reaction of aminal **57** to methylmorpholine **48**.

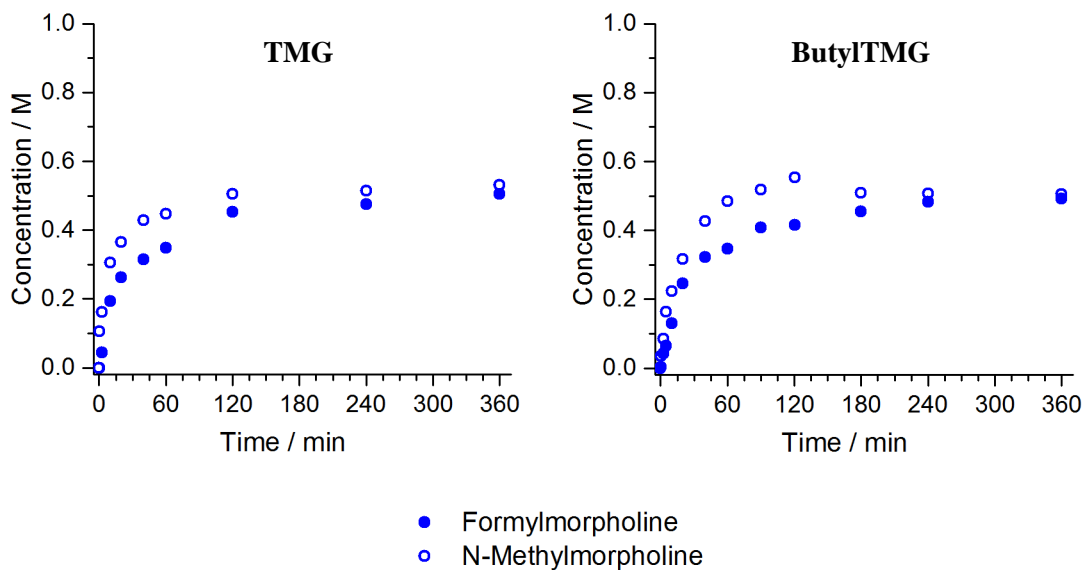
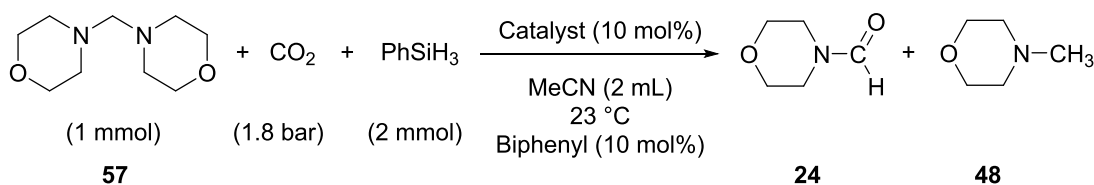


Figure 5.14: Kinetic profiles (GC) of products **24** and **48** from reaction of **57** under standard reaction conditions at 23 °C a) TMG and b) ButylTMG

The rate of formation of the aminal in the reaction of morpholine with CO₂ with butylTMG was investigated at 60 °C by ¹H NMR monitoring, Figure 5.15. The aminal **57** rapidly forms and reaches a maximum of 32 % after 6 minutes, before being partially consumed to give a final yield of 10 % **57** and 22 % **24** after 6 hours. This is contrasting to the corresponding reaction with TMG whereby the maximum concentration of aminal **57** at 20 % was only reached after 120 minutes, Figure 5.4. As the reaction with butylTMG at 60 °C also gave aminal **57** as the final product, this further suggests that PhSiH₃ is consumed faster in the reaction and is thus unavailable to reduce the aminal **57** to **48** and **24**.

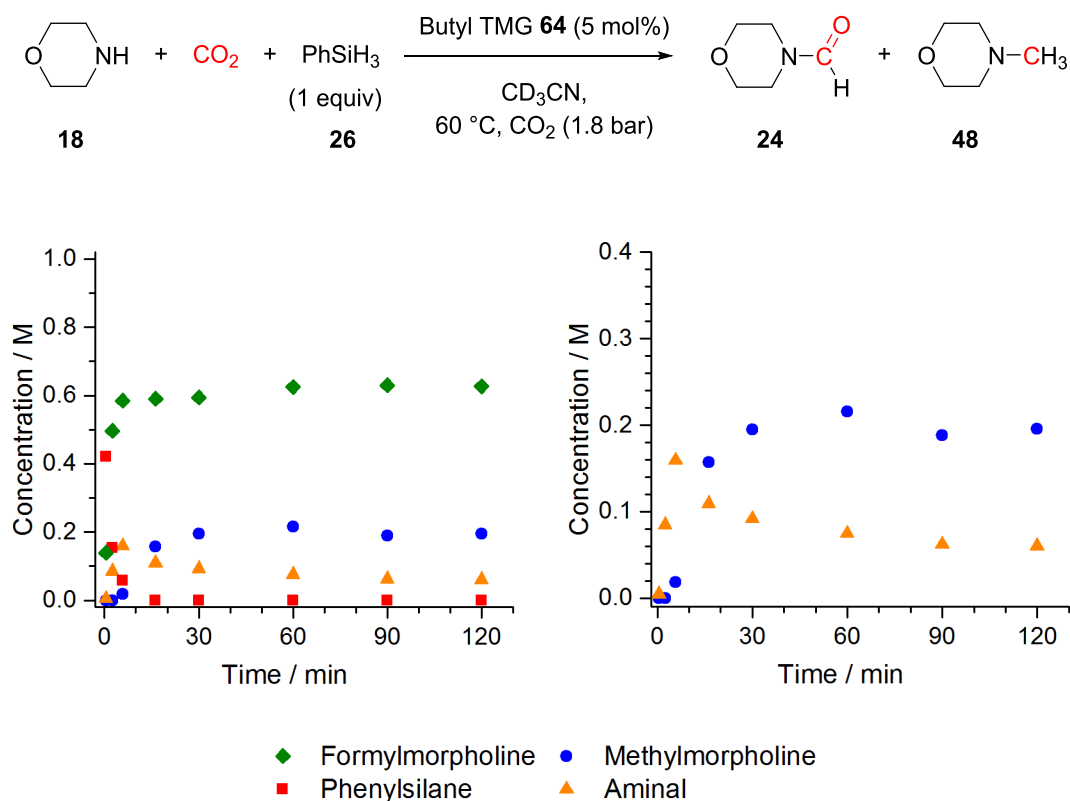


Figure 5.15: ¹H NMR kinetics of morpholine reaction at 60 °C. Reaction conditions: **18** (2 mmol), PhSiH₃ (2 mmol), CD₃CN (2 mL), ButylTMG (0.1 mmol), 1,3,5-trimethoxybenzene (0.1 mmol), CO₂ (1.8 bar), 60 °C a) full reaction profile b) enlarged region displaying aminal and methylmorpholine trends only

These results suggest that as well as preventing catalyst deactivation, alkylating TMG also promotes the reduction of CO₂ to the bis(silyl)acetal species **80**, which can react with morpholine to give aminal **57**. The mechanism by which the alkylated catalyst promotes the rate of CO₂ reduction to the bis(silyl)acetal species is unclear. However, earlier proposals (Chapter 3) led to the suggestion that at high temperatures TMG promotes the reduction by coordination of the TMG to the Si species to form a hypervalent species, activating the Si-H bond for reaction with CO₂, Figure 5.16. Thus alkylating TMG with electron donating groups may increase the nucleophilicity of the catalyst and promote this activation mode. However, the nucleophilicity of alkylated TMGs has not been reported and further investigation is required to determine if this is the cause for increased rate of reduction.

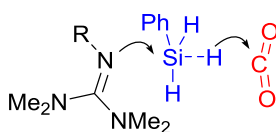
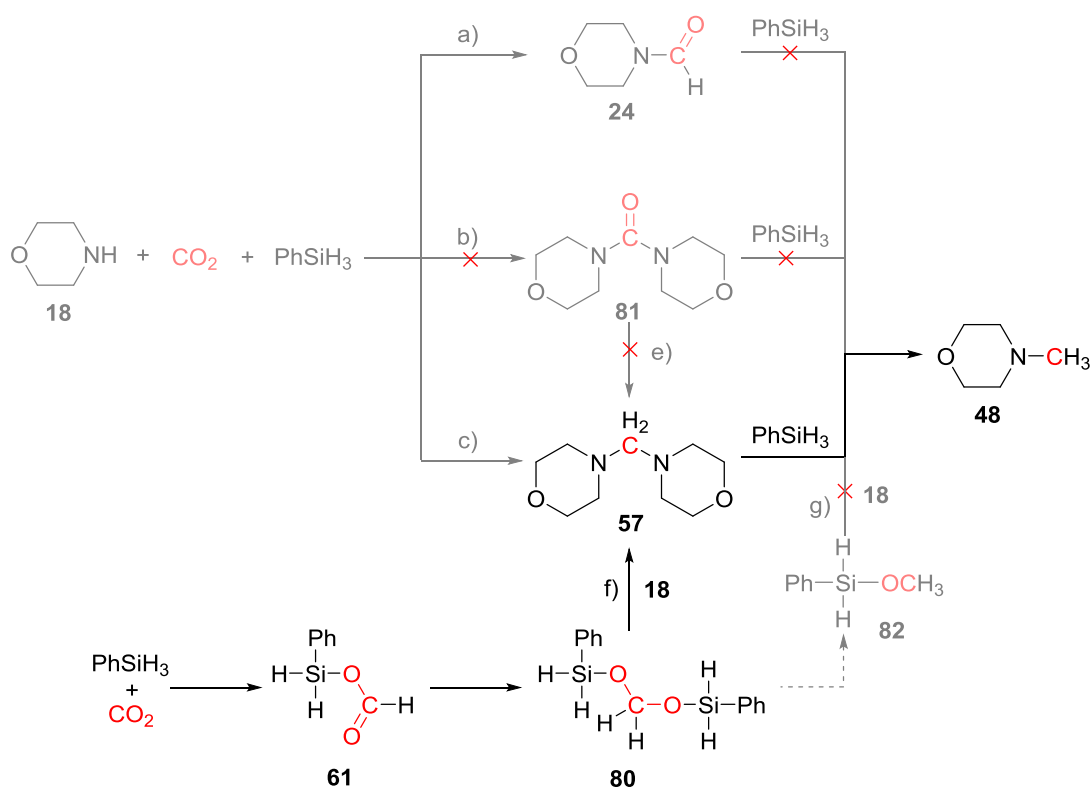


Figure 5.16: Proposed activation of Si-H by nucleophilic attack from catalyst

5.7 Summary of Pathways to Methylmorpholine

The results of the mechanistic study suggest that in the guanidine catalysed reductive functionalisation of CO₂ with morpholine and hydrosilane, the dominant pathway to methylmorpholine is via the formation of an aminal intermediate. The potential reduction of formylmorpholine **24** to methylmorpholine **48** was found not be feasible under the reaction conditions, (Pathway a, Scheme 5.17), contrasting to similar studies with fluoride and borane catalysts.^{77, 92} Similarly, the involvement of a methoxysilane species **82** (Pathway g),⁹³ or the involvement of a urea intermediate **81** (Pathways b & e), can also be discounted.



Scheme 5.17: Pathways investigated for the production of methylmorpholine in the reductive functionalisation of CO₂ with morpholine and phenylsilane – dominant pathway in bold

The proposed pathway to methylmorpholine involves reduction of CO₂ with phenylsilane to give formoxysilanes **61** and subsequent reductive coupling to yield bis(silyl)acetals **80**. This reduction was only found to occur at high temperatures, consistent with the observation that methylmorpholine is produced in larger yields at 60 °C than at 23 °C. Sequential nucleophilic attack of morpholine on silylacetal **80** yields the aminal species **57**. The aminal **57** was shown to be reduced to give methylmorpholine **48** and formylmorpholine **24** as the products and occurred rapidly at 23 and 60 °C. To proceed, the reaction required CO₂, PhSiH₃ and TMG. A mechanism for reduction of aminal **57** was proposed which involves activation of the aminal through reaction with CO₂ and PhSiH₃, the formed iminium species is stabilised by TMG,

enabling reduction by the hydrosilane to give **48**. The silylcarbamate species is also formed in a 50:50 ratio with **48**, which can then undergo subsequent reaction to give either formylmorpholine **24** at low temperatures, or a mixture of formyl- **24** and methylmorpholine **48** at high temperatures as discussed in Chapter 3, Scheme 5.18.

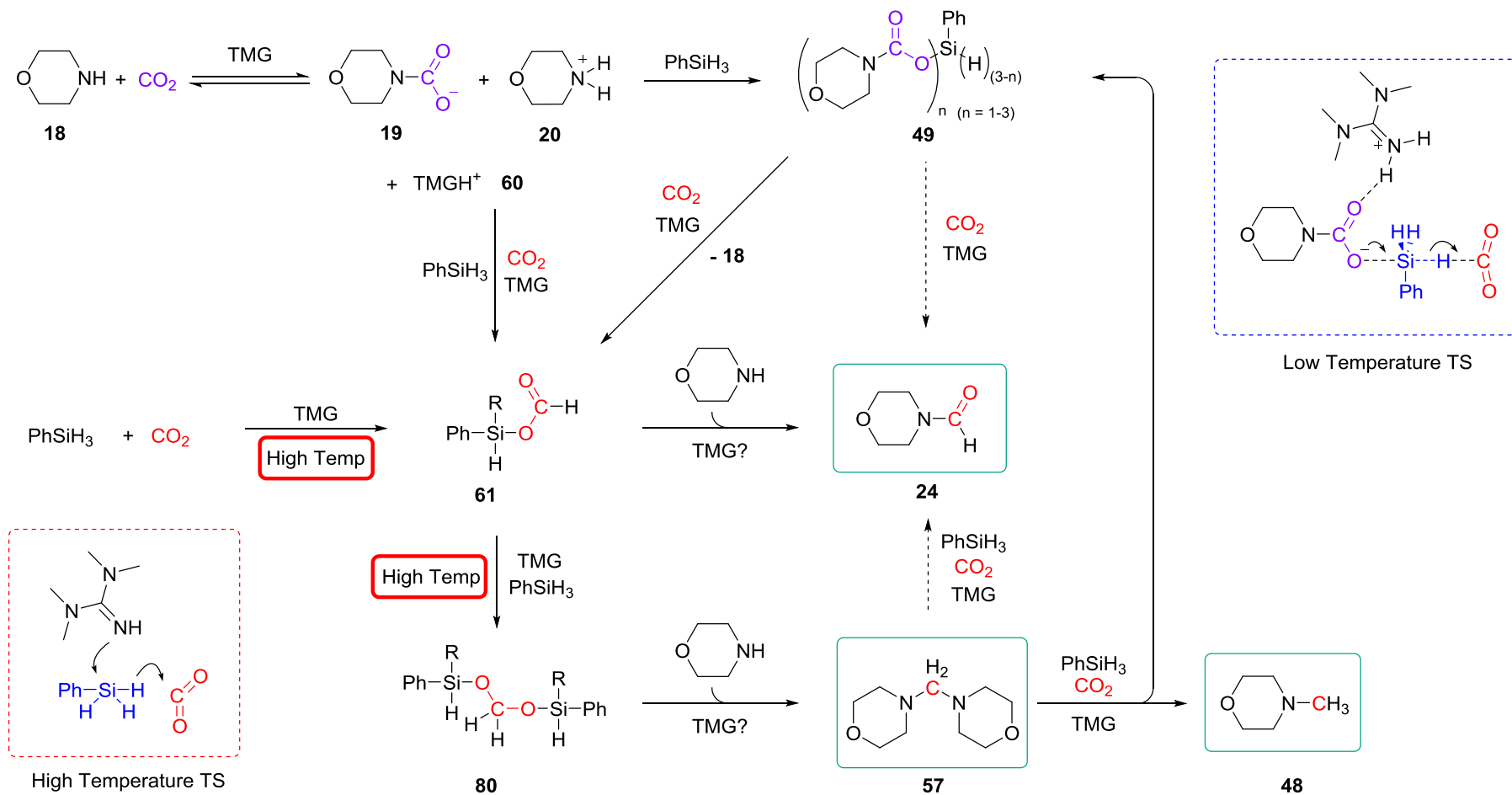
5.8 Summary of Product Selectivity

The guanidine catalysed reductive functionalisation of CO₂ with morpholine and phenylsilane has been shown to produce three main products: formylmorpholine **24**, methylmorpholine **48** and the aminor, dimorpholinomethane **57**. The results of the mechanistic study discussed in Chapters 3 – 5, have shown that the pathways to these products are all closely linked and intertwined, as summarised in Scheme 5.18.

The product ratio of **24**, **48** and **57** is dependent upon which pathway is favoured and this can be effected by reaction temperature, stoichiometry and order of reagent addition. At low temperatures the formylmorpholine **24** product can be formed with high selectivity (98 %), the pathway involves activation of PhSiH₃ via a silylcarbamate species to formoxysilane **61**, which undergoes transformylation with morpholine to yield **24**. At higher temperatures an alternative activation mode to formoxysilane **61** can operate, this leads to further reduction of formoxysilane **61** to bis(silyl)acetal **80**, reaction with morpholine can lead to aminor **57**, and if unreacted silane is still present this can be further reduced to give either **24** or **48** products, and hence may explain the second stage increase in formylmorpholine **24** in some kinetic profiles at higher temperatures.

Higher equivalents of PhSiH₃ have been shown to increase formation of methylmorpholine **48**. Based on the proposed mechanism, this is due to a higher proportion of PhSiH₃ being able to react with CO₂ via the high temperature pathway to give more of the bis(silyl)acetal species, this then competes with the formoxysilane **61** for reaction with morpholine to give aminor **57**. This also explains why the addition of morpholine added last gives formation of aminor **57** rather than methylmorpholine **48**. In this case, with no morpholine to react with, more of the formoxysilane **61** species is reduced to the bis(silyl)acetal **80**, addition of morpholine after completion leads to aminor **57**; as all of the silane has been consumed by this point, the aminor cannot be reacted further to give either **24** or **48** and is hence a stable product.

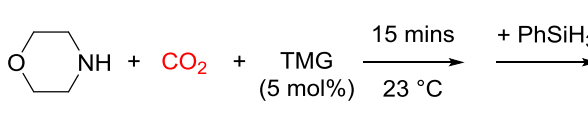
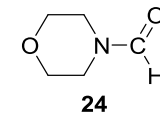
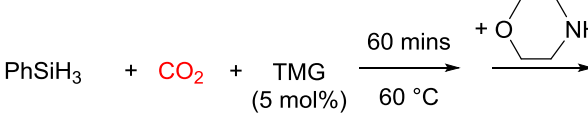
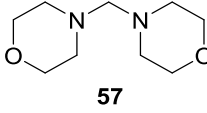
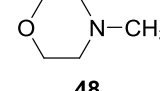
Alkylated catalysts have been shown to promote formation of methylmorpholine **48** and aminor **57** compared to use of TMG as the catalyst. This again is proposed to be due to the promoted reduction of formoxysilane **61** to bis(silyl)acetal species **80**.



Scheme 5.18: Summary of proposed active pathways in the guanidine catalysed reductive functionalisation of CO₂ with morpholine and phenylsilane to formylmorpholine, methylmorpholine and aминаl products. Low and high temperature activation modes are highlighted

The highest product selectivity achieved for each product reported so far and the corresponding reaction conditions are given in Table 5.5. Whilst high selectivity for formylmorpholine **48** (98 %) has been achieved, the selectivity for aminal **57** and methylmorpholine **48** are low at 32 % and 28 % respectively. However, these results do not represent optimised conditions. On the basis of the mechanistic study it is proposed that yields of aminal **57** could be improved by optimising the length of pre-reaction time between PhSiH₃, CO₂ and catalyst, as well as increasing the reaction temperature and using methylTMG **65** as the catalyst. Similarly, to gain high selectivity for methylmorpholine **48**, higher reaction temperatures, increased equivalents of PhSiH₃ and use of butylTMG would be expected to favour methylmorpholine.

Table 5.5: Reaction conditions that have led to the highest selectivity reported for each product

Reaction condition	Product	Yield (%)
	 24	98
	 57	32
	 48	28

A recent study by He on the reductive functionalisation of CO₂ with amines and hydrosilanes with glycine betaine as the organocatalyst has reported the ability to control the product ratios between formamides, aminals, and methylamines.¹⁶¹ By increasing the reaction temperature and reducing the amount of CO₂, methylamines and aminals were produced with high selectivity. However, aromatic substrates were found to favour methylation compared to aliphatic amines, and similarly when aminals were targeted, the maximum reported yield for aliphatic amines was 43 %, compared 90% for some anilines. This is in line with observations from the substrate scope investigations for the guanidine catalysed process reported in Chapter 4, whereby higher yields of the methylamine products were observed with anilines with electron withdrawing substituents. These observations may suggest that the lower nucleophilicity of aromatic amines leads to a lower rate of transformylation of the amine with formoxysilane **61** and thus more of the formoxysilane **61** is reduced to the bis(silyl)acetal species **80**, enabling subsequent reaction to the corresponding aminal and methylamine product.

5.9 Conclusions and Future Work

In conclusion, guanidine catalysts have been shown to be highly efficient catalysts for the reductive functionalisation of CO₂ with morpholine and phenylsilane. Experimental evidence has supported that multiple, intertwined pathways can operate to produce methylamines, formylamides and amination products. Silylcarbamates, formoxysilanes and bis(silyl)acetals were shown to all be important intermediates in the reaction, and experimental evidence has been provided to support previously computationally proposed activation modes.⁸³ Through understanding the factors affecting each of these activation modes at high and low temperatures, the different product ratios observed can be explained. These results are important to guide the future rational development of reductive functionalisation reactions with high product selectivity.

Whilst a broad substrate scope has been demonstrated for the amine formylation reaction with PhSiH₃, the mechanistic study has only been focussed on the aliphatic amine, morpholine. Previous studies have suggested that aliphatic and aromatic amines display different reactivity and may alter product selectivity.^{59, 97, 161} Therefore the reactivity of aromatic amines in the pathways proposed in Scheme 5.18 should be investigated. In particular the lower nucleophilicity of aniline may alter the equilibrium between the amine and CO₂ as well as affecting silylcarbamate formation. Furthermore, the primary amine benzylamine was shown to form the corresponding urea under standard formylation reaction conditions. This highlights that other reaction pathways may be feasible for primary amines, in particular the formation of isocyanate intermediates may be involved and as such needs to be investigated further.

Phenylsilane has been shown to be an active reductant for this transformation; however, it is relatively expensive compared to other hydrosilanes and its moisture sensitivity make it less favourable for use in CO₂ utilisation reactions due to the requirement for dry CO₂. Alternatively, the mechanistic investigation could be extended to encompass PMHS as a reductant, to enable the development of a more sustainable process. This was demonstrated to work with guanidine catalysts in Chapter 4, however with a lower activity and methylamine and amination products were not observed.

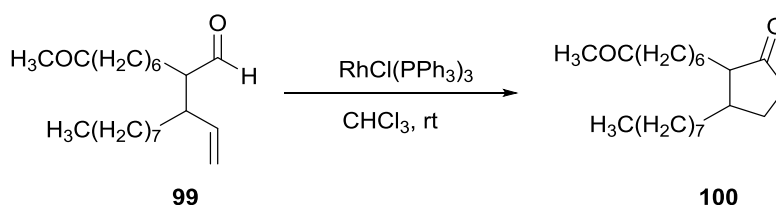
The guanidine catalyst can have a large effect on the reactivity and selectivity of the reaction. However it is not always clear as to how the structure relates to the activity of the catalyst, as it does not appear to be a linear relationship with pK_a. To further investigate this the effect of a series of substituted phenylTMG catalysts (suggestion by Matthew Hughes, Syngenta) for which the pK_as in acetonitrile have been well studied, would enable a direct comparison between the effect of pK_a and catalyst activity.¹⁶²

Chapter 6

Developing a Process for Reaction of CO₂ with Biomass Derived Compounds

6.1 Introduction to Hydroacylation Reactions

Hydroacylation reactions typically involve the addition of an aldehyde into a C=C double bond in both intra- and intermolecular reactions and are highly atom-economical transformations.¹⁶³ The first example of a hydroacylation reaction was reported by Sakai in 1972, whereby the synthesis of cyclopentanone **100** was achieved by intramolecular hydroacylation using stoichiometric amounts of rhodium to promote the reaction, Scheme 6.1.¹⁶⁴



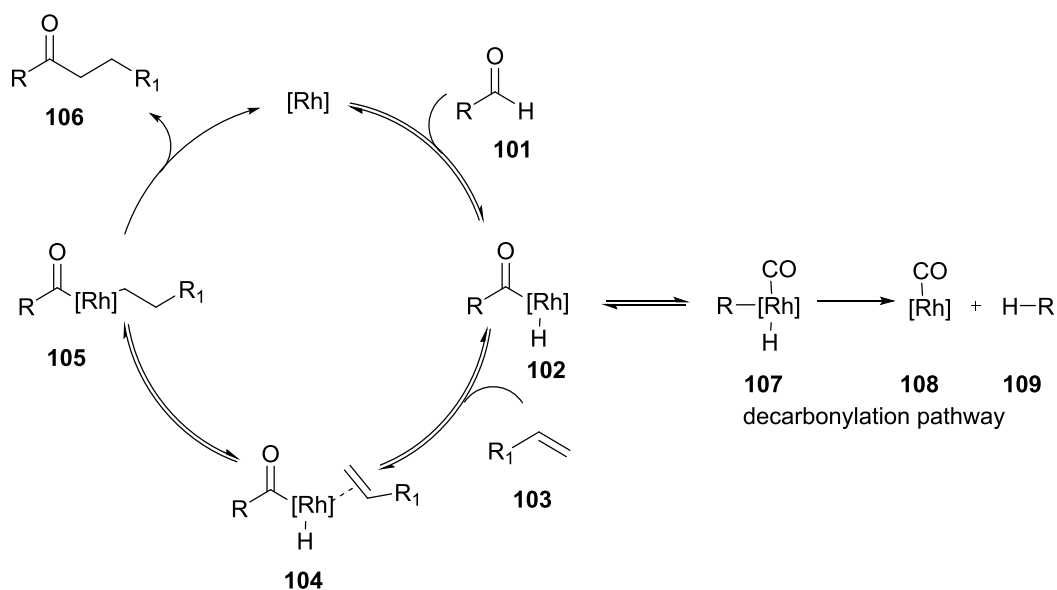
Scheme 6.1: First reported Rh catalysed intramolecular hydroacylation reaction by Sakai¹⁶⁴

The subsequent development of intermolecular versions posed a challenge due to the instability of the intermediates leading to irreversible decarbonylation of the aldehyde once bound to the catalyst. This is a predominant problem in Rh and Ir catalysis, leading to decomposition of the substrate and deactivation of the catalyst.¹⁶⁵ Rhodium complexes are the most commonly used catalysts for hydroacylation reactions, although other transition metal complexes including Co,^{166, 167} Ir,^{168, 169} Ru,^{170, 171} and Ni¹⁷² have been reported.

6.1.1 Mechanistic Overview

The first step in the hydroacylation reaction is oxidative addition of the aldehyde **101** across the C-H bond to the Rh catalyst, generating an acyl metal hydride complex **102**, identified by NMR spectroscopy.^{173, 174} Following this, the alkene component coordinates and the hydride is inserted into the unsaturated C-C bond. The ketone product **106** is released via reductive elimination which is the turnover limiting step and the catalyst is reformed, Scheme 6.2.¹⁷⁴⁻¹⁷⁷

A significant side reaction in the intermolecular hydroacylation reaction is decarbonylation of the aldehyde from the acyl metal hydride **102** to form a carbonyl complex **108** and the corresponding alkane **109**, Scheme 6.2. The formed metal carbonyl complexes are stable and reduce catalytic reactivity.^{178, 179}



Scheme 6.2: General proposed catalytic cycle for alkene hydroacylation with a Rh catalyst, including completing decarbonylation pathway

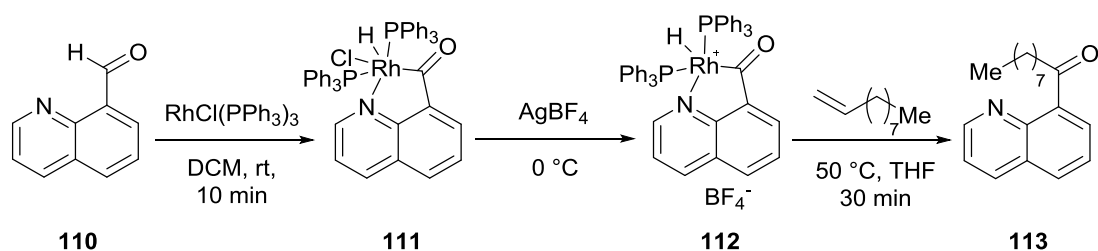
A variety of approaches have been used to inhibit the decarbonylation pathway, to be discussed, which is thought to occur through a coordinatively unsaturated metal centre and an unstabilised aldehyde substrate.¹⁷⁶

6.1.2 Substrate Control

One approach to reduce decarbonylation has been modification of the substrate. Intramolecular hydroacylation reactions were found to be more successful due to coordination of the internal alkene to the catalyst, preventing decarbonylation. This led to the development of substrates with heteroatom chelating groups that can coordinate to the metal, forming a five membered ring, such as nitrogen, phosphorus, sulfur and oxygen.¹⁷⁵

6.1.2.1 N-Chelation

Suggs initially proposed using quinoline-8-carbaldehyde **110**, which has a coordinating nitrogen atom, to enable an acyl rhodium(III) hydride intermediate to be isolated from reaction with Wilkinson's complex $[\text{RhCl}(\text{PPh}_3)_3]$, Scheme 6.3.¹⁷⁸ The isolation and characterisation of this complex demonstrated that a five-membered acylmetallacycle was formed which prevented decarbonylation of the aldehyde due to the formation of an 18-electron complex inhibiting acyl to alkyl rearrangement.¹⁷⁸ The five-membered ring **111** is further thought to disfavour decarbonylation, as the decarbonylation pathway would require a strained four-membered ring to be formed in the process.¹⁷⁶ This would inhibit the reverse reaction, preventing reductive elimination of the original aldehyde.¹⁷⁸



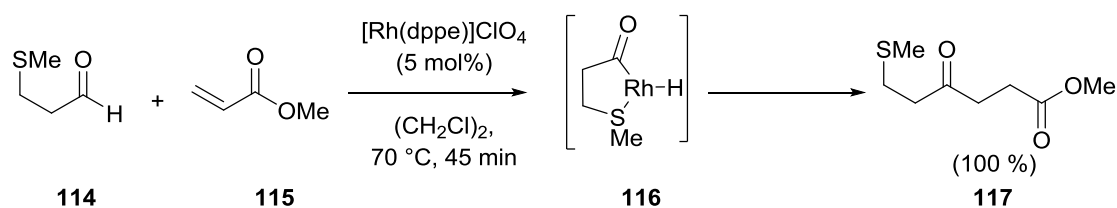
Scheme 6.3: Isolation of acylrhodium(III) hydride intermediate and subsequent hydroacylation reaction on introduction of alkene ^{18, 20}

The addition of AgBF_4 generates a catalytically active, coordinatively unsaturated complex **112** which does not undergo decarbonylation, demonstrating the stability of this coordinating aldehyde.¹⁷⁸ On addition of an alkene, the ketone hydroacylation product **113** is produced and released via reductive elimination, Scheme 6.3.^{178, 180}

Jun further developed the use of quinoline-8-carbaldehyde **110** to demonstrate a broader variety of alkene substrates, e.g. styrene and vinylcyclohexane, with Wilkinson's complex. Use of $[\text{RhCl}(\text{COE})_2]_2$ trimethylphosphite (COE: cyclooctene) to promote reductive elimination also led to an increased range of alkenes that could be used.¹⁸¹ While this method has been successful in isolating the reaction intermediates and demonstrating the advantages of coordinating substrates, the product has limited synthetic applications due to the challenges associated with converting the coordinating nitrogen into synthetically useful functional groups.¹⁷⁵

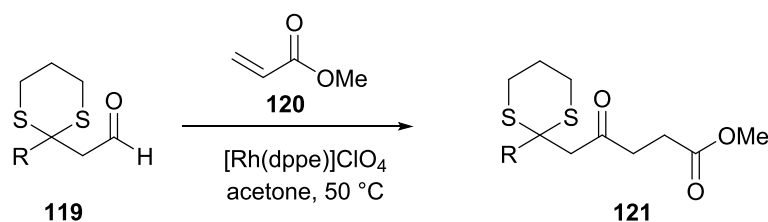
6.1.2.2 S-Chelation

The use of S-chelation in intermolecular hydroacylation reactions was first developed by Willis.¹⁸² β -Methylsulfide propanal **114** was initially investigated with $[\text{Rh}(\text{dppe})]\text{ClO}_4$, which was successful in the hydroacylation reaction with electron-poor alkenes, Scheme 6.4.¹⁸² The methyl sulfide substituent was proposed to coordinate to the rhodium, forming a five-membered intermediate **116**, which prevented decarbonylation through stabilisation; whilst still enabling hydroacylation to occur.^{8, 183}



Scheme 6.4: Example of optimal sulfur coordinating substrate and hydroacylation conditions developed by Willis ¹⁸²

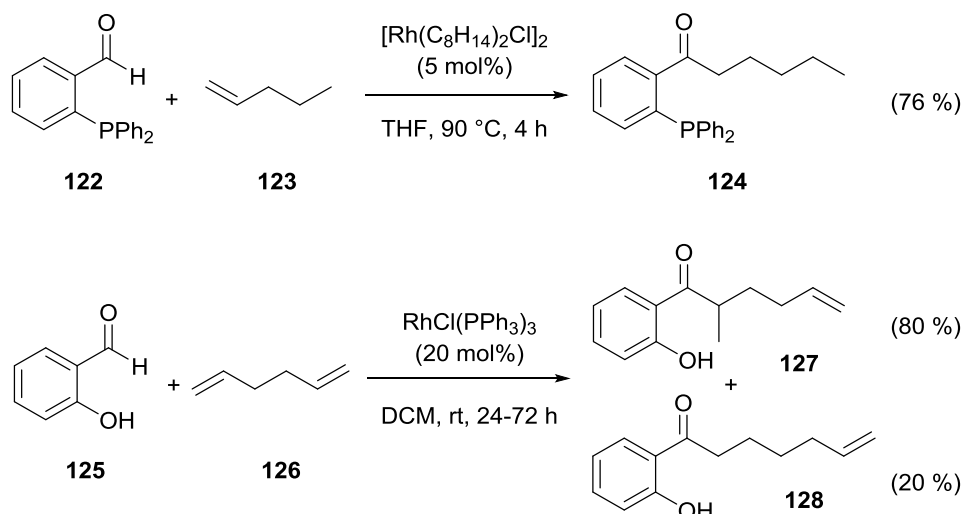
However, key limitations were the requirement for electron-poor alkenes and the limited synthetic application of the products.¹⁷⁷ Use of $[\text{Rh}(\text{COD})\text{Cl}]_2$ and DPEphos ligand, eliminated the requirement for electron poor alkenes and use of 2-methylthiobenzaldehyde **118** further increased substrate scope.^{176, 177} β -Thioacetal-substituted aldehyde **119** (Scheme 6.5) enabled a broader scope of product functionalization, as the thioacetal could readily be transformed to ketones, alcohols, carboxylic acids or alkanes.¹⁸⁴



Scheme 6.5: Improved β -thioacetal-substituted aldehyde to enable greater synthetic scope from the hydroacylation product¹⁸⁴

6.1.2.3 *P*- and *O*- Chelation

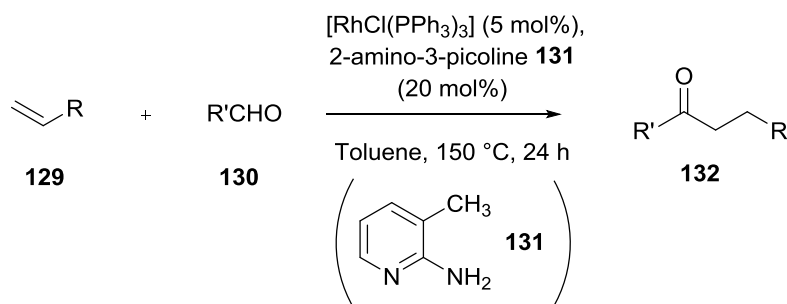
P-chelating aldehydes such as 2-(diphenylphosphino)benzaldehyde **122** are also successful in preventing decarbonylation and form the corresponding ketone product **124**, Scheme 6.6.¹⁸⁵ Tanaka demonstrated the success of salicylaldehydes **125** in comparison to benzaldehyde in work with dienes and showed that the OH group is required for chelation to the rhodium.¹⁸³



Scheme 6.6: Further chelation control of substrate: a) use of 2-(diphenylphosphino)benzaldehyde as a *P*-chelating aldehyde,¹⁸⁵ b) use of salicylaldehydes as a *O*-chelating substrate¹⁸³

6.1.2.4 Via Imine Formation

An alternative approach to widen the synthetic scope of aldehydes has been developed by Jun. It was reported that by using amines, such as 2-amino-3-picoline **131**, the picolyl imine can be formed from the aldehyde **130** which then acts to stabilise the substrate through chelation to the rhodium, Scheme 6.7.¹⁸⁶



Scheme 6.7: Use of picolyl imines in promoting hydroacylation reactions¹⁸⁶

6.1.3 Additive Control

An alternative approach to preventing decarbonylation by creating a coordinatively saturated metal intermediate is through the use of an ethene or carbon monoxide atmosphere at high pressure.^{165, 170, 171} The ethene and carbon monoxide ligands are proposed to be labile, enabling exchange with the aldehyde while maintaining coordinative saturation to limit the decarbonylation pathway.^{165, 170, 171}

6.1.4 Catalyst Control

The initial catalysts used in hydroacylation reactions, e.g. $[\text{RhCl}(\text{PPh}_3)_3]$ and $[\text{Rh}(\text{dppe})\text{-acetone}]_2\text{ClO}_4$, have many limitations including a limited substrate scope and the requirement for *in situ* hydrogenation. This provided a need for an improved and easily accessible catalyst system.^{176, 182} $[\text{Rh}(\text{COD})\text{Cl}]_2$, DPEphos (2 equiv) and $\text{Ag}(\text{ClO}_4)$ (1 equiv), was highlighted by Weller and Willis as an improved system for use with β -substituted aldehydes.¹⁷⁶

The hemi-labile ligand, DPEphos **133**, was compared to similar, more rigid, ligands such as Xanphos **134**, Figure 6.1. DPEphos showed significant catalytic activity over Xanphos, indicating that flexibility in the conformation of the ligand is important to enable the rhodium centre to progress through different geometries and oxidation states during the catalytic cycle.¹⁷⁶ The use of a chelating aldehyde also ensured that hydrogenation was not required for the reaction. DPEphos is thought to be a successful ligand due to temporarily binding to vacant sites on the Rh, this limits their availability for decarbonylation of the aldehyde; however, the oxygen coordination site is labile enough to still enable the hydroacylation reaction to occur.¹⁷⁷

Similar comparisons with thioether ligands **135** indicated that the sulfur bound too strongly to the rhodium, resulting in a permanently coordinatively saturated complex, preventing the hydroacylation reaction.¹⁷⁶

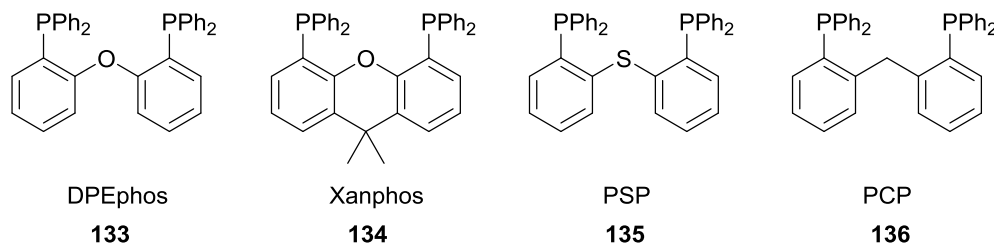


Figure 6.1: Ligands investigated by Willis and Weller: DPEphos **133**, Xanphos **134**, PSP **135**, PCP **136**¹⁷⁶

After initial suggestions that the large bite angle of the DPEphos contributed to promoting reductive elimination,¹⁷⁶ a broader investigation into the effects of bite angles was conducted.¹⁸⁷ Using $[\text{Rh}(\text{Ph}_2\text{P}(\text{CH}_2)_n\text{PPh}_2)(\text{H})_2(\text{acetone})][\text{Bar}^{\text{F}}_4]$ (Ar^{F} : 3,5-(CF_3) $_2\text{C}_6\text{H}_3$) complexes, where ($n=2-5$), the effect of the bite angle was investigated, Figure 6.2.

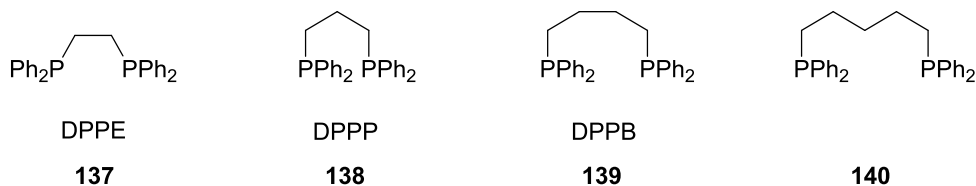


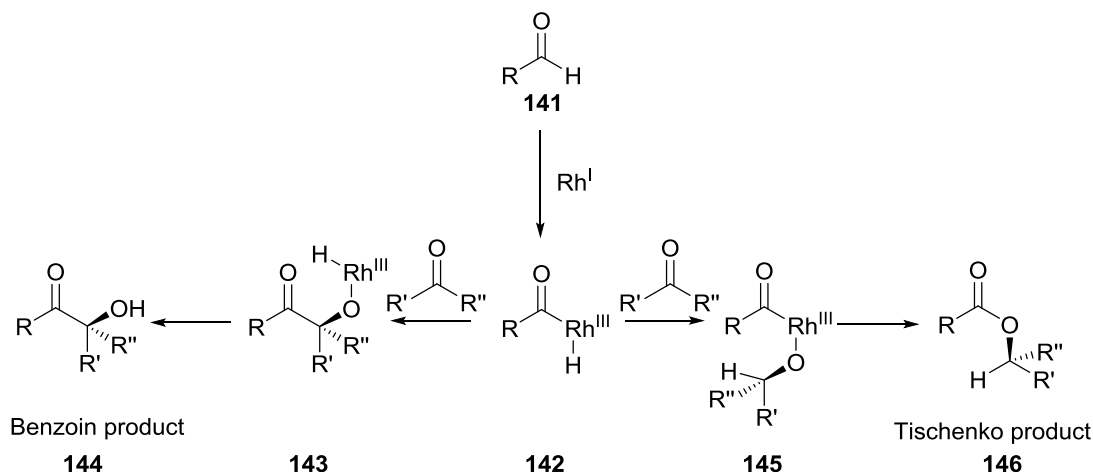
Figure 6.2: Ligands $\text{Ph}_2\text{P}(\text{CH}_2)_n\text{PPh}_3$ where: $n=2$, DPPE **137**; $n=3$, DPPP **138**; $n=4$, DPPB **139**; $n=5$ **140**

It was shown that small bite angles, e.g. $n=2$ **137** (Figure 6.2), successfully catalyse the alkene hydroacylation reaction and produce more effective catalysts. It is speculated that these complexes promote reductive elimination of the product.¹⁸⁸ As the bite angle is increased however, i.e. $n=5$ **140**, there is reduced access to the rhodium; therefore, the coordination of the alkene is disfavoured and aldehyde hydroacylation reaction occurs to give the Tischenko product.¹⁸⁷ If acetone is used as the solvent, acetone adducts may also be observed.¹⁸⁸

6.1.5 Carbonyl Hydroacylation Reactions

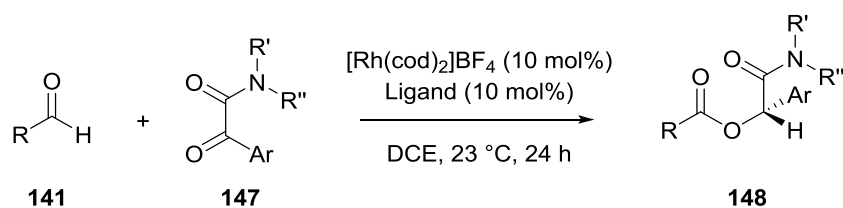
Further interesting developments to hydroacylation reactions is work by Dong *et al.* who have developed intramolecular ketone hydroacylation methodology.^{189, 190} The methodology was developed to provide an alternative approach to lactonisation, with the key advantage of developing a regio- and enantio-selective method.¹⁸⁹

The ketone hydroacylation has the potential to react in two pathways to produce Tishchenko products **146**, via hydrometalation, or benzoin products **144**, via acylmetalation, Scheme 6.8. The development was focused on the Tischenko reaction to form the ester for use in lactone synthesis and no benzoin products were observed under the selected conditions.¹⁸⁹ A catalyst system of 5 mol% [Rh(ligand)]BF₄ was selected and a range of phosphine ligands were examined. It was generally observed that the greater the basicity of the phosphine, the more selective the catalyst is for hydroacylation over competing decarbonylation.¹⁸⁹



Scheme 6.8: Proposed hydrometalation and acylmetalation routes during ketone hydroacylation

Subsequent work demonstrated that an intermolecular ketone hydroacylation reaction could be achieved when a ketone bearing a directing group (an amide) was employed, Scheme 6.9.^{191, 192} The reaction proceeded with use of a rhodium catalyst and bidentate phosphine ligands, preferentially when π -accepting groups and σ -donating groups were present on the ligand.

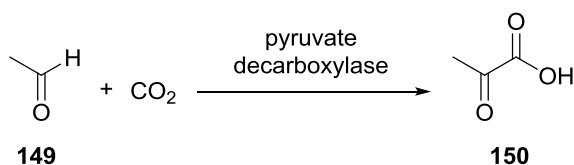


Scheme 6.9: First reported intermolecular ketone hydroacylation reaction¹⁹²

6.1.6 Reaction of CO₂ with Aldehydes

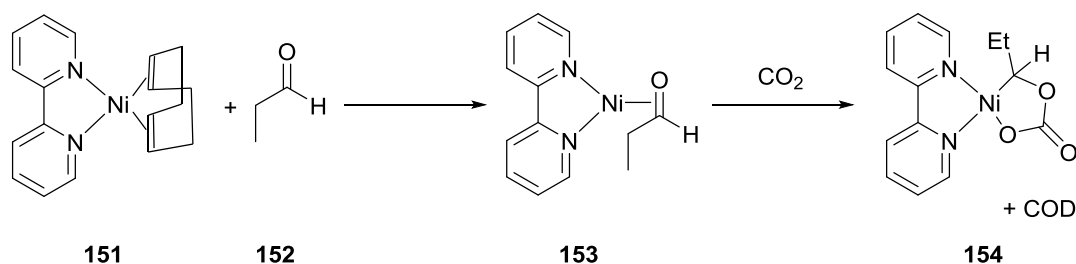
There are currently very few examples for catalytic reactions of CO₂ with aldehydes. One of the few examples involving insertion of CO₂ into the C-H bond of an aldehyde is demonstrated by nature in enzyme catalysis.^{193, 194} Pyruvic acid **150**, a α -ketoacid, was synthesised from

ethanal **149** and CO₂ using pyruvate decarboxylase enzyme in the presence of supercritical CO₂, Scheme 6.10.¹⁹³



Scheme 6.10: Synthesis of pyruvic acid **150** from CO₂ and ethanal **149**

A key example of the reaction of aldehydes with CO₂ at a transition metal centre was first reported by Walther *et al.*^{195, 196} and further developed by Geyer *et al.* during their study of nickel(0) centres.¹⁹⁷ It was shown that using [Ni(bipy)(COD)], aldehydes such as benzaldehyde and propionaldehyde react reversibly with the Ni complex.¹⁹⁷ When CO₂ was introduced into the system it reacted with the nickel propionaldehyde complex **153** undergoing insertion into the Ni-O bond, rather than directly with the [Ni(bipy)(COD)] complex, Scheme 6.11.¹⁹⁷



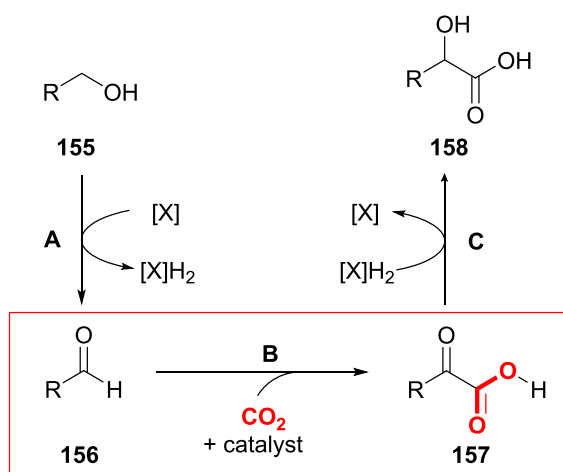
Scheme 6.11: Insertion of CO₂ into Ni-O bond of aldehyde-Nickel complex¹⁹⁷

Following CO₂ insertion, the carbonate complex could not be eliminated from the nickel complex, as is similar with the oxidative coupling of CO₂ and olefins, which requires an aqueous workup to extract the product, deactivating the metal complexes.²³ The release of the product is noted as one of the main limitations of using transition metal complexes in CO₂ reactions.²³

6.2 Aims of Study and Previous Work

This project aimed to design a novel catalytic process to react CO₂ with biomass platform chemicals to develop products of interest to the chemical industry, using conditions accessible for industrial scale synthesis. The overall aim is to devise a catalytic synthesis for the conversion of an alcohol to an α -hydroxycarboxylic acid through reaction with CO₂, Scheme 6.12. For example, using bioethanol as the substrate would lead to formation of lactic acid which is of interest to industry due to its role in polyacetic acid synthesis.

To achieve this conversion an initial hydrogen borrowing approach could enable conversion of the alcohol **155** to an aldehyde **156** (Step A, Scheme 6.12), typically transition metal complexes such as Ir, Ru or Rh are reported for similar reactions. Step B would involve insertion of CO₂ into the aldehyde C-H bond to produce an α -ketocarboxylic acid **157**; again this approach is most likely to be successful through use of a transition metal complex. The final step (Step C) would involve reduction of the α -ketocarboxylic acid **157** to the corresponding α -hydroxycarboxylic acid **158**, through reversal of the initial hydrogen borrowing stage (Scheme 6.12).



Scheme 6.12: Proposed reaction of biomass derived alcohol to the corresponding α -hydroxycarboxylic acid. X = transition metal catalyst, e.g. Rh, Ru or Ir

This chapter reports initial investigations into the insertion of CO₂ into the aldehyde C-H bond (highlighted box, Scheme 6.12). The reaction conditions screened will be focussed on the hydroacylation reactions of aldehydes with alkenes and alkynes using Rh catalysts and chelating substrates. Previous attempts within the Nguyen group to develop this reaction were unsuccessful using low pressures of CO₂ and mild temperatures,^{198, 199} thus higher temperatures and pressures along with alternative catalysts and substrates will be investigated.

6.3 Selection of Reaction Screening Conditions

To commence the study, a number of potential substrates and catalysts were identified for initial investigation. Successful substrates require a chelating group which can form a secondary binding site to the rhodium. This would prevent decarbonylation of the aldehyde, a common problem in hydroacylation reactions, by stabilising the metalacyl complex.^{165, 176} Consequently substrates quinoline-8-carbaldehyde **110** and biomass derived furfural **159** were selected for initial study, Figure 6.3.

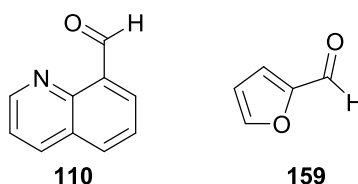
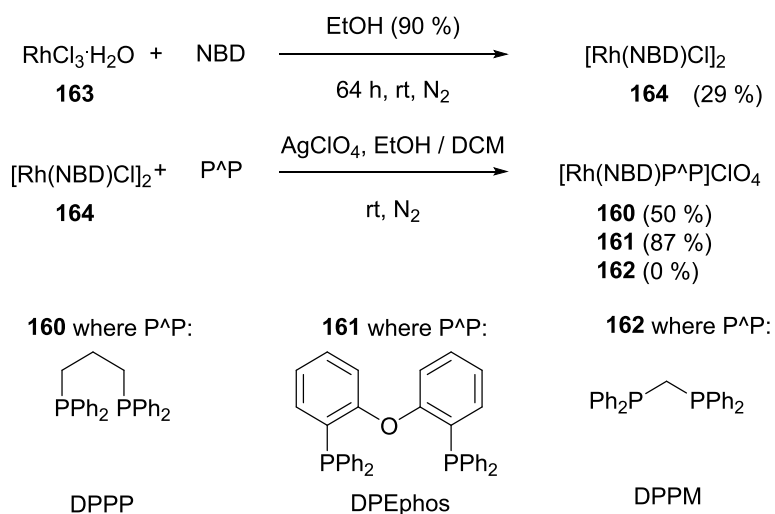


Figure 6.3: Initial substrates selected for testing the insertion of CO₂ into the aldehyde CH bond

Initial catalysts selected for investigation were [Rh(NBD)DPPP]ClO₄ **160**, [Rh(NBD)DPEphos]ClO₄ **161** and [Rh(NBD)DPPM]ClO₄ **162**. These catalysts were selected based on their performance in hydroacylation reactions. [Rh(NBD)DPPM]ClO₄ **162** possesses a small bite angle phosphine ligand which has been demonstrated to be selective for hydroacylation reactions.^{188, 200}

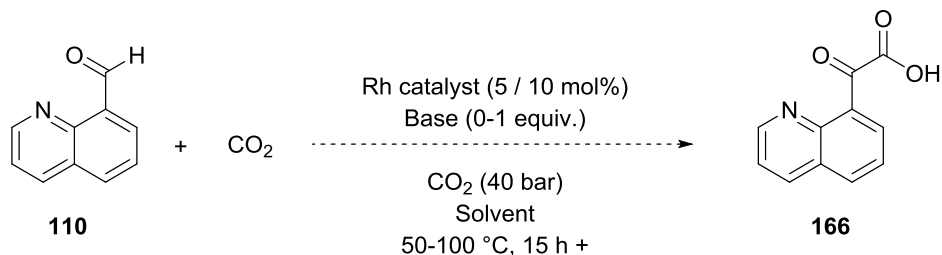
Catalysts **160** and **161** were synthesised from the catalyst precursor [Rh(NBD)Cl]₂ **164** complex in 50 % and 87 % yield respectively. However, attempts to synthesise [Rh(NBD)(DPPM)]ClO₄ **162** from [Rh(NBD)Cl]₂ **164** and DPPM, following the same procedure was unsuccessful; therefore, an alternative small bite-angle ligand, [Rh(NBD)DPPE]ClO₄ **165**, was selected for study.



Scheme 6.13: Synthetic route to Rh catalysts with bidentate phosphorus ligands from [Rh(NBD)Cl]₂ precursor

6.4 Reactions of Quinoline-8-carbaldehyde **110** and CO₂

Quinoline-8-carbaldehyde **110** was selected as the initial substrate for reaction with CO₂ to form the corresponding α -ketocarboxylic acid **166**, Scheme 6.14.



Scheme 6.14: Target reaction for investigation

Catalyst loadings of 5 and 10 mol% were selected and the reaction performed at a substrate concentration of 0.1 M at 100 °C and 40 bar CO₂. The first solvents selected for investigation were toluene and acetonitrile due to their success in alkene hydroacylation. The effect of bases, such as TMG and triethylamine, were also tested. Catalysts and other solid reagents were added to the reaction vessel, sealed and then flushed with nitrogen before solvent or liquid reagents were added. Once the reaction was complete, the products were isolated by evaporating the reaction solvent.

6.4.1 Preliminary Identification of Products

The initial reactions performed with aldehyde **110** and CO₂ at 40 bar and 100 °C were analysed by LC-MS and ¹H NMR spectroscopy, Figure 6.5 & Figure 6.6. Initial analysis suggested no obvious formation of the target keto acid **166** had occurred, however a number of quinoline related products were observed, some of which corresponded with those observed in previous experiments within the group.¹⁹⁹

Each compound was identified using one or two characteristic peaks in ¹H NMR spectra and corresponding LC-MS data, compared to the NMR spectra of the authentic compound or in cases of overlapping peaks, through spiking of the NMR sample with the authentic compound, Figure 6.5 & Table 6.1.

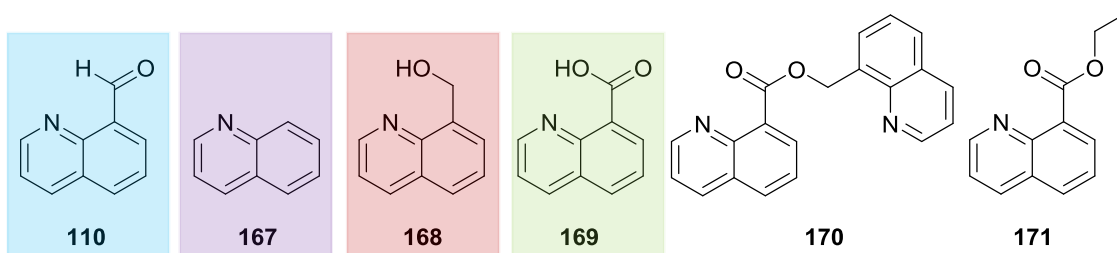


Figure 6.4: Products identified from reactions of aldehyde **110** and CO₂ at 100 °C, 40 bar CO₂ with Rh catalysts

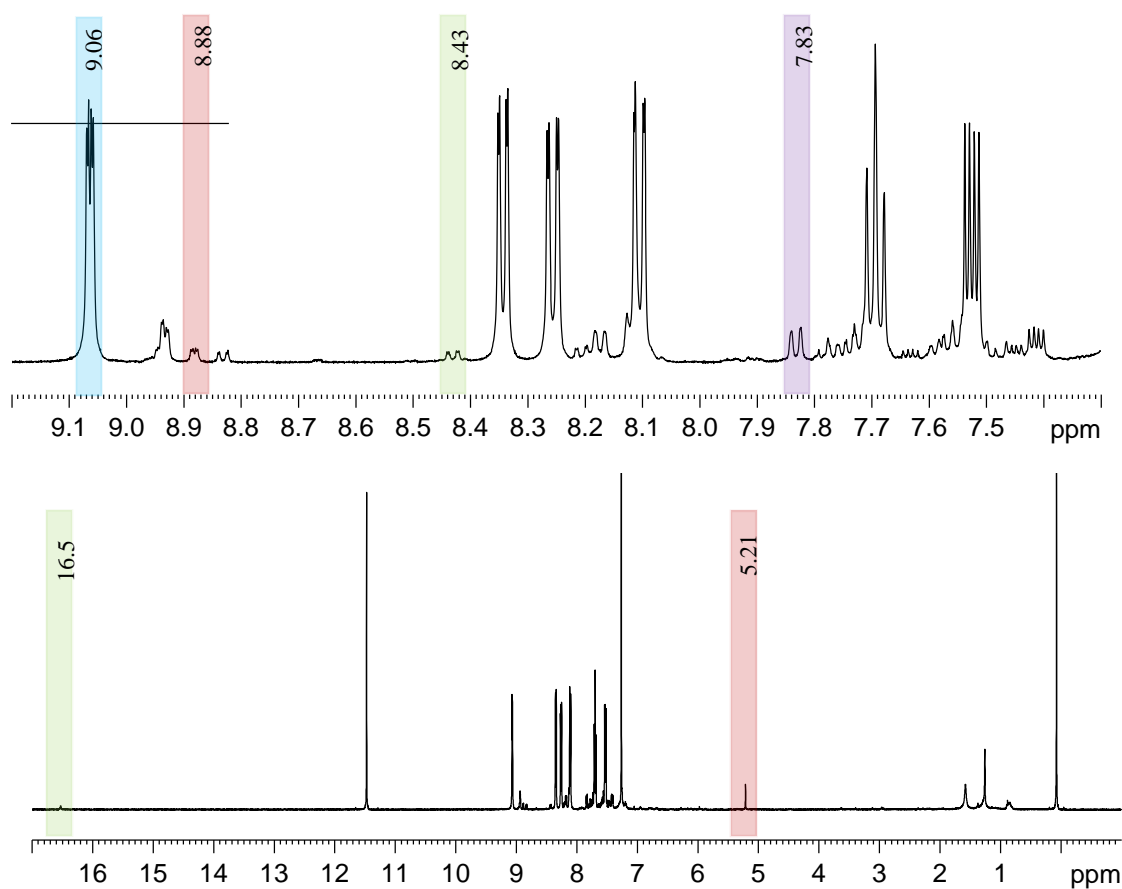
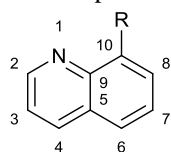
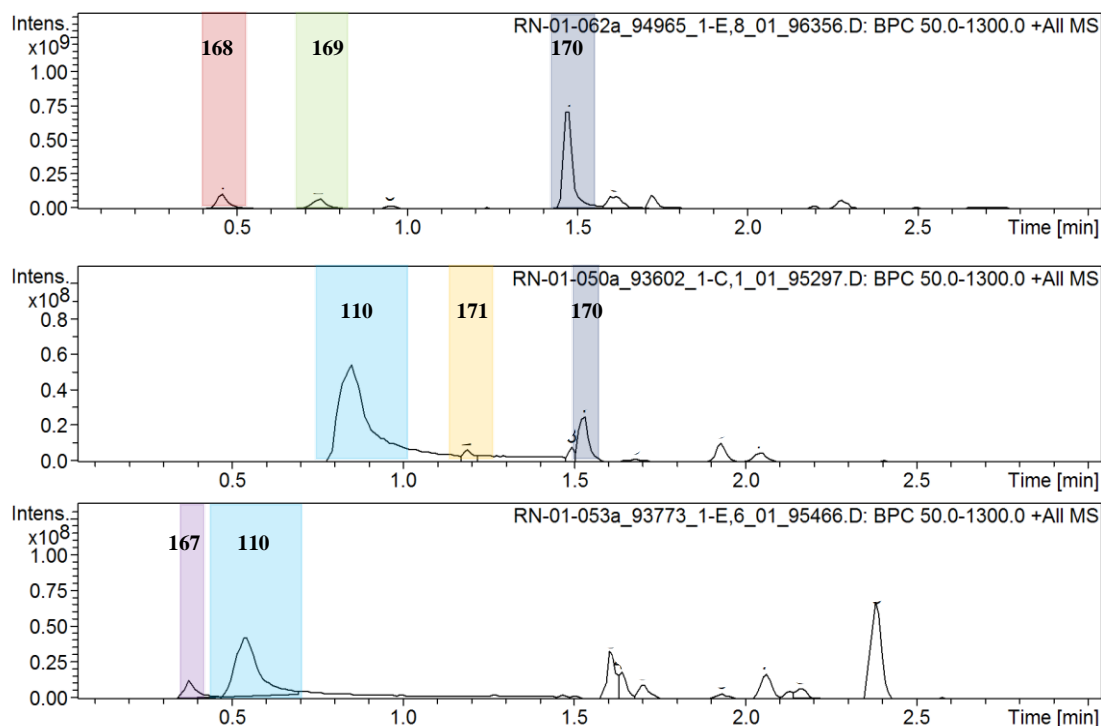
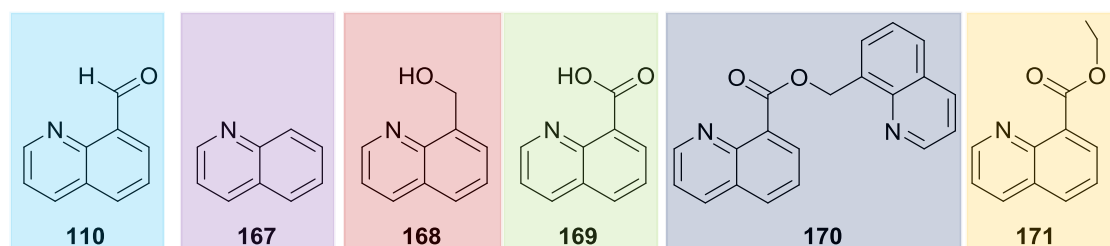


Figure 6.5: Example ¹H NMR from Entry 7 (Table 6.2) used for identification of reaction products

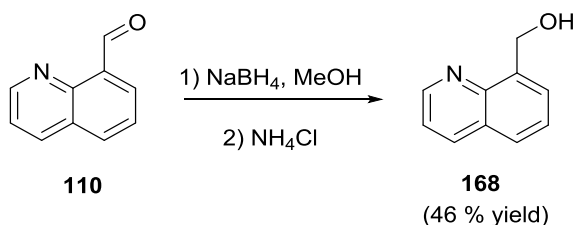
Table 6.1: Diagnostic ^1H NMR peaks for product identification

	110	167²⁰¹	168	169	170	171²⁰²
R:	C(O)H	H	CH ₂ (OH)	C(O)OH	C(O)COCH ₂ C ₁₀ H ₆ N	C(O)OEt
H2	9.07 (dd)	8.94 (d)	8.88 (dd)	8.94 (dd)	9.08 (dd) 8.98 (dd)	9.05 (dd)
H3	7.53 (dd)	7.43 (dd)	7.45 (dd)	7.63 (dd)	7.45 (dd) 7.43 (dd)	7.45 (dd)
H4	8.27 (dd)	8.14 (d)	8.20 (dd)	8.43 (dd)	8.18 (dd) 8.16 (dd)	8.02 (dd)
H6	8.11 (dd)	7.84 (d)	7.76 (dd)	8.12 (dd)	7.92 (dd) 7.79 (dd)	7.93 (dd)
H7	7.70 (dd)	7.61-7.52	7.50 (dd)	7.78 (dd)	7.58-7.52 (m)	7.56 (dd)
H8	8.35 (dd)	7.79-7.70	7.59 (dd)	8.83 (dd)	8.10 (dd) 8.06 (dd)	8.18 (dd)
R	11.48 (s)	8.19 (d)	5.21 (s) 5.06 (s)	16.52 (s)	6.27 (s)	4.55 (q) 1.45 (t)

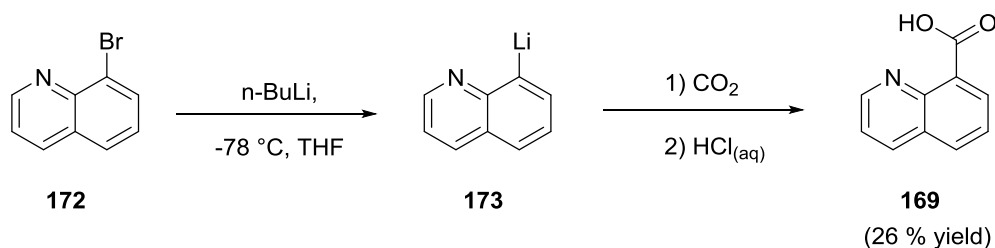
**Figure 6.6:** Example LC-MS traces to analyse reaction products: **110, 167, 168, 169, 170, 171**

Unreacted aldehyde **110** was identified in the ^1H NMR spectrum as a double of doublets at 9.07 ppm. Quinoline **167**, the decarbonylation product, was identified from a double of doublets at 7.83 ppm. A doublet of doublets at 8.88 ppm and a singlet peak at 5.21 ppm, was found to correspond to 8-hydroxymethylquinoline **168**; this was confirmed through synthesis of alcohol **168** following a literature procedure²⁰³ from the reduction of aldehyde **110** with sodium borohydride to give the corresponding alcohol in 46 % yield after purification, Scheme 6.15.

Quinoline-8-carboxylic acid **169** was identified by a doublet of doublets at 8.43 ppm and by a singlet peak at 16.52 ppm. This was also confirmed by spiking experiments with the compound prepared from 8-bromoquinoline **172** following a literature procedure, Scheme 6.16.²⁰⁴ Lithium-halogen exchange using *n*-BuLi produced compound **173**, following which, reaction with dry ice and an acidic work up to pH 5 gave the product **169** in 26 % yield after purification.



Scheme 6.15: Synthetic route to 8-hydroxymethylquinoline **168**²⁰³



Scheme 6.16: Synthetic route to quinoline-8-carboxylic acid **169**²⁰⁴

A singlet peak at 6.27 ppm in some reactions was observed to correlate with an *m/z* ratio of 315.1 [M+H]⁺. Two products potentially corresponded to this signal: either hydroxyketone **174** or ester **170**, Figure 6.7, however the NMR spectra were not available for either compound. The hydroxyketone **174** was prepared from a benzoin condensation reaction of **110** using a thiazolium catalyst and triethylamine, following a modified procedure for a similar substrate, Scheme 6.17.²⁰⁵ Analysis of compound **174** by ^1H NMR showed a singlet in the ^1H NMR spectrum at 6.88 ppm, indicating this product was not the product formed in the catalytic reaction.

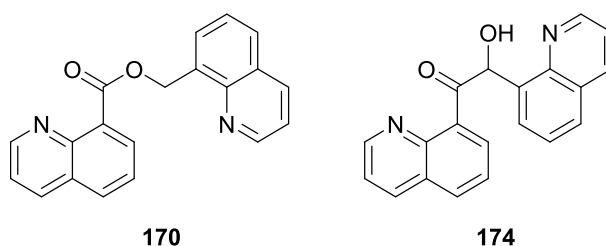
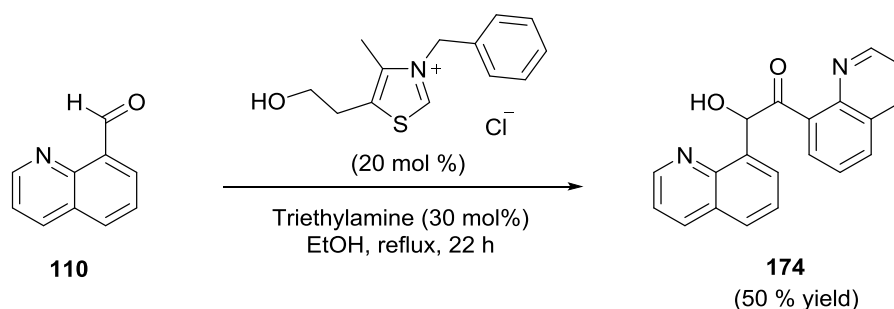


Figure 6.7: Possible products with m/z ratio 315.1

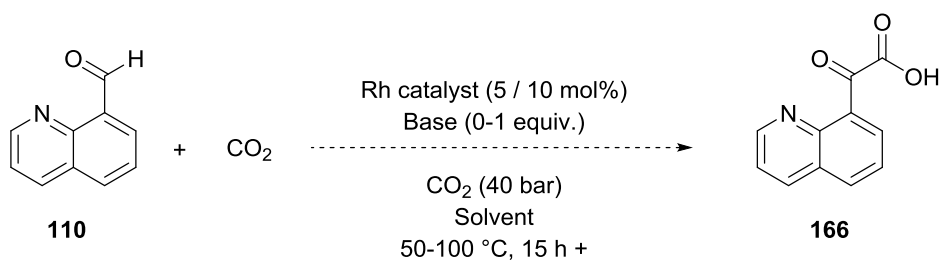


Scheme 6.17: Synthetic route to **174** via a benzoin reaction from quinoline-8-carbaldehyde **110**

To confirm the identify of product with m/z 315.1 the products from the reaction of quinoline-8-carbaldehyde **110** with CO₂ and a Rh catalyst, given in Entry 16 of Table 6.2, were separated by column chromatography. The isolated product corresponding to m/z 315.1 and the singlet in the ¹H NMR spectrum at 6.27 ppm was confirmed to be the ester **170**.

The ethyl ester **171** was characterised by a triplet at 1.46 ppm and a quartet at 4.55 ppm, based on literature NMR data.²⁰²

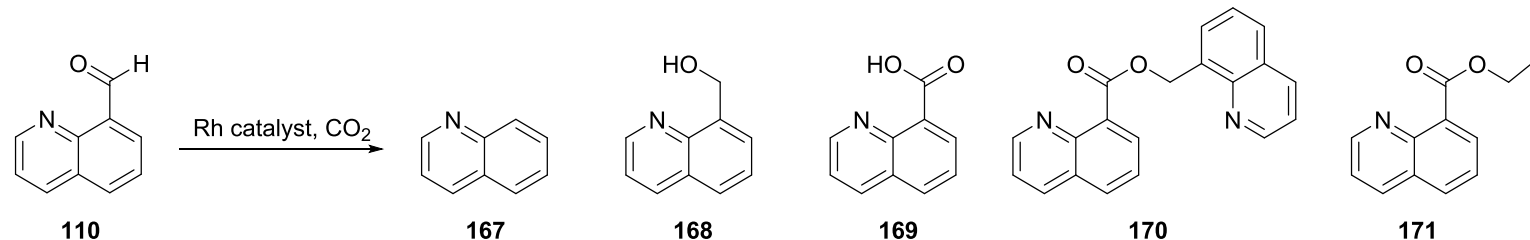
6.4.2 Reaction Outcome



Scheme 6.18: Reaction conditions investigated

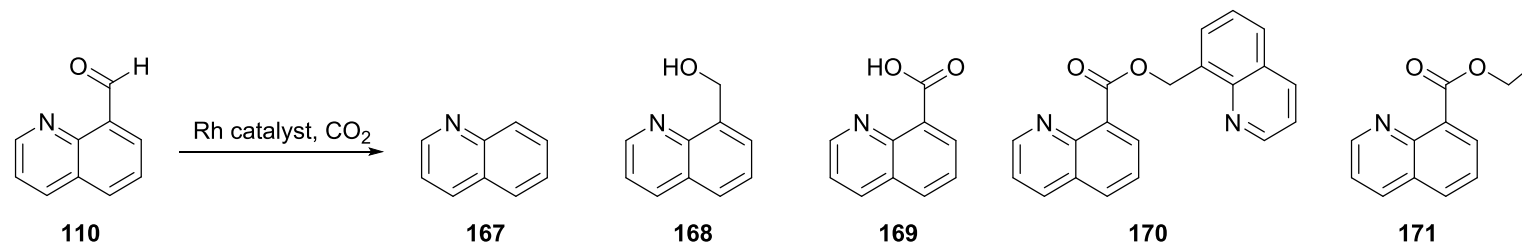
The results of reaction screening of aldehyde **110** with CO₂ under selected conditions (Scheme 6.18) are given in Table 6.2. Approximate conversions to each product were calculated using integration of the ¹H NMR peaks described; however, the yields do not take into account for current unidentified products, however these typically account for <1 % of conversion.

Table 6.2: Results for reaction of quinoline-8-carbaldehyde **110** with CO₂. Conversions calculated from ¹H NMR spectra (continued over page)



Entry	Catalyst System	Gas	Pressure (bar)	Loading (mol %)	Temp (°C)	Solvent	Base	Relative Conversion (%)					
								110	167	168	169	170	171
1	[Rh(NBD) ₂]ClO ₄ + DPPM	CO ₂	40	5	100	Toluene	-	85.3	-	4.4	0.6	8.9	2.9
2	[Rh(NBD) ₂]ClO ₄ + DPEphos	CO ₂	40	5	100	Toluene	-	88.3	-	4.2	0.9	6.5	-
3	[Rh(NBD) ₂]ClO ₄ + DPEphos	CO ₂	40	5	100	Toluene	TMG	97.6	-	2.4	-	0.3	-
4	[Rh(NBD) ₂]ClO ₄ + DPEphos	CO ₂	40	5	100	Toluene	TEA	95.5	-	2.4	1.8	0.6	-
5	[Rh(NBD) ₂]ClO ₄ + DPEphos	CO ₂	40	5	100	Toluene	TEA	53.7	41.1	1.6	3.6	-	-
6	[Rh(NBD)DPEphos]ClO ₄	CO ₂	40	10	100	Toluene	-	98.3	-	0.6	1.1	-	-
7 ^a	[Rh(NBD)DPEphos]ClO ₄	CO ₂	40	10	100	Toluene	-	82.0	11.7	4.1	2.3	-	-
8	[Rh(NBD)DPPE]ClO ₄	CO ₂	40	10	100	Toluene	-	-	21.1	43.7	35.2	-	-
9	[Rh(NBD)DPEphos]ClO ₄	CO ₂	40	10	100	MeCN	-	-	54.4	25.6	20.0	-	-
10	[Rh(NBD)DPEphos]ClO ₄	CO ₂	40	10	100	MeCN	TEA	81.4	-	12.6	5.9	-	-
11 ^a	[Rh(NBD)DPEphos]ClO ₄	CO ₂	40	10	100	MeCN	-	-	21.1	43.7	35.2	-	-
12	[Rh(NBD)DPEphos]ClO ₄	CO ₂	40	10	100	TEA	TEA	90.9	-	9.1	-	-	-
13	[Rh(NBD) ₂]ClO ₄ + DPEphos	N ₂	1	5	100	Toluene	-	97.2	-	1.2	1.3	0.3	-

Table 6.2 continued...

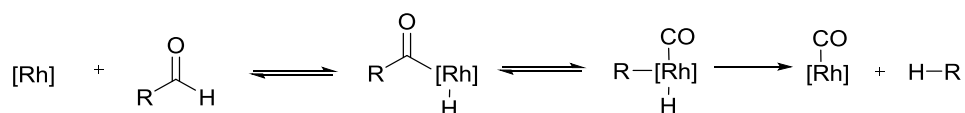


Entry	Catalyst System	Gas	Pressure (bar)	Loading (mol %)	Temp (°C)	Solvent	Base	Relative Conversion (%)					
								110	167	168	169	170	171
14	[Rh(NBD)DPPE]ClO ₄	CO ₂	5	10	50	MeCN	-	-	-	40.7	22.0	37.4	-
15	[Rh(NBD)DPPE]ClO ₄	N ₂	1	10	50	MeCN	-	-	-	29.9	15.3	54.8	-
16	[Rh(NBD)DPPB]ClO ₄	CO ₂	5	10	50	MeCN	-	-	-	45.7	36.9	17.4	-
17	[Rh(NBD)DPPB]ClO ₄	N ₂	1	10	50	MeCN	-	-	-	38.0	27.8	34.2	-

Reaction conditions: quinoline-8-carbaldehyde **110** (0.25 mmol), Rh catalyst (5-10 mol%) solvent (2.5 mL), base (0-1 equiv), 50 - 100 °C, overnight,

^a – reaction ran in presence of water (1 mL, degassed)

Reactions carried out in toluene (Entries 1-7, Table 6.2) with DPPM and DPEphos as the ligand generally resulted in low conversion of the starting material. The exception occurred when quinoline **167** was formed as the major product, e.g. Entry 5 and 7. Quinoline **167** is produced by decarbonylation of the aldehyde **110** and is a major side reaction in hydroacylation reactions when the Rh centre is coordinatively unsaturated, Scheme 6.19.¹⁶⁵ Use of DPEphos should ensure a coordinatively saturated complex. Therefore, for quinoline to be formed either the catalyst was not formed before introduction of the aldehyde, or air was introduced to the system causing decomposition of the complex.



Scheme 6.19: Proposed decarbonylation pathway of quinoline-8-carbaldehyde **110** to quinoline **167** with a Rh catalyst, where R = quinoline ring

Conversion of aldehyde **110** to the alcohol **168** and carboxylic acid **169** was observed to occur when Rh catalyst when Rh catalyst $[\text{Rh}(\text{NBD})\text{DPPE}]\text{ClO}_4$ was used (Entry 8), and when preformed catalyst $[\text{Rh}(\text{NBD})\text{DPEphos}]\text{ClO}_4$ was used in acetonitrile. The presence of water also appeared to favour the formation of these products (Entry 7 and 11) and reaction in the absence of CO_2 also gave products **168** and **169**, (Entry 15, Table 6.2). Conversion of aldehyde **110** to the alcohol **168** and carboxylic acid **169** are thought to occur via a Cannizzaro type reaction mechanism.¹⁹⁹ Traditionally this would require a base to proceed; however, a rhodium catalyst in the presence of water has previously been demonstrated to facilitate this type of conversion.²⁰⁶

Ethyl ester **171** is thought to be produced from contamination of the equipment with ethanol used to clean the system, (Entry 1, Table 6.2). Once ethanol was not used as a cleaning solvent, and the equipment dried thoroughly, no conversion to the ester was observed.

Conducting the reactions in acetonitrile (Entries 9-11, Table 6.2) rather than toluene led to an increased conversion of aldehyde **110**. This may be due to increased catalytic activity due to increased solubility of the Rh catalyst in acetonitrile over toluene.

Use of TMG or triethylamine as a base was proposed to encourage the formation of product **166** both by deprotonating the formed product and through their potential to form complexes with CO_2 . Results show that use of either base (Entry 3, 4 and 10, Table 6.2) led to reduced conversion, as observed in the previous study where TBD was used.¹⁹⁹ The use of neat triethylamine and triethylamine in toluene led to the formation of an orange/red precipitate on

the walls of the reaction flask. By ^1H NMR spectroscopy the precipitate appears to have a different composition to the main solution, in particular the presence of peaks at 9.27, 8.65, 7.92 and 7.32 ppm in the ^1H NMR spectra. These could either be a new quinoline based species or the effect of either rhodium or triethylamine bound to a quinoline derivative. These results were not observed in the previous study. A ^{31}P NMR spectrum showed the presence of phosphorous in the sample (Figure 6.8); suggesting that either the ligand or a Rh complex is present in the precipitate. As the peaks do not correspond with those of free DPEphos or the $[\text{Rh}(\text{NBD})\text{DPEphos}]\text{ClO}_4$ **161** catalyst, the phosphorous present may either have been oxidised during the work up or exist as an alternate Rh complex formed during the reaction.

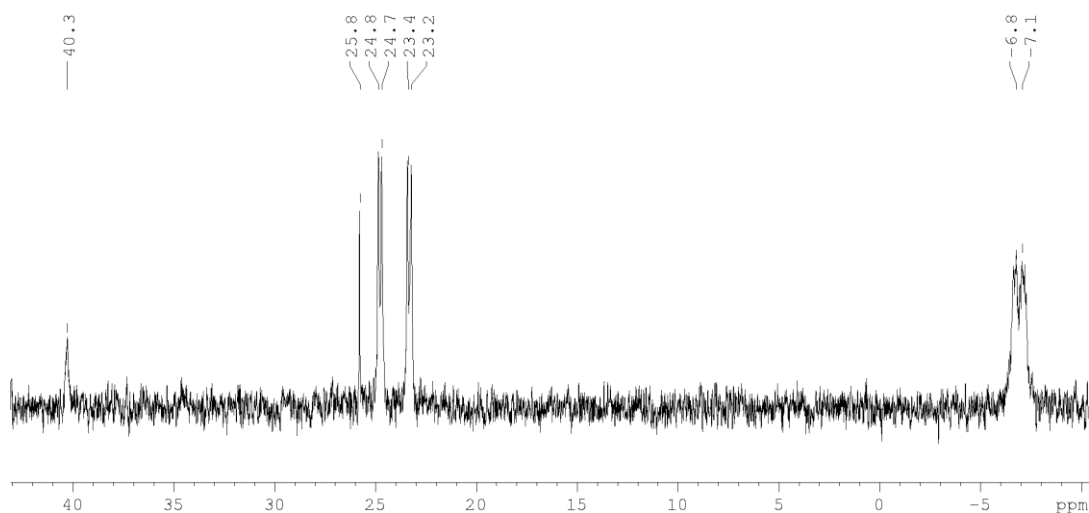


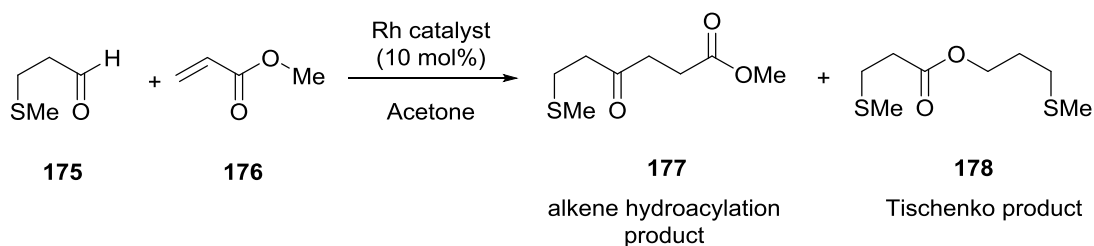
Figure 6.8: ^{31}P NMR spectrum of red/orange precipitate formed in Entry 12 of Table 6.2

Ester **170** was formed in small quantities (<10 %) in toluene when $[\text{Rh}(\text{NBD})_2]\text{ClO}_4$ **164** was used as the catalyst precursor with either DPPM or DPEphos as the ligand (Entries 1-5). However, no conversion to **170** was observed when the pre-prepared catalysts $[\text{Rh}(\text{NBD})\text{DPEphos}]\text{ClO}_4$ and $[\text{Rh}(\text{NBD})\text{DPPE}]\text{ClO}_4$ were used instead.

The use of ligands DPPE and DPPB in acetonitrile at lower temperatures and pressures (Entries 14 & 16, Table 6.2) led to increased conversion of **110** to the ester **170**, with relative conversions of 37 & 17 %. Repeating both reactions at atmospheric pressure under N_2 , in the absence of CO_2 , again led to complete conversion of **110** giving the ester **170** in 55 & 34 % yields, Entries 15 & 17, Table 6.2. This indicated that CO_2 is not incorporated into the product and actually reduces the formation of the ester product **170** favouring the Cannizzaro products **168** & **169** instead.

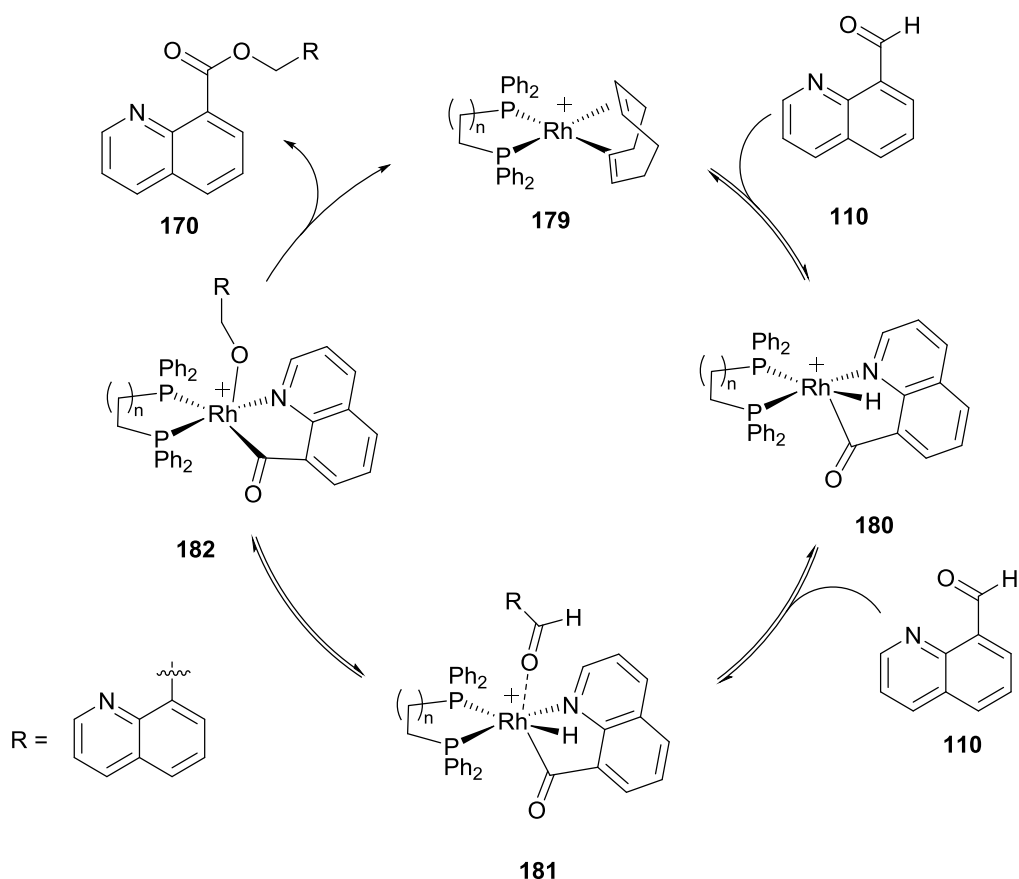
Ester **170** is proposed to form from aldehyde **110** via a Tischenko reaction, which has been shown to occur via rhodium catalysis^{207, 208} and has previously been observed in hydroacylation

studies by Weller and Willis with comparable chelating substrates and rhodium catalysts, Scheme 6.20.¹⁸⁷



Scheme 6.20: Hydroacylation reaction with previously observed hydroacylation and Tischenko products, reported by Weller and Willis¹⁸⁷

The proposed mechanism for formation of **170**, Scheme 6.21, involves initial addition of the quinoline-8-carbaldehyde **110** to give acyl-hydride complex **180** followed by coordination of a second equivalent of **110** through the oxygen. Hydride transfer occurs to give complex **182**, from which the product **170** is released.

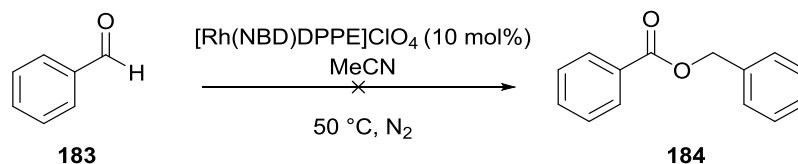


Scheme 6.21: Proposed reaction pathway for Tischenko reaction for product **170** from **110**¹⁸⁷

This proposed mechanism accounts for the increased formation of **170** when DPPE and DPPB are used as the ligand compared to DPEphos. DPEphos is hemi-labile and has a third

coordination site, this would hinder the formation of **181** by restricting coordination of the second aldehyde and therefore reduce conversion to the ester. This is in agreement with work by Weller and Willis who found that hemilabile ligands significantly reduced the formation of the Tischenko product **178** and instead favoured the hydroacylation product **177**, Scheme 6.20. The reduced conversion to **170** at high pressures of CO₂ could therefore be explained by coordination of CO₂ to the rhodium, preventing coordination of a second equivalent of **110**, therefore hindering the ester **170** forming.

Performing the reaction under the same conditions (Entry 15, Table 6.2) with benzaldehyde **183** gave no conversion to the corresponding ester **184**, Scheme 6.22, indicating the importance of the nitrogen chelation group in the quinoline ring **110** for the conversion to occur.



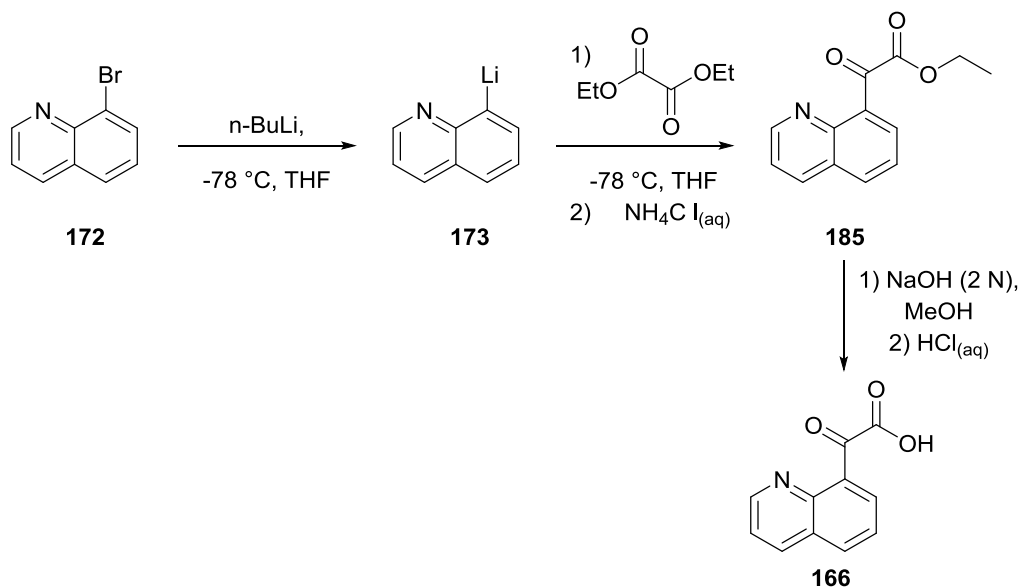
Scheme 6.22: Reaction of benzaldehyde **183** under comparable reactions conditions led to no conversion to ester **184**

A major limitation of the study so far is the identification of reaction products and identifying an appropriate reaction work up. Currently ¹H and COSY NMR spectroscopy have been employed; however, as previously discussed the overlapping region of quinoline protons makes analysis challenging. There was therefore a need to synthesise the authentic α -ketocarboxylic acids to enable their stability under the reaction conditions and characteristic ¹H or ¹³C NMR chemical shifts to be identified.

6.4.3 Synthesis of Target Product **166**

To synthesise the target product **166**, the keto ester equivalent **185** was first synthesised following a literature procedure.²⁰⁹ 8-Bromoquinoline **172** was lithiated and reacted with diethyloxalate to produce the keto ester **185**, Scheme 6.23. A variety of approaches were attempted to hydrolyse the ester **185** to give the product **166**. Hydrolysis with LiCl in pyridine under reflux gave no conversion to the ketoacid, although this method is more well known for methyl esters. Hydrolysis was successful with NaOH in H₂O/MeOH. The reaction solution was washed with ethylacetate and extraction at a range of pH 2-6 into organic solvents were attempted. It was found that the product was present in the aqueous layer and was isolated at pH 5. pH control of the isolated product is essential to prevent the formation of a zwitterionic species due to the basic quinoline group and the acidic carboxylic acid group. After purification of the keto acid **166** by crystallisation, colourless needles were produced, which analysis by x-

ray crystallography demonstrated it to exist as a sodium acetate salt, Figure 6.9. The presence of the acetate group arose from reaction with ethylacetate used in attempt to extract the product during hydrolysis.



Scheme 6.23: Synthetic route to authentic reaction product **166**

Each unit of the crystal consists of two molecules of the keto acid **166**, one acetate anion and three sodium cations, giving the molecular formula: $C_{11}H_6NO_3 \cdot 0.5(C_2H_3O_2) \cdot 1.5Na$. Each sodium is bound to the oxygen with bond lengths between 2.3-2.6 Å. A weak bond between the sodium and the nitrogen atom of the quinoline was also observed, Figure 6.9.

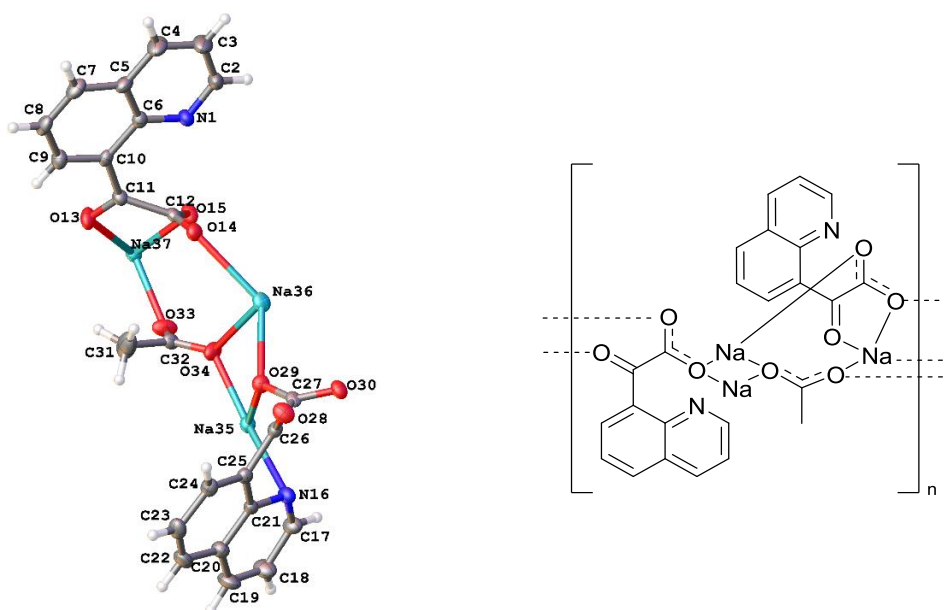


Figure 6.9: Crystal structure of authentic α -ketocarboxylic acid **166**, the target product from the reaction of CO_2 with quinoline-8-carbaldehyde **110**

Although ketoacid **166** was not isolated as the free acid, NMR spectra were studied for characteristic chemical shifts that could be used to identify the target product. Firstly NMR spectra were run in deuterated DMSO due to poor solubility in CDCl_3 . Characteristic carbonyl shifts were identified in the ^{13}C spectrum representing the ketone and carboxylic carbonyl at 199.5 and 168.7 ppm. Previously any reactions with CO_2 were analysed through evaporation of the solvent and NMR analysis in CDCl_3 . As the isolated product was found to be insoluble in CDCl_3 , but soluble in MeOH, water and DMSO, a small selection of the reactions were re run. ^{13}C NMR spectra were run in DMSO in case the formed product was previously not observed due to poor solubility. However, no new products were observed.

As the alpha-keto acid has not yet been isolated in its pure form, an alternative approach was to trap the product as a sodium salt at the end of the CO_2 reaction, thus allowing direct comparison with the synthesised product. However, addition of NaOH to the NMR sample of the keto acid resulted in decomposition of the product, as observed by the loss in carbonyl peaks at 199.5 and 168.7 ppm in the ^{13}C spectrum, Figure 6.10. Although it is also possible that hydration of the ketoacid occurred to give the corresponding gem-diol, this is unlikely to have occurred as the carbonyl peaks would still be present – but have shifted to a lower chemical shift.²¹⁰

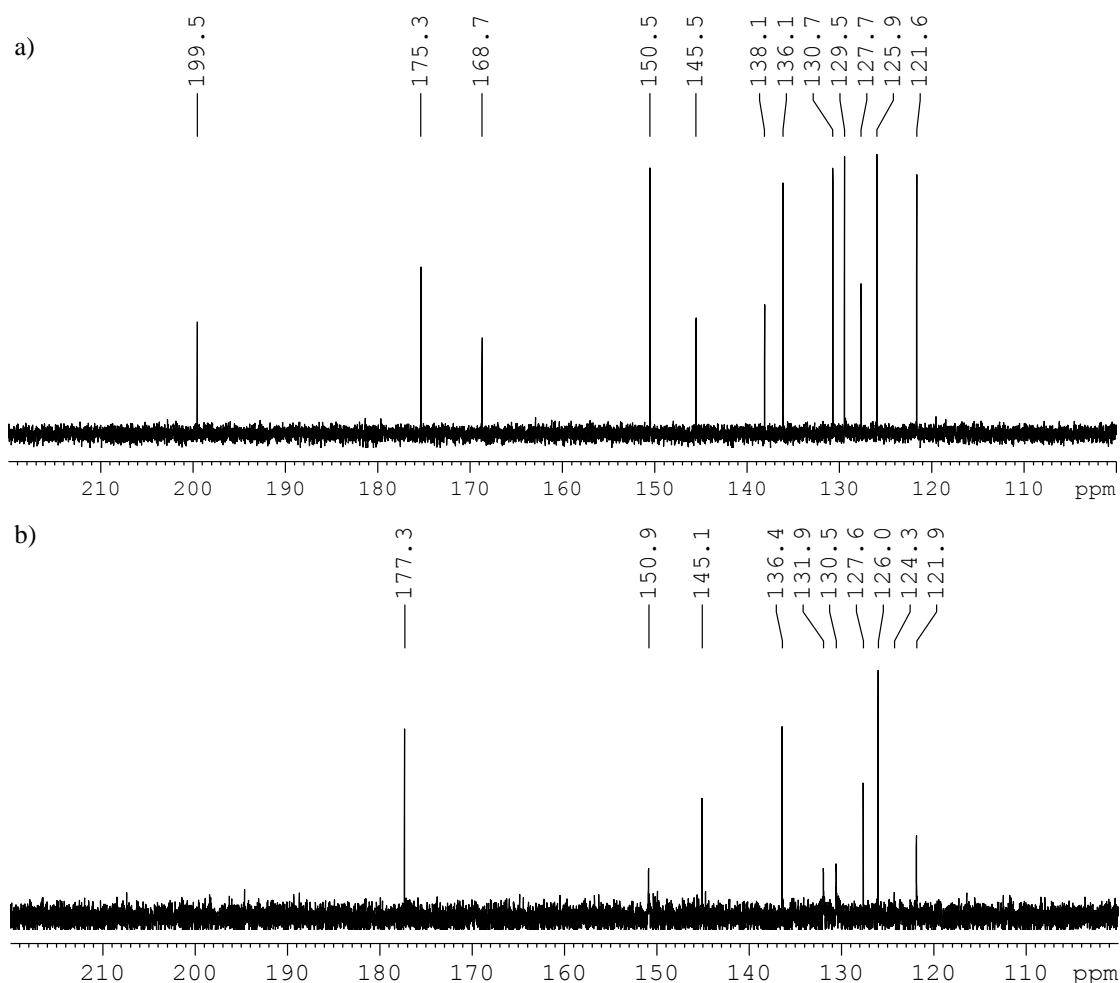


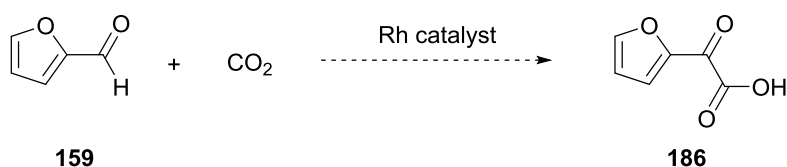
Figure 6.10: ^{13}C NMR spectra of a) α -ketoacid **166**, b) α -ketoacid **166** + 2N NaOH

The hydrolysis was also repeated using NaOH, a wash of diethyl ether to prevent formation of the acetate and acidification to pH 3 resulted in a yellow solid. However, differences in the NMR spectra suggested that the protonated quinoline may have been formed.

Due to difficulties isolating the product and its questionable stability under strongly basic conditions,²¹¹ it was decided to focus on an alternative target, which is known in the literature, for initial investigations.

6.5 Reactions of Furfural and CO₂

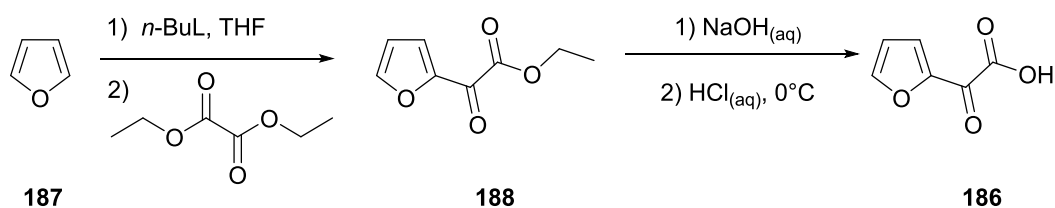
As no incorporation of CO₂ was observed in reactions with quinoline-8-carbaldehyde **110**, a second substrate was investigated. Furfural **159** was selected to study its reactions with CO₂ to give the target product **186**, Scheme 6.24. Furfural was proposed to be a suitable substrate due to its potential to stabilise the hydro-acyl rhodium intermediate by coordination of the furyl oxygen, preventing decarbonylation from occurring. Furthermore, furfural is derived from biomass and its electron rich nature would match the electron poor coupling partner CO₂.



Scheme 6.24: Target reaction of furfural **159** with CO₂ to give α -ketoacid **186**

6.5.1 Preliminary Results and Comparison with Authentic Product **186**

Two preliminary reactions of furfural **159** with [Rh(DPEphos)NBD]ClO₄ in toluene were carried out both in the presence of CO₂ (40 bar) and under a N₂ atmosphere and analysed by ¹H NMR spectroscopy (Figure 6.11b & c). Both reactions showed the presence of furfural **159** at the end (Figure 6.11a), suggesting that decarbonylation is not a significant reaction under these conditions. Of great interest were the new peaks observed when the reaction was carried out in CO₂ (red highlight, Figure 6.11b), which were not observed when carried out under nitrogen (Figure 6.11c), suggesting that a reaction with CO₂ may have taken place.



Scheme 6.25: Synthetic route to authentic α -ketoacid target product **186**²¹²

Comparison of the NMR spectra of the reaction of furfural with CO_2 (Figure 6.11b) to the ^1H NMR spectrum of the target keto acid **186**, synthesised by an alternative route, (Scheme 6.25) indicated that the target compound **186** was not formed, Figure 6.11d. The keto acid **186** would be identified by doublets at 8.19, 7.86 and a doublet of doublets at 6.70 ppm in the ^1H NMR spectrum, Figure 6.11d. Other characteristic signals used to identify the keto acid **186** from the reaction mixture would be signals at 169.9 and 159.1 ppm in the ^{13}C NMR spectra – characteristic of the α -keto carboxylic acid group, Figure 6.11e.

The new chemical shifts in the ^1H NMR spectrum observed after the reaction of furfural with CO_2 (Figure 6.11b) were observed at 7.60 ppm and a series of doublets and multiplets between 7.8 and 8.3 ppm. If the compounds were furan derived, the furan ring must be more electron deficient than furfural **159** as demonstrated by the higher chemical shifts. The reaction was repeated to enable further characterisation of the products derived from the reaction of **159** with CO_2 ; however the same results could not be reproduced despite multiple attempts (Table 6.3, Entries 6-9). Therefore the identity of the new signals remains unknown.

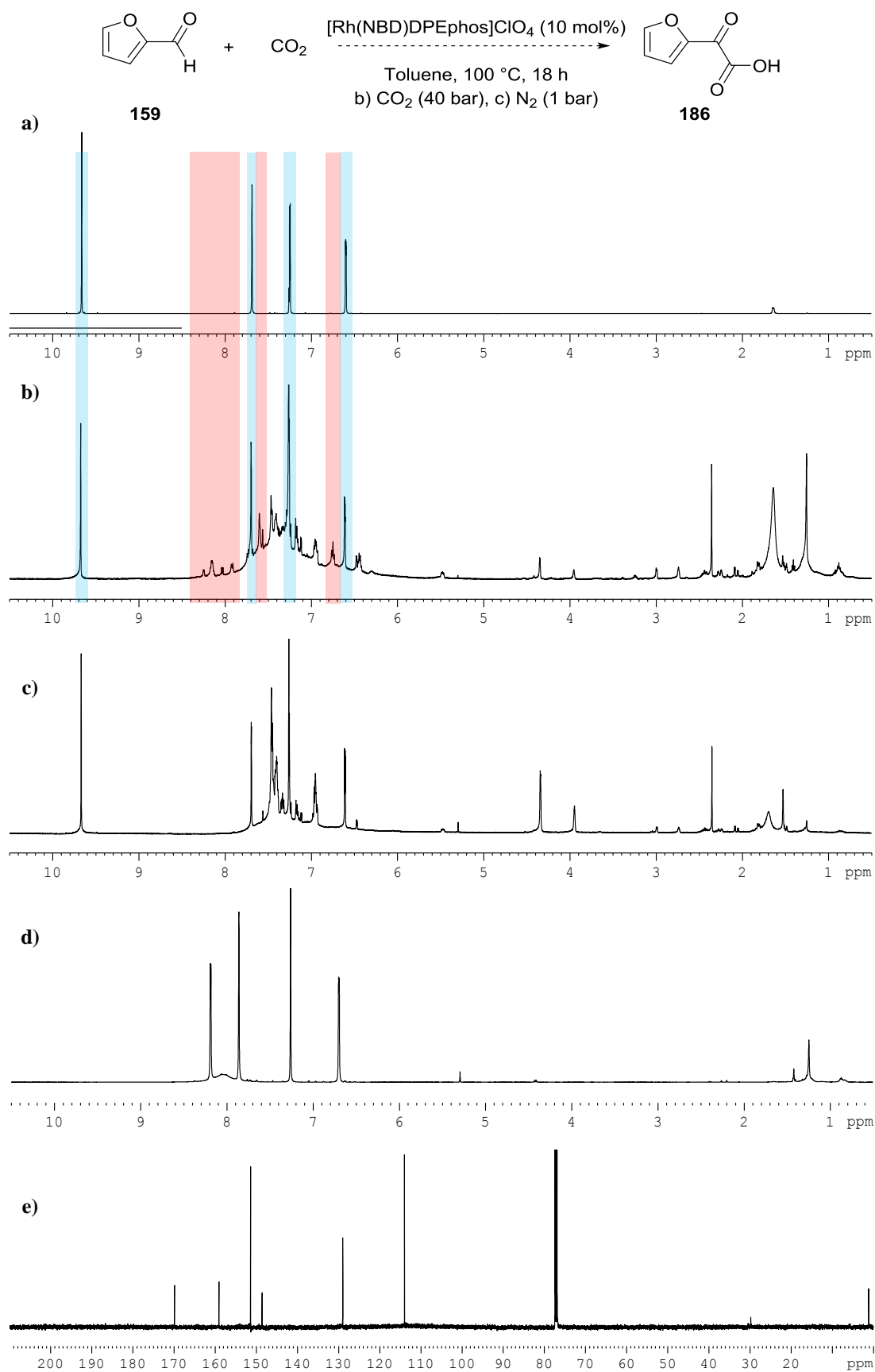
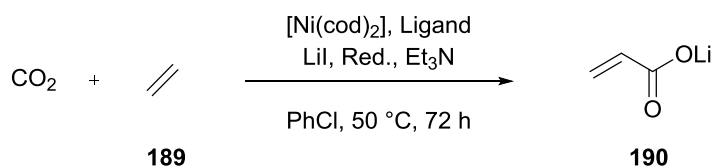


Figure 6.11: ¹H NMR spectra of: a) Furfural **159**, b&c) reaction product under b) CO₂ (40 bar), c) N₂ (1 bar) (blue highlight – furfural, red highlight – new signals seen only under CO₂); d) Target keto acid **186** e) ¹³C NMR of target keto acid **186**

6.5.2 Reaction Screening

Initially reactions of furfural with CO₂ were investigated under similar conditions as were used with quinoline-8-carbaldehyde **110**. Reactions using NBD derived rhodium catalysts with either DPPP, DPPE or DPEphos as the ligand (Entries 1 - 12, Table 6.3), did not show any significant conversion of furfural **159** into other products. This is contrasting to the case with quinoline-8-carbaldehyde **110** where many of the same reaction conditions led to significant and clean conversion of the substrate into clearly identifiable products.

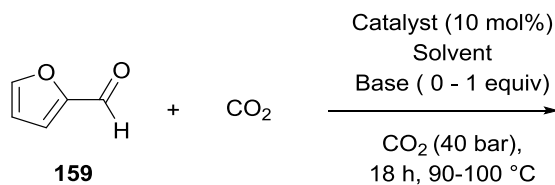
Due to a lack of conversion an alternative catalyst system and the use of a range of bases was investigated. Cyclooctadiene (COD) complexes were used instead of NBD complexes due to their more widely use in hydroacylation reactions and are proposed to be more active than the corresponding NBD derived catalysts in the hydroacylation reactions. Bases investigated included organic bases such as triethylamine (TEA) and 1,1,3,3-tetramethylguanidine (TMG) and inorganic lithium salts such as LiI, LiCl and Li₂CO₃. Lithium bases were selected based on their success in promoting the catalytic synthesis of lithium acrylate **190** from ethene and CO₂, Scheme 6.26.²¹³



Scheme 6.26: Example of use of lithium salts to promote synthesis of catalytic lithium acrylate²¹³

In all cases with COD based complexes, (Entries 13- 24, Table 6.3) only a small amount of conversion of furfural was observed. The use of lithium bases did not lead to any significant difference in conversion of the furfural (Entries 22- 24, Table 6.3); however the use of triethylamine with 1,4-dioxane as the solvent (Entry 18, Table 6.3) resulted in new peaks in the ¹H NMR spectrum, Figure 6.12a. Any changes in the ¹H NMR spectra after reaction with CO₂ (Figure 6.12a) were also observed when the reaction was performed under N₂ (Figure 6.12b) suggesting that no CO₂ has been incorporated into the reaction products (Entries 18-19, Table 6.3).

Despite any observed reaction products being independent of CO₂, they were investigated to understand the processes that are occurring in the reaction and to attempt to identify the reasons for the lack of reaction with CO₂. Three regions of interest were identified as potential products of the reaction, Figure 6.12c.

Table 6.3: Reaction conditions trialled for reaction of furfural **159** with CO₂

Entry	Catalyst System	Solvent	Base	
1	[Rh(NBD)DPPP]ClO ₄	Toluene	-	
2	[Rh(NBD)DPPP]ClO ₄	1,4-Dioxane	-	
3	[Rh(NBD)DPPP]ClO ₄	Acetonitrile	TEA	
4	[Rh(NBD)DPPE]ClO ₄	Toluene	-	
5	[Rh(NBD)DPPE]ClO ₄	DME	-	
6	[Rh(NBD)DPEphos]ClO ₄	Toluene	-	
7*	[Rh(NBD)DPEphos]ClO ₄	Toluene	-	N ₂
8	[Rh(NBD)DPEphos]ClO ₄	Toluene	-	
9	[Rh(NBD)DPEphos]ClO ₄	Toluene	-	
10	[Rh(NBD)DPEphos]ClO ₄	Toluene	-	
11	[Rh(NBD)DPEphos]ClO ₄	Acetonitrile	-	
12	[Rh(NBD)DPEphos]ClO ₄	1,4-Dioxane	TEA	
13	[Rh(COD)DPEphos]ClO ₄	Toluene	-	
14	[Rh(COD)DPEphos]ClO ₄	1,4-Dioxane	-	
15	[Rh(COD) ₂]ClO ₄ + DPPF	1,4-Dioxane	-	
16	[Rh(COD) ₂]ClO ₄ + DPPE	1,4-Dioxane	-	
17	[Rh(COD) ₂]ClO ₄ + DPPM	1,4-Dioxane	-	
18	[Rh(COD)DPEphos]ClO ₄	1,4-Dioxane	TEA	
19*	[Rh(COD)DPEphos]ClO ₄	1,4-Dioxane	TEA	N ₂
20	[Rh(COD)DPEphos]ClO ₄	DCE	TEA	
21	[Rh(COD)DPEphos]ClO ₄	1,4-Dioxane	TMG	
22	[Rh(COD)DPEphos]ClO ₄	1,4-Dioxane	LiI + TEA	
23	[Rh(COD)DPEphos]ClO ₄	1,4-Dioxane	LiCl	
24	[Rh(COD)DPEphos]ClO ₄	1,4-Dioxane	Li ₂ CO ₃	
25*	-	1,4-Dioxane	TEA	N ₂

Reaction conditions: Furfural **159** (0.6 mmol), Rh catalyst (0.06 mmol), solvent (3 mL), CO₂ (40 bar), 100 °C, 15 h +

* Reaction under N₂ at atmospheric pressure

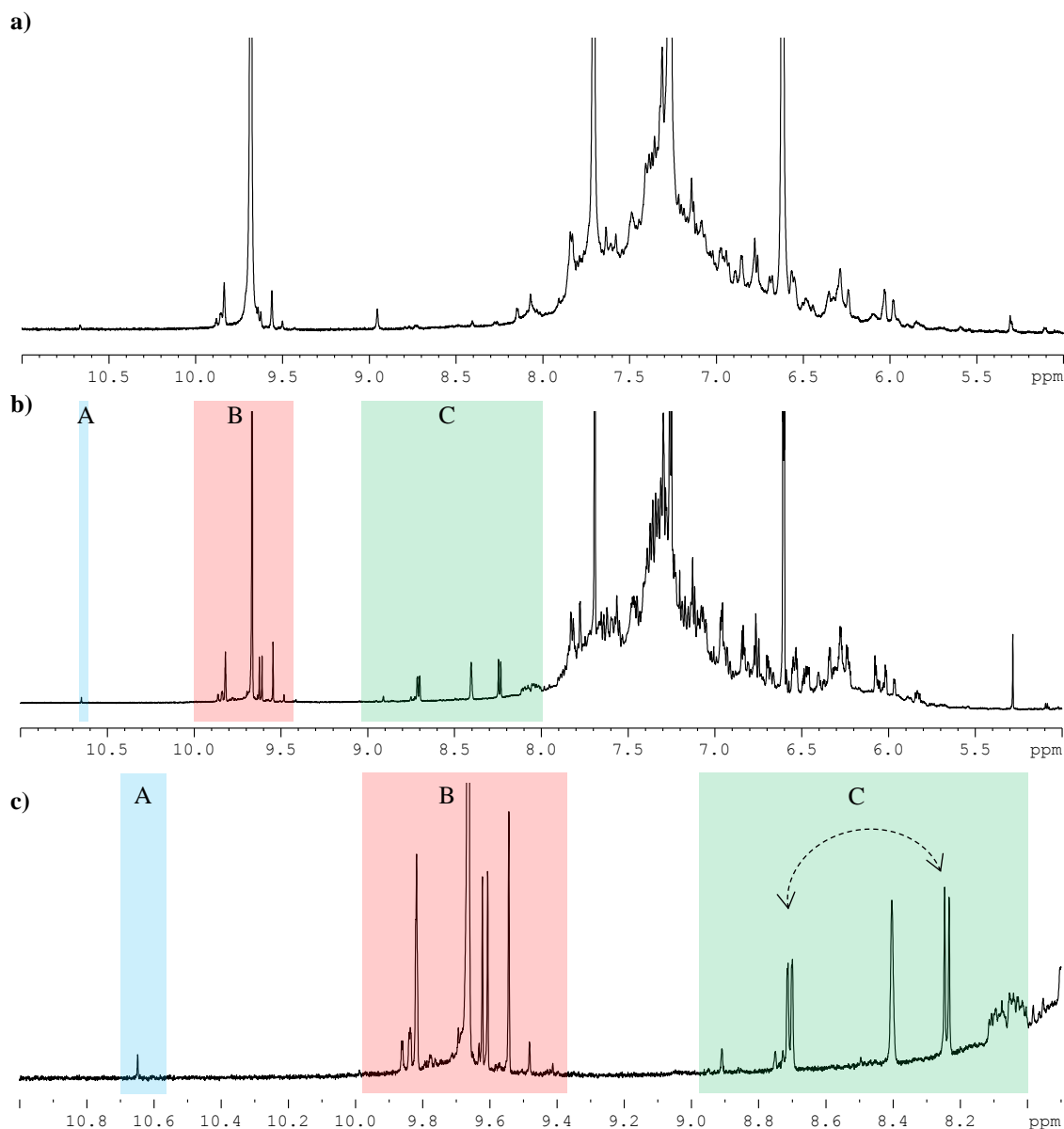


Figure 6.12: ^1H NMR spectra of an example reaction of furfural, $[\text{Rh}(\text{COD})\text{DPEphos}]\text{ClO}_4$, dioxane and triethylamine with a) CO_2 (40 bar) Entry 18, b) N_2 Entry 19, c) expanded spectrum with key regions of interest highlighted

6.5.3 Identification of Reaction Products

Identifying the compounds by analysis of the reaction mixture by NMR has been unsuccessful. Attempts to resolve the compounds present by DOSY also failed to give any further understanding of the components present.

Analysis by mass spectrometry proved challenging due to overwhelming ions from fragmentation of the oxidised phosphine ligands used in reaction. For example, when DPEphos was used as a ligand the dominant signals observed were at m/z 371.1183 and 571.1662 corresponding to compounds **191** and **192** respectively (calculated: 371.1195 and 571.1586), Figure 6.13. The presence of these compounds was also confirmed by peaks in ^{31}P NMR spectra at 24-30 ppm, (^{31}P NMR chemical shift of triphenylphosphine oxide in CDCl_3 is 29.3 ppm).²¹⁴

Similarly, in reactions where DPPE or DPPF ligands were used, the dominant ions in the mass spectra were again due to the oxidised ligands.

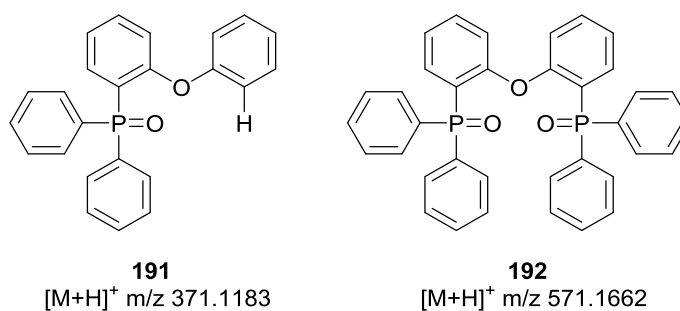


Figure 6.13: Dominant ions in mass spectra of reaction mixtures arisen due to oxidised ligands of the catalyst

Due to the above described limitations in identifying the products of the reaction while still as a mixture; column chromatography was performed on one reaction of key interest (Entry 14, Table 6.3), at a larger scale, to enable isolation of some of the minor components, Figure 6.14.

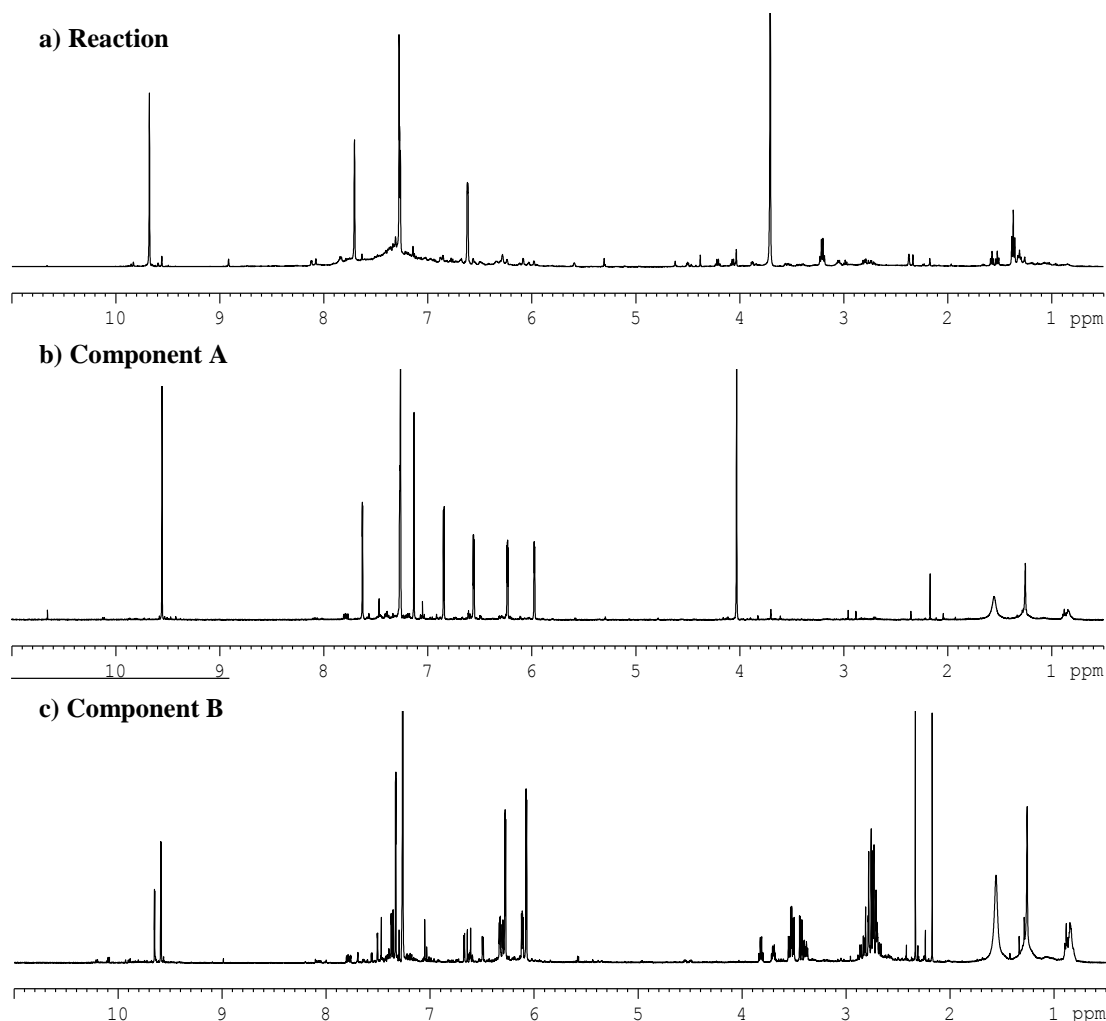
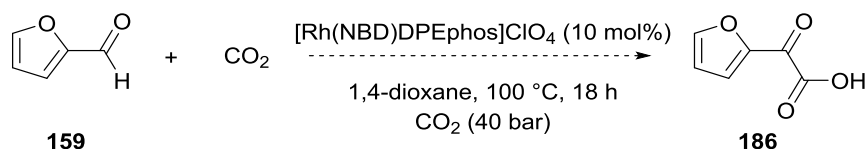


Figure 6.14: Example ^1H NMR spectra from furfural reaction with $[\text{Rh}(\text{COD})\text{DPEphos}]\text{ClO}_4$ and CO_2 in dioxane, b) ^1H NMR spectra of component A, c) ^1H NMR spectra of component B

The structure of component A, **193** was assigned by ^1H & ^{13}C NMR spectroscopy along with corresponding 2D experiments, Figure 6.14b (see Appendix 5 for 2D spectra). Stereochemistry around the double bond was confirmed through coupling constants and correlations between H_3 & H_8 and between H_5 & H_7 in the NOE spectrum.

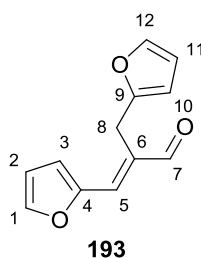
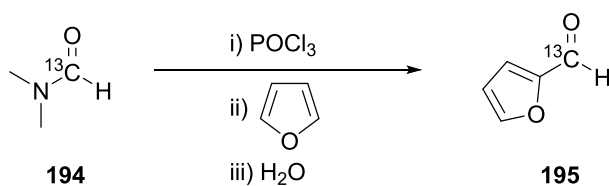


Figure 6.15: Structure of isolated compound, component A, **193**

Two characteristic singlet peaks in ^1H NMR at 9.55 and 4.03 ppm enabled identification of **193** in the reaction mixtures and was observed in entries 18, and 19, Table 6.3. In all cases $[\text{Rh}(\text{COD})\text{DPEphos}]\text{ClO}_4$ was used as the catalyst, 1,4-dioxane as the solvent and triethylamine was present, however its formation was independent on the presence of CO_2 .

Currently the mechanism of formation of **193** under reaction conditions is unclear and further control reactions are required to determine the conditions required for formation. For example, the reaction should be repeated in different solvents to see if 1,4-dioxane has an effect on the products formation and other organic bases should be investigated. Alternatively, an isotopic labelling experiment using furan-2- ^{13}C carboxaldehyde **195** under reaction conditions would enable the origin of the connecting carbons between the two furan rings to be determined. They may either originate from a fragmented and rearranged furan ring, the carbonyl of furfural, or from an external carbon source, e.g. solvent or catalyst. The labelled substrate **195** could be synthesised by a Vilsmeier-Haack reaction from *N,N*-dimethyl ^{13}C formamide **194**, Scheme 6.27.²¹⁵



Scheme 6.27: Proposed synthesis of furan-2- ^{13}C carboxaldehyde **195** via a Vilsmeier-Haack reaction²¹⁵

The identity of component B is unclear; however, more insights into its structure are known from the ^1H NMR spectrum, Figure 6.14c. Peaks at 7.33, 6.28 and 6.07 ppm suggest a furan ring is present with a relatively electron donating substituent on the C-2 position. A multiplet at 2.65 – 2.9 ppm further suggests that diastereomers are also present; however analysis by LC-MS and HR-MS data is inconclusive as the dominant ions are again those of the fragmented DPEphos ligand **191** and **192**. Further work is still required to identify this product.

6.6 Conclusions and Further Work

In summary, this chapter has discussed initial investigations into the insertion of CO₂ into an aldehyde to give α -ketocarboxylic acids. The selected substrates and catalysts for screening were selected based on well-known analogous hydroacylation chemistry.

The reaction of quinoline-8-carboxaldehyde **110** with CO₂ under a range of conditions was screened at high pressure of CO₂ (40 bar) and high temperatures. Conversion of aldehyde **110** was seen; however in no cases was CO₂ incorporated into the final product. Instead the decarbonylation product **167** was formed and carboxylic acids **169** and alcohol **168** were formed, proposed to be via a Cannizzaro type reaction. Ester **170** was also formed by a Tischenko reaction when non hemilabile ligands were used. The target product, an α -ketoacid **166**, was not observed under any of the reaction conditions. To assist in identifying reaction products and identifying potential reaction conditions the authentic product was targeted for synthesis. The product was produced as a sodium acetate salt, as confirmed by x-ray crystallography with the molecular formula: C₁₁H₆NO₃·0.5(C₂H₃O₂)·1.5Na. Although the product was not isolated in its free acid form, the species isolated has enabled characteristic peaks in the ¹³C NMR spectrum of a ketoacid at 199.5 and 168.7 ppm to be identified. These may allow for improved identification of the products after reaction of the substrate with CO₂.

A second substrate, furfural **159**, was also investigated under similar hydroacylation conditions. In this case only a small conversion of the substrate was observed and only one product derived from furfural was identified **193**. As with the quinoline-8-carbaldehyde **110** substrate, no incorporation of CO₂ was observed.

The lack of CO₂ incorporation into either substrate suggests that either harsher reaction conditions or alternative catalysts should to be investigated. For example hydroacylation reactions are also known to occur with Ru, Co, Ni and Ir catalysts.¹⁶³ To develop this further the reaction of furfural under the above conditions needs to be well understood. The coordination of quinoline-8-carbaldehyde **110** to rhodium complexes has been well characterised and it is known that the nitrogen group in the quinoline ring is paramount for stabilising the hydro-acyl rhodium intermediate.^{178, 180, 181} Without this stabilisation effect decarbonylation would occur and the reaction would not proceed to give the hydroacylation products. In this study quinoline-8-carbaldehyde **110** gave high conversion to products, whereas the furfural substrate did not. This may suggest that furfural is less effective at stabilising the hydro-acyl intermediate, preventing a hydroacylation reaction from occurring. To overcome this, additives may be used to assist in providing an additional coordination site to stabilise the complex. For example, in a previous hydroacylation study of furfural with an alkene, the use of

2-amino-3-picoline with either Cp_2ZrCl_2 or Cp_2TiCl_2 led to a much increased conversion of furfural to the hydroacylation product.²¹⁶ This may result in increased use of furfural in hydroacylations which could be an important method to utilise biomass, even if reaction with CO_2 is not achieved.

To further progress this project, further understanding of the catalyst speciation during the reaction is required. For example, currently it is not known how, or even if, CO_2 binds to the metal catalyst under these conditions. To address this, sequential, stoichiometric reaction should be carried out, with the catalyst structure and binding studied at each stage. Furthermore, the stability of the target keto acid under reaction conditions needs to be further examined. Ketoacids are known to regularly undergo hydration under aqueous conditions, and have a large number of decomposition pathways.²¹¹ By controlling the form of the final product, they may be more easily extracted and isolated from solution.

Chapter 7 Experimental

7.1 General Considerations

All reactions were carried out under N₂ atmosphere in oven dried glassware unless otherwise stated. For moisture sensitive reactions standard Schlenk line techniques were used and all glassware was cooled under vacuum and backfilled with nitrogen three times before use. Anhydrous solvents were obtained via a Dow-Grubbs type system (Pure Solv MD - Innovative Technology) or were obtained from Sigma-Aldrich.

TLC was performed using silica gel 60 backed aluminium plates and visualised under UV light or stained using potassium permanganate solution. Column chromatography was performed using silica gel (40-60 μm) in glass columns.

¹H, ¹³C NMR spectra were recorded on Bruker Avance 500, Bruker AV3 400 or Bruker Avance 300 spectrometers at 25 °C. ²⁹Si NMR spectra were recorded on Bruker Avance 500 or Bruker AV3 400 spectrometers. Chemical shifts (δ_H and δ_C) are referenced to the deuterated solvent peak and are reported in parts per million (ppm). Coupling constants (J) are given in Hertz (Hz) and multiplicities are reported as: s – singlet, d – doublet, t – triplet, q – quartet, dd – doublet of doublets, dt – doublet of triplets, ddd – doublet of doublet of doublets, td – triplet of doublets or m – multiplet. CDCl₃ was stored over molecular sieves and deuterated acetonitrile was distilled over CaH₂ and stored over molecular sieves before use.

Mass spectra were obtained from a Bruker maXis impact instrument by Electron Spray Ionisation. FT-IR spectra were recorded on a Bruker Alpha Platinum instrument with ATR attachment. X-ray structure measurements were carried out at 120K on an Agilent SuperNova diffractometer equipped with an Atlas CCD detector and connected to an Oxford Cryostream low temperature device using mirror monochromated Cu K_α radiation (λ = 1.54184 Å) from a Microfocus Nova X-ray source. The structure was solved by direct methods using SHELXS²¹⁷ and refined by a full matrix least squares technique based on F² using SHELXL97.²¹⁷

Gas chromatography was performed on an Agilent HP 6890 Series Gas Chromatography system fitted with a FID detector and an Agilent DB-624 column (30 m x 250 μm x 1.4 μm). GC/MS data was obtained using Agilent HP6890 series GC system, fitted with an Agilent HP-5MS column (30 m x 0.32 mm x 0.25 μm) and an Agilent HP5973 mass selective detector in EI mode.

7.2 Chapter 2: Role of Guanidine Catalysts in the Reaction of Propargylamines and CO₂

7.2.1 General Procedures

General procedure for reaction testing with propargylamine 40:

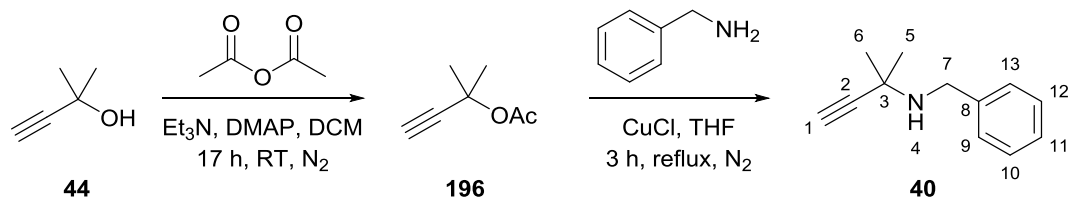
A solution of benzyl-(1,1-dimethylprop-2-ynyl)amine (0.15 g, 0.866 mmol, 1 equiv.) in the selected solvent (3 mL) was prepared in a vial under nitrogen. The catalyst (0.0868 mmol, 0.1 equiv. / 0.00868 mmol, 0.01 equiv.) was added to the reaction. A stainless steel high pressure reaction vessel was flushed with CO₂ and the solution injected into the cell. The vessel was further flushed with CO₂ and heated to 75 °C. After thermal equilibrium was reached the vessel was pressurised to 5 bar and stirred for 18 h. The vessel was cooled, vented through solvent and reaction solvent removed under vacuum. Conversions were calculated from ¹H NMR spectra of the crude reaction. Reactions in DMSO required an extraction: reaction mixture was diluted with H₂O (30 mL) washed with diethyl ether (3 x 40 mL) ether and washed with water (70 mL). The organic solution was dried over MgSO₄, filtered and the solvent evaporated under vacuum.

General procedure for reaction testing with 2-methyl-3-butyn-2-ol 44:

A solution of 2-methyl-3-butyn-2-ol (97 μL, 1 mmol, 1 equiv.) in the selected solvent (3 mL) was prepared in a vial under nitrogen. The catalyst (0.1 mmol, 0.1 equiv. / 0.01 mmol, 0.01 equiv.) was added to the reaction. A stainless steel high pressure reaction vessel was flushed with CO₂ and the solution injected into the cell. The vessel was further flushed with CO₂, pressurised to 40 bar, heated to 100 °C and stirred for 23 h. The vessel was cooled, vented through solvent and reaction solvent removed under vacuum. Reactions in DMSO required an extraction: reaction mixture was diluted with H₂O (30 mL), washed with diethyl ether (3 x 40 mL) and washed with brine (100 mL). The organic solution was dried over MgSO₄, filtered and the solvent evaporated under vacuum.

7.2.2 Substrate Synthesis

Benzyl-(1,1-dimethylprop-2-ynyl)amine 40:²¹⁸



Triethylamine (23.7 mL, 170 mmol, 1.1 equiv) and dimethylaminopyridine (0.472 g, 3.87 mmol, 0.025 equiv.) were added to a solution of 2-methyl-3-butyn-2-ol (15 mL, 155 mmol, 1

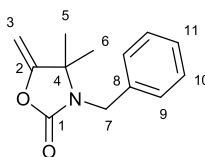
equiv) in DCM (110 mL). The solution was cooled to 0 °C and acetic anhydride (17.7 mL, 186 mmol, 1.2 equiv) was added dropwise over 25 min. A yellow solution formed which was stirred for 17 h until the reaction was complete. The solution was diluted with an aqueous NH₄Cl solution (100 mL) and extracted with DCM (3 x 100 mL). The organic solution was dried over MgSO₄, filtered and the solvent evaporated. The product was purified by column chromatography (7:1, pentane-EtOAc, *R_f*: 0.57) to give 1,1-dimethyl-2-propynyl acetate **196** as a yellow oil (13.5 g, 69 %).

1,1-Dimethyl-2-propynyl acetate **196** (13.5 g, 107 mmol, 1 equiv) and CuCl (0.529 g, 5.35 mmol, 0.05 equiv) were added to a solution of benzylamine (23.3 ml, 213 mmol, 2 equiv.) in degassed THF (200 mL), upon which the reaction turned turquoise. The reaction was stirred and heated under reflux for 3 h until complete. The navy solution was cooled to rt and the solvent evaporated. Product was purified by column chromatography, (DCM, *R_f*: 0.16) and further purified through distillation of remaining benzylamine to yield a yellow solid **40** (5.17 g, 32 %).

¹H NMR (500 MHz, CDCl₃) δ: 7.40-7.23 (5H, m, ArH), 3.88 (2H, s, H₇), 2.36 (1H, s, H₁), 1.43 (6H, s, H₅,H₆), 1.30 (1H, s, H₄); ¹³C NMR (125 MHz, CDCl₃) δ: 140.76 (Ar), 128.57 (Ar), 128.55 (Ar), 127.07 (Ar), 89.17 (C₁), 69.97 (C₂), 50.15 (C₃), 49.11 (C₇), 29.69 (C₅/C₆); MS (ESI): found [M+H]⁺: 174.1279 (calculated: 174.1277); M.p.: 45.5-49 °C; ATR-FT-IR (cm⁻¹): 3301, 3123, 2979, 2832, 2080, 1457, 1438, 1380, 1362, 1188, 750, 701, 548, 504. Spectral data are consistent with the literature.²¹⁸

7.2.3 Product Characterisation

N-benzyl-4,4-dimethyl-5-methylen-2-oxazolidinone **41**:



¹H NMR (500 MHz, CDCl₃) δ: 7.33-7.27 (5H, m, ArH), 4.67 (1H, d, *J*= 3.3 Hz, H₃), 4.45 (2H, s, H₇), 4.21 (1H, s, *J*= 3.3 Hz, H₃), 1.30 (6H, s, H₅/H₆). ¹³C NMR (125 MHz, CDCl₃) δ: 160.93 (C₁), 154.98 (C₂), 137.74 (C₈), 128.81 (Ar), 127.91 (Ar), 127.88 (Ar), 84.28 (C₃), 61.69 (C₄), 44.24 (C₇), 27.77 (C_{5/6}). MS (ESI): found [M+H]⁺: 218.1173 (calculated: 218.1176). Mp: 74.5-75.3 °C; ATR-FT-IR (cm⁻¹): 3031 (w, CH stretch), 2980 (w, CH stretch), 2919 (w), 1771 (s, C=O stretch), 1664 (m), 1397 (m). Spectral data are consistent with the literature²¹⁹

7.3 Chapters 3-5: Guanidine Catalysed Reductive Functionalisation of CO₂

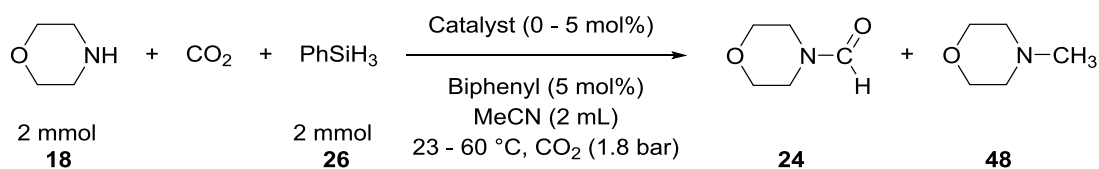
7.3.1 General Considerations

Pharmaceutical grade CO₂ was purchased from BOC and handled on a Schlenk line. Morpholine (99.5 %) was purchased from Acros Organics, phenylsilane (97 %) was purchased from Acros Organics and Sigma Aldrich and 1,1,3,3-tetramethylguanidine (99 %) purchased from Alfa Aesar. All other reagents were obtained from commercial sources and used without further purification unless otherwise stated.

For entire reaction monitoring, ATR-IR spectra were collected using a AgX DiComp fiber optic probe connected to a ReactIR 15 system (Mettler Toledo). Spectra were collected every 15-30 s over range of 650 - 2500 cm⁻¹ at 8 cm⁻¹ resolution. Data analysis was performed using a combination of iC IR 4.3 (Mettler Toledo) or MATLAB software.

Further IR probe studies for individual pathways were studied using an MB3000 FTIR spectrometer (ABB Bomem Inc.) connected to a diamond tip ATR probe. Data analysis and processing performed using Horizon MB (ABB Bohem Inc.) and MATLAB.

7.3.2 Standard Reaction Procedure



A 50 mL oven dried Schlenk tube and stirrer bar fitted with a subaseal was evacuated and backfilled with CO₂. A solution of morpholine (175 μl, 2 mmol, 1 equiv), biphenyl (15.4 mg, 0.1 mmol, 5 mol%) and guanidine catalyst (0.002 - 0.1 mmol, 0.1 - 5 mol%) in acetonitrile (2 mL) was prepared under a N₂ atmosphere and added to the CO₂ flushed Schlenk tube. The solution was stirred at 1000 rpm at reaction temperature, 1.8 bar CO₂, for 15 mins. Phenylsilane (247 μl, 2 mmol, 1 equiv) was added to commence the reaction.

The reaction was monitored by either NMR, IR, GC or HRMS, the details of which can be found in relevant sections.

N-Formylmorpholine **24**:

¹H NMR (300 MHz, CDCl₃) δ: 8.06 (1H, s, CHO), 3.72-3.65 (4H, m, O(CH₂)₂), 3.60-3.56 (2H, m, N(CH₂)₂), 3.41-3.38 (2H, m, N(CH₂)₂); ¹³C NMR (126 MHz, CDCl₃) δ: 161.0 (CHO), 67.4

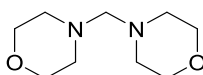
(O(CH₂)₂), 66.6 (O(CH₂)₂), 45.9 (N(CH₂)₂), 40.8 (N(CH₂)₂); EI-MS (rel. int.) m/z = 115.1 (M⁺, 100 %), 100.1 (56), 86.1, (37), 57.1 (45), 56.1 (49)

N-Methylmorpholine **48**:

¹H NMR (400 MHz, CDCl₃) δ: 3.72 (4H, m, O(CH₂)₂), 2.40 (4H, m, N(CH₂)₂), 2.29 (3H, s, NCH₃); ¹³C NMR (126 MHz, CDCl₃) δ: 67.1 (O(CH₂)₂), 55.6 (N(CH₂)₂), 46.6 (NCH₃); EI-MS (rel. int.) m/z = 101.1 (M⁺, 100 %), 100.1 (34), 71.1 (47), 70.1 (11), 56.1 (9)

7.3.3 Synthesis of Organic Compounds

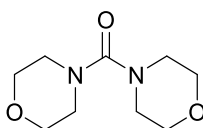
7.3.3.1 Synthesis of Ainal - Dimorpholinomethane **57**



Prepared following a procedure reported by Huang.¹⁴⁹ Morpholine (8.7 mL, 100 mmol, 1 equiv) was added to a solution of paraformaldehyde (3.00 g, 100 mmol, 1 equiv) in anhydrous dioxane (20 mL) and heated at 85 °C for 8 h. After cooling to RT the solvent was removed under reduced pressure, to give a pale yellow oil. The product was purified by reduced pressure distillation (<0.1 mmHg, 58-60 °C) to yield a colourless oil (5.51 g, 59 %).

¹H NMR (400 MHz, CDCl₃) δ: 3.69 (8 H, t, *J* = 4.6 Hz, O(CH₂)₂), 2.90 (2 H, s, NCH₂N), 2.49 (8 H, t, *J* = 4.6 Hz, N(CH₂)₂); ¹³C NMR (101 MHz, CDCl₃) δ: 81.8 (NCH₂N), 67.2 (O(CH₂)₂), 52.2 (N(CH₂)₂); EI-MS (rel. int.) m/z = 186.1 (M⁺, 0.4 %), 100.1 (100), 87.1 (7), 56.1 (11). Spectral data are consistent with the literature²²⁰

7.3.3.2 Synthesis of Urea – Dimorpholinomethanone **81**

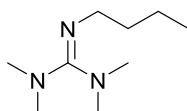


Prepared following a modified procedure reported by Albericio.¹⁵³ Triethylamine (2.8 mL, 20 mmol, 1 equiv.) was added slowly to a solution of morpholine (1.75 mL, 20 mmol, 1 equiv.) in anhydrous DCM at 0 °C. Morpholine-4-carbonyl chloride (2.8 mL, 24 mmol, 1.2 equiv) was added dropwise and the solution slowly warmed to RT and stirred for 5 h to give a pale yellow/orange solution and precipitate. The solution was cooled to 0 °C and an aqueous NaOH solution (20 mL, 10 %) was added and the resulting layers separated. The aqueous layer was washed with DCM (2 × 20 mL), the organics combined and washed with water (2 × 20 mL), brine (2 × 20 mL) and dried over MgSO₄. The solution was filtered and the solvent removed

under reduced pressure to give a yellow solid (3.92 g) which was purified by recrystallisation in ethanol to yield the product as a pure white solid (2.62 g, 65 %).

^1H NMR (500 MHz, CDCl_3) δ : 3.68 (8H, t, $J = 4.7$ Hz, $\text{O}(\text{CH}_2)_2$), 3.27 (8H, t, $J = 4.7$ Hz, $\text{N}(\text{CH}_2)_2$); ^{13}C NMR (500 MHz, CDCl_3) δ : 163.8 ($\text{C}=\text{O}$), 66.6 ($\text{O}(\text{CH}_2)_2$), 47.3 ($\text{N}(\text{CH}_2)_2$); HRMS (ESI): $[\text{M}+\text{H}]^+$ m/z = found: 201.1246. Calculated: 201.1234. Spectral data are consistent with the literature^{221, 222}

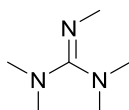
7.3.3.3 2-Butyl-1,1,3,3-tetramethylguanidine **64**



Prepared following a modified procedure reported by Hodson.¹⁴⁶ Oxalyl chloride (4.8 mL, 56.6 mmol, 1.7 equiv) was added dropwise to a stirred solution of tetramethylurea (4.0 mL, 33.3 mmol, 1 equiv) in anhydrous dichloroethane (38 mL). The resulting yellow/green solution was heated to 60 °C for 2 h, cooled to RT and the solvent removed under vacuum. The yellow solid was dissolved in anhydrous acetonitrile (27 mL), cooled to 0 °C and a solution of butylamine (9.9 mL, 100 mmol, 3 equiv) in acetonitrile (30 mL) was added dropwise. The solution was slowly warmed to RT and heated under reflux for 4 h. After cooling to RT the solvent was removed under vacuum yielding a green oil to which diethyl ether (100 mL) was added and cooled to 0 °C. A solution of sodium hydroxide (6.5 g, 163 mmol) in water (40 mL) saturated with potassium carbonate was added and the two phases separated. The aqueous layer was washed with diethyl ether (2 × 50 mL), the organics were combined, dried over MgSO_4 , filtered and the solvent removed under vacuum. The product was purified by Kugelrohr distillation (0.1 mbar, 23 – 40 °C) to yield a colourless oil (1.63 g, 29 %).

^1H NMR (300 MHz, CDCl_3) δ : 3.09 (2H, t, $J = 6.9$ Hz, NCH_2), 2.72 (6H, s, $\text{N}(\text{CH}_3)_2$), 2.63 (6H, s, $\text{N}(\text{CH}_3)_2$), 1.54-1.44 (2H, m, $\text{CH}_2\text{CH}_2\text{CH}_2$), 1.39 – 1.26 (2H, m, CH_2CH_3), 0.89 (3H, t, $J = 7.2$ Hz, CH_2CH_3); ^{13}C NMR (101 MHz, CDCl_3) δ : 160.0 ($\text{C}=\text{N}$), 49.3 (NCH_2), 39.8 ($\text{N}(\text{CH}_3)_2$), 39.0 ($\text{N}(\text{CH}_3)_2$), 35.1 ($\text{CH}_2\text{CH}_2\text{CH}_2$), 20.7 (CH_2CH_3), 14.1 (CH_2CH_3); HRMS (ESI): $[\text{M}+\text{H}]^+$ m/z = Found: 172.1809. Calculated: 172.1808. Spectral data are consistent with the literature.²²³

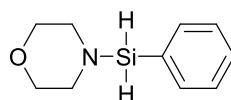
7.3.3.4 Pentamethylguanidine **65**



Prepared following a procedure reported by Elabd.¹⁴⁷ Oxalyl chloride (5.65 mL, 64.8 mmol, 1.6 equiv) was added dropwise to a stirred solution of tetramethylurea (4.8 mL, 40 mmol, 1 equiv) in anhydrous dichloroethane (50 mL). The resulting yellow/green solution was heated to 60 °C for 2.5 h, cooled to RT and the solvent removed under vacuum. The yellow solid was dissolved in anhydrous ethanol (27 mL), stirred and cooled to 0 °C. A solution of methylamine in ethanol (33 mL, 33 wt%, 355 mmol, 8.9 equiv) was added dropwise over 30 mins, slowly warmed to RT, heated under reflux for 4 h and stirred overnight at RT to give a yellow/brown solution. The solvent was evaporated under reduced pressure to yield a yellow oil/solid to which diethyl ether (120 mL) was added, cooled to 0 °C. A solution of NaOH (8.15 g, 204 mmol) in water (50 mL) saturated with potassium carbonate was added and the two layers separated. The aqueous layer was extracted with diethylether (2 × 80 mL), the organics were combined, dried over MgSO₄, filtered and solvent evaporated under reduced pressure. The product was purified by Kugelrohr distillation (0.2 mbar, 23 °C) to yield a colourless oil (0.97 g, 19 %).

¹H NMR (400 MHz, CDCl₃) δ: 2.90 (3H, s, NCH₃), 2.73 (6H, s, N(CH₃)₂), 2.61 (6H, s, N(CH₃)₂); ¹³C NMR (101 MHz, CDCl₃) δ: 161.7 (C=N), 39.7 (N(CH₃)₂), 39.0 (N(CH₃)₂), 37.2 (NCH₃); HRMS (ESI): [M+H]⁺ m/z = found: 130.1341. Calculated: 130.1339. Spectral data are consistent with the literature²²⁴

7.3.3.5 *N*-Phenylsilylmorpholine **53**



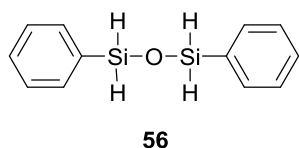
A modified protocol reported by Ripoll was followed.¹²³ Under an N₂ atmosphere, triethylamine (1.4 mL, 10 mmol, 1 equiv) was added to a solution of morpholine (875 μl, 10 mmol, 1 equiv) in anhydrous, degassed DCM (10 mL). After cooling to -40 °C, chlorophenylsilane (1.36 ml, 10 mmol, 1 equiv) was added dropwise over 15 mins leading to the formation of a white precipitate. The solution was stirred at -40 °C for 60 mins before slowly warming to RT and stirred overnight. Degassed, anhydrous hexane (10 mL) was added to the solution and filtered via filter paper and cannula and the solvent evaporated to give a yellow oil. Further hexane (25 mL) was added to the resulting oil, leading to further precipitation of a white solid which was removed via cannula filtration, and the solvent removed under vacuum to give a yellow oil. The resulting oil was purified by vacuum distillation (0.1 mbar, 53.5-54.5 °C) to yield a clear colourless oil (1.24 g, 64 %).

¹H NMR (400 MHz, CD₃CN) δ: 7.66–7.63 (2H, m, ArH), 7.49-7.41 (3H, m, ArH), 4.85 (2H, s, SiH₂), 3.52 (4H, t, *J* = 4.6 Hz, O(CH₂)₂), 2.92 (4H, t, *J* = 4.6 Hz, N(CH₂)₂); ¹³C NMR (101 MHz, CD₃CN) δ: 135.8 (Ar-C), 131.3 (Ar-C), 129.2 (Ar-C), 68.7 (O(CH₂)₂), 47.9 (N(CH₂)₂), (partial

assignments due to overlap with decomposition product). ^{29}Si NMR (79 MHz, CD_3CN) δ : -23.3 (t, $J = 205.8$ Hz). FTIR / ATR (1 M solution in MeCN) (cm^{-1}): 1257, 1113, 968, 918, 877, 742, 703

The product was found to be very sensitive to moisture and on exposure to moisture in the air or water would decompose to 1,3-diphenyldisiloxane **56** and morpholine **18** and thus was stored under N_2 at -18 °C.

1,3-Diphenyldisiloxane **56**



^1H NMR (400 MHz, CDCl_3) δ : 7.68 – 7.33 (10H, m, ArH), 5.13 (s, 4H); EI-MS (rel. int.) $m/z = 230.1$ (M^+ , 48 %), 152.0 (100), 151.0 (97), 107.0 (40), 105.0 (25), 74.0 (38). Spectral data are consistent with the literature.¹²⁵

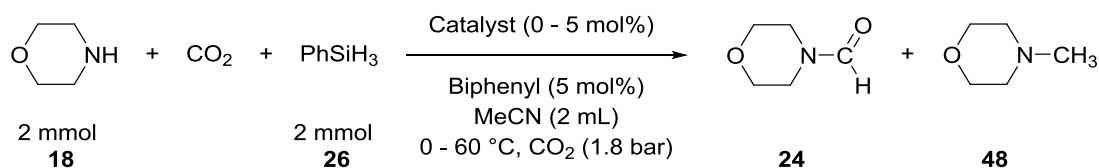
7.3.3.6 Stabilisation of morpholine carbamate by diphenylthiourea **46**

(Prepared by B.N. Nguyen)

A 14 mL vial with septum was charged with a solution of TMG (100 μL , 0.797 mmol), diphenylthiourea **46** (182.0 mg, 0.797 mmol) and morpholine (69.7 μL , 0.797 mmol) in toluene (8 mL) under nitrogen. A balloon of dried CO_2 with a 25G needle was introduced to the vial without stirring. CO_2 was allowed to slowly diffuse into the solution at room temperature to afford colourless cubic crystals overnight. For details of structure see Appendix 1.

7.3.4 Procedure for Reaction Monitoring by GC

7.3.4.1 Standard Procedure



A 50 mL oven dried Schlenk tube and stirrer bar fitted with a subaseal was evacuated and backfilled with CO_2 . A solution of morpholine (175 μl , 2 mmol, 1 equiv), biphenyl (15.4 mg, 0.1 mmol, 5 mol%) and guanidine catalyst (0 - 0.1 mmol, 0 - 5 mol%) in acetonitrile (2 mL) was prepared under a N_2 atmosphere and added to the CO_2 flushed Schlenk tube. The solution was stirred at 1000 rpm at reaction temperature, 1.8 bar CO_2 , for 15 mins. Phenylsilane (247 μl , 2 mmol, 1 equiv) was added to commence the reaction and kinetic monitoring started. Regular

samples (approx. 0.02 mL) were taken and diluted in methanol to quench the reaction for analysis by GC.

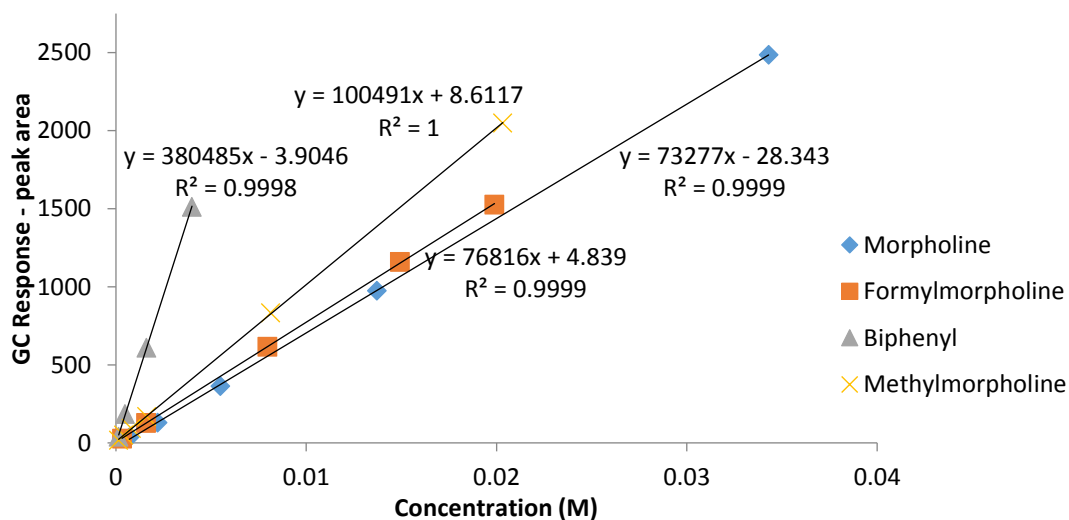
The reaction outcome was further confirmed by GCMS analysis (0.1 mL of reaction mixture in 1 mL DCM) and solvent evaporated from the remaining reaction mixture under reduced pressure for analysis by NMR.

7.3.4.2 GC Analysis

GC samples were analysed on an Agilent HP 6890 Series Gas Chromatography system fitted with a FID detector and an Agilent DB-624 column (30 m x 250 μ m x 1.4 μ m). Temperature method: held for 3 mins 40 $^{\circ}$ C, increased to 140 $^{\circ}$ C at 12 $^{\circ}$ C / min, to 200 $^{\circ}$ C at 5 $^{\circ}$ C / min and held at 200 $^{\circ}$ C for 15 mins. Gas flow rate of 3.0 mL/min at 15 psi.

To determine product yields calibration curves were prepared using commercial samples with biphenyl as an internal standard (IS). Standard solutions of morpholine, *N*-formylmorpholine, *N*-methylmorpholine and biphenyl in methanol from 0.0001 M – 0.04 M were prepared and their response in peak area measured.

7.3.4.3 Calibration Curves



Compound	Retention Time / min	Gradient	Response Factor relative to IS
Morpholine 18	8.0	73277	0.1926
Formylmorpholine 24	15.3	76816	0.2019
Methylmorpholine 48	7.6	100491	0.2641
Biphenyl	19.9	380485	1

Concentration of reaction component calculated by:

$$\text{Response Factor} = \frac{\text{gradient}(\text{component})}{\text{gradient}(\text{IS})}$$

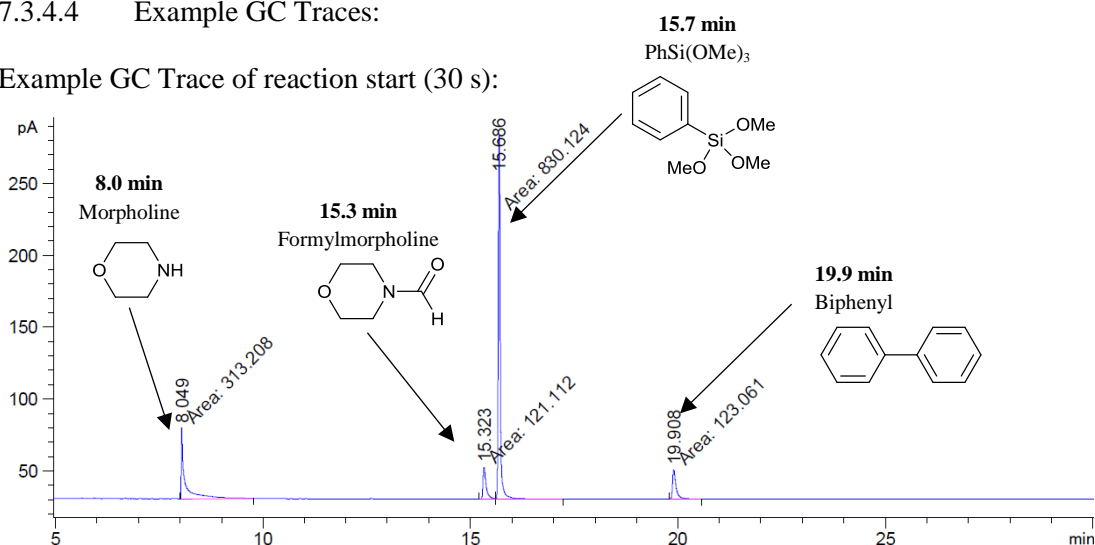
$$\frac{\text{response}(\text{component})}{\text{response}(\text{IS})} = \text{Response Factor} \times \frac{[\text{component}]}{[\text{IS}]}$$

Thus:

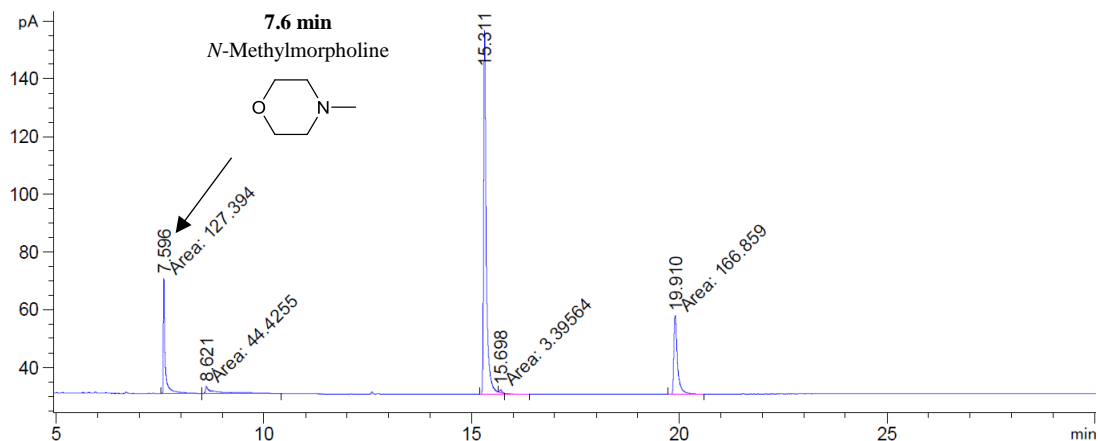
$$[\text{Component}] = \frac{\text{response}(\text{component})}{\text{response}(\text{IS})} \times \frac{[\text{IS}]}{\text{Response Factor}}$$

7.3.4.4 Example GC Traces:

Example GC Trace of reaction start (30 s):

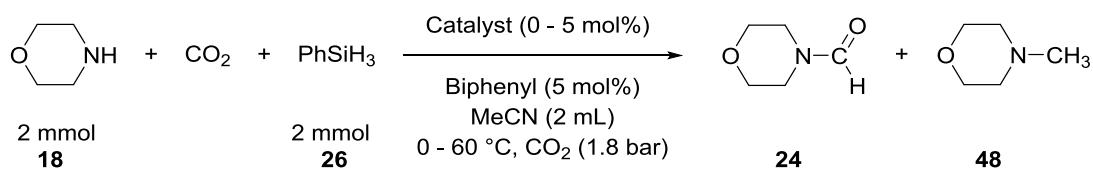


Example GC Trace near reaction end (4 h):



The formation of dimorpholinomethane **57** in some reactions could be observed in the GC trace; however due to its decomposition on the column and subsequent overlap with the morpholine signal neither morpholine nor dimorpholinomethane **57** could be reliably quantified during many cases of reaction monitoring where dimorpholinomethane **57** is a significant intermediate.

7.3.4.5 Kinetic Experiments – reaction conditions used



Reactions were performed using the standard procedure outlined in Section 7.3.4.1. Variations to reagent conditions as outlined below:

Entry	18 (mmol)	PhSiH₃ (mmol)	Catalyst	Catalyst loading (mol%)	Temp (°C)	CO₂ Pressure (bar)
1	2	2	TMG	5	60	1.8
2	2	2	TMG	5	23	1.8
3	2	2	TMG	5	0	1.8
4	2	2	TMG / 46	5 / 5	60	1.8
5	2	2	TMG / 46	5 / 5	23	1.8
6	2	2	TBD	5	60	1.8
7	2	2	TBD	5	23	1.8
8	2	2	TMG	1	60	1.8
9	2	2	TMG	1	23	1.8
10	2	4	TMG	5	60	1.8
11	2	1	TMG	5	60	1.8
12	2	1	TMG	5	23	1.8
13	2	2	TMG	5	23	1.2
14 ^{a)}	2	2	TMG	5	23	1 ^{a)}
15	1	1	TMG	5	23	1.8
16	0.2	0.2	TMG	5	23	1.8
17	1	1	TMG	10	23	1.8
18	2	2	-	0	60	1.8
19	2	2	-	0	23	1.8
20 ^{b)}	2	2	TMG	5	60	1.8

^{a)} Reaction at 1 bar CO₂ performed on CO₂ line with bubbler open at 1-2 bubbles a second

^{b)} 10 mol% water added

7.3.4.6 Kinetic Experiments – kinetic data:

Entry 1			
Time / min	18 / M	24 / M	48 / M
0.00	0.9794	0.0000	0.0000
0.17	0.9028	0.0499	0.0000
2.50	0.6781	0.3011	0.0000
5.00	0.5878	0.4131	0.0000
10.00	0.5078	0.4736	0.0021
20.00	0.4735	0.5121	0.0029
30.00	0.3988	0.5229	0.0035
45.00	0.3634	0.5861	0.0075
60.00	0.3058	0.6256	0.0132
90.00	0.1366	0.7309	0.0340
120.00	0.1892	0.7255	0.0568
150.00	0.0454	0.7818	0.0674
180.00	0.0456	0.7788	0.0801
240.00	0.0250	0.8214	0.0928
300.00	0.0023	0.8720	0.1156
360.00	0.0211	0.8902	0.1204

Entry 2			
Time / min	18 / M	24 / M	48 / M
0.00	1.0357	0.0000	0.0000
0.17	0.9595	0.0180	0.0000
2.50	0.7581	0.2195	0.0000
5.00	0.5818	0.3657	0.0000
10.00	0.4123	0.4941	0.0000
20.00	0.2462	0.6542	0.0038
30.00	0.1868	0.7371	0.0071
45.00	0.1159	0.8381	0.0127
60.00	0.0000	0.8462	0.0142
90.00	0.0000	0.8781	0.0198
120.00	0.0000	0.8875	0.0231
150.00	0.0000	0.9091	0.0254
180.00	0.0000	0.8859	0.0277
240.00	0.0000	0.9424	0.0218
300.00	0.0000	0.9545	0.0250
360.00	0.0000	0.9737	0.0242

Entry 3			
Time / min	18 / M	24 / M	48 / M
0.00	1.0385	0.0000	0.0000
0.30	0.4547	0.0068	0.0000
2.67	0.7682	0.0149	0.0000
6.00	0.7532	0.0604	0.0000
11.00	0.7047	0.1279	0.0000
16.67	0.6867	0.1773	0.0000
25.18	0.6403	0.2887	0.0000
35.67	0.5907	0.3879	0.0000
45.25	0.5283	0.4640	0.0000
60.33	0.4501	0.5411	0.0000
90.67	0.4253	0.5871	0.0000
123.08	0.4017	0.6202	0.0000
153.33	0.3312	0.6202	0.0000
182.00	0.3623	0.6660	0.0000
215.00	0.2795	0.7436	0.0000
243.00	0.2361	0.7809	0.0000
361.50	0.0000	0.7528	0.0000
480.00	0.0000	0.8356	0.0000
1320.0	0.0000	1.0466	0.0000

Entry 4			
Time / min	18 / M	24 / M	48 / M
0.00	1.0006	0.0000	0.0000
0.33	0.9333	0.0157	0.0000
2.50	0.7867	0.1250	0.0000
5.08	0.7864	0.1913	0.0000
10.00	0.6761	0.2720	0.0000
20.08	0.5843	0.3155	0.0000
30.08	0.5851	0.3495	0.0031
45.00	0.6375	0.3701	0.0045
60.83	0.4937	0.4063	0.0055
90.17	0.3427	0.5575	0.0120
120.00	0.0000	0.6655	0.0387
183.08	0.0000	0.7603	0.0903
240.50	0.0000	0.8075	0.1239
364.00	0.0000	0.8309	0.1316

Entry 5			
Time / min	18 / M	24 / M	48 / M
0.00	0.9842	0.0000	0.0000
0.33	0.9348	0.0006	0.0000
2.58	0.8758	0.0626	0.0000
5.08	0.8507	0.0996	0.0000
10.58	0.7189	0.2109	0.0000
20.08	0.6060	0.3354	0.0000
30.00	0.4961	0.4184	0.0000
45.17	0.3988	0.5188	0.0000
60.17	0.3122	0.6053	0.0023
90.08	0.2238	0.6988	0.0060
120.00	0.1432	0.8078	0.0107
180.00	0.1310	0.8352	0.0206
240.00	0.0000	0.8706	0.0198
360.00	0.0000	0.9326	0.0246

Entry 6			
Time / min	18 / M	24 / M	48 / M
0.00	1.0742	0.0000	0.0000
0.17	0.9551	0.0170	0.0000
2.50	0.8797	0.1165	0.0000
5.00	0.7550	0.2431	0.0000
10.00	0.5859	0.4038	0.0000
20.00	0.4489	0.4672	0.0000
30.00	0.4390	0.5198	0.0000
45.00	0.3991	0.5886	0.0079
60.00	0.2915	0.6863	0.0197
90.00	0.2260	0.7253	0.0559
120.00	0.1727	0.7642	0.0815
150.00	0.0965	0.8065	0.1202
180.00	0.0234	0.8657	0.1491
241.00	0.0000	0.9065	0.1623
300.00	0.0000	0.9146	0.1546
360.00	0.0000	0.9202	0.1657

Entry 7			
Time / min	18 / M	24 / M	48 / M
0.00	1.0688	0.0000	0.0000
0.33	0.7264	0.0000	0.0000
2.50	0.9016	0.0441	0.0000
5.00	0.7931	0.0743	0.0000
10.00	0.7833	0.1364	0.0000
20.00	0.7002	0.2196	0.0000
30.00	0.6761	0.3101	0.0000
45.00	0.5049	0.3445	0.0000
60.00	0.4425	0.4083	0.0000
90.00	0.4403	0.5560	0.0021
120.00	0.4055	0.5671	0.0045
150.00	0.3565	0.6400	0.0098
180.00	0.2425	0.7617	0.0155
241.00	0.1683	0.8247	0.0234
300.00	0.1357	0.8723	0.0313
360.00	0.0897	0.9287	0.0373

Entry 8			
Time / min	18 / M	24 / M	48 / M
0.50	0.8616	0.0394	0.0000
2.50	0.6450	0.2389	0.0000
5.33	0.5021	0.3537	0.0000
7.50	0.4749	0.3951	0.0000
10.00	0.4636	0.4106	0.0000
15.00	0.4605	0.4307	0.0000
20.17	0.4361	0.4432	0.0000
30.00	0.3887	0.4632	0.0000
45.00	0.3984	0.4766	0.0000
60.00	0.3798	0.4934	0.0000
90.00	0.3798	0.5133	0.0038
120.00	0.3656	0.5245	0.0064
152.66	0.2804	0.6143	0.0107
180.66	0.2782	0.6094	0.0157
240.00	0.2323	0.6106	0.0294
300.00	0.1861	0.6684	0.0430
360.00	0.2175	0.6485	0.0659
480.00	0.1717	0.6642	0.0082

Entry 9			
Time / min	18 / M	24 / M	48 / M
0.33	1.0735	0.0047	0.0000
2.83	0.8722	0.0839	0.0000
5.00	0.7926	0.1629	0.0000
7.50	0.7410	0.2284	0.0000
10.00	0.6654	0.2524	0.0000
15.00	0.5887	0.3469	0.0000
20.00	0.5882	0.3836	0.0000
30.00	0.5185	0.4626	0.0000
45.25	0.4772	0.5023	0.0012
60.00	0.4771	0.5044	0.0020
90.00	0.4346	0.5549	0.0035
120.50	0.3405	0.5944	0.0049
150.50	0.3838	0.6030	0.0066
180.00	0.3551	0.6304	0.0083
240.00	0.3211	0.6659	0.0112
300.00	0.1597	0.8099	0.0162
360.00	0.1860	0.8423	0.0366
480.00	0.0000	0.8858	0.0382

Entry 10			
Time / min	18 / M	24 / M	48 / M
0.00	0.9708	0.0000	0.0000
0.17	0.8427	0.0511	0.0000
2.50	0.6439	0.2254	0.0000
5.00	0.5278	0.2806	0.0000
7.50	0.4845	0.3229	0.0035
10.00	0.4768	0.3421	0.0028
14.50	0.4338	0.3841	0.0037
20.00	0.4276	0.4269	0.0074
30.00	0.3396	0.4984	0.0108
45.17	0.2581	0.6015	0.0343
60.66	0.0000	0.6670	0.0890
90.00	0.0000	0.6879	0.2756
120.00	0.0000	0.6958	0.2687
150.00	0.0000	0.6952	0.2742
180.00	0.0000	0.6924	0.2806
241.43	0.0000	0.6773	0.3028
300.00	0.0000	0.6962	0.2690
361.00	0.0000	0.6910	0.2693

Entry 11			
Time / min	18 / M	24 / M	48 / M
0.18		0.0441	0.0000
2.68		0.4151	0.0000
5.00		0.4025	0.0000
7.50		0.4285	0.0000
10.00		0.4319	0.0000
15.00		0.4347	0.0000
20.00		0.4569	0.0000
30.00		0.4485	0.0000
90.50		0.4964	0.0000
120.33		0.5066	0.0000
301.00		0.5061	0.0000
365.50		0.5145	0.0000

Entry 12			
Time / min	18 / M	24 / M	48 / M
0.00	1.0726	0.0000	0.0000
0.30	1.0788	0.0021	0.0000
2.50	0.8865	0.1652	0.0000
10.00	0.5272	0.3818	0.0000
20.00	0.5005	0.4762	0.0000
40.00	0.4505	0.5393	0.0000
60.00	0.4813	0.5732	0.0000
120.00	0.4426	0.6110	0.0000
240.00	0.4011	0.6356	0.0000
360.00	0.4195	0.6393	0.0000

Entry 13

Time / min	18 / M	24 / M	48 / M
0.00	1.0379	0.0000	0.0000
0.33	0.8373	0.0033	0.0000
2.50	0.8127	0.1267	0.0000
10.00	0.6330	0.3433	0.0000
20.00	0.4949	0.4904	0.0000
40.00	0.3571	0.6231	0.0000
60.00	0.2625	0.6356	0.0055
120.00	0.2149	0.7853	0.0113
240.00	0.0000	0.8542	0.0217
360.00	0.0000	0.9184	0.0240

Entry 14

Time / min	18 / M	24 / M	48 / M
0.00	1.0184	0.0000	0.0000
0.30	0.9495	0.0128	0.0000
2.58	0.9329	0.0855	0.0000
10.00	0.7365	0.1971	0.0000
20.00	0.6303	0.2584	0.0011
41.00	0.6018	0.4070	0.0023
60.00	0.4220	0.4006	0.0023
120.00	0.4023	0.5021	0.0027
240.00	0.0000	0.6029	0.0068
360.00	0.0000	0.6948	0.0134
532.00	0.0000	0.9004	0.0221
1320.0	0.0000	0.9941	0.0750

Entry 15

Time / min	18 / M	24 / M	48 / M
0.00	0.4923	0.0000	0.0000
0.33	0.3938	0.0000	0.0000
2.50	0.4091	0.0814	0.0000
5.08	0.3339	0.1579	0.0000
10.50	0.2542	0.2233	0.0000
20.00	0.1460	0.3057	0.0000
30.00	0.1137	0.3265	0.0000
60.00	0.0430	0.4194	0.0069
90.00	0.0027	0.4404	0.0101
121.00	0.0018	0.4589	0.0125
183.00	0.0000	0.4797	0.0134
242.50	0.0024	0.4709	0.0129
300.00	0.0015	0.4799	0.0125
360.00	0.0000	0.4866	0.0139

Entry 16

Time / min	18 / M	24 / M	48 / M
0.00	0.1142	0.0000	0.0000
2.50	0.1041	0.0015	0.0000
10.00	0.0785	0.0278	0.0000
20.00	0.0544	0.0499	0.0000
41.00	0.0289	0.0743	0.0000
60.00	0.0194	0.0839	0.0000
120.00	0.0079	0.0976	0.0000
240.00	0.0052	0.0992	0.0000
360.00	0.0000	0.1023	0.0000

Entry 17			
Time / min	18 / M	24 / M	48 / M
0.33	0.4795	0.0041	0.0000
2.50	0.3553	0.1549	0.0000
10.00	0.1722	0.3306	0.0016
20.18	0.0747	0.4249	0.0040
40.18	0.0000	0.4823	0.0069
60.00	0.0000	0.5153	0.0132
120.00	0.0000	0.5331	0.0173
240.18	0.0000	0.5264	0.0173
360.00	0.0000	0.5421	0.0171

Entry 18			
Time / min	18 / M	24 / M	48 / M
0.5	0.6053	0.0081	
30	0.0709	0.0396	
60	0.5558	0.0516	
120	0.5660	0.0569	
240	0.6062	0.0728	
1650	0.5141	0.2304	
4128	0.4891	0.3647	
5550	0.4880	0.3927	
8430	0.4017	0.3971	
11070	0.4523	0.4039	

Entry 19			
Time / min	18 / M	24 / M	48 / M
0.20	0.5572	0.0000	
120.00	0.9993	0.0431	
240.00	0.9167	0.0465	
510.00	0.9698	0.0664	
1170.0	0.8864	0.1164	
1710.0	0.8589	0.1526	
2730.0	0.7980	0.2227	
3030.0	0.7503	0.2324	
4560.0	0.6401	0.3424	
5400.0	0.5899	0.4211	
5880.0	0.5425	0.4548	
6840.0	0.4312	0.4879	
7320.0	0.4398	0.5328	
8280.0	0.4068	0.6063	

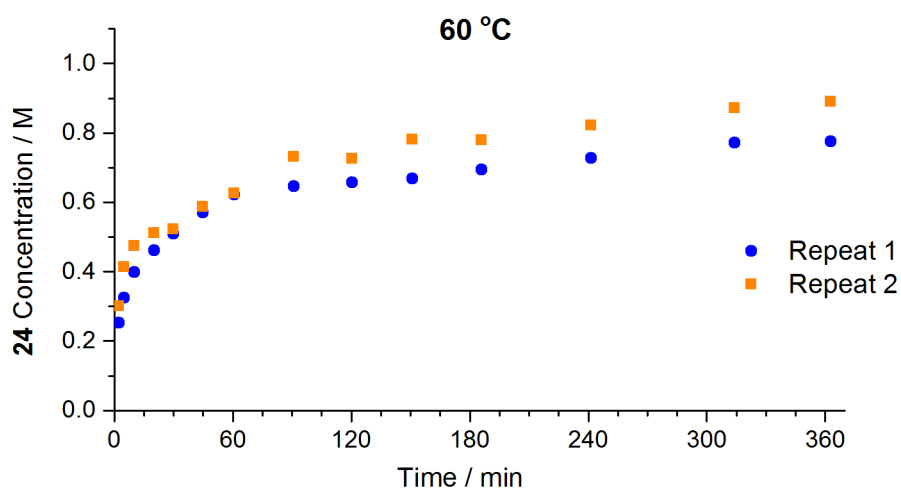
Entry 20			
Time / min	18 / M	24 / M	48 / M
0.3	0.5281	0.0803	0.0000
15	0.2752	0.4824	0.0000
30	0.2393	0.5501	0.0000
45	0.1782	0.6305	0.0000
60	0.1588	0.7068	0.0112
92	0.0000	0.7424	0.0390
122	0.0000	0.7519	0.0697
152	0.0000	0.7716	0.0822
181	0.0000	0.7869	0.1034
244	0.0000	0.8619	0.1307
299	0.0000	0.8312	0.1846
368	0.0000	0.8928	0.1429

7.3.4.7 Error Calculation

To determine the error in kinetic measurements, two reactions (Entry 1 – 60 °C and Entry 2 – 23 °C) were repeated. Standard deviation from the two repeats for conversion to formylmorpholine was used to calculate an average error of 9 % for reactions at 60 °C and 3 % for reactions at 23 °C. As to be expected, the error in the first 20 minutes of the reaction is greater, due to the faster rate of concentration change leading to error in sampling time.

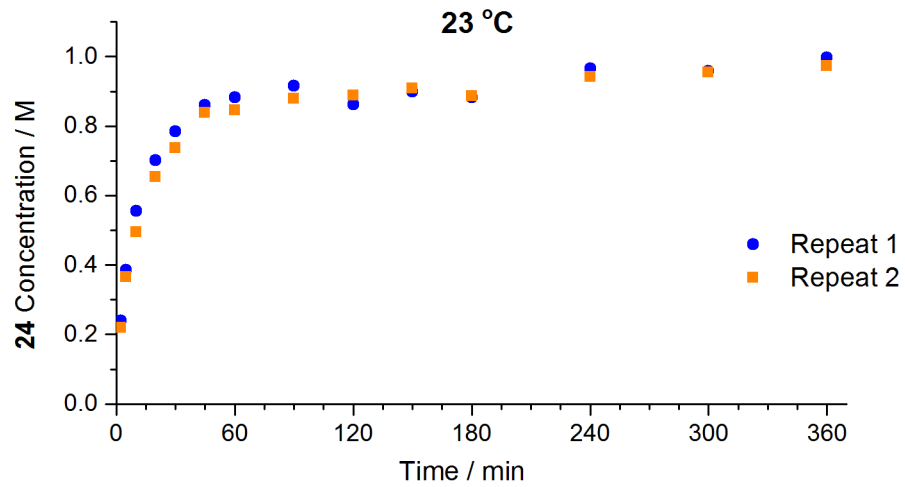
Repeats at 60 °C

Time / min	Repeat 1 24 / M	Repeat 2 24 / M	Standard Deviation	% Error
2.50	0.2533	0.3011	0.0338	13.33
5.00	0.3245	0.4131	0.0627	19.32
10.00	0.3980	0.4736	0.0535	13.44
20.17	0.4612	0.5121	0.0360	7.81
30.00	0.5096	0.5229	0.0094	1.84
45.00	0.5711	0.5861	0.0106	1.86
60.66	0.6216	0.6256	0.0028	0.45
90.83	0.6460	0.7309	0.0600	9.29
120.33	0.6579	0.7255	0.0478	7.26
151.00	0.6675	0.7818	0.0809	12.12
186.00	0.6936	0.7788	0.0603	8.69
241.50	0.7279	0.8214	0.0661	9.08
314.00	0.7725	0.8720	0.0704	9.11
362.66	0.7762	0.8902	0.0806	10.39

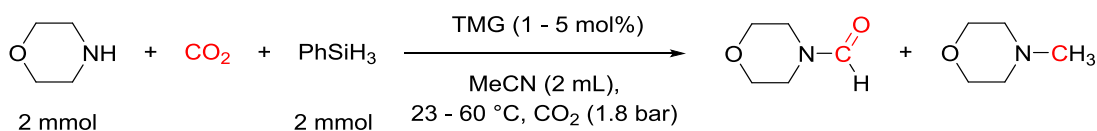


Repeats at 23 °C

Time / min	Repeat 1 24 / M	Repeat 2 24 / M	Standard Deviation	% Error
2.50	0.2398	0.2195	0.0144	6.55
5.00	0.3859	0.3657	0.0142	3.89
10.00	0.5550	0.4941	0.0431	8.72
20.00	0.7011	0.6542	0.0332	5.08
30.00	0.7839	0.7371	0.0331	4.50
45.00	0.8599	0.8381	0.0155	1.84
60.00	0.8826	0.8462	0.0257	3.04
90.00	0.9153	0.8781	0.0263	3.00
120.00	0.8621	0.8875	0.0180	2.02
150.00	0.8983	0.9091	0.0077	0.85
180.00	0.8820	0.8859	0.0027	0.31
240.00	0.9654	0.9424	0.0162	1.72
300.00	0.9588	0.9545	0.0030	0.32
360.00	0.9979	0.9737	0.0171	1.76



7.3.5 Procedure for Reaction Monitoring by *In Situ* IR



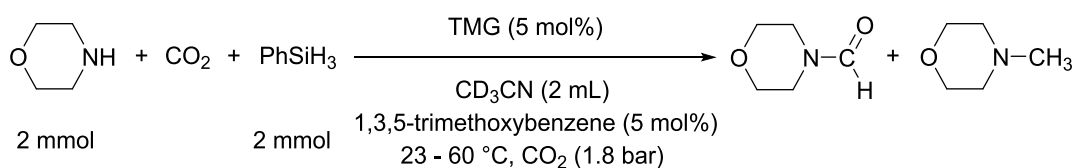
A 50 mL oven dried Schlenk tube and stirrer bar fitted with an IR probe was evacuated and backfilled with CO_2 . A solution of morpholine (175 μL 2 mmol, 1 equiv) and TMG (0.02 - 0.1 mmol, 1 - 5 mol%) in acetonitrile (2 mL) was prepared under a N_2 atmosphere and added to the CO_2 flushed Schlenk tube. The solution was stirred at 1000 rpm at reaction temperature (23 or 60 °C), 1.8 bar CO_2 and monitored by IR for 5 - 15 mins until an equilibrium was reached. Phenylsilane (247 μl , 2 mmol, 1 equiv) was added to commence the reaction.

ATR-IR spectra were collected using a AgX DiComp fiber optic probe connected to a ReactIR 15 system (Mettler Toledo). Spectra were collected every 15-30 s over range of 650 - 2500 cm^{-1} at 8 cm^{-1} resolution. Data analysis was performed using a combination of iC IR 4.3 (Mettler Toledo) or MATLAB software.

Trends are displayed based on the peak height with the solvent (MeCN) background subtracted and displayed relative to the maximum intensity of each trend.

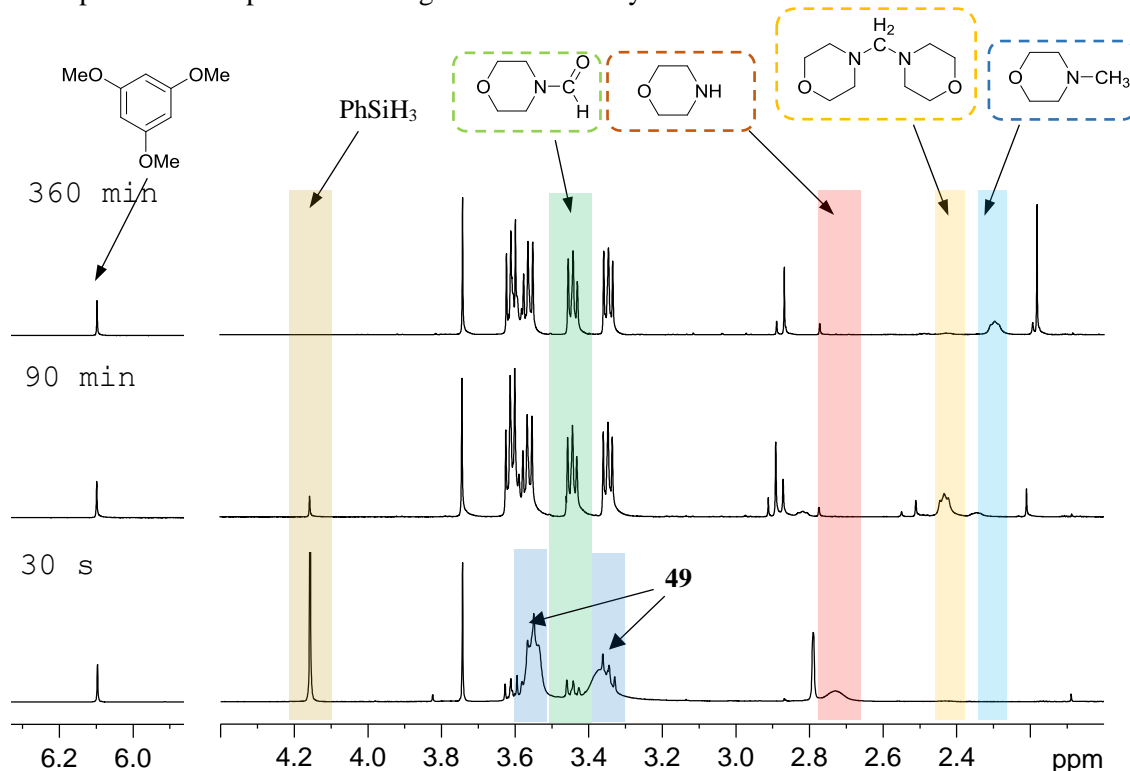


7.3.6 Procedure for Reaction Monitoring by NMR



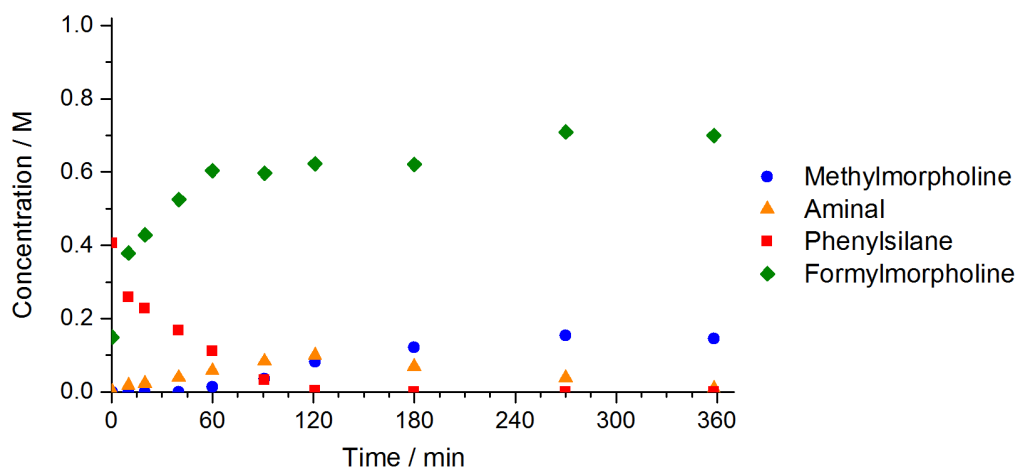
A 50 mL oven dried Schlenk tube and stirrer bar fitted with a subaseal was evacuated and backfilled with CO₂. A solution of morpholine (175 μl, 2 mmol, 1 equiv), 1,3,5-trimethoxybenzene (16.8 mg, 0.1 mmol, 5 mol%) and TMG (12.5 μl, 0.1 mmol, 5 mol%) in CD₃CN (2 mL) was prepared under a N₂ atmosphere and added to the CO₂ flushed Schlenk tube. The solution was stirred at 1000 rpm at 23 / 60 °C, 1.8 bar CO₂, for 15 mins. Phenylsilane (247 μl, 2 mmol, 1 equiv) was added to commence the reaction and kinetic monitoring started. Regular samples were taken and diluted in either CD₃CN or CDCl₃ in a N₂ flushed NMR tube. ¹H NMR spectra were collected and referenced relative to the residual acetonitrile peak at 1.94 ppm.

Example ¹H NMR spectra and assignments used for yield calculation for reaction at 60 °C:



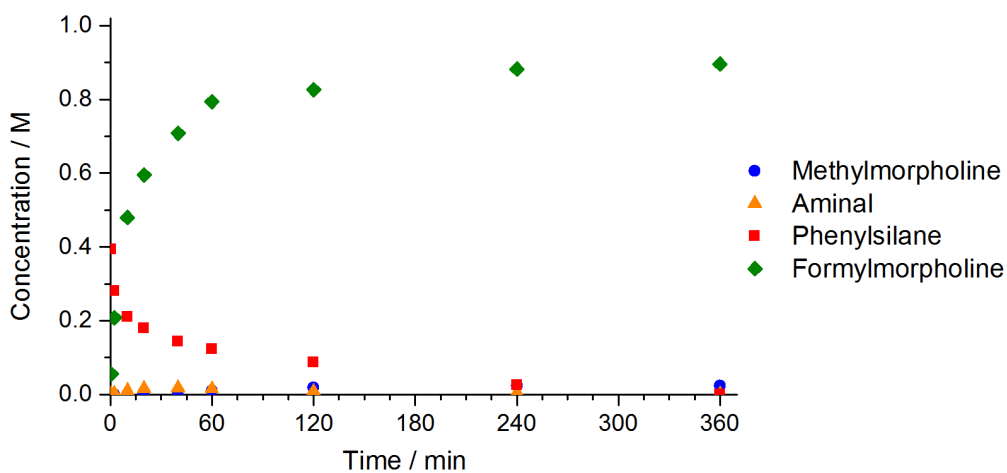
Results for reaction at 60 °C with ¹H NMR monitoring:

Time / min	18 / M	[PhSiH ₃] / M	24 / M	57 / M	48 / M
0.5	0.1876	0.4053	0.1488	0.0000	0.0000
10	0.1125	0.2589	0.3786	0.0168	0.0000
20	0.0857	0.2275	0.4282	0.0226	0.0000
40	0.1170	0.1682	0.5249	0.0388	0.0000
60	0.1160	0.1113	0.6041	0.0575	0.0127
91	0.0000	0.0314	0.5971	0.0835	0.0350
121	0.0000	0.0026	0.6225	0.0990	0.0811
180	0.0000	0.0000	0.6213	0.0688	0.1209
270	0.0000	0.0000	0.7091	0.0379	0.1545
360	0.0000	0.0000	0.7001	0.0088	0.1453

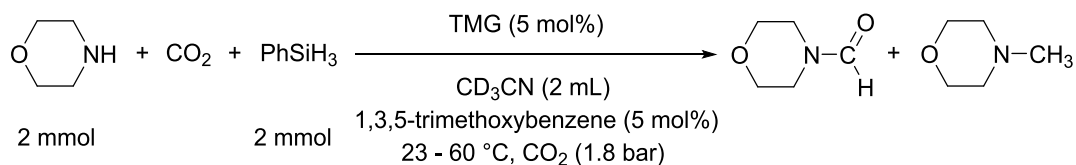


Results for reaction at 23 °C with ¹H NMR monitoring:

Time / min	18 / M	[PhSiH ₃] / M	24 / M	57 / M	48 / M
0.5	0.4173	0.3930	0.0554	0.0000	0.0000
2.5	0.0571	0.2796	0.2083	0.0028	0.0000
10	0.0247	0.2101	0.4794	0.0106	0.0000
20	0.0236	0.1795	0.5953	0.0157	0.0017
40	0.0167	0.1430	0.7084	0.0171	0.0058
60	0.0000	0.1231	0.7940	0.0147	0.0102
120	0.0000	0.0871	0.8268	0.0076	0.0190
240	0.0000	0.0258	0.8821	0.0041	0.0229
360	0.0000	0.0000	0.8959	0.0000	0.0228

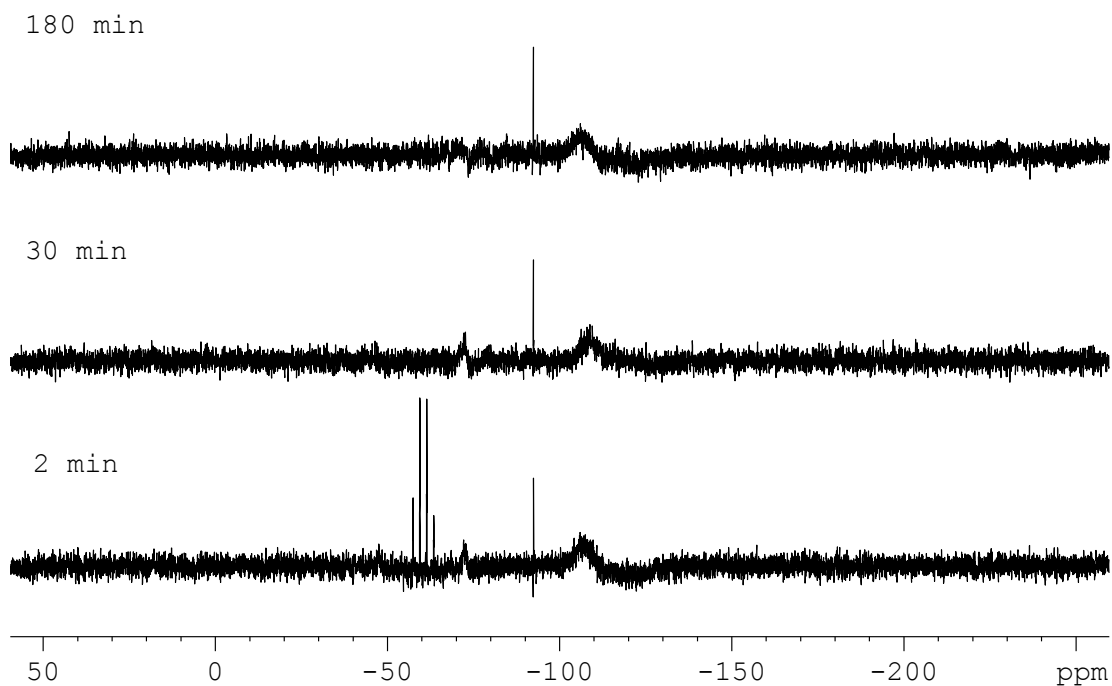


7.3.6.1 Reaction Monitoring by ^{29}Si NMR

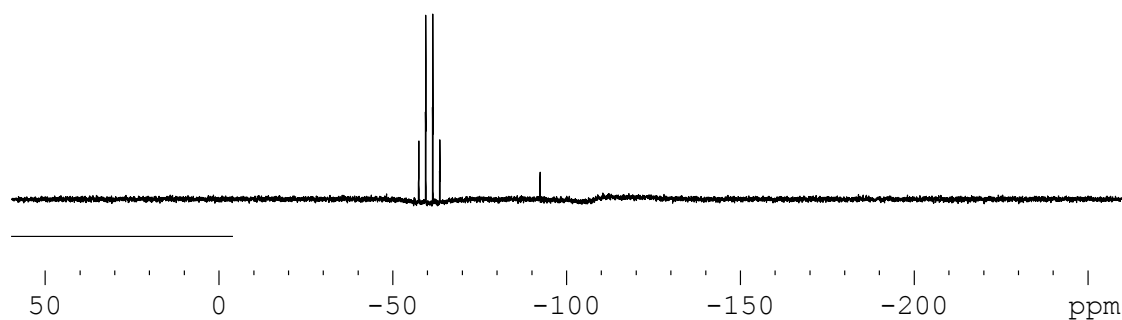


Following the previously described standard reaction procedure, 0.5 mL samples of the reaction were taken into a N₂ flushed NMR tube. Non-decoupled ^{29}Si NMR spectra were collected. Signals at -90 and -105 ppm are due to background signals.

Reaction at 60 °C (CD₃CN, 99.4 MHz):



Phenylsilane spectra:

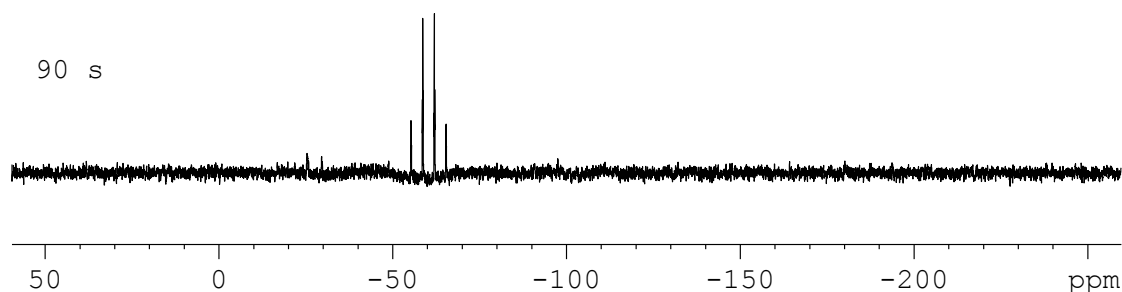


Reaction at 23 °C (CD₃CN, 99.4 MHz):

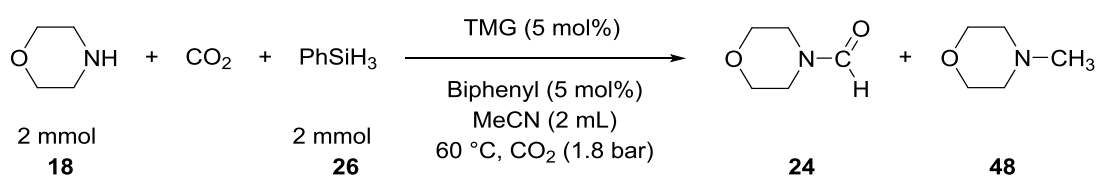
30 min



90 s

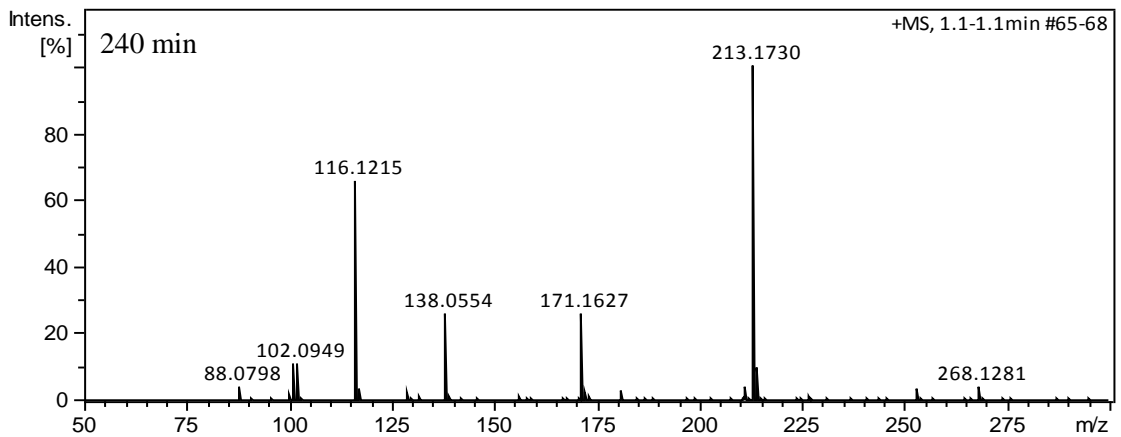
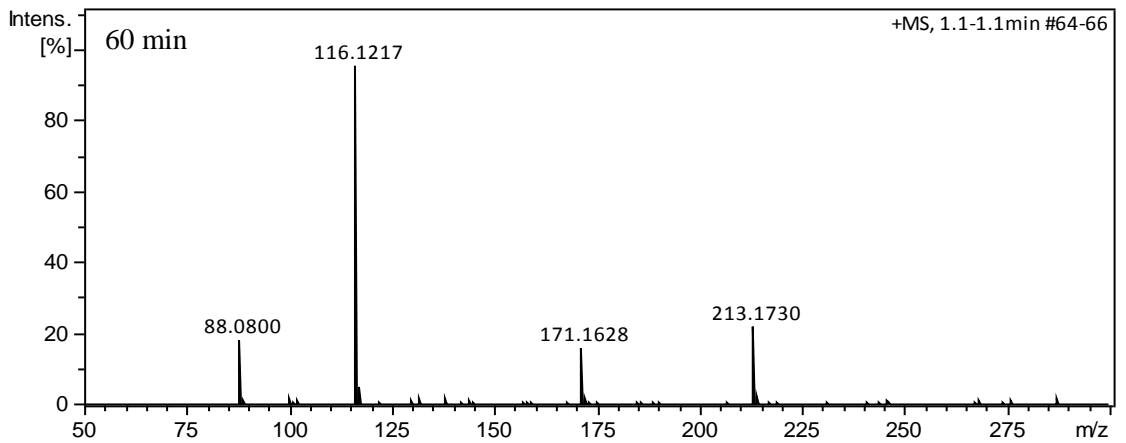
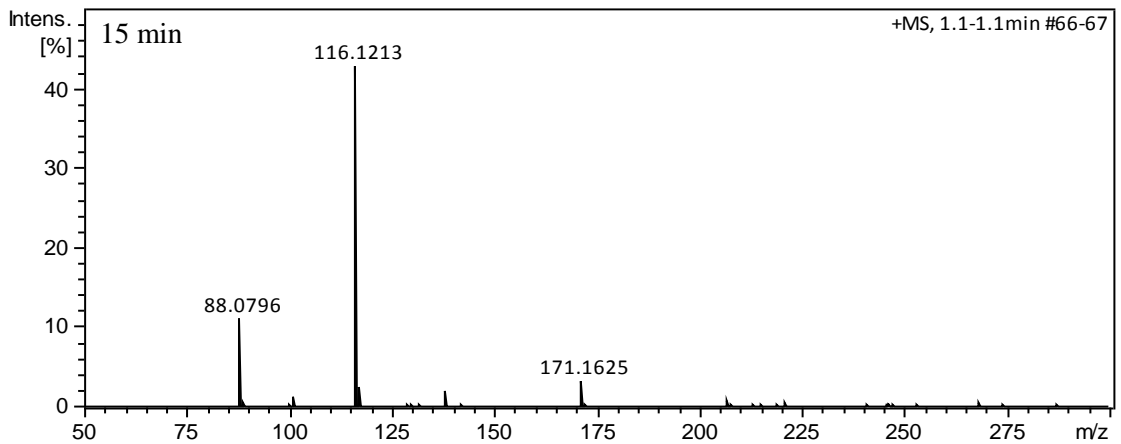
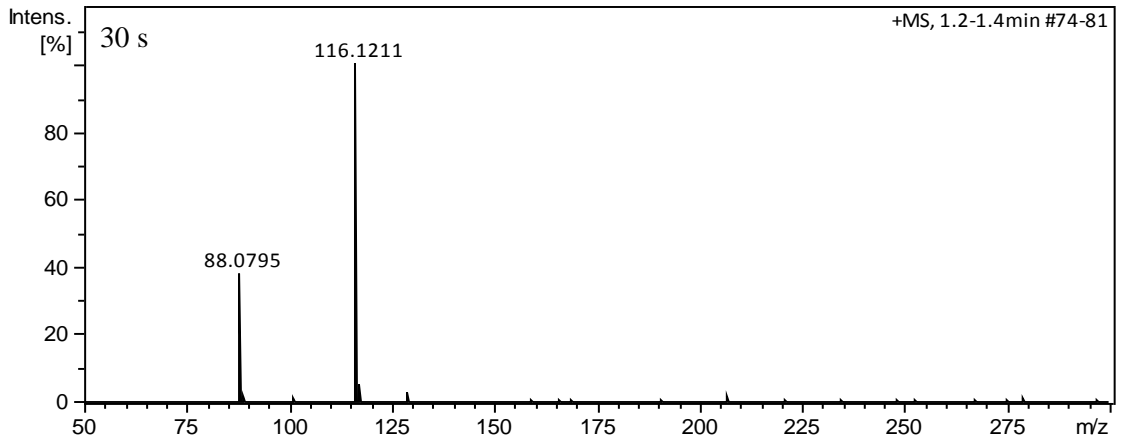


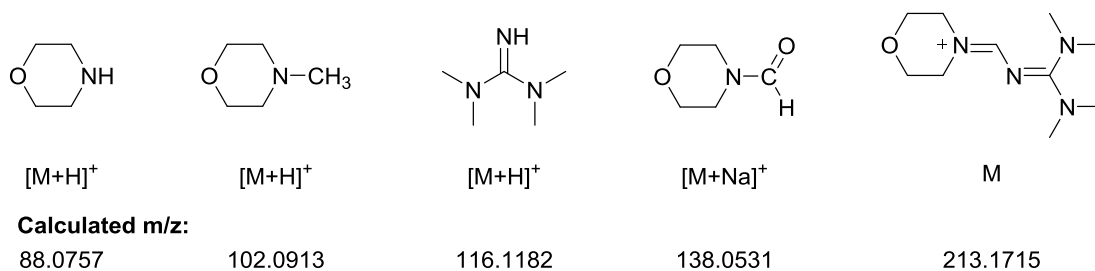
7.3.7 Procedure for Reaction Monitoring by HRMS



A 50 mL oven dried Schlenk tube and stirrer bar fitted with a subseal was evacuated and backfilled with CO₂. A solution of morpholine (175 μ l, 2 mmol, 1 equiv), biphenyl (15.4 mg, 0.1 mmol, 5 mol%) and TMG (0.1 mmol, 5 mol%) in acetonitrile (2 mL) was prepared under a N₂ atmosphere and added to the CO₂ flushed Schlenk tube. The solution was stirred at 1000 rpm at 60 °C, 1.8 bar CO₂, for 15 mins. Phenylsilane (247 μ l, 2 mmol, 1 equiv) was added to commence the reaction and kinetic monitoring started. Regular samples were taken and diluted in methanol for analysis by mass spectrometry on a Bruker maXis impact instrument by Electron Spray Ionisation in positive ionisation mode.

Example results:





7.3.8 Relative Solubility of CO₂ in MeCN at 23 and 60 °C

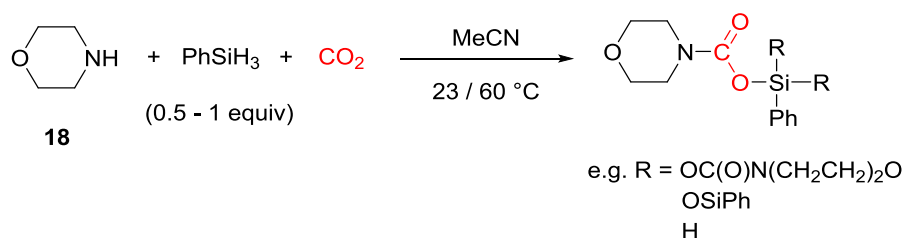
A 50 mL oven dried Schlenk tube and stirrer bar fitted with an IR probe was evacuated and backfilled with N₂. Acetonitrile (2 mL) was added and a vacuum applied for 60 s, following which CO₂ was introduced at 1.8 bar.

ATR-IR spectra were collected using a AgX SiComp fiber optic probe connected to a ReactIR 15 system (Mettler Toledo). Spectra were collected every 15 s over range of 650 - 3000 cm⁻¹ at 8 cm⁻¹ resolution. Data analysis was performed using a combination of iC IR 4.3 (Mettler Toledo) or MATLAB software. The peak height of the CO₂ band at 2342 cm⁻¹ (asymmetric CO₂ stretch) was used to monitor the absorption of CO₂ into solution.

7.3.9 Procedures for Role of Silylcarbamate Intermediate Studies

All IR spectra discussed in this section were collected using an MB3000 FTIR spectrometer (ABB Bomem Inc.) connected to a diamond tip ATR probe. Spectra were collected every 30 s over range of 600 - 1900 cm⁻¹ at 4 cm⁻¹ resolution. Data analysis and processing performed using Horizon MB (ABB Bohem Inc.) and MATLAB.

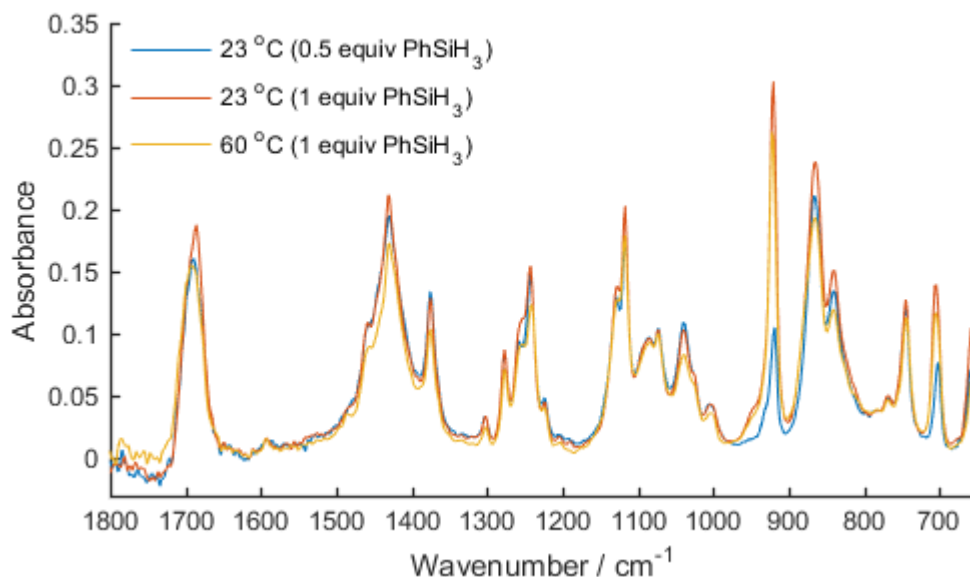
7.3.9.1 Formation kinetics of silylcarbamate by *in situ* IR



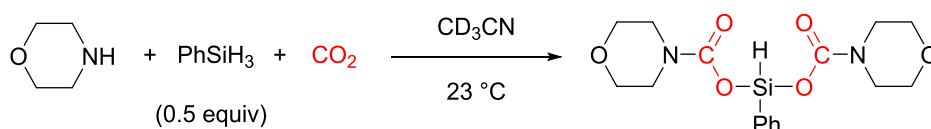
A 75 mL oven dried Schlenk tube and stirrer bar fitted with the IR probe was evacuated and backfilled with CO₂. A solution of morpholine (175 μl, 2 mmol, 1 equiv.), and phenylsilane (1 - 2 mmol, 0.5 - 1 equiv.) in acetonitrile (2 mL) was prepared under a N₂ atmosphere and added

to the CO₂ flushed Schlenk tube. The solution was stirred at 1000 rpm at reaction temperature (23 or 60 °C) at 1.8 bar CO₂ and IR spectra recorded.

FTIR / ATR (1 M in MeCN) (cm⁻¹): 1697 (C=O stretch), 1430 (Si-Ph ring stretch), 1253 (C-O stretch), 1242 (C-O stretch), 866 cm⁻¹ (Si-H and Si-H₂ stretch)



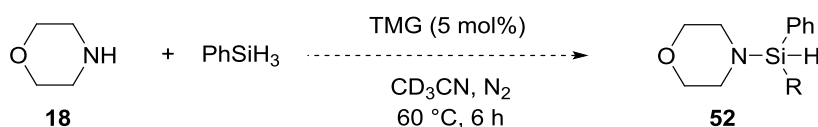
7.3.9.2 Characterisation by NMR



A solution of morpholine (52 μl , 0.6 mmol, 1 equiv), and phenylsilane (37 μl , 0.3 mmol, 0.5 equiv) in CD₃CN (0.6 mL) was prepared under a N₂ atmosphere in a Young's tap NMR tube. Whilst under N₂, the solution was frozen using liq. N₂ and evacuated and backfilled with CO₂ at 1.1 bar for two cycles. The solution was slowly left to warm to RT and regularly shaken to ensure adequate transfer of CO₂ into solution.

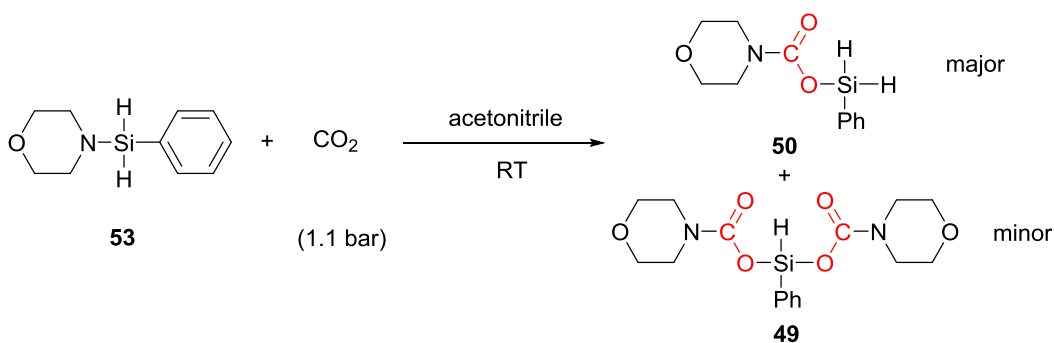
¹H NMR (500 MHz, CD₃CN) δ : 7.87-7.78 (2 H, m, ArH), 7.57-7.44 (3 H, m, ArH), 5.47 (1 H, s, Si-H), 3.62-3.58 (8 H, t, $J = 4.8$ Hz, O(CH₂)₂), 3.45-3.43 (8 H, t, $J = 4.9$ Hz, N(CH₂)₂); ¹³C NMR (126 MHz, CD₃CN) δ 153.8 (NC(O)O), 135.1 (Ar-C), 132.6 (Ar-C), 131.5 (Ar-C), 67.0 (O(CH₂)₂), 45.3 (N(CH₂)₂) (partial assignment due to overlap of signals); ²⁹Si NMR (99 MHz, CD₃CN) δ : -31.18 ppm (td, $J = 281.6, 6.3$ Hz)

7.3.9.3 Reaction under N₂ to probe for silylmorpholine species **52**



A solution of morpholine (53 μl, 0.6 mmol, 1 equiv), phenylsilane (74 μl, 0.3 mmol, 0.5 equiv) and TMG (3.8 μL, 0.03 mmol, 5 mol%) in CD₃CN (0.6 mL) was prepared under a N₂ atmosphere in a Young's tap NMR tube. The solution was heated to 60 °C in an oil bath, and removed briefly to collect NMR spectra at regular intervals.

7.3.9.4 Insertion of CO₂ into phenylsilylmorpholine **53**

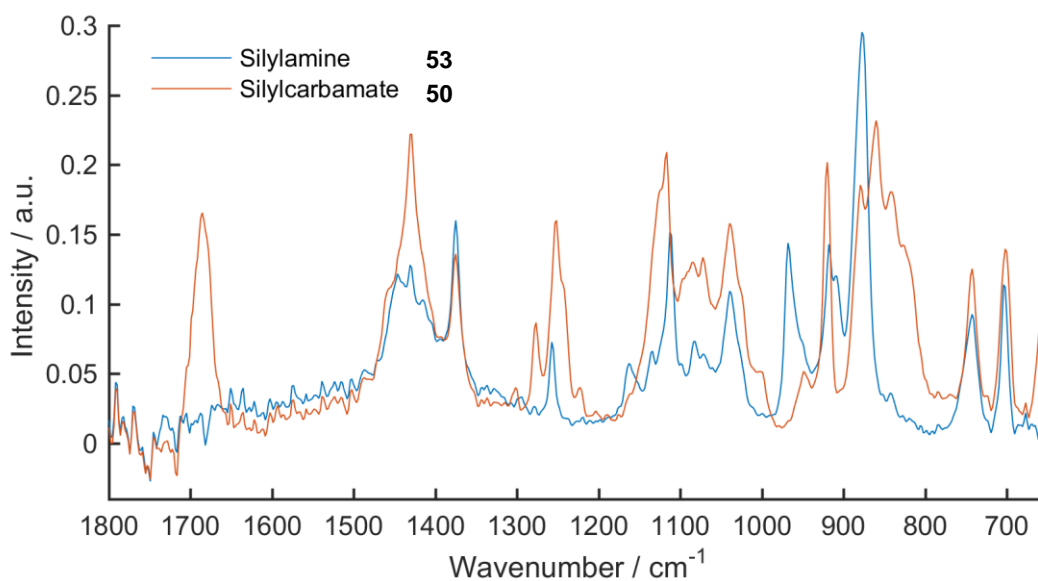


Monitoring by NMR:

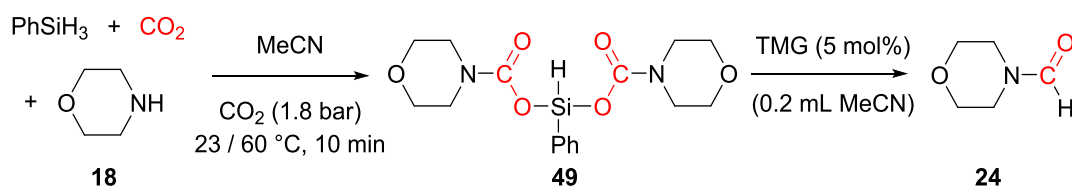
A solution of *N*-phenylsilylmorpholine (116 mg, 0.6 mmol) in CD₃CN (0.6 mL) was prepared under N₂ in a Young's tap NMR tube. The solution was frozen using liq. N₂, evacuated and backfilled with CO₂ at 1.1 bar. The solution was slowly warmed to RT and regularly shaken to ensure adequate transfer of CO₂ into solution.

Monitoring by FT-IR:

A 75 mL oven dried Schlenk tube and stirrer bar fitted with the IR probe was evacuated and backfilled with N₂. A solution of *N*-phenylsilylmorpholine (390 mg, 2 mmol) in MeCN (2 mL) was prepared and added to the Schlenk tube at RT. IR spectra were recorded every 30 s, and the Schlenk tube was flushed with CO₂ for 60 s, and then pressurised to 1.8 bar CO₂. Insertion of CO₂ was complete within 10 minutes.

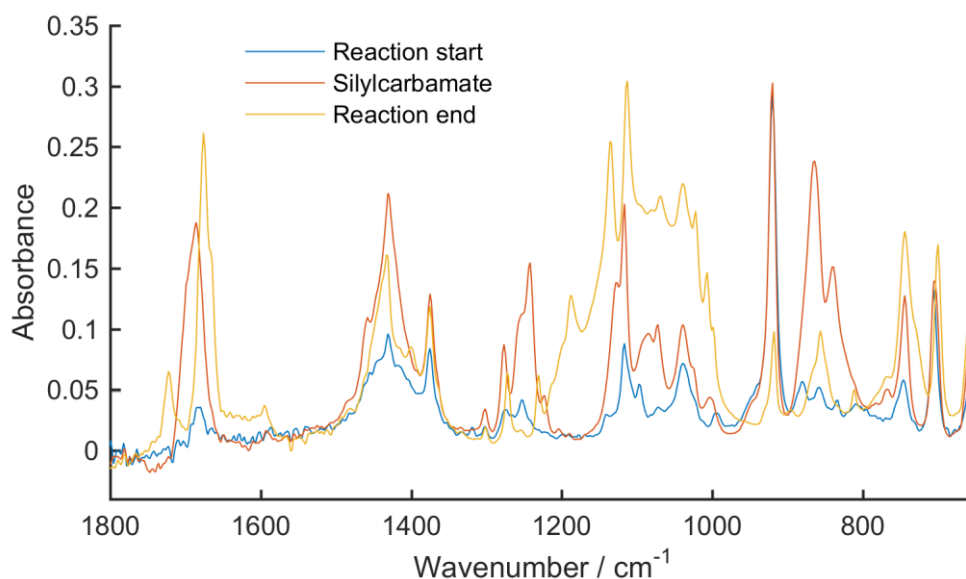


7.3.9.5 Reactivity of Silylcarbamate Intermediate

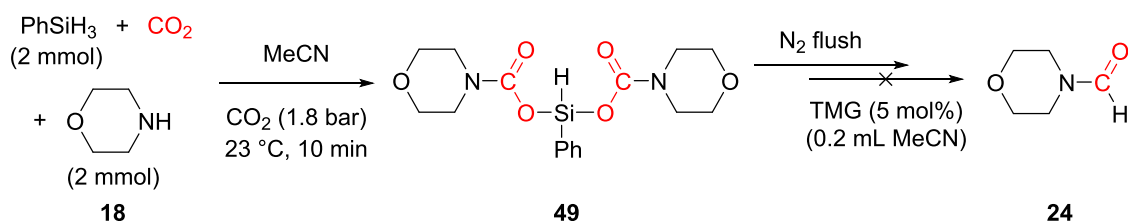


A 75 mL oven dried Schlenk tube and stirrer bar fitted with the IR probe was evacuated and backfilled with CO₂. A solution of morpholine (175 μ l, 2 mmol, 1 equiv.), and phenylsilane (1 – 2 mmol, 0.5 – 1 equiv.) in acetonitrile (2 mL) was prepared under a N₂ atmosphere and added to the CO₂ flushed Schlenk tube. The solution was stirred at 1000 rpm at 23 or 60 $^\circ$ C at 1.8 bar CO₂ for 10 minutes until the silylcarbamate species had formed. After 10 mins a solution of TMG (12.5 μ l, 0.1 mmol, 5 mol%) in acetonitrile (0.2 mL) was added to the reaction and reaction monitored for further 4 – 6 h.

Example IR spectra of reaction at 23 $^\circ$ C at the start of reaction, the silylcarbamate (before TMG addition) and the end of the reaction:



7.3.9.6 Reactivity of silylcarbamate intermediate with TMG after 60 mins N₂ flush:



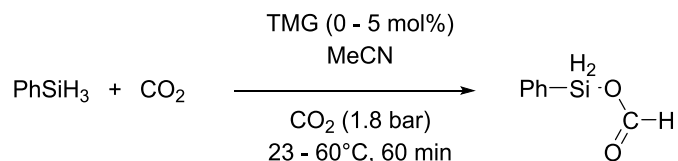
A 75 mL oven dried Schlenk tube and stirrer bar fitted with the IR probe was evacuated and backfilled with CO₂. A solution of morpholine (175 μl , 2 mmol, 1 equiv.), and phenylsilane (247 μl , 2 mmol, 1 equiv.) in acetonitrile (2 mL) was prepared under a N₂ atmosphere and added to the CO₂ flushed Schlenk tube. The solution was stirred at 1000 rpm at 23 or 60 °C at 1.8 bar CO₂ for 10 minutes until the silylcarbamate species had formed. After 10 min the reaction was flushed with N₂ for 60 mins to remove all CO₂ from solution and head space (Removal of CO₂ was monitored by IR band at 660 cm⁻¹ until reached a stable level). Following this, a solution of TMG (12.5 μl , 0.1 mmol, 5 mol%) in acetonitrile (0.2 mL) was added to the reaction and reaction monitored for further 4 h.

7.3.9.7 Reaction of silylcarbamate intermediate with monitoring by GC:

To give accurate conversion data for the reactivity of the silylcarbamate intermediate, the above reactions were repeated with sampling for GC analysis. Conversions calculated relative to internal standard of biphenyl (5 mol%) using methods describe in Section 7.3.4.

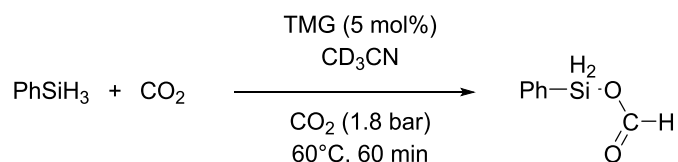
7.3.10 Procedures for Role of Formoxsilane Intermediate Studies

7.3.10.1 Monitoring reduction of CO₂ with PhSiH₃ by *in situ* FT-IR



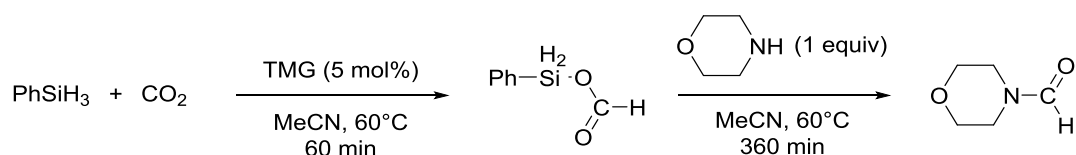
A 75 mL oven dried Schlenk tube and stirrer bar fitted with the IR probe was evacuated and backfilled with CO₂. A solution of TMG (0 - 0.1 mmol, 0 - 5 mol%) in acetonitrile (2 mL) was prepared under a N₂ atmosphere and added to the CO₂ flushed Schlenk tube. The solution was stirred at 1000 rpm at 23 or 60 °C at 1.8 bar CO₂ for 15 minutes to allow for temperature equilibration. Phenylsilane (247 μl, 2 mmol, 1 equiv) was added and spectra collected every 30 s for a further 60 mins.

7.3.10.2 Monitoring reduction of CO₂ with PhSiH₃ by ¹H NMR



A 50 mL oven dried Schlenk tube and stirrer bar fitted with a suba seal was evacuated and backfilled with CO₂. A solution of TMG (12.5 μl, 0.1 mmol, 5 mol%) and 1,3,5-trimethoxybenzene (16.8 mg, 0.1 mol, 5 mol%) in acetonitrile (2 mL) was prepared under a N₂ atmosphere and added to the CO₂ flushed Schlenk tube. The solution was stirred at 1000 rpm at 23 or 60 °C at 1.8 bar CO₂ for 15 minutes to allow for temperature equilibration. Phenylsilane (247 μl, 2 mmol, 1 equiv) was added and regular samples (0.1 mL) taken and diluted in CDCl₃ (0.5 mL) for ¹H & ¹³C NMR analysis.

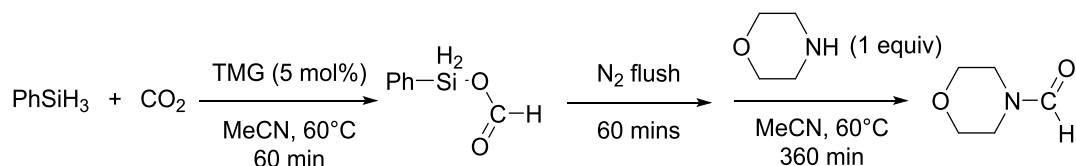
7.3.10.3 Monitoring addition of morpholine to product of reduction between CO₂ and PhSiH₃ by FT-IR



A 75 mL oven dried Schlenk tube and stirrer bar fitted with the IR probe was evacuated and backfilled with CO₂. A solution of TMG (12.5 μl, 0.1 mmol, 5 mol%) in acetonitrile (2 mL) was prepared under a N₂ atmosphere and added to the CO₂ flushed Schlenk tube. The solution was stirred at 1000 rpm at 60 °C at 1.8 bar CO₂ for 15 minutes to allow for temperature equilibration. Phenylsilane (247 μl, 2 mmol, 1 equiv) was added and spectra collected every 30

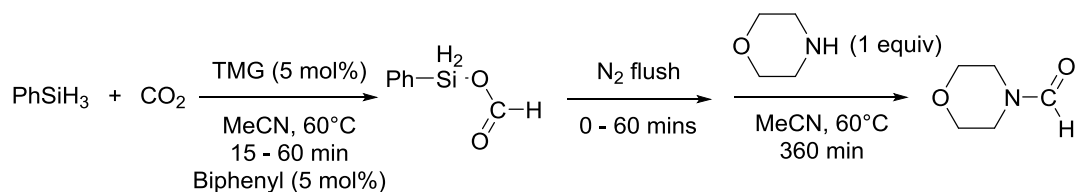
s for a further 60 mins. After 60 mins morpholine (175 μ l, 2 mmol, 1 equiv) in MeCN (0.2 mL) was added to the reaction.

7.3.10.4 Monitoring addition of morpholine to product of reduction between CO₂ and PhSiH₃ by FT-IR



A 75 mL oven dried Schlenk tube and stirrer bar fitted with the IR probe was evacuated and backfilled with CO₂. A solution of TMG (12.5 μ l, 0.1 mmol, 5 mol%) in acetonitrile (2 mL) was prepared under a N₂ atmosphere and added to the CO₂ flushed Schlenk tube. The solution was stirred at 1000 rpm at 60 °C at 1.8 bar CO₂ for 15 minutes to allow for temperature equilibration. Phenylsilane (247 μ l, 2 mmol, 1 equiv) was added and spectra collected every 30 s for a further 60 mins. After 60 min the reaction was flushed with N₂ for 60 mins to remove all CO₂ from solution and head space (Removal of CO₂ was monitored by IR band at 660 cm⁻¹ until reached a stable level). Following this, a solution of morpholine (175 μ l, 2 mmol, 1 equiv) in MeCN (0.2 mL) was added to the reaction.

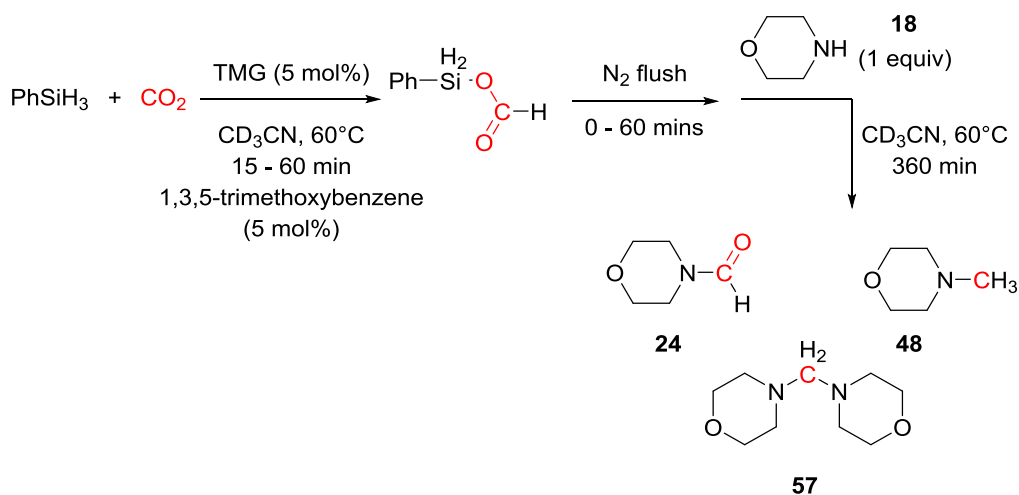
7.3.10.5 Monitoring addition of morpholine to product of reduction between CO₂ and PhSiH₃ by GC



To give accurate rate of conversion for addition of morpholine to the formoxysilane intermediate, the above reactions were repeated with sampling for GC analysis. Conversions were calculated relative to internal standard of biphenyl (5 mol%) using method describe in Section 7.3.4.

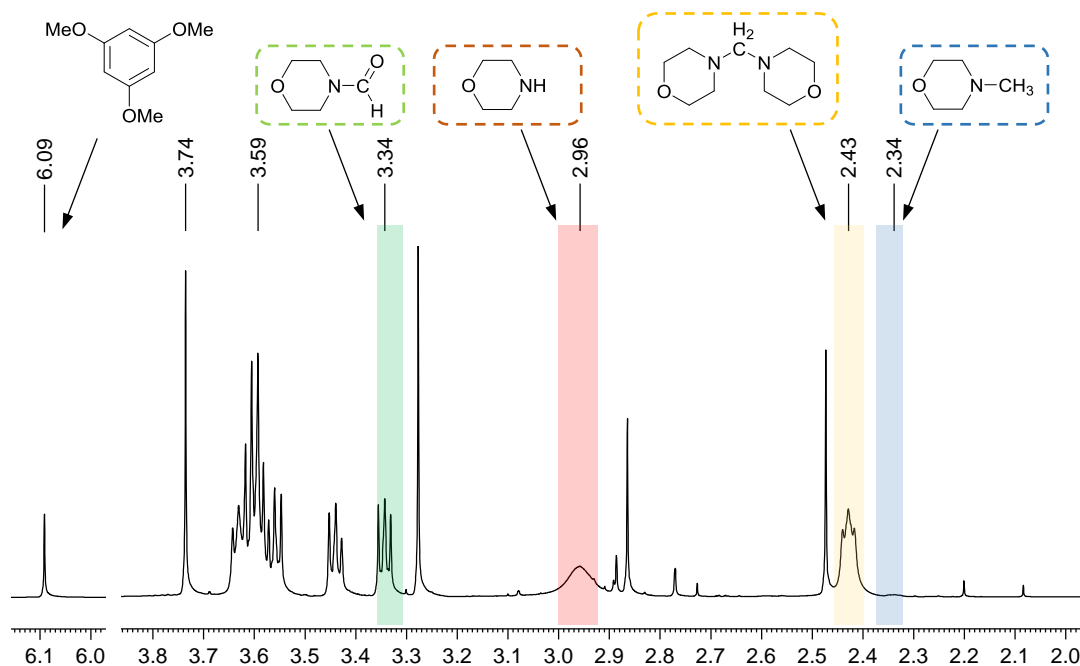
7.3.10.6 Monitoring addition of morpholine to product of reduction between CO₂ and PhSiH₃ by NMR

Monitoring the reaction by GC and IR did not enable accurate conversion of the aminoral **57** species, thus reactions were repeated using the procedure described above in CD₃CN with monitoring by ¹H NMR.



Entry	Time / min	% Conversion			
		18	24	48	57
1	15	0	75	1	24
2	60	28	38	1	32
3*	60 + N ₂ flush	51	26	0	23

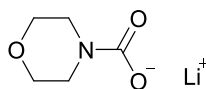
Example ¹H NMR spectra for product ratio determination:



The peaks highlighted represent those used for conversion calculation relative to integration of the internal standard, 1,3,5-trimethoxybenzene. The multiplet at 3.59 ppm represents an overlap of all four morpholine products (CH₂), in cases where the morpholine peak at 2.96 ppm overlapped with other reaction components, the integration of the morpholine signal was determined from the integration of the multiplet at 3.59 ppm with the other morpholine species subtracted from it.

7.3.11 Role of Morpholinium Carbamate 19 & 20

7.3.11.1 Preparation Lithium Morpholine Carbamate 58



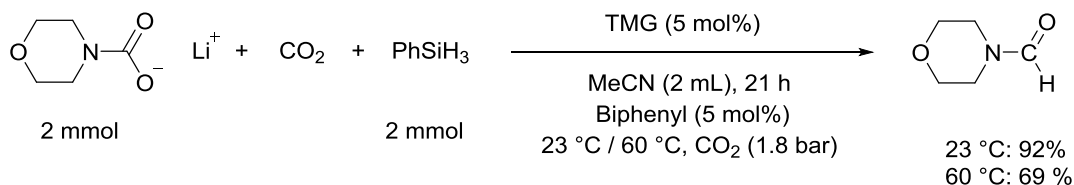
Prepared using a modified procedure.¹³⁷ A solution of morpholine (1.75 mL, 20 mmol, 1 equiv) in anhydrous, degassed diethylether was cooled to $-78\text{ }^{\circ}\text{C}$ and *n*-BuLi (13.3 mL, 1.5 M in hexanes, 20 mmol, 1 equiv) added dropwise over 15 mins. The solution was stirred for 60 mins and slowly warmed to RT. After cooling back to $-78\text{ }^{\circ}\text{C}$, CO_2 was introduced via a balloon and stirred for 2 h before slowly warming to RT. The solvent was removed by cannula filtration and the white solid washed with hexane ($3 \times 15\text{ mL}$) and dried under vacuum to give a white solid (1.84 g, 67 %).

FTIR / ATR (cm^{-1}): 2960, 2896, 2855, 1554 (NCO_2), 1473, 1424, 1302, 1279, 1111, 811, 608, 567. Poor solubility prevented characterisation by NMR.

Literature for sodium morpholine carbamate:²²⁵ IR frequencies: 1570, 1432, 1280, 810 cm^{-1}

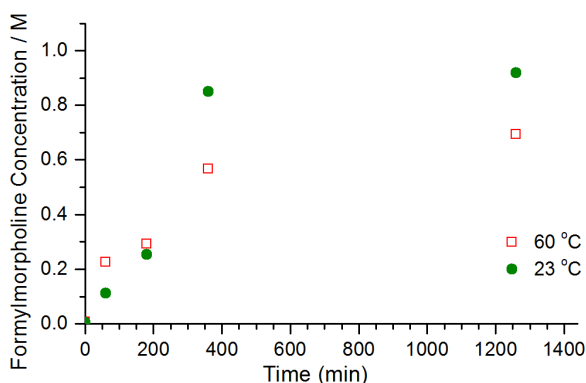
7.3.11.2 Procedure for reaction of Lithium morpholine carbamate 58

Reaction under CO_2 :

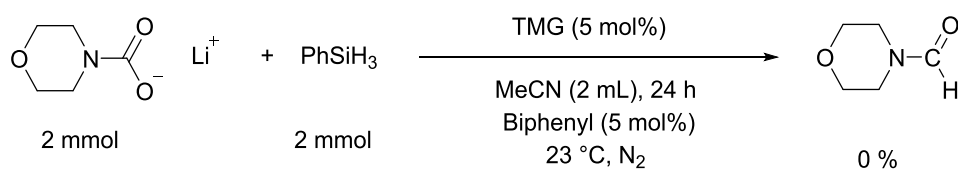


Lithium morpholine carbamate (274 mg, 2 mmol, 1 equiv) was added to a 50 mL oven dried Schlenk tube and stirrer bar which was evacuated and backfilled with CO_2 . A solution of biphenyl (15.4 mg, 0.1 mmol, 5 mol%) and TMG (12.5 μl , 0.1 mmol, 5 mol%) in acetonitrile (2 mL) was prepared under a N_2 atmosphere and added to the CO_2 flushed Schlenk tube. The solution was stirred at 1000 rpm at $23\text{ }^{\circ}\text{C}$ or $60\text{ }^{\circ}\text{C}$, 1.8 bar CO_2 , for 15 mins. Phenylsilane (247 μl , 2 mmol, 1 equiv) was added to commence the reaction. Regular samples were taken and filtered for analysis by GC. After 21 h the solvent was removed under vacuum for further confirmation by NMR.

Time / min	Formylmorpholine / M	
	23 °C	60 °C
1	0.0043	0.0077
60	0.1111	0.2263
180	0.2538	0.2928
360	0.8490	0.5673
1260	0.9181	0.6922

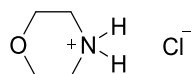


Under N₂ atmosphere:



Lithium morpholine carbamate (274 mg, 2 mmol, 1 equiv) was added to a 50 mL oven dried Schlenk tube and stirrer bar which was evacuated and refilled with N₂. A solution of biphenyl (15.4 mg, 0.1 mmol, 5 mol%) and TMG (12.5 μl, 0.1 mmol, 5 mol%) in acetonitrile (2 mL) was prepared under a N₂ atmosphere and added to the CO₂ flushed Schlenk tube. The solution was stirred at 1000 rpm at 23 °C for 15 mins. Phenylsilane (247 μl, 2 mmol, 1 equiv) was added to commence the reaction. After stirring for 24 h at 23 °C, the reaction was filtered for analysis by GC and solvent removed under vacuum for further confirmation by NMR.

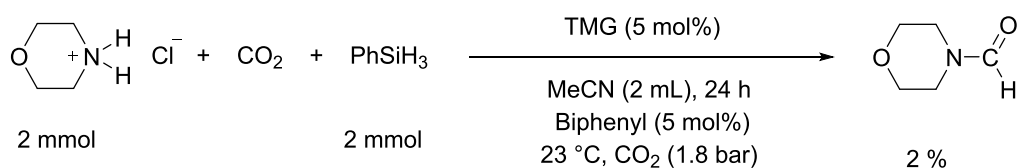
7.3.11.3 Preparation of Morpholinium Hydrochloride **59**



Prepared following a procedure reported by List.¹³⁸ Hydrogen chloride in diethyl ether (1.1 mL, 2 M, 2.2 mmol, 1.1 equiv.) was added dropwise to a solution of morpholine (175 μL, 2 mmol, 1 equiv) in diethylether (4 mL) at 0 °C and stirred at RT for 1 h yielding a white precipitate. The solvent was removed by cannula filtration and the white solid washed with diethylether (3 × 4 mL) and pentane (2 × 4 mL) and dried under vacuum to give a white solid (207 mg, 84 %).

¹H NMR (400 MHz, (CD₃)₂SO) δ: 9.56 (2H, s, ⁺NH₂), 3.79 (4H, t, *J* = 4.9 Hz, (CH₂)₂O), 3.05 (4H, t, *J* = 4.9 Hz, (CH₂)₂N); ¹³C NMR (101 MHz, (CD₃)₂SO) δ: 63.1 ((CH₂)₂O), 42.6 ((CH₂)₂N). Spectral data are consistent with the literature.¹³⁸

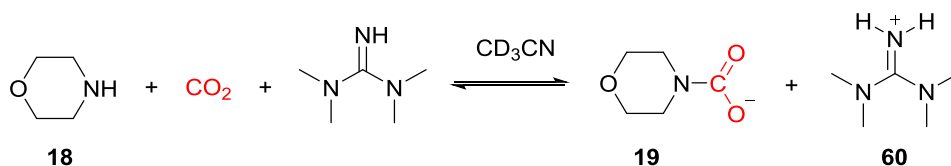
7.3.11.4 Procedure for reaction of Morpholinium Hydrochloride **59**



Morpholinium hydrochloride (2 mmol) was prepared in situ in a 50 mL oven dried Schlenk tube and stirrer bar, evacuated and backfilled with CO_2 . A solution of biphenyl (15.4 mg, 0.1 mmol, 5 mol%) and TMG (12.5 μl , 0.1 mmol, 5 mol%) in acetonitrile (2 mL) was prepared under a N_2 atmosphere and added to the CO_2 flushed Schlenk tube. The solution was stirred at 1000 rpm at 23 $^\circ\text{C}$, 1.8 bar CO_2 , for 15 mins. Phenylsilane (247 μl , 2 mmol, 1 equiv) was added to commence the reaction. After stirring for 24 h at RT, the reaction was analysed by GC and solvent removed under vacuum for further confirmation by NMR.

7.3.12 Role of TMG Studies

7.3.12.1 Stoichiometric reaction of Morpholine + TMG + CO_2



A solution of morpholine (26 μl , 0.3 mmol, 1 equiv), and 1,1,3,3-tetramethylguanidine (38 μl , 0.3 mmol, 1 equiv) in CD_3CN (0.6 mL) was prepared under a N_2 atmosphere in a Young's tap NMR tube. Whilst under N_2 , the solution was frozen using liq. N_2 and evacuated and backfilled with CO_2 at 1.1 bar for two cycles. The solution was slowly left to warm to RT and regularly shaken to ensure adequate transfer of CO_2 into solution.

^1H NMR (500 MHz, CD_3CN) δ : 9.71 (2H, s, $^+\text{NH}_2$), 3.48 (4H, t, $J = 4.8$ Hz, $\text{O}(\text{CH}_2)_2$), 3.27 (4H, t, $J = 4.8$ Hz, $\text{N}(\text{CH}_2)_2$), 2.88 (12H, s, $\text{N}(\text{CH}_3)_2$); ^{13}C NMR (126 MHz, CD_3CN) δ : 163.8, 162.4, 67.9 ($\text{O}(\text{CH}_2)_2$), 45.7 ($\text{N}(\text{CH}_2)_2$), 40.0 ($\text{N}(\text{CH}_3)_2$).

7.3.12.2 Role of TMG in activation of CO_2

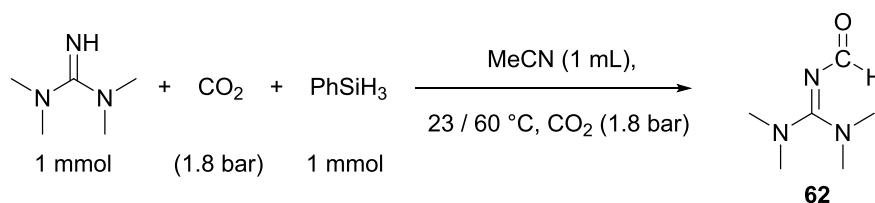
A 75 mL oven dried Schlenk tube and stirrer bar fitted with the IR probe was evacuated and backfilled with N_2 . A solution of 1,1,3,3-tetramethylguanidine (250 μl , 2 mmol) in MeCN (2 mL) was prepared and added to the Schlenk tube at RT. IR spectra were recorded every 30 s, and the Schlenk tube was flushed with CO_2 for 60 s, and then pressurised to 1.8 bar CO_2 .

7.3.12.3 Role of TMG in activation of phenylsilane

A solution of phenylsilane (62 μ l, 0.5 mmol, 1 equiv), in CD_3CN (0.6 mL) was prepared under a N_2 atmosphere in a Young's tap NMR tube. NMR spectra were recorded and 1,1,3,3-tetramethylguanidine (63 μ l, 0.5 mmol, 1 equiv) was then added to NMR tube and NMR spectra measured.

7.3.13 Stoichiometric Catalyst Deactivation Studies

7.3.13.1 Stoichiometric reaction of TMG with PhSiH_3 and CO_2



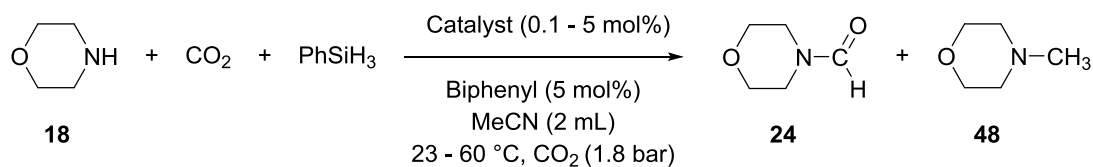
An oven dried Schlenk tube and stirrer bar fitted with a subseal was evacuated and backfilled with CO_2 . A solution of TMG (126 μ l, 1 mmol, 1 equiv) and biphenyl (7.9 mg, 0.05 mmol, 5 mol%) in acetonitrile (2 mL) was prepared under a N_2 atmosphere and added to the Schlenk tube. The solution was stirred at 1000 rpm at $23 / 60^\circ\text{C}$, 1.8 bar CO_2 , for 15 mins. Phenylsilane (124 μ l, 1 mmol, 1 equiv) was added to commence the reaction and continued for 120 mins. Regular samples were taken and diluted in methanol for analysis by MS. After completion, the solvent was removed under vacuum, and analysed by NMR spectroscopy. The same reaction procedure was also used to monitor the reaction with *in situ* IR.

Two species were observed in the ^1H and ^{13}C NMR species in approximate ratio 1:0.3.

Dominant species: ^1H NMR (400 MHz, CDCl_3) δ : 8.46 (1 H, s, CHO), 2.90 (12 H, s, $\text{N}(\text{CH}_3)_2$); ^{13}C NMR (101 MHz, CDCl_3) δ : 170.1 (CHO), 163.0 (C=N), 40.5 ($\text{N}(\text{CH}_3)_2$); HRMS (ESI): $[\text{M}+\text{H}]^+$ m/z = found 144.1189. Calculated: 144.1131. FTIR / ATR (in MeCN) ν = 1664 (C=O), 1609 (C=N) cm^{-1} . Spectral data are consistent with the literature.¹⁴⁴

7.3.14 Evaluating Catalytic Activity of Alkylated Catalysts

7.3.14.1 General procedure:



A 50 mL oven dried Schlenk tube and stirrer bar fitted with a subseal was evacuated and backfilled with CO₂. A solution of morpholine (175 μ l, 2 mmol, 1 equiv), biphenyl (15.4 mg, 0.1 mmol, 5 mol%) and guanidine catalyst (0.002 - 0.1 mmol, 0.1 - 5 mol%) in acetonitrile (2 mL) was prepared under a N₂ atmosphere and added to the CO₂ flushed Schlenk tube. The solution was stirred at 1000 rpm at 23 / 60 °C, 1.8 bar CO₂, for 15 mins. Phenylsilane (247 μ l, 2 mmol, 1 equiv) was added to commence the reaction and regular samples (approx. 0.02 mL) were taken for analysis by GC.

Yields are given relative to the amine substrate and determined by GC analysis relative to biphenyl as an internal standard using the method described in Section 7.3.4. For reactions which resulted in aminal **57** the yield of **57** was determined by ¹H NMR.

Entry	18 (mmol)	PhSiH ₃ (mmol)	Catalyst	Catalyst loading (mol%)	Temp (°C)	CO ₂ Pressure (bar)
1	2	2	Butyl TMG	5	60	1.8
2	2	2	Butyl TMG	5	23	1.8
3	2	2	Butyl TMG	1	60	1.8
4	2	2	Butyl TMG	1	23	1.8
5	2	2	Butyl TMG	0.1	23	1.8
6*	2	2	Butyl TMG	5	23	1.8
7	2	2	Methyl TMG	5	60	1.8
8	2	2	Methyl TMG	5	23	1.8
9	2	2	Methyl TMG	1	23	1.8

* With 40 mol% water present

7.3.14.2 Kinetic data:

Entry 1			
Time / min	18 / M	24 / M	48 / M
0.00	1.0007	0.0000	0.0000
0.33	0.7931	0.1133	0.0000
2.67	0.0000	0.4881	0.0078
5.08	0.0000	0.5861	0.0316
10.17	0.0000	0.5917	0.0395
20.17	0.0000	0.6268	0.0913
40.17	0.0000	0.6770	0.1382
60.33	0.0000	0.7104	0.1620
90.33	0.0000	0.7155	0.1615
120.17	0.0000	0.7262	0.1723
151.00	0.0000	0.7333	0.1769
184.83	0.0000	0.7337	0.1717
250.67	0.0000	0.7309	0.1766
305.75	0.0000	0.7278	0.1888
360.00	0.0000	0.7218	0.1883

Entry 2			
Time / min	18 / M	24 / M	48 / M
0.00	0.9934	0.0000	0.0000
0.30	0.9470	0.0208	0.0000
2.50	0.5659	0.3478	0.0000
5.00	0.4531	0.4882	0.0027
10.00	0.0000	0.6252	0.0049
15.00	0.0000	0.6935	0.0079
20.00	0.0000	0.7556	0.0109
30.00	0.1898	0.7853	0.0144
45.00	0.0000	0.8710	0.0236
60.00	0.0000	0.9119	0.0311
90.00	0.0000	0.9248	0.0409
120.00	0.0000	0.9624	0.0428
150.00	0.0000	0.9590	0.0476
180.00	0.0000	0.9752	0.0542
240.00	0.0000	0.9309	0.0523
300.00	0.0000	0.9893	0.0487
360.00	0.0000	0.9924	0.0575
480.00	0.0000	1.0080	0.0575

Entry 3			
Time / min	18 / M	24 / M	48 / M
0.00	0.9376	0.0000	0.0000
0.50	0.8951	0.0727	0.0000
2.50	0.5334	0.3755	0.0000
5.33	0.4750	0.5012	0.0016
10.00	0.3979	0.5218	0.0040
15.00	0.3917	0.5380	0.0054
20.00	0.3558	0.5695	0.0061
30.00	0.3879	0.5512	0.0091
45.00	0.3579	0.5848	0.0118
60.00	0.3386	0.5977	0.0161
90.00	0.2837	0.6500	0.0245
120.00	0.2577	0.6525	0.0286
150.00	0.2221	0.6905	0.0336
180.00	0.2303	0.7086	0.0385
240.00	0.1863	0.7159	0.0433
300.00	0.1770	0.7553	0.0479
360.00	0.2239	0.7019	0.0541
480.00	0.1192	0.8046	0.0598

Entry 4			
Time / min	18 / M	24 / M	48 / M
0.00	1.0941	0.0000	0.0000
0.30	0.9728	0.0101	0.0000
2.50	0.7106	0.1639	0.0000
5.25	0.7435	0.2820	0.0000
10.08	0.5578	0.3629	0.0000
15.00	0.0000	0.4192	0.0000
20.18	0.4815	0.4404	0.0000
30.00	0.4271	0.5489	0.0000
45.00	0.3753	0.6295	0.0054
60.00	0.3722	0.6123	0.0000
90.00	0.3147	0.7001	0.0175
120.00	0.2527	0.7546	0.0314
150.18	0.0000	0.9216	0.0345
180.50	0.0000	0.9060	0.0448
240.33	0.0000	0.9652	0.0532
314.00	0.0000	0.9783	0.0608
361.75	0.0000	0.9858	0.0657
482.58	0.0000	1.0073	0.0681

Entry 5			
Time / min	18 / M	24 / M	48 / M
0.00	0.7973	0.0000	0.0000
0.30	0.9345	0.0083	0.0000
5.00	0.8889	0.0525	0.0000
10.00	0.8624	0.0926	0.0000
20.00	0.8443	0.1392	0.0000
40.00	0.8198	0.1766	0.0000
60.00	0.7744	0.2150	0.0000
90.00	0.7542	0.2503	0.0000
120.00	0.7138	0.2583	0.0000
180.00	0.6945	0.2830	0.0000
240.00	0.6543	0.3317	0.0000
300.00	0.6157	0.3587	0.0000
360.00	0.5539	0.4208	0.0000
540.00	0.4534	0.5478	0.0060
1440.0	0.1732	0.8233	0.0266
1800.0	0.1656	0.8143	0.0425
2880.0	0.0000	0.8829	0.0723

Entry 6			
Time / min	18 / M	24 / M	48 / M
0.00	0.8488	0.0000	0.0000
0.33	0.9313	0.0000	0.0000
2.50	0.6782	0.2571	0.0000
5.00	0.5686	0.3422	0.0000
10.18	0.4530	0.4385	0.0000
20.00	0.3936	0.5263	0.0000
40.50	0.0000	0.6106	0.0000
60.50	0.0000	0.6564	0.0000
90.00	0.2347	0.7094	0.0000
122.75	0.2236	0.7437	0.0000
180.00	0.0000	0.7329	0.0000
285.00	0.0000	0.8294	0.0000

Entry 7			
Time / min	18 / M	24 / M	48 / M
0.00	0.9921	0.0000	0.0046
0.58	0.7278	0.1562	0.0047
2.83	0.4135	0.4915	0.0027
5.08	0.3165	0.5814	0.0088
10.18	0.0000	0.6486	0.0129
20.25	0.0000	0.6651	0.0177
40.92	0.0000	0.7118	0.0242
60.00	0.0000	0.7421	0.0341
90.08	0.0000	0.7453	0.0426
120.00	0.0000	0.7549	0.0461
150.00	0.0000	0.7607	0.0521
182.00	0.0000	0.7646	0.0485
248.08	0.0000	0.7559	0.0566
302.00	0.0000	0.7594	0.0544
360.00	0.0000	0.7565	0.0548

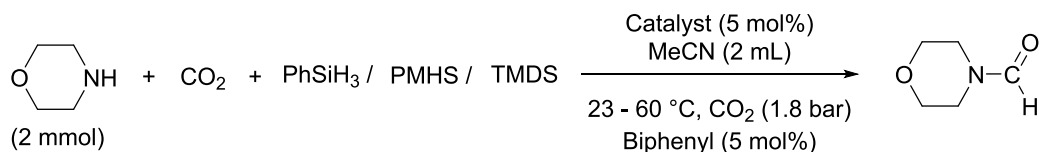
Entry 8			
Time / min	18 / M	24 / M	48 / M
0.00	0.9961	0.0000	0.0000
0.33	0.8166	0.0116	0.0000
2.50	0.5637	0.3313	0.0000
5.08	0.4779	0.4551	0.0000
10.00	0.3261	0.6213	0.0046
15.17	0.2651	0.6913	0.0064
20.00	0.2269	0.7339	0.0103
30.00	0.0000	0.8134	0.0153
45.08	0.0000	0.8656	0.0199
60.00	0.0000	0.8782	0.0249
90.00	0.0000	0.9258	0.0374
120.00	0.0000	0.9372	0.0449
149.83	0.0000	0.9575	0.0468
179.18	0.0000	0.9946	0.0573
240.00	0.0000	0.9819	0.0526
360.00	0.0000	0.9956	0.0581
480.00	0.0000	0.9828	0.0583

Entry 9

Time / min	18 / M	24 / M	48 / M
0.00	0.2875	0.0000	0.0000
0.30	1.1404	0.0025	0.0000
2.50	0.8636	0.1261	0.0000
5.00	0.7481	0.2397	0.0000
10.00	0.6747	0.3279	0.0000
15.00	0.6561	0.3689	0.0000
20.00	0.6064	0.4026	0.0000
30.00	0.5654	0.4647	0.0000
45.00	0.5112	0.4947	0.0038
60.00	0.4106	0.5824	0.0060
90.00	0.4019	0.6030	0.0134
120.00	0.3459	0.6553	0.0212
150.18	0.0000	0.8793	0.0257
180.00	0.0000	0.8776	0.0333
240.00	0.0000	0.9323	0.0441
311.57	0.0000	0.9745	0.0510
360.00	0.0000	0.9512	0.0572
480.00	0.0000	0.9917	0.0709

7.3.15 Procedure for Use of Alternative Reductants

7.3.15.1 General procedure



A 50 mL oven dried Schlenk tube and stirrer bar fitted with a subseal was evacuated and backfilled with CO₂. A solution of morpholine (175 μ l, 2 mmol, 1 equiv), biphenyl (15.4 mg, 0.1 mmol, 5 mol%) and guanidine catalyst (0.1 mmol, 5 mol%) in acetonitrile (2 mL) was prepared under a N₂ atmosphere and added to the CO₂ flushed Schlenk tube. The solution was stirred at 1000 rpm at 23 / 60 °C, 1.8 bar CO₂, for 15 mins. The reductant (3 Si-H equiv.) was added to commence the reaction and regular samples (approx. 0.02 mL) were taken for analysis by GC.

Yields are given relative to the amine substrate and determined by GC analysis relative to biphenyl as an internal standard using the method described in Section 7.3.4.

7.3.15.2 Table of reactions with reagent quantities

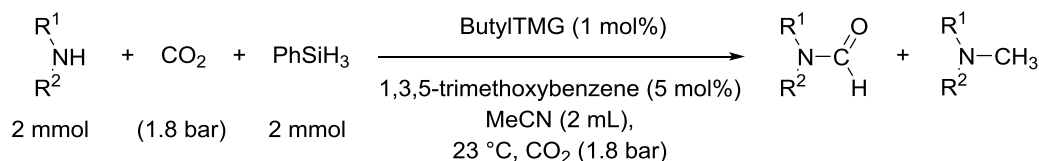
Entry	18 (mmol)	Reductant	Reductant (μ L)	Reductant equiv.	Catalyst	Catalyst loading (mol%)	Temp (°C)
1	2	TMDS	530	3 Si-H eq	TMG	5	60
2	2	PMHS	359	3 Si-H eq	TMG	5	60
3	2	PMHS	359	3 Si-H eq	Butyl TMG	5	60
4	2	PMHS	359	3 Si-H eq	Butyl TMG	5	23
5	2	PMHS	359	3 Si-H eq	TBD	5	60

TMDS = Tetramethyldisiloxane

PMHS = Poly(methylhydrosiloxane)

7.3.16 Substrate Scope

7.3.16.1 General procedure



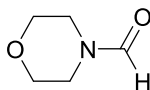
A 50 mL oven dried Schlenk tube and stirrer bar fitted with a subaseal was evacuated and backfilled with CO₂. A solution of amine (2 mmol, 1 equiv), 1,3,5-trimethoxybenzene (16.8 mg, 0.1 mmol, 5 mol%) and ButylTMG **64** (3.4 mg, 0.02, 1 mol%) in acetonitrile (2 mL) was prepared under a N₂ atmosphere and added to the CO₂ flushed Schlenk tube. The solution was stirred at 1000 rpm at 23 °C, 1.8 bar CO₂ for 15 mins. Phenylsilane (247 μl, 2 mmol, 1 equiv) was added to commence the reaction. Reaction samples were analysed by GCMS at 8 and 22 h. After completion, the solvent was removed under vacuum and conversions of the products were calculated by ¹H NMR of the crude product mixture relative to 1,3,5-trimethoxybenzene. The major formylamide products were purified by column chromatography (pentane:ethylacetate, gradient 95:5 to 0:100, with <1 % triethylamine) to confirm identity of products.

7.3.16.2 Characterisation of Products

Characterisation data for the major isolated compounds are given below. The minor methylamine side products were characterised by GC-MS data and comparison of the crude NMR spectra to literature spectra. Literature spectral data are given along with the corresponding peaks in the ¹H NMR spectra of the crude reaction mixture that were used to calculate the yield.

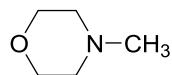
7.3.16.3 Characterisation of all Isolated Products

N-Formylmorpholine **24**



¹H NMR (300 MHz, CDCl₃) δ: 8.06 (1H, s, CHO), 3.72-3.65 (4H, m, O(CH₂)₂), 3.60-3.56 (2H, m, N(CH₂)₂), 3.41-3.38 (2H, m, N(CH₂)₂); ¹³C NMR (126 MHz, CDCl₃) δ: 161.0 (CHO), 67.4 (O(CH₂)₂), 66.6 (O(CH₂)₂), 45.9 (N(CH₂)₂), 40.8 (N(CH₂)₂); EI-MS (rel. int.) m/z = 115.1 (M⁺, 100 %), 100.1 (56), 86.1, (37), 57.1 (45), 56.1 (49)

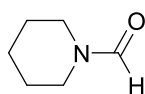
***N*-Methylmorpholine 48:**



NMR of commercial sample: ^1H NMR (400 MHz, CDCl_3) δ : 3.72 (4H, m, $\text{O}(\text{CH}_2)_2$), 2.40 (4H, m, $\text{N}(\text{CH}_2)_2$), 2.29 (3H, s, NCH_3); ^{13}C NMR (126 MHz, CDCl_3) δ : 67.1 ($\text{O}(\text{CH}_2)_2$), 55.6 ($\text{N}(\text{CH}_2)_2$), 46.6 (NCH_3); Crude mixture: EI-MS (rel. int.) m/z = 101.1 (M^+ , 100 %), 100.1 (34), 71.1 (47), 70.1 (11), 56.1 (9)

CH_2 signal at 3.72 ppm used for yield calculation

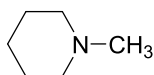
***N*-Formylpiperidine 32**



NMR of commercial sample: ^1H NMR (500 MHz, CDCl_3): 7.97 (1H, s), 3.45 – 3.43 (2H, m), 3.28 – 3.26 (2H, m), 1.67 – 1.62 (2H, m), 1.57 -1.48 (4H, m); ^{13}C NMR (126 MHz, CDCl_3): 160.9, 46.9, 40.7, 26.7, 25.1, 24.8; Crude mixture: EI-MS (rel. int.) m/z = 113.1 (M^+ , 100 %), 112.1 (30), 98.1 (30), 84.1 (36), 56.1 (30)

CH_2 signal at 3.27 ppm used for yield calculation

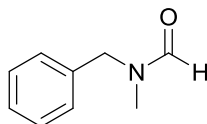
***N*-Methylpiperidine 98**



NMR of commercial sample: ^1H NMR (500 MHz, CDCl_3): 2.32 (4H, br), 2.23 (3H, s), 1.60 – 1.56 (4H, m), 1.40 (2H, br); ^{13}C NMR (126 MHz, CDCl_3): 55.7, 47.0, 26.1, 23.9; Crude mixture: EI-MS (rel. int.) m/z = 99.1 (M^+ , 39 %), 98.1 (100), 71.1 (7), 70.1 (15), 58.1 (8)

Yield determined by GC relative to internal standard calibration

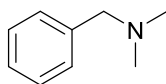
***N*-Methyl-*N*-benzylformamide 69**



Two rotamers observed (1:0.73). ^1H NMR (500 MHz, CDCl_3) δ : 8.29 (1H, s, CHO , major), 8.16 (1H, s, minor, CHO), 7.39-7.20 (5 H, m, major & minor, ArH), 4.52 (2H, s, minor, NCH_2), 4.39 (2H, s, major, NCH_2), 2.85 (3H, s, minor, NCH_3), 2.78 (3H, s, major, NCH_3); ^{13}C NMR (126 MHz, CDCl_3) δ : 162.8 (CHO , major), 162.6 (CHO , minor), 136.1 (ArC), 135.8 (ArC), 128.9 (ArC), 128.7 (ArC), 128.3 (ArC), 128.1 (ArC), 127.7 (ArC), 127.4 (ArC), 53.5 (NCH_2 , major), 47.8 (NCH_2 , minor), 34.1 (NCH_3 , minor), 29.5 (NCH_3 , major); EI-MS (rel. int.) m/z = 149.1

(M⁺, 100 %), 120.1 (8), 106.1 (20), 91.1 (45), 79.1 (14). Spectral data are consistent with the literature⁸⁸

***N,N*-Dimethyl-*N*-benzylamine 197**

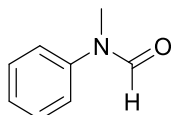


Not isolated

Literature characterisation:²²⁶ ¹H NMR (400 MHz, CDCl₃) δ: 7.33-7.28 (m, 4 H), 7.26-7.21 (m, 1 H), 3.41 (s, 2 H), 2.23 (s, 6 H); ¹³C NMR (100 MHz, CDCl₃) δ: 138.9, 129.1, 128.3, 127.1, 64.5, 45.4.; Crude mixture: EI-MS (rel. int.) m/z = 135.1 (M⁺, 100 %), 134.1 (74), 91.1 (78), 65.1 (17), 58.1 (82).

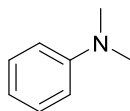
CH₂ and CH₃ signals at 4.02 ppm and 2.60 ppm used for yield calculation

***N*-Methyl-*N*-phenylformamide 70**



Two rotamers observed (1:0.05). ¹H NMR (500 MHz, CDCl₃) δ: 8.48 (1H, s, major, CHO), 8.67 (1H, s, minor, CHO), 7.43-7.40 (2H, m, Ar-H₃), 7.30-7.26 (1H, m, Ar-H₄), 7.19-7.17 (2H, m, Ar-H₂), 3.36 (3H, s, minor, NCH₃) 3.33 (3H, s, major, NCH₃); ¹³C NMR (126 MHz, CDCl₃) δ: 162.2 (major, CHO), 162.1 (minor, CHO), 142.1 (major, Ar-C₁), 140.1 (minor, Ar-C₁), 129.5 (major, Ar-C₃), 128.9 (minor, Ar-C₃), 126.3 (major, Ar-C₄), 126.1 (minor, Ar-C₄), 123.5 (minor, Ar-C₂), 122.2 (major, Ar-C₂), 36.7 (minor, NCH₃), 31.9 (major, NCH₃); EI-MS (rel. int.) m/z = 135.1 (M⁺, 87 %), 106.1 (100), 107.1 (16), 77.1 (26). Spectral data are consistent with the literature:⁷⁶

***N,N*-Dimethyl-*N*-phenylformamide 39**

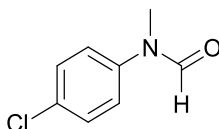


Not isolated

Literature characterisation:²²⁷ ¹H NMR (400 MHz, CDCl₃): δ 7.26 (m, 2H), 6.76 (m, 3H), 2.94 (s, 6H); ¹³C NMR (75 MHz, CDCl₃): δ 150.7, 129.1, 116.7, 112.7, 40.7. Crude mixture: EI-MS (rel. int.) m/z = 121.1 (M⁺, 76 %), 120.1 (100), 105.1 (11), 104.1 (12), 77.1 (16)

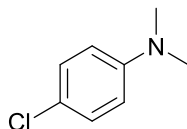
CH₃ signal at 2.96 ppm used for yield calculation

***N*-(4-Chlorophenyl)-*N*-methylformamide 72**



Two rotamers observed (1:0.08). ^1H NMR (500 MHz, CDCl_3) δ : 8.37 (1H, s, major, CHO), 8.35 (1H, s, minor, CHO), 7.30 (2H, m, Ar- H_3), 7.04 (2H, m, Ar- H_2), 3.34 (3H, s, minor, NCH_3), 3.22 (3H, s, major, NCH_3); ^{13}C NMR (126 MHz, CDCl_3) δ : 162.2 (minor, CHO), 162.0 (major, CHO), 140.8 (major, Ar- C_1), 138.7 (minor, Ar- C_1), 132.0 (major, Ar- C_4), 131.4 (minor, Ar- C_4), 129.8 (major, Ar- C_3), 129.1 (minor, Ar- C_3), 124.6 (minor, Ar- C_2), 123.5 (major, Ar- C_2), 36.7 (minor, NCH_3) 32.1 (major, NCH_3); EI-MS (rel. int.) m/z = 171.0 ($^{37}\text{Cl} - \text{M}^+$, 25 %), 169.0 ($^{35}\text{Cl} - \text{M}^+$, 74), 142.0 (32), 140.0 (100), 130.0 (8), 128.0 (27). Spectral data are consistent with the literature⁷⁵

***N*-(4-Chlorophenyl)-*N,N*-Dimethylformamide 198**

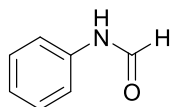


Not isolated

Literature characterisation:⁹⁰ ^1H NMR (300 MHz, CDCl_3) δ : 7.22 (2H, d, J = 8.4 Hz), 6.65 (2H, d, J = 8.4 Hz), 2.95 (6H, s); ^{13}C NMR (75 MHz, CDCl_3) δ : 149.0, 128.8, 121.5, 113.9, 40.7; Crude mixture: EI-MS (rel. int.) m/z = 157.1 ($^{37}\text{Cl} - \text{M}^+$, 24 %), 156.0 (38), 155.1 (76), 154.0 (100), 140.0 (7), 139.0 (15), 138.0 (12).

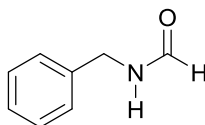
CH_3 signal at 2.92 ppm used for yield calculation

***N*-Phenylformamide 76**



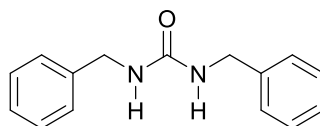
Two rotamers observed (1:0.98). ^1H NMR (500 MHz, CDCl_3) δ : 8.69 (1H, d, J = 11.5 Hz, major, CHO), 8.39 (1H, d, J = 1.3 Hz, minor, CHO), 7.75 (1H, br, NH), 7.54 (1H, m, Ar- H_2), 7.38 – 7.33 (2H, m, Ar- H_3), 7.22-7.13 (1H, m, Ar- H_4), 7.09 (1H, m, Ar- H_2); ^{13}C NMR (126 MHz, CDCl_3) δ : 163.0 (CHO), 159.4 (CHO), 137.0 (Ar- C_1), 136.9 (Ar- C_1), 129.8 (Ar- C_3), 129.2 (Ar- C_3), 125.4 (Ar- C_4), 124.9 (Ar- C_4), 120.2 (Ar- C_2), 118.9 (Ar- C_2); EI-MS (rel. int.) m/z = 121.0 (M^+ , 100 %), 93.0 (65), 66.1 (34). Spectral data are consistent with the literature²²⁸

***N*-Benzylformamide 78**



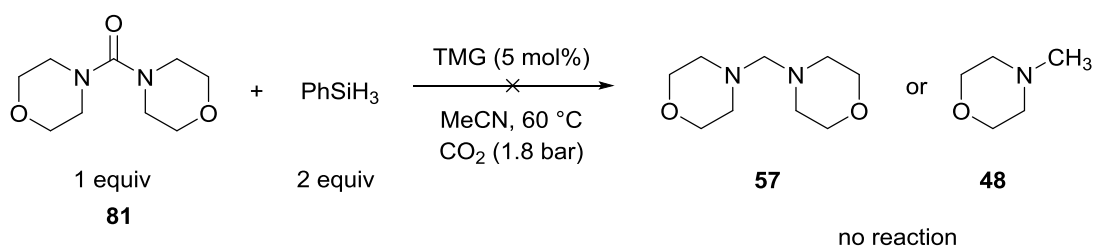
Two rotamers observed (1:0.18). ^1H NMR (400 MHz, CDCl_3) δ : 8.27 (1H, s, major, *CHO*), 8.19 (1H, d, $J = 11.8$ Hz, minor, *CHO*), 7.39 – 7.25 (5H, m, *Ar-H*), 5.86 (1H, s, br, *NH*), 4.49 (2H, d, $J = 6.0$ Hz, major, *NCH*₂), 4.42 (2H, d, $J = 6.5$ Hz, minor, *NCH*₂); ^{13}C NMR (126 MHz, CDCl_3) δ : 164.7 (minor, *CHO*), 161.1 (major, *CHO*), 137.7 (major, *Ar-C*₁), 137.6 (minor, *Ar-C*₁), 129.1 (*Ar-C*), 128.9 (*Ar-C*), 128.1 (*Ar-C*), 127.9 (*Ar-C*), 127.8 (*Ar-C*), 127.1 (*Ar-C*), 45.8 (minor, *NCH*₂), 42.3 (major, *NCH*₂); EI-MS (rel. int.) $m/z = 135.1$ (M^+ , 100 %), 134.1 (47), 106.1 (26), 91.1 (29), 79.1 (19), 77.1 (14). Spectral data are consistent with the literature²²⁹

***N,N'*-Dibenzylurea 79**



^1H NMR (300 MHz, CDCl_3) δ : 7.35 – 7.23 (10H, m, *Ar-H*), 4.61 (2H, s, *NH*), 4.39 (4H, d, $J = 5.8$ Hz, *NCH*₂); ^{13}C NMR (101 MHz, CDCl_3) δ : 158.2 (*C=O*), 139.2 (*Ar-C*), 128.8 (*Ar-C*), 127.6 (*Ar-C*), 127.5 (*Ar-C*), 44.7 (*NCH*₂); EI-MS (rel. int.) $m/z = 240.1$ (M^+ , 71 %), 149.0 (24), 107.1 (16), 106.1 (100), 91.1 (50), 79.1 (16), 77.1 (13). Spectral data are consistent with the literature²³⁰

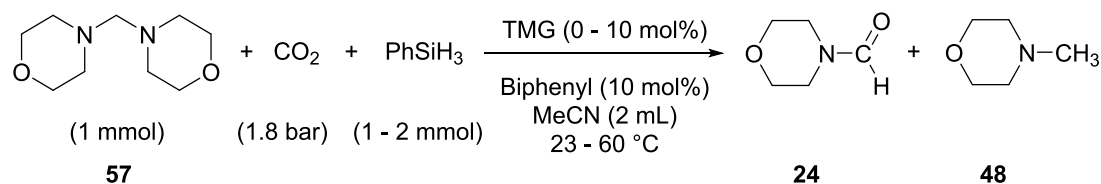
7.3.17 Reduction of Urea 81



A 50 mL oven dried Schlenk tube and stirrer bar fitted with a subaseal was evacuated and backfilled with CO_2 for two cycles. A solution of dimorpholinemethanone (199 mg, 1 mmol, 1 equiv), biphenyl (15.4 mg, 0.1 mmol, 10 mol%) and TMG (12.5 μl , 0.1 mmol, 10 mol%) in acetonitrile (2 mL) was prepared under a N_2 atmosphere and added to the CO_2 flushed Schlenk tube. The solution was stirred at 1000 rpm at 60 °C, 1.8 bar CO_2 for 15 mins. Phenylsilane (247 μl , 2 mmol, 2 equiv) was added to commence the reaction and regular samples taken for analysis by GC. After 24 h no conversion to either aminal or methylmorpholine was observed by GC or NMR.

7.3.18 GC Kinetics of Reaction of Aminal **57** to Methyl and Formylmorpholine

General Procedure:



A 50 mL oven dried Schlenk tube and stirrer bar fitted with a subaseal was evacuated and backfilled with CO₂. A solution of dimorpholinomethane **57** (186 mg, 1 mmol, 1 equiv), biphenyl (0.1 mmol, 10 mol%) and guanidine catalyst (0.002 - 0.1 mmol, 0 - 10 mol%) in acetonitrile (2 mL) was prepared under a N₂ atmosphere and added to the CO₂ flushed Schlenk tube. The solution was stirred at 1000 rpm at reaction temperature, at selected CO₂ pressure used) for 15 mins. Phenylsilane (1 - 2 mmol, 1 - 2 equiv) was added to commence the reaction and kinetic monitoring started. Regular samples (approx. 0.02 mL) were taken and diluted in methanol (to quench the reaction) for analysis by GC. Product concentrations are determined by GC analysis relative to biphenyl as an internal standard using the method described in Section 7.3.4.

The reaction outcome was further confirmed by GCMS analysis (0.1 mL of reaction in mixture in 1 mL DCM) and solvent evaporated from the remaining reaction mixture under reduced pressure for analysis by NMR.

Table of reaction conditions investigated:

Entry	57 (mmol)	PhSiH ₃ (mmol)	Catalyst	Catalyst loading (mol%)	Temp (°C)	CO ₂ Pressure (bar)
1	1	2	TMG	10	60	1.8
2	1	2	TMG	10	23	1.8
3	1	2	TBD	10	23	1.8
4	1	2	ButylTMG	10	23	1.8
5	1	2	-	-	60	1.8
6 ^a	1	2	TMG	10	60	
7	1	1	TMG	10	23	1.8
8 ^b	1	2	TMG	10	23	1.8
9	1	2	TMG	10	23	1.2
10	1	2	TMG	10	23	1

a) Reaction under N₂

b) Reaction with 40 mol% water present

Kinetic Data:

Entry 1:		
Time	24	48
/ min	/ M	/ M
0.00	0.0000	0.0000
0.33	0.0000	0.0793
2.50	0.0924	0.2571
5.17	0.1137	0.2820
10.00	0.1388	0.3280
20.00	0.1748	0.4031
40.00	0.2258	0.4611
60.17	0.2568	0.4751
90.00	0.3058	0.5042
120.25	0.3416	0.5333
180.50	0.3754	0.6525
242.00	0.3758	0.6230
360.00	0.3645	0.5818

Entry 2:		
Time	24	48
/ min	/ M	/ M
0.00	0.0000	0.0000
0.30	0.0000	0.1052
2.50	0.0431	0.1610
10.00	0.1924	0.3058
20.00	0.2630	0.3651
40.00	0.3147	0.4281
60.00	0.3480	0.4470
120.00	0.4534	0.5052
240.00	0.4742	0.5142
360.00	0.5044	0.5310

Entry 3:		
Time	24	48
/ min	/ M	/ M
0.00	0.0000	0.0000
0.30	0.0000	0.0680
2.50	0.0076	0.0741
10.00	0.0545	0.1680
20.00	0.1030	0.2369
40.00	0.1508	0.3280
60.00	0.1720	0.3565
120.00	0.3170	0.4823
240.00	0.3500	0.5408
360.00	0.4290	0.5800

Entry 4:		
Time	24	48
/ min	/ M	/ M
0.00	0.0005	0.0000
0.30	0.0035	0.0355
2.50	0.0414	0.0847
5.00	0.0640	0.1635
10.00	0.1305	0.2226
20.00	0.2455	0.3162
40.00	0.3224	0.4264
60.18	0.3463	0.4843
90.25	0.4073	0.5172
120.50	0.4155	0.5534
180.00	0.4552	0.5085
240.00	0.4827	0.5068
360.00	0.4911	0.5055

Entry 5:		
Time	24	48
/ min	/ M	/ M
0.00	0.0006	0.0000
0.25	0.0000	0.0858
5.08	0.0000	0.0375
20.43	0.0072	0.1125
49.43	0.0154	0.1396
120.08	0.0248	0.1738
178.25	0.0317	0.1955
238.58	0.0390	0.2016
361.00	0.0478	0.2444
1260.0	0.1748	0.3818
1800.0	0.2224	0.4442

Entry 6:		
Time	24	48
/ min	/ M	/ M
0.00	0.0000	0.0000
5.00	0.0000	0.0000
30.00	0.0000	0.0000
59.50	0.0000	0.0000
120.00	0.0000	0.0000
240.00	0.0000	0.0000
420.00	0.0000	0.0000

Entry 7:		
Time	24	48
/ min	/ M	/ M
0.00	0.0007	0.0000
0.30	0.0009	0.0471
2.50	0.0370	0.0994
10.00	0.1328	0.1974
20.00	0.2412	0.3735
40.00	0.2834	0.3584
60.00	0.3238	0.4205
120.00	0.3741	0.4924
240.00	0.4286	0.5152
360.00	0.4828	0.5012

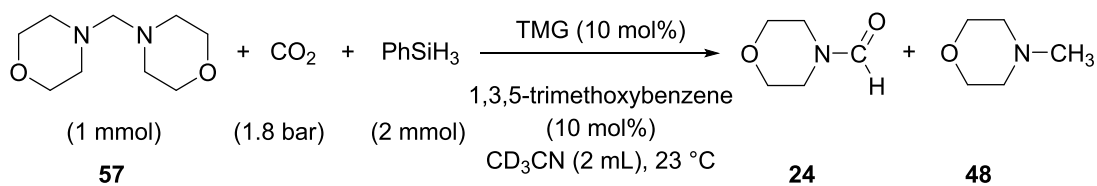
Entry 8:		
Time	24	48
/ min	/ M	/ M
0.00	0.0000	0.0000
0.33	0.0000	0.1052
2.50	0.0338	0.1416
10.00	0.1593	0.2828
20.00	0.2090	0.2806
40.00	0.3212	0.4523
60.00	0.3525	0.4914
120.00	0.3957	0.5265
240.00	0.4548	0.5253
360.00	0.4844	0.5233

Entry 9:		
Time	24	48
/ min	/ M	/ M
0.00	0.0000	0.0000
0.30	0.0000	0.0711
2.50	0.0261	0.1220
10.00	0.1212	0.2467
20.00	0.1970	0.3087
40.00	0.2833	0.4299
60.00	0.3222	0.4723
120.00	0.3728	0.5165
240.00	0.4346	0.5508
360.00	0.4633	0.5496

Entry 10:		
Time	24	48
/ min	/ M	/ M
0.00	0.0000	0.0000
0.30	0.0000	0.0710
2.50	0.0234	0.0516
10.00	0.0968	0.2267
20.00	0.1708	0.3027
40.00	0.2674	0.4082
60.00	0.2914	0.4260
120.00	0.3232	0.4954
240.00	0.3459	0.4778
360.00	0.4474	0.5348
532.00	0.4644	0.5281
1320.0	0.4780	0.5089

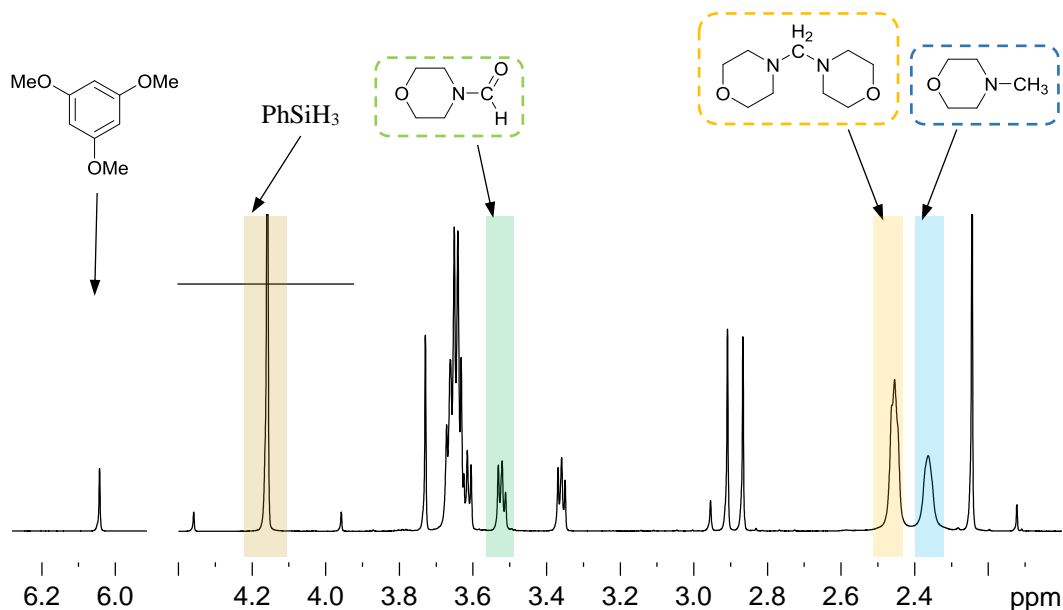
7.3.19 Mechanistic Study of Aminal 57 Reactivity

7.3.19.1 NMR monitoring of aminal to methyl and formylmorpholine

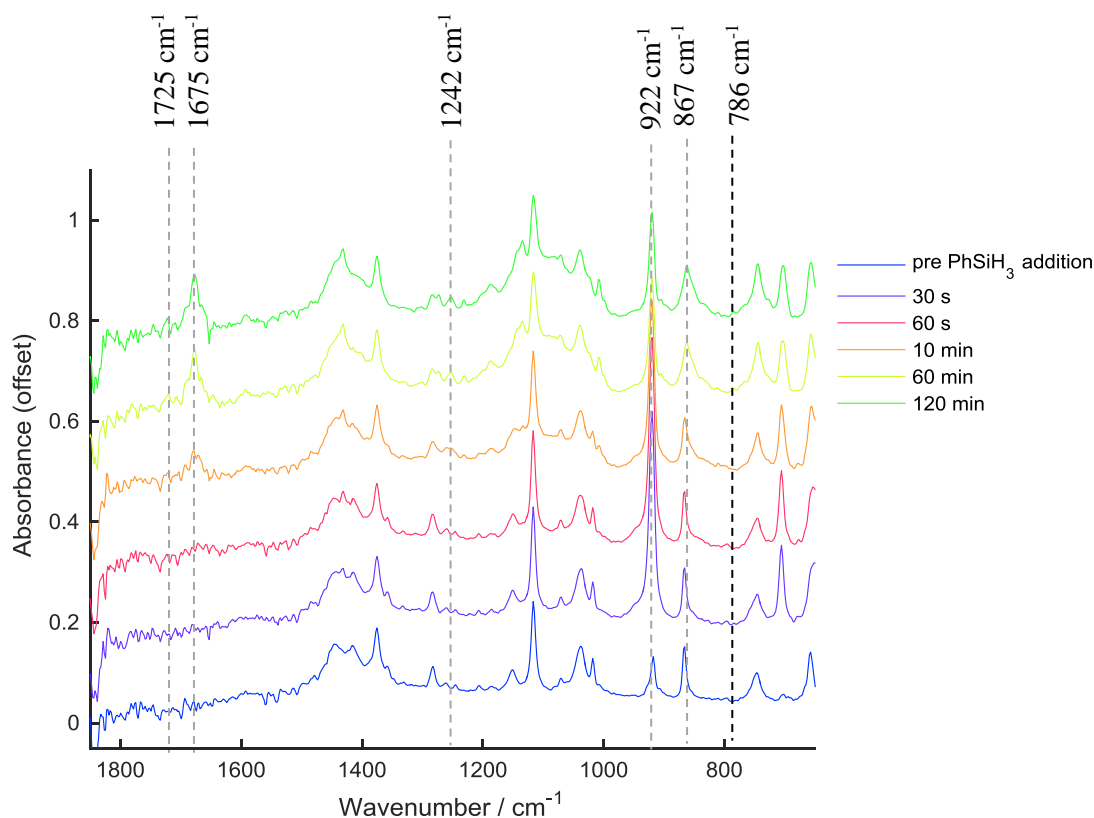


A 50 mL oven dried Schlenk tube and stirrer bar fitted with a subseal was evacuated and backfilled with CO_2 . A solution of dimorpholinomethane (186 mg, 1 mmol, 1 equiv), 1,3,5-trimethoxybenzene (16.8 mg, 0.1 mmol, 10 mol%) and TMG (12.5 μL , 0.1 mmol, 10 mol%) in CD_3CN (2 mL) was prepared under a N_2 atmosphere and added to the CO_2 flushed Schlenk tube. The solution was stirred at 1000 rpm at reaction temperature, at selected CO_2 pressure used) for 15 mins. Phenylsilane (247 μL , 2 mmol, 2 equiv) was added to commence the reaction and kinetic monitoring started. Regular samples (approx. 0.1 mL) were taken and diluted in mL CDCl_3 (0.5 mL) in a N_2 flushed NMR tube. ^1H & ^{13}C NMR spectra were collected and referenced relative to the residual acetonitrile peak at 1.94 ppm (^1H spectra) or CDCl_3 peak at 77.16 ppm (^{13}C spectra).

Example ^1H NMR spectra and assignments used for yield calculation:

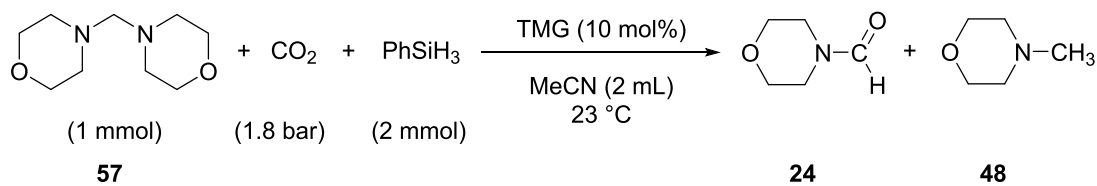


IR spectra of reaction with peak heights used for trend analysis:



(Formoxysilane (1725 cm^{-1}), Formylmorpholine (1675 cm^{-1}), Silylcarbamate (1242 cm^{-1}), PhSiH_3 (922 cm^{-1}), N-methylmorpholine (867 cm^{-1}) and TMG (786 cm^{-1}))

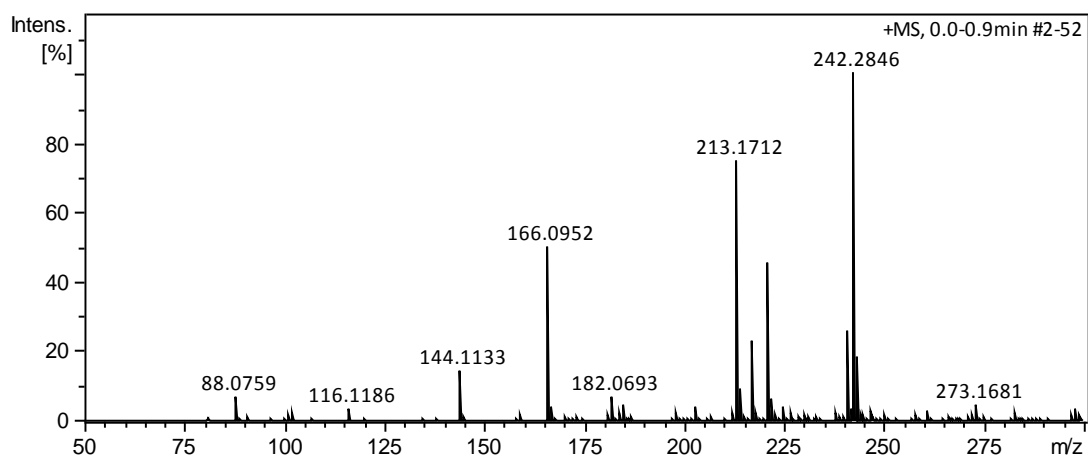
7.3.19.3 MS and MSMS monitoring of ainal to methyl and formylmorpholine



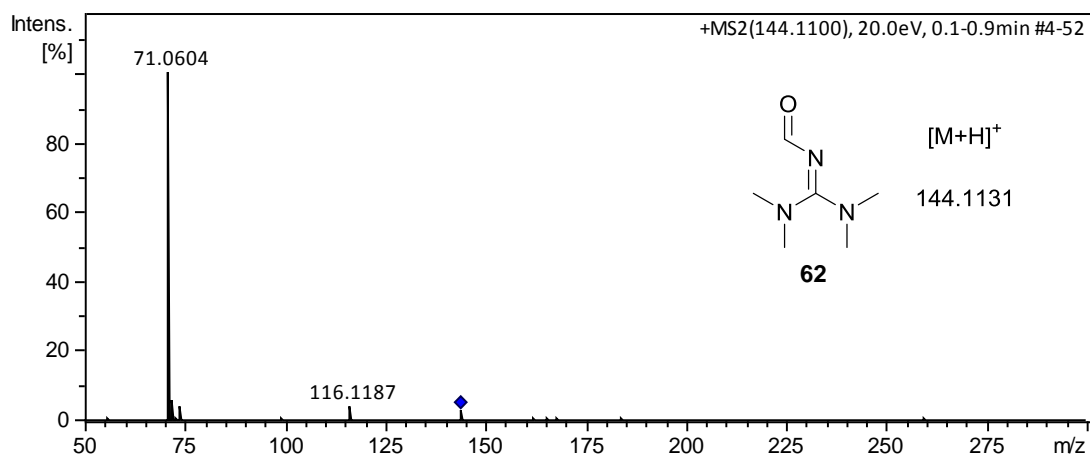
A 50 mL oven dried Schlenk tube and stirrer bar fitted with a subseal was evacuated and backfilled with CO_2 . A solution of dimorpholinomethane **57** (186 mg, 1 mmol, 1 equiv), biphenyl (0.1 mmol, 10 mol%) and TMG (12.5 μL , 0.1 mmol, 10 mol%) in acetonitrile (2 mL) was prepared under a N_2 atmosphere and added to the CO_2 flushed Schlenk tube. The solution was stirred at 1000 rpm at $23\text{ }^\circ\text{C}$, at 1.8 bar CO_2 for 15 mins. Phenylsilane (247 μL , 2 mmol, 2 equiv) was added to commence the reaction and kinetic monitoring started. Regular samples (approx. 0.02 mL) were taken and diluted in methanol to quench the reaction for analysis by HRMS.

MSMS analysis was performed on a sample taken at 60 minutes.

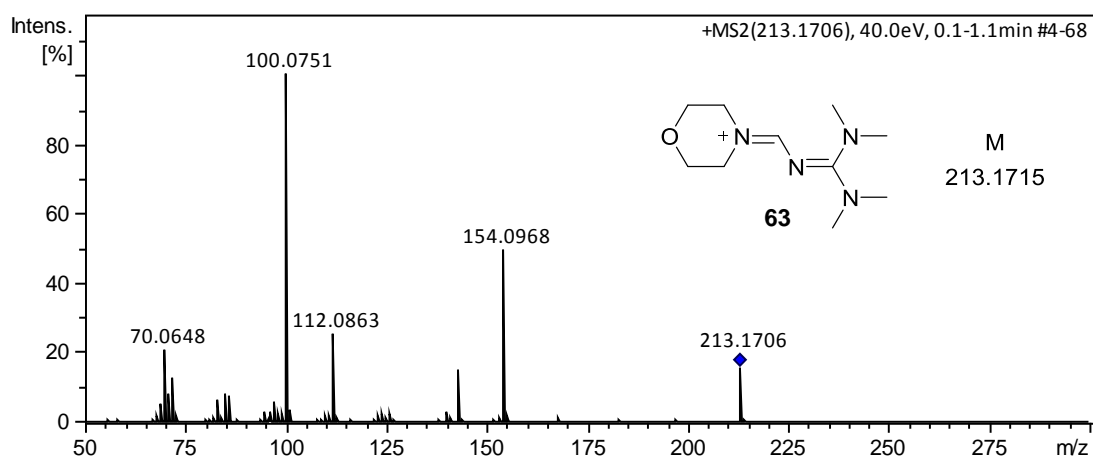
Whole spectra – 60 min



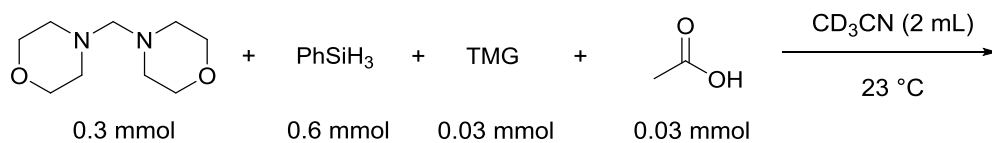
144.1131 fragment



213.1715 fragment

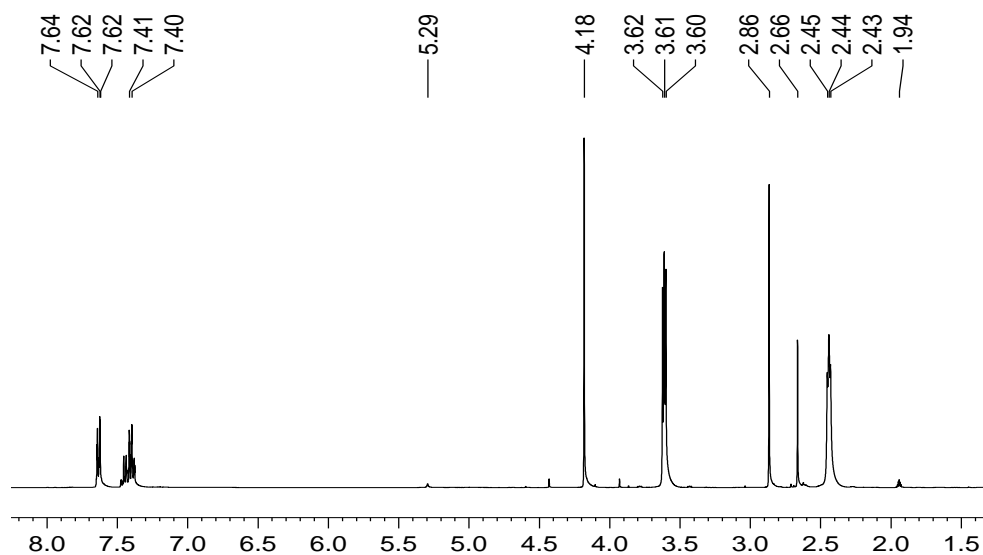


7.3.19.4 Acid catalysed reaction pathway investigation by ^1H NMR

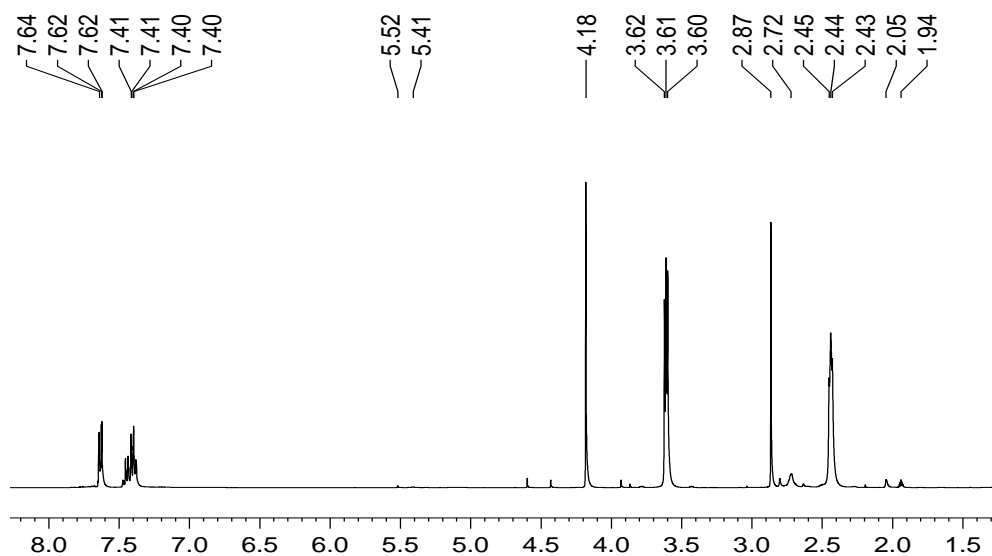


A solution of dimorpholinomethane (56.2 mg, 0.3 mmol, 1 equiv), phenylsilane (74 μL , 0.6 mmol, 2 equiv) and TMG (3.8 μL , 0.03 mmol, 0.1 equiv) in CD_3CN (0.6 mL) was prepared under a N_2 atmosphere in a Young's tap NMR tube. ^1H NMR spectra were collected. Acetic acid (1.7 μL , 0.03 mmol, 0.1 equiv) was added to the solution and ^1H NMR spectra collected.

^1H NMR spectra of aminal + PhSiH_3 + TMG (10 mol%):

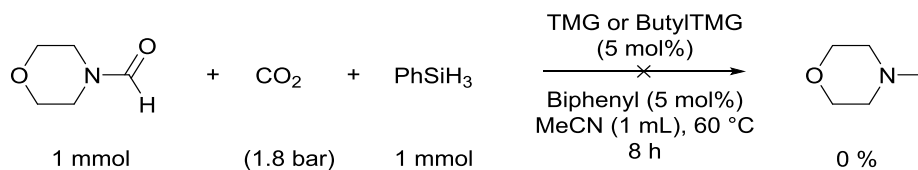


^1H NMR spectra of aminal + PhSiH_3 + TMG (10 mol%) + acetic acid (10 mol%)



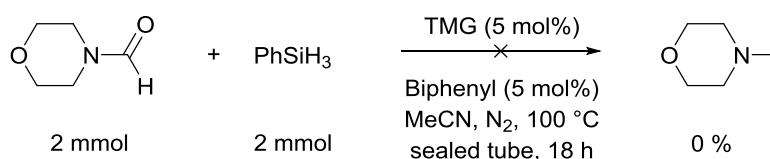
7.3.20 Reduction of Formylmorpholine 24 to Methylmorpholine 48

7.3.20.1 Reaction at 60 °C with CO₂



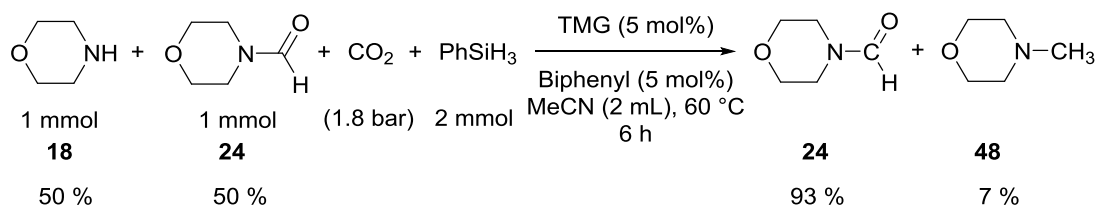
A 50 mL oven dried Schlenk tube and stirrer bar fitted with a subseal was evacuated and backfilled with CO₂ for two cycles. A solution of formylmorpholine (101 μl, 1 mmol, 1 equiv), biphenyl (7.6 mg, 0.05 mmol, 5 mol%) and TMG (6.3 μl, 0.05 mmol, 5 mol%) in acetonitrile (1 mL) was prepared under a N₂ atmosphere and added to the CO₂ flushed Schlenk tube. The solution was stirred at 1000 rpm at 60 °C, 1.8 bar CO₂ for 15 mins. Phenylsilane (124 μl, 1 mmol, 1 equiv) was added to commence the reaction and regular samples taken for analysis by GC. After 8 h no conversion of formylmorpholine was observed.

7.3.20.2 Reaction at 100 °C in N₂



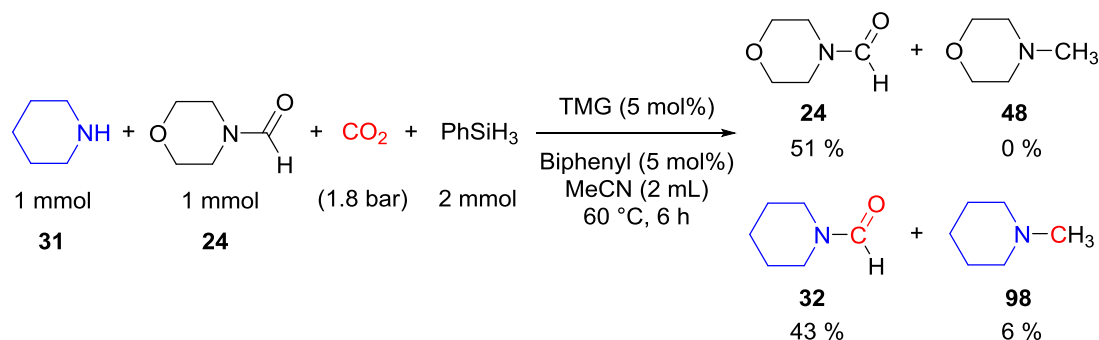
A solution of formylmorpholine (200 μl, 2 mmol, 1 equiv), biphenyl (15.4 mg, 0.1 mmol, 5 mol%), TMG (12.5 μl, 0.1 mmol, 5 mol%) and phenylsilane (247 μl, 2 mmol, 1 equiv) in acetonitrile (2 mL) was prepared under a N₂ atmosphere and added to an N₂ flushed pressure tube. The solution was stirred at 100 °C for 18 h. Analysis by GC and NMR showed no conversion of formylmorpholine to methylmorpholine.

7.3.20.3 Reaction with 50 % Formylmorpholine 24

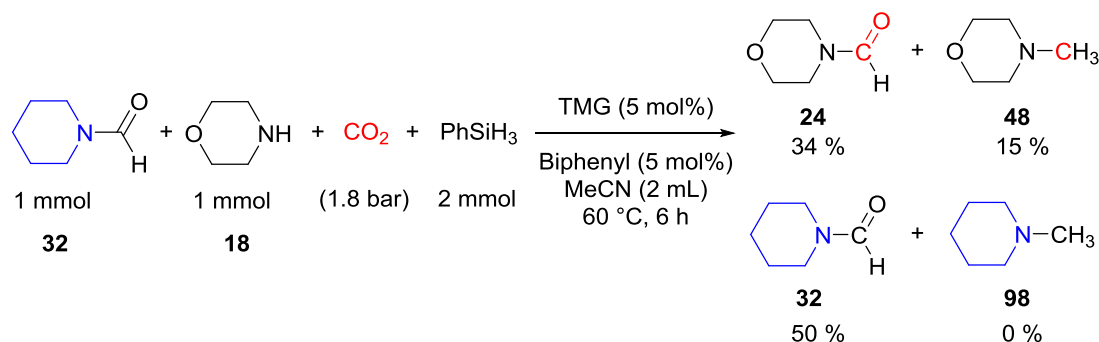


A 50 mL oven dried Schlenk tube and stirrer bar fitted with a subseal was evacuated and backfilled with CO₂ for two cycles. A solution of morpholine (87.5 μl, 1 mmol, 0.5 equiv), formylmorpholine (101 μl, 1 mmol, 0.5 equiv), biphenyl (15.4 mg, 0.1 mmol, 5 mol%) and TMG (12.5 μl, 0.1 mmol, 5 mol%) in acetonitrile (2 mL) was prepared under a N₂ atmosphere and added to the CO₂ flushed Schlenk tube. The solution was stirred at 1000 rpm at 60 °C, 1.8

7.3.20.5 Crossover reactions

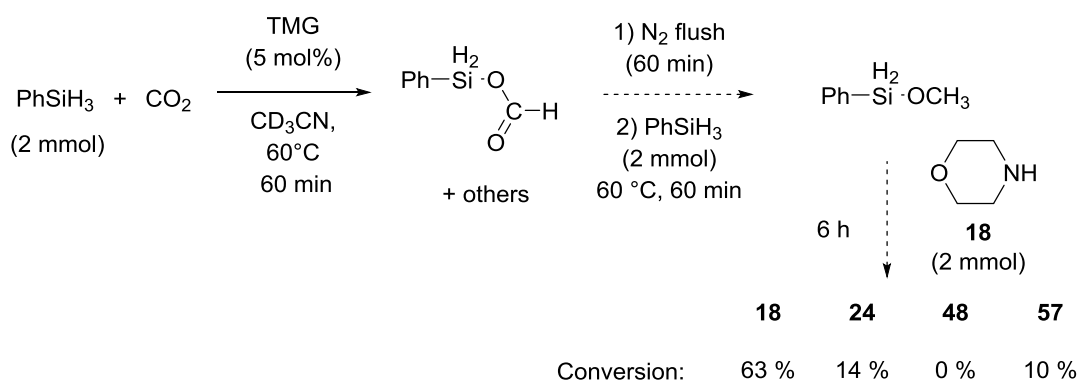


A 50 mL oven dried Schlenk tube and stirrer bar fitted with a subaseal was evacuated and backfilled with CO₂ for two cycles. A solution of piperidine (99.0 μl, 1 mmol, 0.5 equiv), formylmorpholine (101 μl, 1 mmol, 0.5 equiv), biphenyl (15.4 mg, 0.1 mmol, 5 mol%) and TMG (12.5 μl, 0.1 mmol, 5 mol%) in acetonitrile (2 mL) was prepared under a N₂ atmosphere and added to the CO₂ flushed Schlenk tube. The solution was stirred at 1000 rpm at 60 °C, 1.8 bar CO₂ for 15 mins. Phenylsilane (247 μl, 2 mmol, 1 equiv) was added to commence the reaction and kinetic monitoring by GC started.



A 50 mL oven dried Schlenk tube and stirrer bar fitted with a subaseal was evacuated and backfilled with CO₂ for two cycles. A solution of morpholine (87.5 μl, 1 mmol, 0.5 equiv), formylpiperidine (111 μl, 1 mmol, 0.5 equiv), biphenyl (15.4 mg, 0.1 mmol, 5 mol%) and TMG (12.5 μl, 0.1 mmol, 5 mol%) in acetonitrile (2 mL) was prepared under a N₂ atmosphere and added to the CO₂ flushed Schlenk tube. The solution was stirred at 1000 rpm at 60 °C, 1.8 bar CO₂ for 15 mins. Phenylsilane (247 μl, 2 mmol, 1 equiv) was added to commence the reaction and kinetic monitoring by GC started.

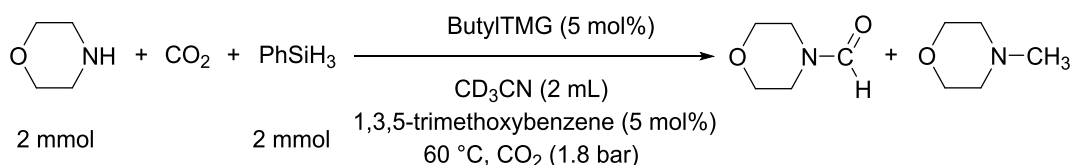
7.3.21 Involvement of Methoxysilane Species



A 50 mL oven dried Schlenk tube and stirrer bar fitted with a subseal was evacuated and backfilled with CO_2 . A solution of phenylsilane (247 μl , 2 mmol, 1 equiv), 1,3,5-trimethoxybenzene (16.8 mg, 0.1 mmol, 0.05 equiv), and TMG (12.5 μl , 0.1 mmol, 5 mol%) in CD_3CN (2 mL) was prepared under a N_2 atmosphere and added to the CO_2 flushed Schlenk tube. The solution was stirred at 1000 rpm at 60 °C, 1.8 bar CO_2 for 60 mins, flushed with N_2 for 60 mins to remove CO_2 and a second equivalent of phenylsilane (247 μl , 2 mmol, 1 equiv) added. After 60 mins a solution of morpholine (175 μl , 2 mmol, 1 equiv) in CD_3CN (0.2 mL), prepared under N_2 , was added. After 6 h the neat reaction mixture was analysed by NMR spectroscopy to determine conversions.

7.3.22 Rate Enhancement with Alkylated Catalysts

7.3.22.1 NMR study with butylTMG catalyst



A 50 mL oven dried Schlenk tube and stirrer bar fitted with a subseal was evacuated and backfilled with CO_2 . A solution of morpholine (175 μl , 2 mmol, 1 equiv), 1,3,5-trimethoxybenzene (16.8 mg, 0.1 mmol, 5 mol%) and ButylTMG (17.1 mg, 0.1 mmol, 5 mol%) in CD_3CN (2 mL) was prepared under a N_2 atmosphere and added to the CO_2 flushed Schlenk tube. The solution was stirred at 1000 rpm at 60 °C, 1.8 bar CO_2 , for 15 mins. Phenylsilane (247 μl , 2 mmol, 1 equiv) was added to commence the reaction and kinetic monitoring started. Regular samples were taken and diluted in CD_3CN in a N_2 flushed NMR tube. ^1H NMR spectra were collected and referenced relative to the residual acetonitrile peak at 1.94 ppm.

Time / min	PhSiH₃ / M	57 / M	24 / M	48 / M
0.50	0.4208	0.0046	0.1388	0.0000
2.50	0.1534	0.0844	0.4966	0.0000
5.80	0.0568	0.1589	0.5843	0.0180
16.25	0.0000	0.1091	0.5905	0.1569
30.00	0.0000	0.0915	0.5943	0.1947
60.00	0.0000	0.0746	0.6252	0.2155
90.00	0.0000	0.0620	0.6297	0.1884
120.00	0.0000	0.0601	0.6267	0.1958
240.00	0.0000	0.0509	0.6893	0.2242

7.4 Chapter 6: Process Development for Reaction of CO₂ with Biomass Derived Compounds

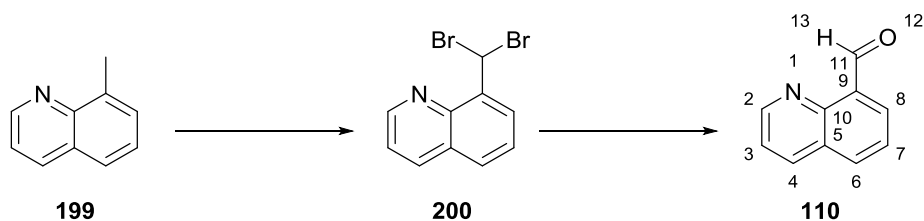
7.4.1 General Procedures for Quinoline-8-carbaldehyde **110** Substrate

General procedure for screening reaction of quinoline-8-carbaldehyde **110** with CO₂:

Quinoline-8-carbaldehyde **110** (0.25 mmol, 1 equiv.), Rh catalyst (0.025 mmol, 10 mol%) and a magnetic stirrer bar were placed in a high pressure reaction vessel and flushed with nitrogen. Degassed solvent (2.5 mL), and base if used (0.25 mmol, 1 equiv.), was added to the vessel, sealed and flushed with CO₂. The vessel was pressurised to 40 bar with CO₂, heated to 100 °C and stirred overnight. The vessel was cooled, vented through solvent and the reaction products were isolated through evaporation of the solvent under vacuum.

7.4.2 Substrate Synthesis

Quinoline-8-carbaldehyde **110**



N-bromosuccinimide (2.37 g, 13.3 mmol, 0.4 equiv) was added to a solution of degassed carbon tetrachloride (55 mL) and freshly distilled 8-methyl-quinoline **199** (4.5 mL, 33.2 mmol, 1 equiv). A spatula tip of dibenzoylperoxide was added and heated to 90 °C. *N*-bromosuccinimide (9.46 g, 53.2 mmol, 1.6 equiv) was added in four portions over 90 min. After 46 h the orange solution was cooled to 0 °C, filtered and washed with aqueous NaOH (2 N, 50 mL), sodium sulfite solution (50 mL), water (50 mL) and brine (2 × 50 mL). The organics were dried over sodium sulphate and the solvent evaporated to yield 8-(dibromomethyl)-quinoline **200** (9.84 g, 98 %) as a yellow solid.

Crude 8-(dibromomethyl)-quinoline **200** (9.84 g, 32.7 mmol) in H₂O (90 mL) was heated under reflux for 2 h and filtered whilst hot. After cooling to rt, aqueous NaOH (2 N, 75 mL) was added to produce a white precipitate which was extracted with diethyl ether (3 × 100 mL). The organics were washed with water to neutrality (2 × 100 mL) and dried over sodium sulphate. Solvent evaporation yielded a yellow solid which was recrystallised (H₂O) to give colourless needles **110** (1.43 g, 28 %).

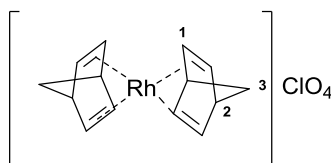
^1H NMR (500 MHz, CDCl_3) δ : 11.48 (1H, s, H_{13}), 9.07 (1H, dd, $J = 4.1, 1.4$ Hz, H_2), 8.35 (1H, dd, $J = 7.1, 0.8$ Hz, H_8), 8.27 (1H, dd, $J = 8.3, 1.4$ Hz, H_4), 8.11 (1H, dd, $J = 8.2, 0.8$ Hz, H_6), 7.70 (1H, t, $J = 7.7$ Hz, H_7), 7.53 (1H, dd, $J = 8.3, 4.1$ Hz, H_3). ^{13}C NMR (125 MHz, CDCl_3) δ : 193.0 (C_{11}), 151.7 (C_2), 148.0 (C_{10}), 136.7 (C_4), 134.6 (C_6), 132.1 (C_9), 129.7 (C_8), 128.7 (C_5) 126.6 (C_7), 122.2 (C_3); HRMS (ESI): found $[\text{M}+\text{H}]^+$ 158.0600, (calculated: 158.0600); mp: 97–98.5 °C; ATR-FT-IR (cm^{-1}): 2865 (w, CH stretch), 1679 (m, C=O stretch), 1570 (m, C-C in ring stretch), 1246 (m, CH bend), 869 (m), 827 (m), 785 (s, CH wag), 764 (s, CH wag), 641 (m). Spectral data are consistent with the literature.²³¹

7.4.3 Catalyst Preparation

$[\text{Rh}(\text{NBD})\text{Cl}]_2$

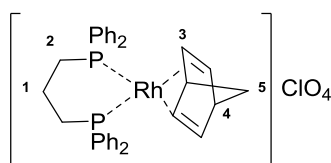
NBD (2.90 mL, 28.2 mmol, 5.9 equiv.) was added to RhCl_3 hydrate (1.00 g, 4.78 mmol, 1 equiv.) in degassed, ethanol (90 %, 14.5 mL). After stirring at rt for 64 h the yellow precipitate was isolated by filtration, washed with ice cold ethanol (5 mL), and dried under vacuum to give $[\text{Rh}(\text{NBD})\text{Cl}]_2$ as a yellow solid (0.636 g, 29 %).

$[\text{Rh}(\text{NBD})_2]\text{ClO}_4$



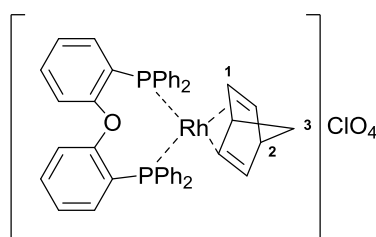
A solution of $[\text{Rh}(\text{NBD})\text{Cl}]_2$ (0.200 g, 0.434 mmol, 1 equiv.) and AgClO_4 (0.150 g, 0.868 mmol, 2 equiv.) in degassed DCM (4 mL) was stirred at rt overnight. After allowing to settle, the solution was removed and the remaining precipitate washed with DCM (2×2 mL). The solvent was evaporated and the product crystallised by layering diethylether (4 mL) onto DCM (4 mL) and leaving to stand overnight. A second recrystallisation with DCM (2 mL) and pentane (2 mL) gave the product as red crystals which were washed (4:1, DCM—pentane, 1 mL) and dried under vacuum (0.081 g, 48 %). ^1H NMR (500 MHz, CDCl_3) δ : 5.19 (8H, m, H_1), 4.11 (4H, m, H_2), 1.50 (4H, m, H_3). Comparison to literature characterisation:²³² ^1H NMR (400 MHz, CD_2Cl_2) δ : 5.67 (dd, 8 H), 4.28 (br m, 4 H), 1.65 (t, 4 H)

$[\text{Rh}(\text{NBD})\text{DPPP}]\text{ClO}_4$



DPPP (0.179 g, 0.434 mmol, 2 equiv.) was added to $[\text{Rh}(\text{NBD})\text{Cl}]_2$ (0.100 g, 0.217 mmol, 1 equiv) and AgClO_4 (0.0900 g, 0.434 mmol, 2 equiv.) in degassed, anhydrous ethanol. After stirring overnight the solvent was removed under vacuum and the resulting red solid dissolved in DCM (2 mL). The reaction mixture was filtered and washed with DCM (3×2 mL). The product was crystallised from the filtrate (1:1, DCM—pentane) to produce red crystals which were filtered and dried under vacuum (0.152 g, 50 %). ^1H NMR (500 MHz, CDCl_3) δ : 7.54-7.38 (20 H, m, Ar-H), 4.69 (4 H, s, H_3), 4.08 (2 H, s, H_4), 2.81-2.75 (4H, m, H_2), 1.96-1.84 (2H, m, H_1), 1.55 (2 H, s, H_5); ^{31}P NMR (121 MHz, CDCl_3) δ : 14.86 (d, $J= 149.3$ Hz). Spectral data are consistent with the literature.¹⁹⁹

$[\text{Rh}(\text{NBD})\text{DPEphos}]\text{ClO}_4$

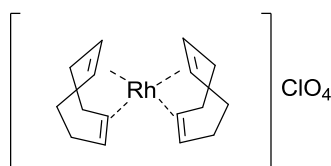


DPEphos (0.246 g, 0.456 mmol, 2.1 equiv.) was added to a stirred solution of $[\text{Rh}(\text{NBD})\text{Cl}]_2$ (0.100 g, 0.217 mmol, 1 equiv.), AgClO_4 (0.0945 g, 0.456 mmol, 2.1 equiv.) and degassed DCM (2 mL). Reaction mixture was stirred overnight, allowed to stand and solution transferred to a second flask. The remaining filtrate was washed with DCM (2×2 mL) and the combined solutions evaporated under vacuum until 2 mL of solvent remained. Product crystallised through layering of pentane (2 mL) on the remaining DCM layer. The resulting red crystals were washed (4:1, DCM—pentane, 2×1 mL) and dried under vacuum (0.313 g, 87 %). ^1H NMR (500 MHz, CDCl_3) δ : 7.49-7.31 (22 H, m, ArH), 6.99-6.92 (6 H, m, ArH), 4.36 (4 H, m, H_1), 3.97-3.94 (2H, m, H_2), 1.54-1.52 (2H, m, H_3); ^{31}P NMR (121 MHz, CDCl_3) δ : 17.11 (d, $J= 158.6$ Hz). Spectral data are consistent with the literature¹⁷⁷

$[\text{Rh}(\text{COD})\text{Cl}]_2$

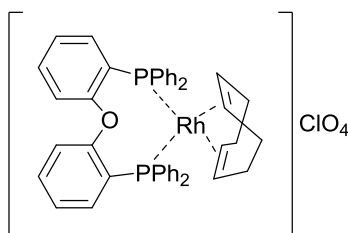
RhCl_3 hydrate (1.00 g, 4.78 mmol, 1 equiv.) was added to a solution of freshly distilled 1,5-cyclooctadiene (3.80 mL, 31.1 mmol, 6.5 equiv.) in degassed ethanol (90 %, 25 mL) and stirred under reflux for 15 h. The formed yellow/orange precipitate was isolated by filtration, washed with ice cold degassed ethanol (90 %, 2×5 mL) and dried under vacuum to give $[\text{Rh}(\text{COD})\text{Cl}]_2$ as a yellow solid (0.658 g, 28 %). ^1H NMR (500 MHz, CDCl_3) δ : 4.22 (4H, s), 2.57 – 2.42 (4H, m), 1.81 – 1.69 (4H, m); ^{13}C NMR (125 MHz, CDCl_3) δ : 78.9, 78.8, 31.0

[Rh(COD)₂]ClO₄



Freshly distilled 1,5-cyclooctadiene (0.10 mL, 0.811 mmol, 2 equiv.) was added to a solution of [Rh(COD)Cl]₂ (0.200 g, 0.406 mmol, 1 equiv.) and AgClO₄ (0.167 g, 0.811 mmol, 2 equiv.) in degassed DCM (4 mL) and stirred at rt for 3 h. After allowing to settle, the dark red solution was removed and the remaining grey/yellow precipitate washed with degassed DCM (3 × 2 mL). The solvent was evaporated and the product crystallised by layering pentane (3 mL) on DCM (3 mL) forming red/brown needles (0.134 g, 79 %). ¹H NMR (500 MHz, CDCl₃) δ: 5.35 (4H, s), 2.76 – 2.35 (8H, m)

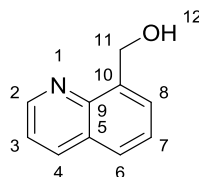
[Rh(COD)DPEphos]ClO₄



DPEphos (0.459 g, 0.852 mmol, 2.1 equiv.) was added to a stirred solution of [Rh(COD)Cl]₂ (0.200 g, 0.406 mmol, 1 equiv.), AgClO₄ (0.176 g, 0.852 mmol, 2.1 equiv.) and degassed DCM (4 mL) producing a red solution which was stirred at rt for 1 h. After leaving to stand the solution was transferred to a second flask and the remaining yellow precipitate washed with DCM (3 × 2 mL) and the combined solutions evaporated under vacuum until 4 mL of solvent remained. The product was crystallised through layering of hexane (4 mL). The resulting red crystals were washed (1:1, DCM—hexane, 2 × 1 mL) and dried under vacuum (0.506 g, 73 %). ¹H NMR (500 MHz, CDCl₃) δ: 7.50-7.31 (22 H, m, ArH), 7.04 – 6.95 (6 H, m, ArH), 4.45 (4H, s), 2.40 – 2.31 (4H, m), 2.17 – 2.09 (4H, m); ³¹P NMR (121 MHz, CDCl₃) δ: 12.99 (d, *J* = 146.4 Hz); MS (ESI): found *M*⁺: 749.1591 (calculated: 749.1609)

7.4.4 Authentic Product Synthesis

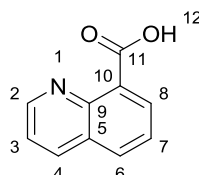
8-Hydroxymethylquinoline **168**



Following a procedure reported by Gurney,²⁰³ NaBH₄ (26.6 mg, 0.703 mmol, 1.1 equiv) was added to a solution of quinoline-8-carbaldehyde **110** (0.100 g, 0.636 mmol, 1 equiv.) in MeOH (4 mL). After stirring for 3 h at rt the reaction was quenched with aqueous NH₄Cl (2 mL) to pH 6, extracted with EtOAc (3 × 15 mL) and washed with brine (30 mL). The organic solution was dried over MgSO₄, filtered and the solvent evaporated to yield a yellow solid. (0.103 g). The product was purified by column chromatography (2:1, pentane—ethylacetate) to give an off white solid **168** (46.3 mg, 46 %).

¹H NMR (500 MHz, CDCl₃) δ: 8.88 (1H, dd, *J*= 4.3, 1.5 Hz, H₂), 8.20 (1H, dd, *J*= 8.4, 1.5 Hz, H₄), 7.76 (1H, d, *J*= 8.3 Hz, H₆), 7.59 (1H, d, *J*= 6.9 Hz, H₈), 7.50 (1H, t, *J*= 8.1 Hz, H₇), 7.45 (1H, dd, *J*= 8.4, 4.3 Hz, H₃), 5.21 (2H, s, H₁₁), 5.06 (1H, s, H₁₂); ¹³C-NMR (125 MHz, CDCl₃) δ: 149.18 (C₂), 147.32 (C₉), 138.30 (C₁₀), 136.97 (C₄), 128.64 (C₅), 127.89 (C₆), 127.56 (C₆), 126.57 (C₇), 121.32 (C₃), 64.99 (C₁₁); Mp: 78-80 °C; MS (ESI): found [M+H]⁺ 160.0758, (calculated: 160.0757). Spectral data are consistent with the literature²³¹

Quinoline-8-carboxylic acid **169**

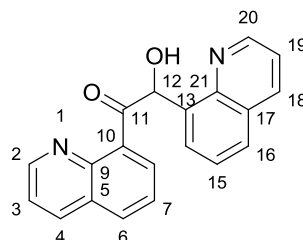


Following a procedure reported by Douglas,²⁰⁴ *n*-BuLi (0.86 mL, 1.38 mmol, 1.2 equiv.) was added dropwise to a stirred solution of 8-bromoquinoline (0.15 mL, 1.15 mmol, 1 equiv) in THF (5 mL) at -78°C. After 30 min the brown solution was poured onto dry ice and stirred and once excess CO₂ had sublimed, the mixture was diluted with water (4 mL) and 1N HCl added to pH 5. The product was extracted with DCM (3 × 30 mL), washed with brine (100 mL), dried over Na₂SO₄ filtered and the solvent evaporated to give a yellow solid (0.164 g) which was recrystallised (EtOH) to give the product (44.3 mg, 26 %).

¹H NMR (500 MHz, CDCl₃) δ: 16.52 (1H, s, H₁₂), 8.94 (1H, dd, *J*= 4.4, 1.6 Hz, H₂), 8.83 (1H, dd, *J*= 7.3, 1.3 Hz, H₈), 8.43 (1H, dd, *J*= 8.3, 1.6 Hz, H₄), 8.12 (1H, dd, *J*= 8.1, 1.3 Hz, H₆), 7.78, (1H, dd, *J*= 8.1, 7.3 Hz, H₇), 7.63 (1H, dd, *J*= 8.3, 4.4 Hz, H₃); ¹³C-NMR (125 MHz,

CDCl₃) δ : 167.31 (C₁₁), 148.62 (C₂), 145.52 (C₉), 138.88 (C₄), 135.59 (C₈), 133.14 (C₆), 128.42 (C₅), 127.54 (C₇), 124.90 (C₁₀), 121.83 (C₃); MS (ESI): found [M+H]⁺ 174.0562. Spectral data are consistent with the literature:²⁰⁴

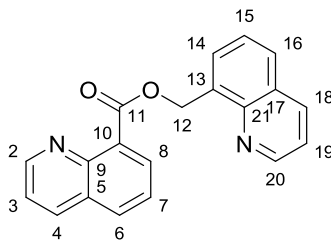
2-Hydroxy-1,2-di(quinolyl-8)ethanone 174



Prepared following a modified procedure for similar compound reported by Blencowe.²⁰⁵ Triethylamine (0.135 mL, 0.957 mmol) was added to a stirred solution of quinoline-8-carbaldehyde (500 mg, 3.18 mmol) in anhydrous ethanol (10 mL). 3-Benzyl-5-(2-hydroxyethyl)-4-methyl-1,3-thiazolium chloride (0.173 g, 0.637 mmol) was added resulting in a deep pink / purple solution. After heating under reflux for 22.5 h the deep red solution was quenched with water (60 mL) and extracted with DCM (3 x 60 mL) and sodium chloride. The orange organic layer was washed with brine (100 mL), dried over MgSO₄, filtered and the solvent removed under vacuum to yield an orange oil. The product was purified by column chromatography (hexane:ethylacetate 1:1, R_f: 0.36), to give a pale yellow oil (0.248 g, 50 %). The product was recrystallised from DCM and pentane to give colourless crystals (No yield obtained as due to instability of the product, multiple small scale recrystallisations were performed before each analysis).

¹H NMR (500 MHz, CDCl₃) δ : 8.99 (1H, dd, J = 4.3, 1.7 Hz, H₂), 8.74 (1H, dd, J = 4.3, 1.7 Hz, H₂₀), 8.20 (1H, dd, J = 8.2, 1.7 Hz, H₄), 8.09 (1H, dd, J = 8.2, 1.7 Hz, H₁₈), 7.91 (1H, d, J = 7.1 Hz, H₁₄), 7.89 – 7.86 (2H, m, H₆ & H₈), 7.68 (1H, dd, J = 8.2, 1.1 Hz, H₁₆), 7.50 (1H, dd, J = 8.0, 7.3 Hz, H₇), 7.48 (1H, dd, J = 8.3, 4.2 Hz, H₃), 7.46 (1H, dd, J = 8.1, 7.4 Hz, H₁₅), 7.34 (1H, dd, J = 8.3, 4.2 Hz, H₁₉), 6.98 (1H, s, OH), 6.88 (1H, s, H₁₂); ¹³C NMR (125 MHz, CDCl₃) δ : 204.7 (C₁₁), 150.3 (C₂), 149.1 (C₂₀), 145.9 (C₂₁), 145.2 (C₉), 139.0 (C₁₀), 137.4 (C₁₃), 137.1 (C₄), 136.4 (C₁₈), 131.4 (C₈), 131.1 (C₆), 129.1 (C₁₄), 128.3 (C₅ / C₁₇), 128.1 (C₅ / C₁₇), 127.7 (C₁₆), 126.5 (C₇), 126.5 (C₁₅), 121.6 (C₃), 121.1 (C₁₉), 77.6 (C₁₂); ATR-FT-IR (cm⁻¹): 3037 (br, OH stretch), 2895 (w, CH stretch), 1674 (m, C=O stretch), 1609, 1593 (m, C-C in ring stretch), 1568 (m, C=C stretch), 1498 (m, C=C stretch); HRMS (ESI): found [M+H]⁺: 315.1132 (calculated: 315.1128).

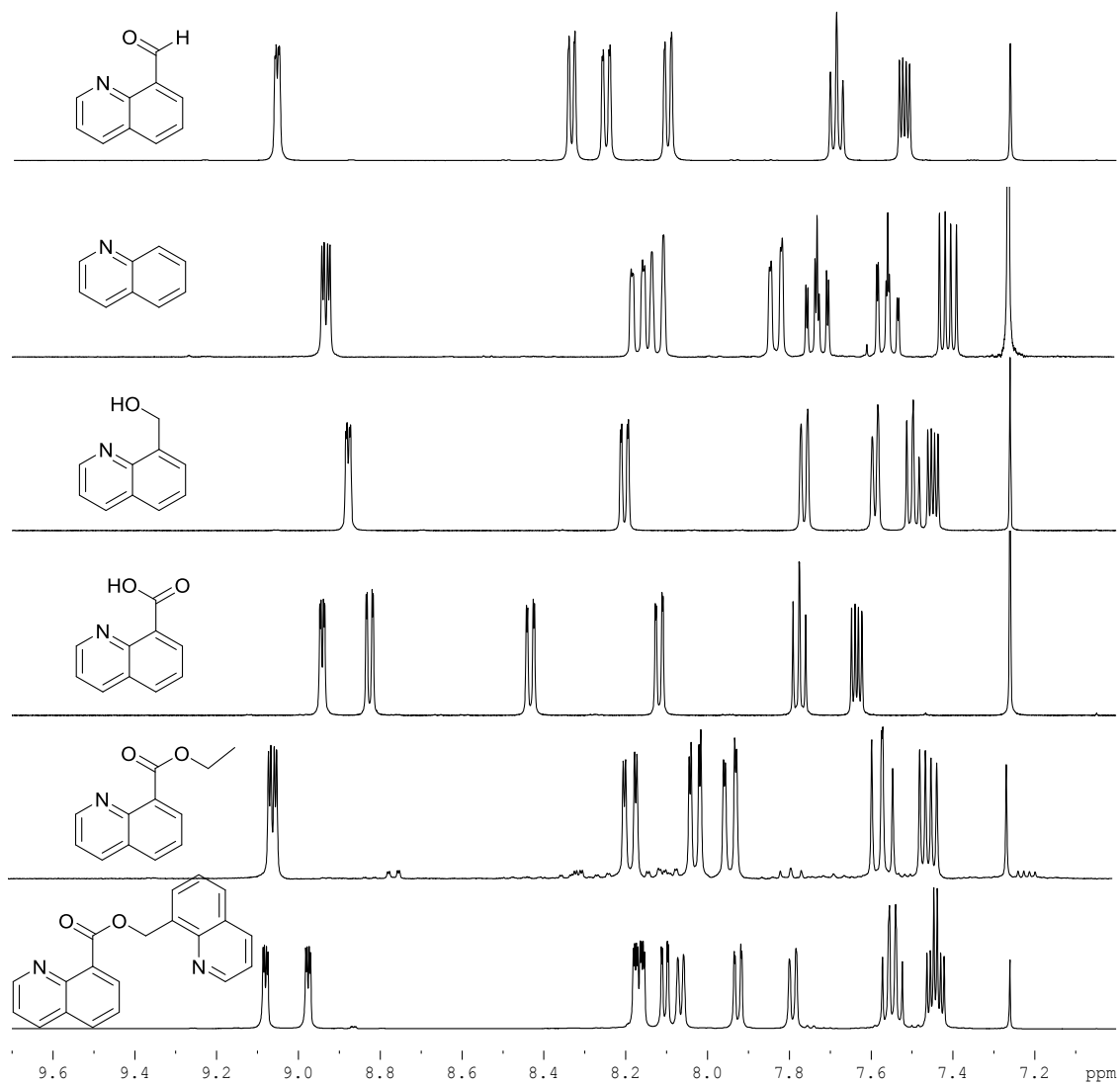
Quinolin-8-ylmethyl 8-quinolate 170



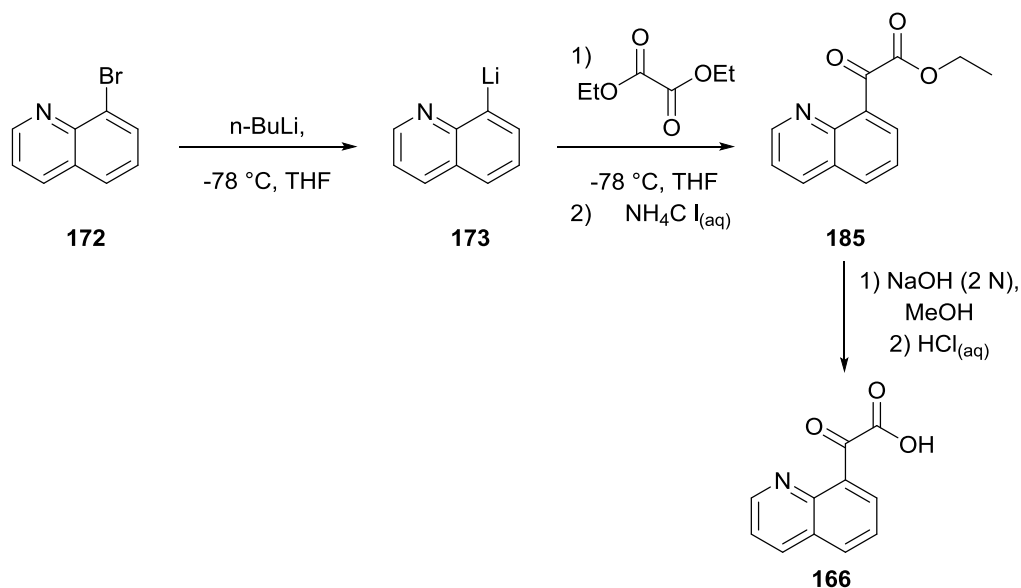
Quinoline-8-carbaldehyde (0.119 g, 0.759 mmol, 1 equiv.), [Rh(NBD)DPPB]ClO₄ (0.053 g, 0.075, 0.1 equiv.) in degassed, anhydrous acetonitrile was stirred at 50 °C for 18 h. After cooling, the solvent was evaporated under vacuum and the product purified by column chromatography (pentane – ethylacetate, 1:1, R_f: 0.26) to give a colourless oil which crystallised on storage overnight under N₂ (0.055 g, 46 %).

¹H NMR (500 MHz, CDCl₃) δ: 9.08 (1H, dd, *J* = 4.2, 1.8 Hz, H₂), 8.98 (1H, dd, *J* = 4.2, 1.8 Hz, H₂₀), 8.18 (1H, dd, *J* = 3.8, 1.7 Hz, H₄), 8.16 (1H, dd, *J* = 3.8, 1.8 Hz, H₁₈), 8.10 (1H, dd, *J* = 7.1, 1.3 Hz, H₈), 8.06 (1H, dd, *J* = 7.0, 0.6, H₁₄), 7.92 (1H, dd, *J* = 8.3, 1.4, H₆), 7.79 (1H, dd, *J* = 8.0, 0.7 Hz, H₁₆), 7.58 – 7.52 (2H, m, H₇ & H₁₅), 7.45 (1H, dd, *J* = 8.4, 4.2 Hz, H₃), 7.43 (1H, dd, *J* = 8.3, 4.1 Hz), 6.27 (2H, s, H₁₂); ¹³C NMR (125 MHz, CDCl₃) δ: 167.7 (C₁₁), 151.6 (C₂), 149.9 (C₂₀), 146.3 (C₂₁), 145.9 (C₉), 136.3 (C₁₈), 136.2 (C₄), 134.6 (C₁₃), 131.9 (C₁₀), 131.4 (C₆), 130.8 (C₈), 128.8 (C₁₄), 128.5 (C₅ / C₁₇), 128.2 (C₅ / C₁₇), 128.0 (C₁₆), 126.4 (C₇ / C₁₅), 125.7 (C₇ / C₁₅), 121.7 (C₃), 121.4 (C₁₉), 64.0 (C₁₂); ATR-FT-IR (cm⁻¹): 3069 (CH stretch), 3010, (CH stretch), 2958 (CH stretch), 1721 (C=O stretch, ester); HRMS (ESI): found [M+H]⁺ 315.1136 (Calculated: 315.1128)

¹H NMR spectra used to assign products from the reactions of quinoline-8-carbaldehyde:



2-Oxidanylidene-2-quinolin-8-yl-ethanoic acid sodium acetate salt **166**



n-BuLi (1.72 mL, 1.6M, 2.76 mmol, 1.2 equiv.) was added dropwise to a solution of 8-bromoquinoline (0.30 mL, 2.30 mmol, 1 equiv.) in THF (10 mL) at -78 °C resulting in an orange/brown solution. After 70 min the solution was added to diethyl oxalate (0.35 mL, 2.53 mmol, 1.1 equiv.) in THF (1 mL) and stirred for 60 min at -78 °C. The reaction mixture was warmed to rt and quenched with aqueous NH₄Cl (15 mL), extracted with diethyl ether (3 × 20 mL) and washed with brine (50 mL). Organics were dried over MgSO₄, filtered and the solvent evaporated to give an orange oil **185** (0.446 g, 85 %) which was used in next step without purification.

A solution of keto ester **185** (217 mg, 0.947 mmol) in MeOH (3 mL) was cooled to 0 °C and aqueous NaOH (3 mL, 2N) added and stirred at rt for 90 min. MeOH was removed under vacuum and the remaining aqueous solution washed at pH 9 with EtOAc (2 x 20 mL). The aqueous solution was acidified to pH 5 with aqueous 1N HCl and washed with EtOAc (2 x 20 mL). The remaining aqueous solution reduced under vacuum to give a white solid (0.231 g) which was dissolved in MeOH and filtered to remove NaCl. Product recrystallised through addition of diethyl ether to a solution of the product in minimum amount of MeOH. Crystals prepared for X-ray analysis through vapour diffusion of diethyl ether into MeOH over three days. For crystal structure see Appendix 3 – measured and resolved by Dr Chris Pask.

¹H NMR (500 MHz, D₆-DMSO) δ: 8.88 (1H, dd, *J* = 4.1, 1.8 Hz, H₂), 8.39 (1H, dd, *J* = 8.3, 1.8 Hz, H₄), 8.08 (1H, dd, *J* = 8.1, 1.3 Hz, H₆), 7.92 (1H, dd, *J* = 7.1, 1.3 Hz, H₈), 7.64 (1H, dd, *J* = 8.1, 7.1 Hz, H₇), 7.55 (1H, dd, *J* = 8.3, 4.1 Hz, H₃), 1.63 (5H, s, Ac). ¹³C NMR (125 MHz, D₆-DMSO) δ: 199.53 (C₁₁), 175.34 (acetate), 168.71 (C₁₂), 150.53 (C₂), 145.54 (C₉), 138.11 (C₁₀), 136.13 (C₄), 130.72 (C₆), 129.46 (C₈), 127.66 (C₅), 125.94 (C₇), 121.64 (C₃), 25.23 (acetate).

MS (ESI): found $[M+H]^+$ 202.0525. ATR-FT-IR (cm^{-1}): 3736 (br, w), 3417 (br, w), 3280 (br, w), 3172 (br, w, CH stretch), 1633 (m, C=O stretch), 1558 (s, CO_2 out of phase stretch), 1408 (s, CO_2 in phase stretch), 790 (m), 641 (m), 623 (m), 510 (s). For crystal structure see Appendix 4 – measured and resolved by Dr Chris Pask

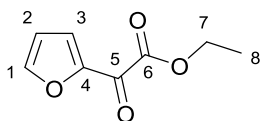
7.4.5 General Procedures Furfural 159 as Substrate

General procedure for screening reaction of Furfural with CO_2 :

Furfural **159** (49.7 μL , 0.6 mmol, 1 equiv.), Rh catalyst (0.06 mmol, 10 mol%) and a magnetic stirrer bar were placed in a high pressure reaction vessel and flushed with nitrogen. Degassed solvent (3 mL), and base if used (0.6 mmol, 1 equiv.), was added to the vessel, sealed and flushed with CO_2 . The vessel was pressurised to 40 bar with CO_2 , heated to 100 $^\circ\text{C}$ and stirred overnight. The vessel was cooled, vented through solvent and the reaction products were isolated through evaporation of the solvent under vacuum.

7.4.6 Authentic Product Synthesis

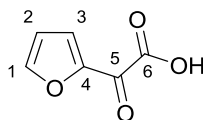
Ethyl 2-(2-furyl)-2-oxo acetate²¹² **188**



Prepared following a procedure reported by de Vries.²¹² *n*-BuLi (4.1 mL, 1.6 M, 6.6 mmol, 1.1 equiv.) was added dropwise at -78 $^\circ\text{C}$ to a stirred solution of furan (0.44 mL, 6 mmol) in THF (18 mL). After warming slowly over 2 h to rt, the resulting pale yellow solution was cooled to -78 $^\circ\text{C}$ and added dropwise over 25 min to a solution of diethyl oxalate (0.90 mL, 6.6 mmol, 1.1 equiv.) in THF (10 mL) at -78 $^\circ\text{C}$. After stirring for 1 h the solution was warmed to rt and quenched with aqueous NH_4Cl , extracted with diethylether (3 x 50 mL) and washed with brine (100 mL). The organics were dried over MgSO_4 , filtered and the solvent evaporated under vacuum to give a yellow/orange oil/solid (0.504 g, 50 %) which was purification by column chromatography (pentane – EtOAc, 6:1, R_f : 0.2) to give the keto ester as a pale yellow oil (0.323 g, 32 %)

^1H NMR (500 MHz, CDCl_3) δ : 7.75 (1H, dd, J = 1.6, 0.7 Hz, H_1), 7.71 (1H, dd, J = 3.7, 0.7 Hz, H_3), 6.62 (1H, dd, J = 3.7, 1.6 Hz, H_2), 4.41 (2H, q, J = 7.1 Hz, H_7), 1.41 (3H, t, J = 7.1 Hz, H_8); ^{13}C NMR (125 MHz, CDCl_3) δ : 171.3 (C_5), 161.2 (C_6), 149.9 (C_4), 149.6 (C_1), 124.8 (C_3), 113.1 (C_2), 62.8 (C_7), 14.1 (C_8) MS (ESI): found $[M+\text{Na}]^+$ 191.0317 (calculated: 191.0315) ATR-FT-IR (cm^{-1}): 3142 (CH stretch), 2986 (CH stretch), 1732 (C=O ester), 1668 (C=O ketone). Spectral data consistent with those reported in literature.²¹²

2-Oxo-2-furan-2-ylacetic acid **186**

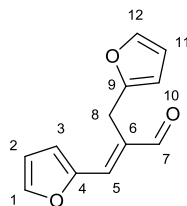


Aqueous NaOH (3.8 mL, 1 M, 3.84 mmol, 2 equiv) was added to a solution of the keto ester **188** (300 mg, 1.78 mmol) in ethanol (7.5 mL) and stirred at rt for 15 min. The solution was acidified to pH 1 at 0 °C with aqueous HCl (2 M), extracted with diethyl ether (2 x 50 mL), dried over MgSO₄, filtered and the solvent evaporated under vacuum to give a red/purple oil which formed a black solid after storing overnight under N₂. The black precipitate would not dissolve and therefore the product was washed with DCM, filtered and solvent removed under vacuum to give a purple / pink solid which was recrystallised by diffusion of pentane into DCM or MeOH to give white crystals. Crystals for X-ray structure obtained by repeating crystallisation.

¹H NMR (500 MHz, CDCl₃) δ: 8.19 (1H, d, *J* = 3.7 Hz, H₃), 8.05 (1H, br s, OH), 7.86 (1H, s, H₁), 6.70 (1H, dd, *J* = 3.6, 1.3 Hz, H₂); ¹³C NMR (125 MHz, CDCl₃) δ: 169.9 (C₅), 159.1 (C₆), 151.3 (C₁), 148.6 (C₄), 129.0 (C₃), 114.0 (C₂); MS (ESI): found [M-H] 139.0052 (calculated: 139.0031 – 15 ppm error); ATR-FT-IR (cm⁻¹): 1742 (C=O ketone), 1630 (COOH out of phase stretch), 1614 (COOH in phase stretch). For crystal structure see Appendix 4 – measured and resolved by Dr Chris Pask.

7.4.7 Characterisation of Reaction Product Component A **193**

3-(Furan-2-yl)-2-[(furan-2-yl)methyl]prop-2-enal **193**



¹H NMR (500 MHz, CDCl₃) δ: 9.55 (1H, s, H₇), 7.63 (1H, d, *J* = 1.6 Hz, H₁), 7.27 (1H, d, *J* = 1.9 Hz, H₁₂), 7.13 (1H, s, H₅), 6.84 (1H, d, *J* = 3.4 Hz, H₃), 6.56 (1H, dd, *J* = 3.5, 1.8 Hz, H₂), 6.23 (1H, dd, *J* = 3.1, 1.9 Hz, H₁₁), 5.97 (1H, m, H₁₀), 4.03 (2H, s, H₈); ¹³C-NMR (125 MHz, CDCl₃) δ: 193.3 (C₇), 152.3 (C₉), 150.9 (C₄), 146.0 (C₁), 141.3 (C₁₂), 136.3 (C₅), 134.6 (C₆), 117.9 (C₃), 112.9 (C₂), 110.5 (C₁₁), 105.9 (C₁₀), 23.9 (C₈); MS (ESI): found [M+H]⁺ 203.0713 (calculated: 203.0703) LCMS (ESI): found 224.9 [M+Na]⁺

References

1. M. North and P. Styring, *Faraday Discuss.*, 2015, **183**, 489-502.
2. M. Aresta and A. Dibenedetto, *Dalton Trans.*, 2007, 2975-2992.
3. W. Leitner, *Coord. Chem. Rev.*, 1996, **153**, 257-284.
4. M. Poliakoff, W. Leitner and E. S. Streng, *Faraday Discuss.*, 2015, **183**, 9-17.
5. C. Song, *Catal. Today*, 2006, **115**, 2-32.
6. M. Bohnet, *Ullmann's encyclopedia of industrial chemistry*, Wiley-VCH, Weinheim, 2003.
7. M. North, R. Pasquale and C. Young, *Green Chem.*, 2010, **12**, 1514-1539.
8. M. North, *Chimica Oggi-Chemistry Today*, 2012, **30**, 3-5.
9. J. Meléndez, M. North and R. Pasquale, *Eur. J. Inorg. Chem.*, 2007, **2007**, 3323-3326.
10. C. Beattie, M. North, P. Villuendas and C. Young, *J. Org. Chem.*, 2013, **78**, 419-426.
11. M. North, B. Wang and C. Young, *Energy Environ. Sci.*, 2011, **4**, 4163-4170.
12. A. M. Chapman, C. Keyworth, M. R. Kember, A. J. J. Lennox and C. K. Williams, *ACS Catal.*, 2015, **5**, 1581-1588.
13. N. Yi, J. Unruangsri, J. Shaw and C. K. Williams, *Faraday Discuss.*, 2015, **183**, 67-82.
14. J. Langanke, A. Wolf, J. Hofmann, K. Bohm, M. A. Subhani, T. E. Muller, W. Leitner and C. Gurtler, *Green Chem.*, 2014, **16**, 1865-1870.
15. N. v. d. Assen, A. Sternberg, A. Katelhon and A. Bardow, *Faraday Discuss.*, 2015, **183**, 291-307.
16. E. E. Benson, C. P. Kubiak, A. J. Sathrum and J. M. Smieja, *Chem. Soc. Rev.*, 2009, **38**, 89-99.
17. <http://carbonrecycling.is/>, Accessed March 2017.
18. E. Graf and W. Leitner, *Chem. Commun.*, 1992, 623-624.
19. P. G. Jessop, T. Ikariya and R. Noyori, *Nature*, 1994, **368**, 231-233.

20. S. Bontemps, L. Vendier and S. Sabo-Etienne, *J. Am. Chem. Soc.*, 2014, **136**, 4419-4425.
21. T. Matsuo and H. Kawaguchi, *J. Am. Chem. Soc.*, 2006, **128**, 12362-12363.
22. K. P. Kuhl, T. Hatsukade, E. R. Cave, D. N. Abram, J. Kibsgaard and T. F. Jaramillo, *J. Am. Chem. Soc.*, 2014, **136**, 14107-14113.
23. M. Cokoja, C. Bruckmeier, B. Rieger, W. A. Herrmann and F. E. Kuhn, *Angew. Chem. Int. Ed. Engl.*, 2011, **50**, 8510-8537.
24. K. Huang, C.-L. Sun and Z.-J. Shi, *Chem. Soc. Rev.*, 2011, **40**, 2435-2452.
25. D. H. Gibson, *Chem. Rev.*, 1996, **96**, 2063-2096.
26. Y. Ito and H. Ushitora, *Tetrahedron*, 2006, **62**, 226-235.
27. C. Perinu, B. Arstad, A. M. Bouzga and K.-J. Jens, *J. Phys. Chem. B*, 2014, **118**, 10167-10174.
28. E. R. Pérez, R. H. A. Santos, M. T. P. Gambardella, L. G. M. de Macedo, U. P. Rodrigues-Filho, J.-C. Launay and D. W. Franco, *J. Org. Chem.*, 2004, **69**, 8005-8011.
29. D. J. Heldebrant, P. G. Jessop, C. A. Thomas, C. A. Eckert and C. L. Liotta, *J. Org. Chem.*, 2005, **70**, 5335-5338.
30. C. Villiers, J.-P. Dognon, R. Pollet, P. Thuéry and M. Ephritikhine, *Angew. Chem. Int. Ed.*, 2010, **49**, 3465-3468.
31. H. A. Duong, T. N. Tekavec, A. M. Arif and J. Louie, *Chem. Commun.*, 2004, 112-113.
32. H. Zhou, G.-X. Wang, W.-Z. Zhang and X.-B. Lu, *ACS Catal.*, 2015, **5**, 6773-6779.
33. C. C. Chong and R. Kinjo, *Angew. Chem. Int. Ed.*, 2015, **54**, 12116-12120.
34. C. M. Mömmling, E. Otten, G. Kehr, R. Fröhlich, S. Grimme, D. W. Stephan and G. Erker, *Angew. Chem. Int. Ed.*, 2009, **48**, 6643-6646.
35. G. Fiorani, W. Guo and A. W. Kleij, *Green Chem.*, 2015, **17**, 1375-1389.
36. M. Costa, G. P. Chiusoli, D. Taffurelli and G. Dalmonego, *J. Chem. Soc., Perkin Trans. I*, 1998, 1541-1546.
37. S. N. Riduan, Y. Zhang and J. Y. Ying, *Angew. Chem. Int. Ed.*, 2009, **48**, 3322-3325.
38. M.-A. Courtemanche, M.-A. Légaré, L. Maron and F.-G. Fontaine, *J. Am. Chem. Soc.*, 2013, **135**, 9326-9329.

39. J. Hu, J. Ma, Q. Zhu, Z. Zhang, C. Wu and B. Han, *Angew. Chem. Int. Ed.*, 2015, **54**, 5399-5403.
40. C. J. Whiteoak, A. Nova, F. Maseras and A. W. Kleij, *ChemSusChem*, 2012, **5**, 2032-2038.
41. Y. Kayaki, M. Yamamoto and T. Ikariya, *Angew. Chem. Int. Ed.*, 2009, **48**, 4194-4197.
42. Y. Tsutsumi, K. Yamakawa, M. Yoshida, T. Ema and T. Sakai, *Org. Lett.*, 2010, **12**, 5728-5731.
43. N. D. Ca, B. Gabriele, G. Ruffolo, L. Veltri, T. Zanetta and M. Costa, *Adv. Synth. Catal.*, 2011, **353**, 133-146.
44. M. H. Anthofer, M. E. Wilhelm, M. Cokoja, I. I. E. Markovits, A. Pothig, J. Mink, W. A. Herrmann and F. E. Kuhn, *Catal. Sci. Technol.*, 2014, **4**, 1749-1758.
45. M. H. Anthofer, M. E. Wilhelm, M. Cokoja, M. Drees, W. A. Herrmann and F. E. Kühn, *ChemCatChem*, 2015, **7**, 94-98.
46. F.-G. Fontaine and D. W. Stephan, *Current Opinion in Green and Sustainable Chemistry*, 2017, **3**, 28-32.
47. F. J. Fernandez-Alvarez, A. M. Aitani and L. A. Oro, *Catal. Sci. Technol.*, 2014, **4**, 611-624.
48. N. J. Lawrence, M. D. Drew and S. M. Bushell, *J. Chem. Soc., Perkin Trans. 1*, 1999, 3381-3391.
49. S. N. Riduan, J. Y. Ying and Y. Zhang, *ChemCatChem*, 2013, **5**, 1490-1496.
50. M.-A. Courtemanche, M.-A. Legare, E. Rochette and F.-G. Fontaine, *Chem. Commun.*, 2015, **51**, 6858-6861.
51. S. N. Riduan, J. Y. Ying and Y. Zhang, *J. Catal.*, 2016, **343**, 46-51.
52. A. Berkefeld, W. E. Piers and M. Parvez, *J. Am. Chem. Soc.*, 2010, **132**, 10660-10661.
53. A. Schafer, W. Saak, D. Haase and T. Muller, *Angew. Chem. Int. Ed.*, 2012, **51**, 2981-2984.
54. M. A. Courtemanche, M. A. Legare, L. Maron and F. G. Fontaine, *J. Am. Chem. Soc.*, 2014, **136**, 10708-10717.
55. C. Das Neves Gomes, E. Blondiaux, P. Thuéry and T. Cantat, *Chem. Eur. J.*, 2014, **20**, 7098-7106.
56. T. Wang and D. W. Stephan, *Chem. Commun.*, 2014, **50**, 7007-7010.

57. A. E. Ashley, A. L. Thompson and D. O'Hare, *Angew. Chem. Int. Ed.*, 2009, **48**, 9839-9843.
58. M.-A. Courtemanche, A. P. Pulis, E. Rochette, M.-A. Legare, D. W. Stephan and F.-G. Fontaine, *Chem. Commun.*, 2015, **51**, 9797-9800.
59. C. Das Neves Gomes, O. Jacquet, C. Villiers, P. Thuéry, M. Ephritikhine and T. Cantat, *Angew. Chem. Int. Ed.*, 2012, **51**, 187-190.
60. A. Tlili, E. Blondiaux, X. Frogneux and T. Cantat, *Green Chem.*, 2015, **17**, 157-168.
61. Z.-Z. Yang, L.-N. He, J. Gao, A.-H. Liu and B. Yu, *Energy Environ. Sci.*, 2012, **5**, 6602-6639.
62. S. Ding and N. Jiao, *Angew. Chem. Int. Ed.*, 2012, **51**, 9226-9237.
63. C. Gerack and L. McElwee-White, *Molecules*, 2014, **19**, 7689.
64. P. Haynes, L. H. Slaugh and J. F. Kohnle, *Tetrahedron Lett.*, 1970, **11**, 365-368.
65. P. G. Jessop, Y. Hsiao, T. Ikariya and R. Noyori, *J. Am. Chem. Soc.*, 1994, **116**, 8851-8852.
66. O. Krocher, R. A. Koppel and A. Baiker, *Chem. Commun.*, 1997, 453-454.
67. J. Liu, C. Guo, Z. Zhang, T. Jiang, H. Liu, J. Song, H. Fan and B. Han, *Chem. Commun.*, 2010, **46**, 5770-5772.
68. C. Ziebart, C. Federsel, P. Anbarasan, R. Jackstell, W. Baumann, A. Spannenberg and M. Beller, *J. Am. Chem. Soc.*, 2012, **134**, 20701-20704.
69. P. Munshi, D. J. Heldebrant, E. P. McKoon, P. A. Kelly, C. C. Tai and P. G. Jessop, *Tetrahedron Lett.*, 2003, **44**, 2725-2727.
70. H. Ishida, H. Tanaka, K. Tanaka and T. Tanaka, *Chem. Lett.*, 1987, **16**, 597-600.
71. M. Oestreich, J. Hermeke and J. Mohr, *Chem. Soc. Rev.*, 2015, **44**, 2202-2220.
72. O. Jacquet, C. D. Gomes, M. Ephritikhine and T. Cantat, *J. Am. Chem. Soc.*, 2012, **134**, 2934-2937.
73. L. Hao, Y. Zhao, B. Yu, Z. Yang, H. Zhang, B. Han, X. Gao and Z. Liu, *ACS Catal.*, 2015, **5**, 4989-4993.
74. S. Das, F. D. Bobbink, S. Bulut, M. Soudani and P. J. Dyson, *Chem. Commun.*, 2016, **52**, 2497-2500.

75. B. Dong, L. Wang, S. Zhao, R. Ge, X. Song, Y. Wang and Y. Gao, *Chem. Commun.*, 2016, **52**, 7082-7085.
76. M. Hulla, F. D. Bobbink, S. Das and P. J. Dyson, *ChemCatChem*, 2016, **8**, 3338-3342.
77. X.-F. Liu, R. Ma, C. Qiao, H. Cao and L.-N. He, *Chem. Eur. J.*, 2016, **22**, 16489-16493.
78. H. Lv, Q. Xing, C. Yue, Z. Lei and F. Li, *Chem. Commun.*, 2016, **52**, 6545-6548.
79. J. Song, B. Zhou, H. Liu, C. Xie, Q. Meng, Z. Zhang and B. Han, *Green Chem.*, 2016, **18**, 3956-3961.
80. B. J. Wang and Z. X. Cao, *RSC Advances*, 2013, **3**, 14007-14015.
81. F. Huang, G. Lu, L. Zhao, H. Li and Z.-X. Wang, *J. Am. Chem. Soc.*, 2010, **132**, 12388-12396.
82. H. Zhou, W.-Z. Zhang, C.-H. Liu, J.-P. Qu and X.-B. Lu, *J. Org. Chem.*, 2008, **73**, 8039-8044.
83. Q. Zhou and Y. Li, *J. Am. Chem. Soc.*, 2015, **137**, 10182-10189.
84. K. Motokura, N. Takahashi, D. Kashiwame, S. Yamaguchi, A. Miyaji and T. Baba, *Catal. Sci. Technol.*, 2013, **3**, 2392-2396.
85. L. González-Sebastián, M. Flores-Alamo and J. J. García, *Organometallics*, 2013, **32**, 7186-7194.
86. X. Frogneux, O. Jacquet and T. Cantat, *Catal. Sci. Technol.*, 2014, **4**, 1529-1533.
87. K. Motokura, M. Naijo, S. Yamaguchi, A. Miyaji and T. Baba, *Chem. Lett.*, 2015, **44**, 1217-1219.
88. D. B. Nale and B. M. Bhanage, *Synlett*, 2016, **27**, 1413-1417.
89. O. Jacquet, X. Frogneux, C. D. Gomes and T. Cantat, *Chem. Sci.*, 2013, **4**, 2127-2131.
90. Y. H. Li, X. J. Fang, K. Junge and M. Beller, *Angew. Chem. Int. Ed.*, 2013, **52**, 9568-9571.
91. S. Das, F. D. Bobbink, G. Laurenczy and P. J. Dyson, *Angew. Chem. Int. Ed.*, 2014, **53**, 12876-12879.
92. Z. Yang, B. Yu, H. Zhang, Y. Zhao, G. Ji, Z. Ma, X. Gao and Z. Liu, *Green Chem.*, 2015, **17**, 4189-4193.
93. H. Niu, L. Lu, R. Shi, C.-W. Chiang and A. Lei, *Chem. Commun.*, 2017.

94. E. Blondiaux, J. Pouessel and T. Cantat, *Angew. Chem. Int. Ed.*, 2014, **53**, 12186-12190.
95. W.-C. Chen, J.-S. Shen, T. Jurca, C.-J. Peng, Y.-H. Lin, Y.-P. Wang, W.-C. Shih, G. P. A. Yap and T.-G. Ong, *Angew. Chem. Int. Ed.*, 2015, **54**, 15207-15212.
96. X.-F. Liu, C. Qiao, X.-Y. Li and L.-N. He, *Green Chem.*, 2017, **19**, 1726-1731.
97. X. Frogneux, E. Blondiaux, P. Thuéry and T. Cantat, *ACS Catal.*, 2015, **5**, 3983-3987.
98. J. E. Taylor, S. D. Bull and J. M. J. Williams, *Chem. Soc. Rev.*, 2012, **41**, 2109-2012.
99. M. Costa, G. P. Chiusoli and M. Rizzardi, *Chem. Commun.*, 1996, 1699-1700.
100. E. R. Pérez, M. O. da Silva, V. C. Costa, U. P. Rodrigues-Filho and D. W. Franco, *Tetrahedron Lett.*, 2002, **43**, 4091-4093.
101. A. Barbarini, R. Maggi, A. Mazzacani, G. Mori, G. Sartori and R. Sartorio, *Tetrahedron Lett.*, 2003, **44**, 2931-2934.
102. W. Clegg, R. W. Harrington, M. North and R. Pasquale, *Chem. Eur. J.*, 2010, **16**, 6828-6843.
103. J. C. Meredith, K. P. Johnston, J. M. Seminario, S. G. Kazarian and C. A. Eckert, *J. Phys. Chem.*, 1996, **100**, 10837-10848.
104. X. Zhang, Y.-B. Jia, X.-B. Lu, B. Li, H. Wang and L.-C. Sun, *Tetrahedron Lett.*, 2008, **49**, 6589-6592.
105. T. Mizuno, N. Okamoto, T. Ito and T. Miyata, *Tetrahedron Lett.*, 2000, **41**, 1051-1053.
106. R. Nicholls, S. Kaufhold and B. N. Nguyen, *Catal. Sci. Technol.*, 2014, **4**, 3458-3462.
107. P. V. Kortunov, M. Siskin, L. S. Baugh and D. C. Calabro, *Energy & Fuels*, 2015, **29**, 5940-5966.
108. P. R. Edwards, J. R. Hiscock and P. A. Gale, *Tetrahedron Lett.*, 2009, **50**, 4922-4924.
109. V. Blažek Bregović, N. Basarić and K. Mlinarić-Majerski, *Coord. Chem. Rev.*, 2015, **295**, 80-124.
110. A. Gennaro, A. A. Isse and E. Vianello, *J. Electroanal. Chem.*, 1990, **289**, 203-215.
111. D. Knausz, A. Meszticzky, L. Szakács, B. Csákvári and K. Ujszászy, *J. Organomet. Chem.*, 1983, **256**, 11-21.
112. M. Mörtl, D. Knausz, Z. Kolos, L. Szakács and B. Csákvári, *J. Organomet. Chem.*, 1994, **482**, 183-185.

113. J. Chen, L. Falivene, L. Caporaso, L. Cavallo and E. Y. X. Chen, *J. Am. Chem. Soc.*, 2016, **138**, 5321-5333.
114. G. Buechi and H. Wuest, *J. Am. Chem. Soc.*, 1978, **100**, 294-295.
115. M. Trommer, W. Sander and A. Patyk, *J. Am. Chem. Soc.*, 1993, **115**, 11775-11783.
116. M. Sawall and K. Neymeyr, "Current Applications of Chemometrics" ed. M. Khanmohammadi, Chapter 6, pages 97-134, Nova Science Publishers 2014.
117. J. Jaumot, R. Gargallo, A. de Juan and R. Tauler, *Chemom. Intell. Lab. Syst.*, 2005, **76**, 101-110.
118. K. Kraushaar, C. Wiltzsch, J. Wagler, U. Böhme, A. Schwarzer, G. Roewer and E. Kroke, *Organometallics*, 2012, **31**, 4779-4785.
119. C. D. F. Konigs, M. F. Muller, N. Aiguabella, H. F. T. Klare and M. Oestreich, *Chem. Commun.*, 2013, **49**, 1506-1508.
120. T. Tsuchimoto, Y. Iketani and M. Sekine, *Chem. Eur. J.*, 2012, **18**, 9500-9504.
121. L. Greb, S. Tamke and J. Paradies, *Chem. Commun.*, 2014, **50**, 2318-2320.
122. R. J. P. Corriu, D. Leclercq, P. H. Mutin, J. M. Planeix and A. Vioux, *J. Organomet. Chem*, 1991, **406**, C1-C4.
123. J.-M. Denis, Z. Pellerin, P. Guenot, M. Letulle and J.-L. Ripoll, *Chem. Ber.*, 1992, **125**, 1397-1399.
124. J. X. Wang, A. K. Dash, J. C. Berthet, M. Ephritikhine and M. S. Eisen, *J. Organomet. Chem*, 2000, **610**, 49-57.
125. N. W. Mitzel, A. Schier, H. Beruda and H. Schmidbaur, *Chem. Ber.*, 1992, **125**, 1053-1059.
126. H. Breederveld, *Recl. Trav. Chim. Pays-Bas*, 1962, **81**, 276-278.
127. R. H. Cragg and M. F. Lappert, *J. Chem. Soc. (A)*, 1966, 82-85.
128. F.-T. Chiu, Y. H. Chang, G. Özkan, G. Zon, K. C. Fichter and L. R. Phillips, *J. Pharm. Sci.*, 1982, **71**, 542-551.
129. M. T. Zoeckler and R. M. Laine, *J. Org. Chem.*, 1983, **48**, 2539-2543.
130. C. J. Smith, T. R. Early, A. B. Holmes and R. E. Shute, *Chem. Commun.*, 2004, 1976-1977.

131. D. Lin-Vien, N. B. Colthup, W. G. Fateley and J. G. Grasselli, in *The Handbook of Infrared and Raman Characteristic Frequencies of Organic Molecules*, Academic Press, San Diego, Editon edn., 1991, pp. 117-154.
132. A. D. Kirilin, A. A. Dokuchaev, I. N. Menchaikina, E. V. Semenova, N. B. Sokova and E. A. Chernyshev, *Russ. Chem. Bull.*, 1996, **45**, 2192-2195.
133. S. Tanaka, T. Yamamura, S. Nakane and M. Kitamura, *Chem. Commun.*, 2015, **51**, 13110-13112.
134. D. Lin-Vien, N. B. Colthup, W. G. Fateley and J. G. Grasselli, in *The Handbook of Infrared and Raman Characteristic Frequencies of Organic Molecules*, Academic Press, San Diego, Editon edn., 1991, pp. 251-261.
135. P. Deglmann, E. Ember, P. Hofmann, S. Pitter and O. Walter, *Chem. Eur. J.*, 2007, **13**, 2864-2879.
136. S. Itagaki, K. Yamaguchi and N. Mizuno, *J. Mol. Catal. A: Chem.*, 2013, **366**, 347-352.
137. C.H. Lee, E.J. Lee, S.W. Jung, J.A. Lee, B.R. Lee, B.Y. Lee, WO2008/84931, 2008.
138. K. Zumbansen, A. Döhring and B. List, *Adv. Synth. Catal.*, 2010, **352**, 1135-1138.
139. I. M. Kolthoff, M. K. Chantooni and S. Bhowmik, *J. Am. Chem. Soc.*, 1968, **90**, 23-28.
140. J. F. Coetzee and G. R. Padmanabhan, *J. Am. Chem. Soc.*, 1965, **87**, 5005-5010.
141. P. Arya, J. Boyer, R. J. P. Corriu, G. F. Lanneau and M. Perrot, *J. Organomet. Chem*, 1988, **346**, C11-C14.
142. T. Kanzian, T. A. Nigst, A. Maier, S. Pichl and H. Mayr, *Eur. J. Org. Chem.*, 2009, **2009**, 6379-6385.
143. F. Brotzel, Y. C. Chu and H. Mayr, *J. Org. Chem.*, 2007, **72**, 3679-3688.
144. W. Kantlehner, I. C. Ivanov and I. Tiritiris, *Z. Naturforsch., B: Chem. Sci.*, 2012, **67**, 331 - 336.
145. L. Belding, P. Stoyanov and T. Dudding, *J. Org. Chem.*, 2016, **81**, 6-13.
146. T. Arthur, J. R. Harjani, L. Phan, P. G. Jessop and P. V. Hodson, *Green Chem.*, 2012, **14**, 357-362.
147. K. M. Meek and Y. A. Elabd, *Macromolecules*, 2015, **48**, 7071-7084.
148. D. Margetic, in *Superbases for Organic Synthesis*, ed. T. Ishikawa, John Wiley & Sons, Ltd, Editon edn., 2009, pp. 9-48.

149. Y. Xie, B. Qian, P. Xie and H. Huang, *Adv. Synth. Catal.*, 2013, **355**, 1315-1322.
150. T. Kimura, K. Kamata and N. Mizuno, *Angew. Chem. Int. Ed.*, 2012, **51**, 6700-6703.
151. M. J. Fuchter, C. J. Smith, M. W. S. Tsang, A. Boyer, S. Saubern, J. H. Ryan and A. B. Holmes, *Chem. Commun.*, 2008, 2152-2154.
152. C. Wu, H. Cheng, R. Liu, Q. Wang, Y. Hao, Y. Yu and F. Zhao, *Green Chem.*, 2010, **12**, 1811-1816.
153. A. El-Faham and F. Albericio, *J. Org. Chem.*, 2008, **73**, 2731-2737.
154. D. Chaturvedi, N. Mishra and V. Mishra, *Monatsh. Chem.*, 2008, **139**, 267-270.
155. F. Bigi, R. Maggi and G. Sartori, *Green Chem.*, 2000, **2**, 140-148.
156. T. Rosenau, A. Potthast and P. Kosma, *Tetrahedron*, 2004, **60**, 301-306.
157. A. Porzelle and C. M. Williams, *Synthesis*, 2006, **2006**, 3025-3030.
158. G. Kinast and L.-F. Tietze, *Angew. Chem. Int. Ed. Engl.*, 1976, **15**, 239-240.
159. B. Hatano, K. Nagahashi and T. Kijima, *J. Org. Chem.*, 2008, **73**, 9188-9191.
160. H. Heaney, G. Papageorgiou and R. F. Wilkins, *Tetrahedron*, 1997, **53**, 2941-2958.
161. X.-F. Liu, X.-Y. Li, C. Qiao, H.-C. Fu and L.-N. He, *Angew. Chem. Int. Ed.*, 2017, **56**, 7425 .
162. P. Pruszynski, *Can. J. Chem.*, 1987, **65**, 626-629.
163. M. C. Willis, *Chem. Rev.*, 2009, **110**, 725-748.
164. K. Sakai, J. Ide, O. Oda and N. Nakamura, *Tetrahedron Lett.*, 1972, **13**, 1287-1290.
165. T. B. Marder, D. C. Roe and D. Milstein, *Organometallics*, 1988, **7**, 1451-1453.
166. C. P. Lenges, P. S. White and M. Brookhart, *J. Am. Chem. Soc.*, 1998, **120**, 6965-6979.
167. C. P. Lenges and M. Brookhart, *J. Am. Chem. Soc.*, 1997, **119**, 3165-3166.
168. S. Hatanaka, Y. Obora and Y. Ishii, *Chem. Eur. J.*, 2010, **16**, 1883-1888.
169. Y. Obora, K. Nakamura and S. Hatanaka, *Chem. Commun.*, 2012, **48**, 6720-6722.
170. T. Kondo, Y. Tsuji and Y. Watanabe, *Tetrahedron Lett.*, 1987, **28**, 6229-6230.

171. T. Kondo, M. Akazome, Y. Tsuji and Y. Watanabe, *J. Org. Chem.*, 1990, **55**, 1286-1291.
172. Y. Hoshimoto, Y. Hayashi, H. Suzuki, M. Ohashi and S. Ogoshi, *Angew. Chem. Int. Ed. Engl.*, 2012, **51**, 10812-10815.
173. I. F. D. Hyatt, H. K. Anderson, A. T. Morehead and A. L. Sargent, *Organometallics*, 2007, **27**, 135-147.
174. D. P. Fairlie and B. Bosnich, *Organometallics*, 1988, **7**, 946-954.
175. C.-H. Jun, E.-A. Jo and J.-W. Park, *Eur. J. Org. Chem.*, 2007, **2007**, 1869-1881.
176. G. L. Moxham, H. Randell-Sly, S. K. Brayshaw, A. S. Weller and M. C. Willis, *Chem. Eur. J.*, 2008, **14**, 8383-8397.
177. G. L. Moxham, H. E. Randell-Sly, S. K. Brayshaw, R. L. Woodward, A. S. Weller and M. C. Willis, *Angew. Chem. Int. Ed. Engl.*, 2006, **45**, 7618-7622.
178. J. W. Suggs, *J. Am. Chem. Soc.*, 1978, **100**, 640-641.
179. D.-Y. Lee, C. W. Moon and C.-H. Jun, *J. Org. Chem.*, 2002, **67**, 3945-3948.
180. J. W. Suggs, M. J. Wovkulich and S. D. Cox, *Organometallics*, 1985, **4**, 1101-1107.
181. J.-S. H. Chul-Ho Jun, Jung-Bu Kang, Sun-Il Kim, *Bull. Korean Chem. Soc.*, 1994, **15**, 204.
182. M. C. Willis, S. J. McNally and P. J. Beswick, *Angew. Chem. Int. Ed.*, 2004, **43**, 340-343.
183. M. Tanaka, M. Imai, Y. Yamamoto, K. Tanaka, M. Shimowatari, S. Nagumo, N. Kawahara and H. Suemune, *Org. Lett.*, 2003, **5**, 1365-1367.
184. M. C. Willis, H. E. Randell-Sly, R. L. Woodward and G. S. Currie, *Org. Lett.*, 2005, **7**, 2249-2251.
185. C.-H. Jun, *Bull. Korean Chem. Soc.*, 1995, **16**, 66-68.
186. C.-H. Jun, H. Lee and J.-B. Hong, *J. Org. Chem.*, 1997, **62**, 1200-1201.
187. R. J. Pawley, G. L. Moxham, R. Dallanegra, A. B. Chaplin, S. K. Brayshaw, A. S. Weller and M. C. Willis, *Organometallics*, 2010, **29**, 1717-1728.
188. I. Pernik, J. F. Hooper, A. B. Chaplin, A. S. Weller and M. C. Willis, *ACS Catal.*, 2012, **2**, 2779-2786.
189. Z. Shen, H. A. Khan and V. M. Dong, *J. Am. Chem. Soc.*, 2008, **130**, 2916-2917.

190. Z. Shen, P. K. Dornan, H. A. Khan, T. K. Woo and V. M. Dong, *J. Am. Chem. Soc.*, 2009, **131**, 1077-1091.
191. K. G. M. Kou, D. N. Le and V. M. Dong, *J. Am. Chem. Soc.*, 2014.
192. K.B. Schenthal, D.G.M. Kou and V.M. Dong, presented at the Organomet. Chem. Conference, Indiana Convention Center, 2013.
193. T. Miyajima, *Japan Pat.*, JP2013000037A, 2013.
194. M. Miyazaki, M. Shibue, K. Ogino, H. Nakamura and H. Maeda, *Chem. Commun.*, 2001, 1800-1801.
195. E. Dinjus, J. Kaiser, J. Sieler and D. Walther, *Z. Anorg. Allg. Chem.*, 1981, **483**, 63-68.
196. J. Kaiser, J. Sieler, U. Braun, L. Golič, E. Dinjus and D. Walther, *J. Organomet. Chem.*, 1982, **224**, 81-87.
197. C. Geyer, E. Dinjus and S. Schindler, *Organometallics*, 1998, **17**, 98-103.
198. D. F. Hahn, Masters Thesis, Imperial College London, Swiss Federal Institute of Technology Zurich, 2012.
199. S. Kaufhold, Masters Thesis, Imperial College London, University Erlangen-Nuremberg, 2012.
200. A. B. Chaplin, J. F. Hooper, A. S. Weller and M. C. Willis, *J. Am. Chem. Soc.*, 2012, **134**, 4885-4897.
201. Z. Shi, M. Boultadakis-Arapinis and F. Glorius, *Chem. Commun.*, 2013, **49**, 6489-6491.
202. H. Tsunoda, N. Fukazawa, H. Nagase, K. Chiba, T. Nakao, N. Asada, T. Yamaki, K. Kibayashi, H. Migita, M. Morikawa, *United States Pat.*, US2003/212100, 2003.
203. J. Singh, M.E. Gurney, *International Pat.*, WO2005/123724, 2005.
204. G. T. Hoang, V. J. Reddy, H. H. K. Nguyen and C. J. Douglas, *Angew. Chem. Int. Ed. Engl.*, 2011, **50**, 1882-1884.
205. A. Blencowe, A. M. Celli, D. Donati, W. C. Hayes, C. Martin, P. J. Murphy, F. Ponticelli and J. K. Melville-Richards, *Tetrahedron*, 2009, **65**, 3858-3862.
206. J. Cook, J. E. Hamlin, A. Nutton and P. M. Maitlis, *J. Chem. Soc., Chem. Commun.*, 1980, 144-145.
207. C. Krug and J. F. Hartwig, *Organometallics*, 2004, **23**, 4594-4607.
208. C. Tejel, M. A. Ciriano and V. Passarelli, *Chem. Eur. J.*, 2011, **17**, 91-95.

209. A. Crespo-Peña, D. Monge, E. Martín-Zamora, E. Álvarez, R. Fernández and J. M. Lassaletta, *J. Am. Chem. Soc.*, 2012, **134**, 12912-12915.
210. G. Fischer, S. Flatau, A. Schellenberger and A. Zschunke, *J. Org. Chem.*, 1988, **53**, 214-216.
211. A. J. L. Cooper, J. Z. Ginos and A. Meister, *Chem. Rev.*, 1983, **83**, 321-358.
212. E. J. de Vries, PhD Thesis, Groningen, 1997.
213. C. Hendriksen, E. A. Pidko, G. Yang, B. Schöffner and D. Vogt, *Chem. Eur. J.*, 2014, **20**, 12037-12040.
214. G. S. Ananthnag, J. T. Mague and M. S. Balakrishna, *Dalton Trans.*, 2015, **44**, 3785-3793.
215. J. E. Semple, P. C. Wang, Z. Lysenko and M. M. Joullie, *J. Am. Chem. Soc.*, 1980, **102**, 7505-7510.
216. C.-H. Jun, D.-Y. Lee and J.-B. Hong, *Tetrahedron Lett.*, 1997, **38**, 6673-6676.
217. G. M. Sheldrick, *Acta. Crystallogr. A*, 2008, **64**, 112.
218. B. Gabriele, P. Plastina, G. Salerno, R. Mancuso and M. Costa, *Org. Lett.*, 2007, **9**, 3319-3322.
219. M. Yoshida, T. Mizuguchi and K. Shishido, *Chem. Eur. J.*, 2012, **18**, 15578-15581.
220. R. Hernandez-Altamirano, V. Y. Mena-Cervantes, S. Perez-Miranda, F. J. Fernandez, C. A. Flores-Sandoval, V. Barba, H. I. Beltran and L. S. Zamudio-Rivera, *Green Chem.*, 2010, **12**, 1036-1048.
221. M. Donnier-Maréchal, D. Goyard, V. Folliard, T. Docsa, P. Gergely, J.-P. Praly and S. Vidal, *Beilstein Journal of Organic Chemistry*, 2015, **11**, 499-503.
222. T. Mizuno, T. Nakai and M. Mihara, *Synthesis*, 2010, **2010**, 4251-4255.
223. J. Gao, L.-N. He, C.-X. Miao and S. Chanfreau, *Tetrahedron*, 2010, **66**, 4063-4067.
224. J. Wang, S. Li and S. Zhang, *Macromolecules*, 2010, **43**, 3890-3896.
225. M. Aresta, A. Dibenedetto and E. Quaranta, *J. Chem. Soc., Dalton Trans.*, 1995, 3359-3363.
226. J. T. Reeves, Z. Tan, M. A. Marsini, Z. S. Han, Y. Xu, D. C. Reeves, H. Lee, B. Z. Lu and C. H. Senanayake, *Adv. Synth. Catal.*, 2013, **355**, 47-52.

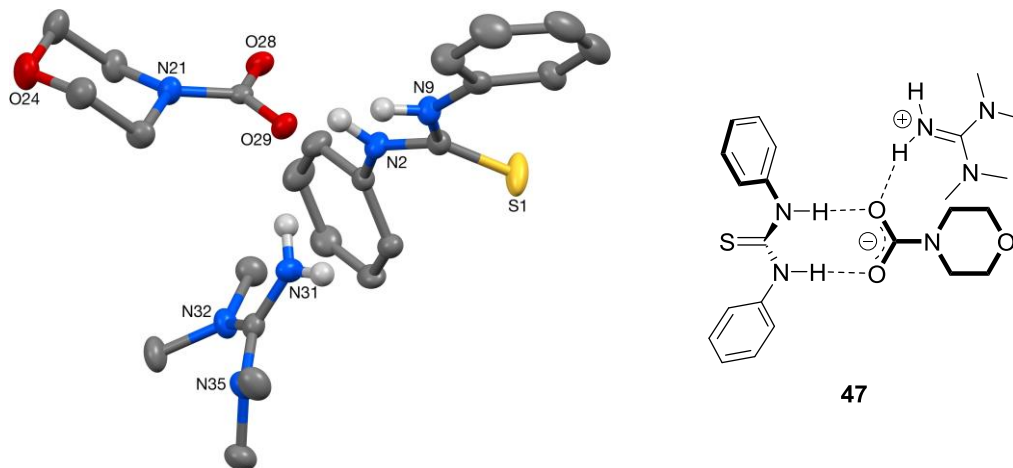
227. D. Wang, D. Kuang, F. Zhang, C. Yang and X. Zhu, *Adv. Synth. Catal.*, 2015, **357**, 714-718.
228. Y. Wei, J. Wu, D. Xue, C. Wang, Z. Liu, Z. Zhang, G. Chen and J. Xiao, *Synlett*, 2014, **25**, 1295-1298.
229. L. Zhang, Z. Han, X. Zhao, Z. Wang and K. Ding, *Angew. Chem. Int. Ed.*, 2015, **54**, 6186-6189.
230. E. S. Smirnova, J. M. Muñoz Molina, A. Johnson, N. A. G. Bandeira, C. Bo and A. M. Echavarren, *Angew. Chem. Int. Ed.*, 2016, **55**, 7487-7491.
231. L. Pokhrel, Y. Kim, T. D. T. Nguyen, A. M. Prior, J. Lu, K.-O. Chang and D. H. Hua, *Bioorg. Med. Chem. Lett.*, 2012, **22**, 3480-3484.
232. D. P. Fairlie and B. Bosnich, *Organometallics*, 1988, **7**, 936-945.

Appendix

Appendix 1 Crystal Structure of Morpholine/Thiourea/CO₂ Complex **47**

X-ray Crystal Structure for Authentic Product **47**

(prepared, measured and resolved by B.N. Nguyen and A.P.White)



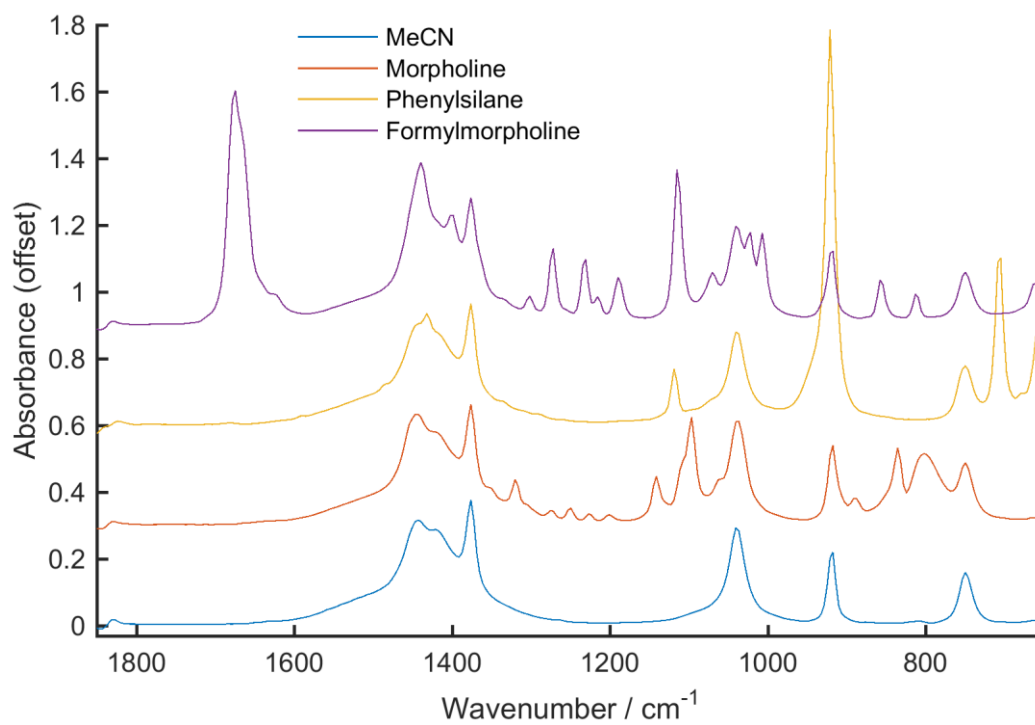
Crystal data and structure refinement

Identification code	Complex 47
Empirical formula	C ₁₃ H ₁₂ N ₂ S, C ₅ H ₈ NO ₃ , C ₅ H ₁₄ N ₃
Formula weight	474.62
Temperature	173 K
Diffractometer, wavelength	OD Xcalibur 3, 0.71073 Å
Crystal system, space group	Monoclinic, P2(1)
Unit cell dimensions	$a = 9.2161(2)$ Å $\alpha = 90^\circ$ $b = 12.7576(3)$ Å $\beta = 95.835(2)^\circ$ $c = 10.9094(2)$ Å $\gamma = 90^\circ$
Volume	1276.03(5) Å ³
Z	2
Density (calculated)	1.235 Mg/mm ³
Absorption coefficient	0.162 mm ⁻¹
F(000)	508
Crystal colour / morphology	Colourless needles
Crystal size	0.39 x 0.07 x 0.05 mm
2 θ range for data collection	3.19 to 32.71°
Index ranges	-13 ≤ h ≤ 13, -16 ≤ k ≤ 19, -14 ≤ l ≤ 16
Reflns collected / unique	14420 / 7060 [R(int) = 0.0220]

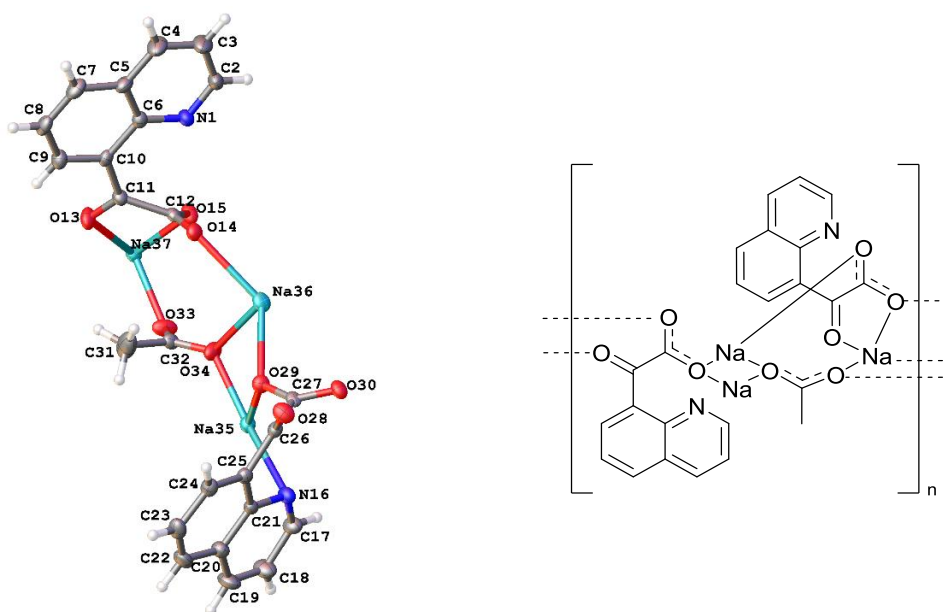
Reflns observed [$F > 4\sigma(F)$]	6099
Absorption correction	Analytical
Max. and min. transmission	0.993 and 0.960
Refinement method	Full-matrix least-squares on F^2
Data / restraints / parameters	7060 / 5 / 319
Goodness-of-fit on F^2	1.038
Final R indices [$F > 4\sigma(F)$]	R1 = 0.0375, wR2 = 0.0838 R1+ = 0.0375, wR2+ = 0.0838 R1- = 0.0380, wR2- = 0.0852
R indices (all data)	R1 = 0.0480, wR2 = 0.0877
Absolute structure parameter	$x_+ = 0.21(5)$, $x_- = 0.79(5)$
Largest diff. peak, hole	0.323, -0.387 $e\text{\AA}^{-3}$
Mean and maximum shift/error	0.000 and 0.000

Appendix 2 IR Spectra of Reaction Standards

IR Spectra of standards:



Appendix 3 X-ray Crystal Structure for Authentic Product 166

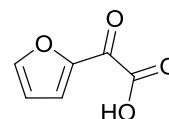
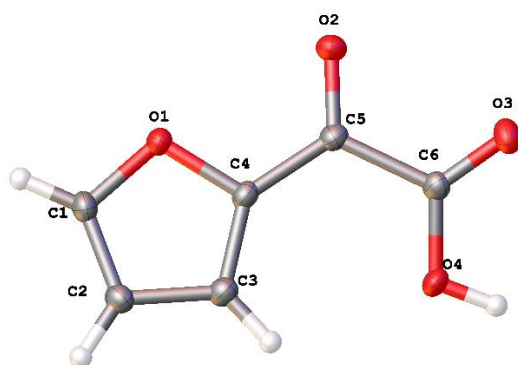


Crystal data and structure refinement:

Identification code	Compound 166	
Empirical formula	$C_{12}H_{7.5}NNa_{1.5}O_4$	
Formula weight	264.17	
Temperature	120.01(19) K	
Crystal system	monoclinic	
Space group	$P2_1/c$	
Unit cell dimensions	$a = 6.1101(5) \text{ \AA}$	$\alpha = 90.00^\circ$
	$b = 22.7075(19) \text{ \AA}$	$\beta = 94.626(7)^\circ$
	$c = 16.1587(12) \text{ \AA}$	$\gamma = 90.00^\circ$
Volume	$2234.6(3) \text{ \AA}^3$	
Z	8	
Density (calculated)	1.570 mg/mm^3	
Absorption coefficient	1.497 mm^{-1}	
F(000)	1080.0	
Crystal size	$0.19 \times 0.04 \times 0.03 \text{ mm}$	
Radiation	$CuK\alpha$ ($\lambda = 1.54184$)	
2θ range for data collection	6.72 to 133.18°	
Index ranges	$-4 \leq h \leq 7, -25 \leq k \leq 26, -18 \leq l \leq 19$	
Reflections collected	7799	

Independent reflections	3943 [$R_{\text{int}} = 0.0585$, $R_{\text{sigma}} = 0.0786$]
Data/restraints/parameters	3943/0/335
Goodness-of-fit on F^2	0.985
Final R indexes [$I \geq 2\sigma(I)$]	$R_1 = 0.0498$, $wR_2 = 0.1088$
Final R indexes [all data]	$R_1 = 0.0891$, $wR_2 = 0.1303$
Largest diff. peak/hole	0.25/-0.29 $e \text{ \AA}^{-3}$

Appendix 4 X-ray Crystal Structure for Authentic Product 186

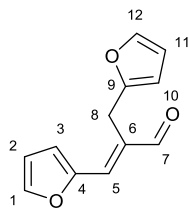


Crystal data and structure refinement

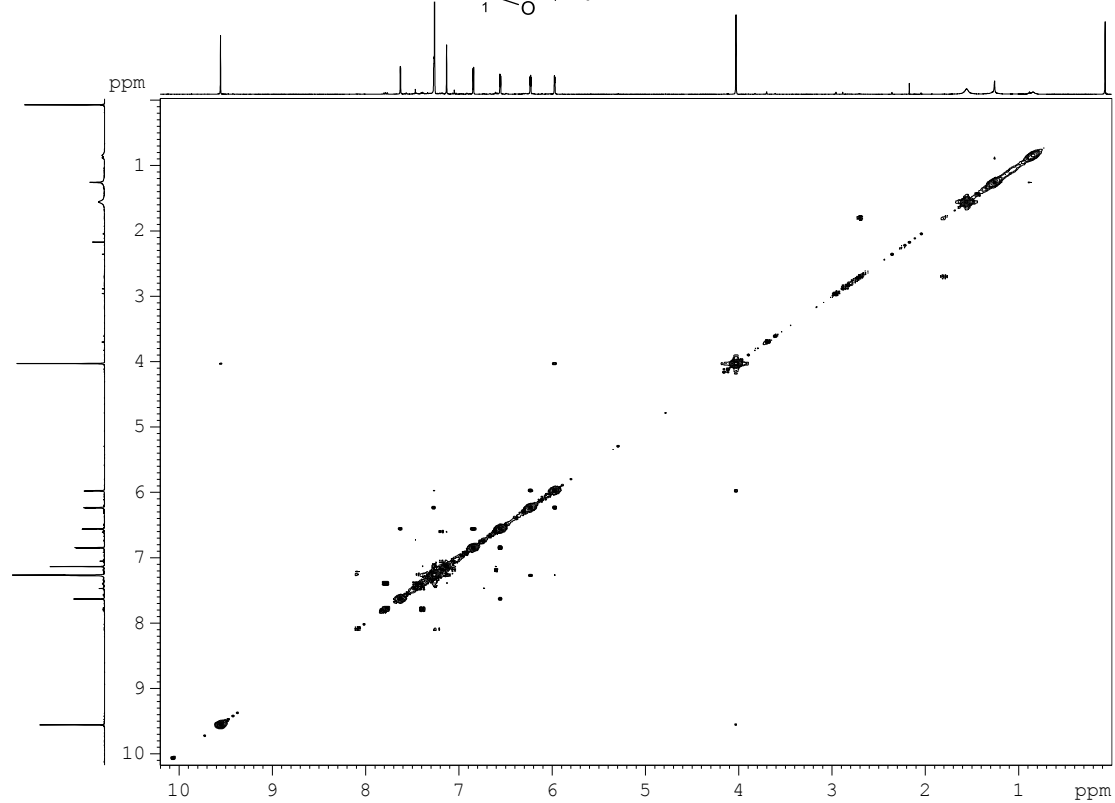
Identification code	Compound 186	
Empirical formula	$C_6H_4O_4$	
Formula weight	140.09	
Temperature	119.99(13) K	
Crystal system	monoclinic	
Space group	$P2_1/c$	
Unit Cell Dimensions	$a = 7.7421(7) \text{ \AA}$	$\alpha = 90.00^\circ$
	$b = 9.7534(9) \text{ \AA}$	$\beta = 94.091(9)^\circ$
	$c = 7.3662(8) \text{ \AA}$	$\gamma = 90.00^\circ$
Volume	$554.82(9) \text{ \AA}^3$	
Z	4	
Density (calculated)	1.677 g/cm^3	
Absorption coefficient	0.145 mm^{-1}	
F(000)	288.0	
Crystal size	$0.14 \times 0.11 \times 0.07 \text{ mm}^3$	
Radiation	$\text{MoK}\alpha$ ($\lambda = 0.71073$)	

2 Θ range for data collection	6.72 to 56.56°
Index ranges	-10 ≤ h ≤ 10, -12 ≤ k ≤ 12, -9 ≤ l ≤ 9
Reflections collected	6877
Independent reflections	1373 [R _{int} = 0.0427, R _{sigma} = 0.0328]
Data/restraints/parameters	1373/0/107
Goodness-of-fit on F ²	1.186
Final R indexes [I ≥ 2σ (I)]	R ₁ = 0.0547, wR ₂ = 0.1054
Final R indexes [all data]	R ₁ = 0.0638, wR ₂ = 0.1084
Largest diff. peak/hole	0.39/-0.23 e Å ⁻³

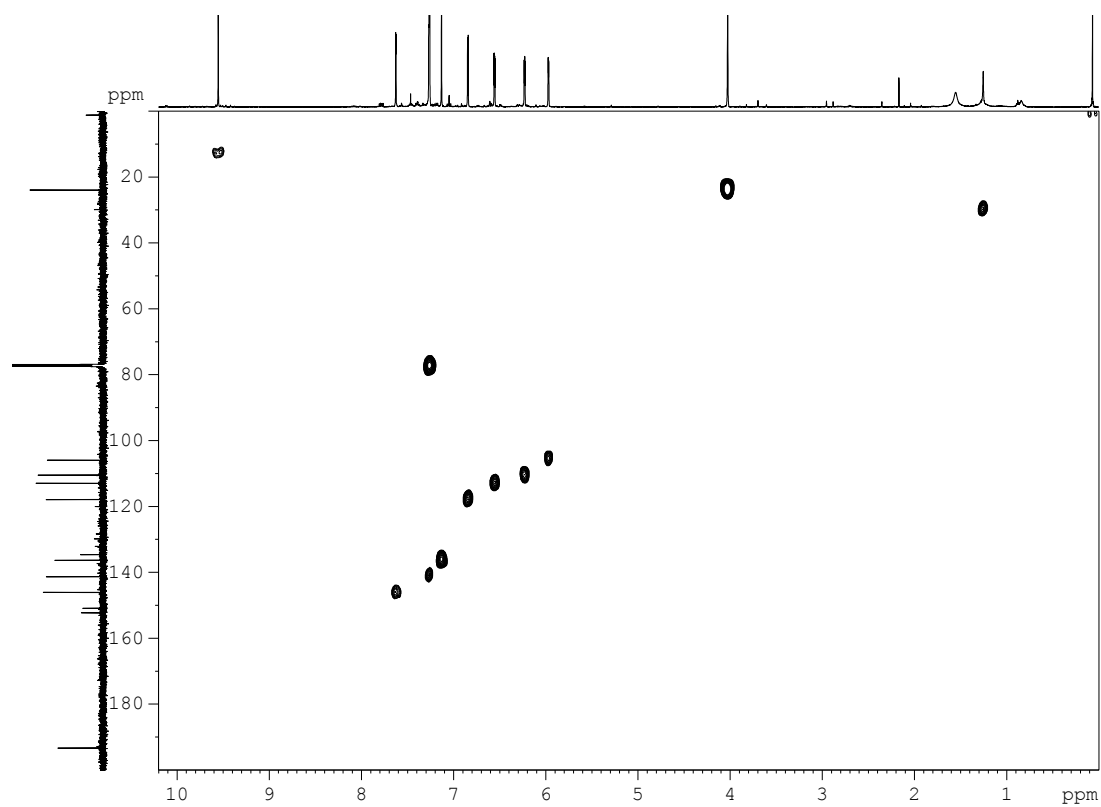
Appendix 5 2D Spectra Used for Identification of Component A 193 :



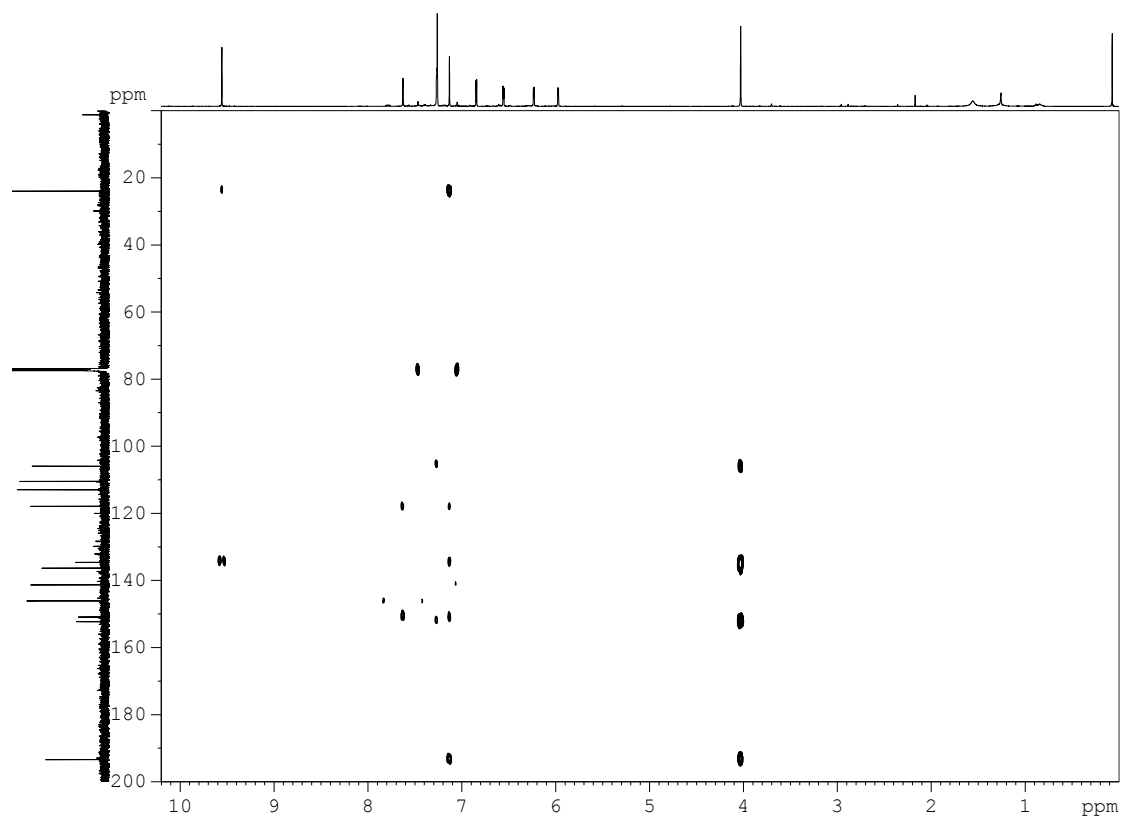
COSY:



HMQC:



HMBC:



NOE spectrum:

